

INTERPRETATION OF GRAVITY DATA

By

Walter W. Hays
U.S. Geological Survey

Open-File Report 76-479

1976

This report is preliminary and has not
been edited or reviewed for conformity
with U.S. Geological Survey standards.

FOREWORD

This report was prepared for use as a text in a short course that was presented in Buenos Aires, Argentina, June-July, 1976. The short course was sponsored by the Naval Hydrographic Service of the Argentine Navy, under the auspices of the Organization of American States. This program was a part of their Multinational Marine Science Project.

The material contained in this report was drawn from many sources. Although an effort was made to give proper credit to the multitude of information sources used to prepare the report, some omissions may have occurred. The author assumes full responsibility for all omissions.

INTERPRETATION OF GRAVITY DATA

I. INTRODUCTION	Page
Force and acceleration.....	2
Gravitational attraction.....	7
Continuously distributed matter--the gravitational field...	13
II. GRAVITY EFFECTS OF CERTAIN GEOMETRICAL FORMS	
Field of force of a straight rod.....	17
Circular disc.....	30
Homogeneous sphere.....	35
Horizontal cylinder.....	39
Vertical fault.....	41
III. ACCURACY OF SUBSURFACE MODEL APPROXIMATIONS	
Thin plate approximation for a fault.....	44
Equivalent sphere approximation.....	46
Vertical cylinder and approximation by axial line element.	47
Vertical cylinder approximated by thin horizontal disc....	49
IV. FACTORS AFFECTING THE CHARACTER OF GRAVITY ANOMALIES	
Effect of size of anomalous mass.....	54
Effect of depth of anomalous mass.....	55
Effect of density contrast of anomalous mass.....	56
Effect of attitude of anomalous mass.....	58
Effect of boundary conditions of anomalous mass.....	59
Effect of shape of sedimentary basin.....	61
Isolation and resolution.....	62
Horizontal attenuation of fault anomalies.....	66
V. DERIVATIVE METHODS OF DATA ENCHANCEMENT	
Sphere.....	67
Infinite horizontal cylinder.....	69
Infinite horizontal slab (fault).....	70
Numerical calculation of 2nd vertical derivative from potential field data.....	72
VI. DEPTH ESTIMATES	
Sphere.....	75
Infinite horizontal cylinder.....	75
Faulted slab.....	77

	<u>Page</u>
VII. CORRECTIONS APPLICABLE TO GRAVITY DATA	
Gravimeters.....	81
Earthtide or drift correction.....	82
Free air correction.....	83
Bouguer correction.....	84
Terrain correction.....	84
Latitude.....	86
VIII. MATHEMATICAL BACKGROUND FOR CORRECTING GRAVITY DATA	
Free air correction.....	88
Bouguer correction.....	89
Terrain correction.....	92
Latitude correction.....	92
Earth tide or drift correction.....	94
IX. SPECIAL INTERPRETATIONAL AIDS	
Skeel's graticule.....	94
Dot chart.....	97
Solid angle chart.....	104
Computation for irregularly shaped 3-D bodies.....	104
Analytical continuation.....	119
Surface fitting.....	121
Stripping.....	123
Frequency analysis.....	125
Two-dimensional filtering.....	128
Example.....	141
REFERENCES	
APPENDICES	
A. Tables for the gravity terrain correction.....	A-1
B. Fortran program for upward and downward continuation...	B-1
C. Basic elements of Fourier transforms and convolution...	C-1
D. Bouguer gravity map of South America.....	D-1
E. Conversion tables, English and metric systems of units.	E-1
F. Problems.....	F-1

INTRODUCTION

The gravity method has a very important place in a well-planned comprehensive geophysical program. The principles of gravitational attraction upon which the method is based are well-established. It follows, therefore, that an interpretation of gravity data which has geological significance must be based on an intelligent use of these underlying physical principles, either directly or indirectly. It follows also that any attempt to interpret gravity data into its geological import without respect to these physical principles cannot be considered scientifically acceptable.

Much time and effort have been spent seeking direct correlations between known geological structures and corresponding gravity measurements. In many cases, such as those of some of the shallow salt domes of the Texas-Louisiana Gulf Coast, very good direct correlations exist. However, there are some shallow salt domes in the same geological province for which the gravity data show practically no anomaly. Hence, interpretation of gravity data is complex.

Various techniques have been developed to aid in interpreting gravity measurements in terms of the subsurface structure. The so-called "curvature" data of torsion balance measurements, are an example. Other techniques, which largely are of a subjective nature, consist in reducing gravity data to a "residual" by various methods of "removing the regional." The so-called "second derivative" method, although often said to be "more mathematical," is also a subjective technique similar to the residual.

Graticules, nomograms, tables and charts are examples of other interpretational techniques which relate gravity measurements to a geologic model. To use these tools, the problem is first reduced in complexity by a reduction in the number of parameters. For example, by assuming that one horizontal dimension of the subsurface structure is infinite in extent, a two-dimensional cross-section is developed. Then by reducing the number of density differentials to only one, the solutions become manageable, although not unique.

This last type of interpretation if used intelligently is scientifically honest in the sense that all these simplifying conditions are clearly understood and that the principles of gravitational attraction are not discarded. However, as is well known, even these methods of subsurface interpretation require careful application. Every person interested in the interpretation of gravity data would do well to go through both types of interpretational techniques to get the "feel" of the complexity of the problem even when it is reduced to relatively simple proportions.

For completeness, the elementary physical concepts, definitions, and mathematical formulations will be reviewed.

Force and Acceleration--The first of the three laws of motion, as stated by Newton, says that a body will persist in its state of rest or of uniform motion in a straight line unless impelled to change that state by external forces. This law gives rise to the concept of force. To understand the consequences of the physical principles embodied in this

law of motion, consider first a body in empty space indefinitely removed in distance from any other body. It would be impossible to make any distinction between that body at rest or that body moving with constant velocity in a straight line, unless we had some point of reference, to which point we would have to ascribe arbitrarily the property of either being at rest or of moving with constant velocity in a straight line. In other words, a body at rest and a body moving uniformly in a straight line are in a very important sense simply relative states of one another.

When a force is applied to such a body, however, things begin to happen. What is a force? A force is a push or a pull. This simple definition will suffice for now, although force is a fundamental concept of mechanics which is studied and understood by its properties. Force is an undefined concept to which properties are ascribed to fit the nature of the physical world as we experience it.

The important attributes--properties--of a force are: (1) Magnitude (How big is it?), and (2) Direction. Intuitively, one may have a feeling for these properties, but force can be defined in a quantitative manner by examining the effects of applying a force to a body.

To do this we start with the elementary units of mechanics: (1) distance (measured in metres or feet or such), (2) mass (measured in grams or pounds or such), and, (3) time (measured in seconds or such). The concepts of distance and time are intuitively understood. But the concept of mass must be dissociated from weight. By the mass of an object, one means the amount of matter in it, regardless of its weight. A gram of matter is the same here or anywhere else in the universe. The weight of this gram of

matter, on the other hand, will depend on its position and the attendant forces. For example, a gram of water is defined as the mass of water, under standard conditions, in a cubic centimetre. The weight of this water on the earth, or anywhere else, for that matter, will vary from point to point. But its mass is one gram. In the same way, the mass of any body is the amount of matter in it, not its weight at some point.

Because it is practical to do so, and for no other reason, a gram of mass of material is defined as the amount of the material whose weight at an arbitrary point is equal to the weight of a gram of water at that same point. Note that the gram of material so defined is the mass in a certain volume, which is the same everywhere.

Next, using a point of reference, consider a body of mass M (grams) moving in a straight line with a velocity v (cm/sec). With no force acting on this body, it will persist in moving at this constant velocity (which may be zero, if it is at rest). The momentum of this body is defined to be the product of its mass and velocity. That is the momentum M of a body of mass m moving with a velocity v .

$$M = mv;$$

and it follows that the units of M are

$$\text{gr. cm./sec.}$$

As an example, a body of 15 grams moving with a velocity of 25 ~~cm~~. /sec. has a momentum of 375 gr.cm./sec. A body at rest has a momentum of zero.

Newton's Second Law of Motion states that rate of change of momentum is proportional to the force acting and takes place in the direction of that force.

The phrase "rate of change" refers to the time rate of change: the change that occurs in the momentum - its increase or decrease - during certain intervals of time. Thus, assuming the rate of change is constant, for purposes of illustration, the rate of change of momentum is the amount by which the momentum is increased (or decreased) each unit of time (second). The unit of this rate of change of momentum is thus seen to be

$$(\text{gr.cm./sec.})/\text{sec.}$$

The Second Law of Motion says essentially that the effect of a force acting on a body is to change the momentum of that body at a rate proportional to the magnitude of that force.

Consider, again, the momentum M of a body of mass m moving in a straight line with constant velocity v .

$$M = mv.$$

Suppose a force - call it F for the present - is now applied in the direction of this moving body. Its momentum will change, according to the Second Law of Motion. The Mass M of the body cannot change; therefore, only the velocity can change with the change of momentum.

By definition, rate of change of velocity is called acceleration. Accordingly, rate of change of momentum is equivalent to the product of the mass of the body and its acceleration.

The Second Law of Motion thus reduces itself to the statement that the product of the mass m of a body and its acceleration a (in a given direction) is proportional to the force F acting to produce that acceleration. The effect of a force, in other words, is to produce an acceleration on a body in direct proportion to its magnitude.

If the factor of proportionality is assumed to be unity, the relation says that

$$F = a$$

In this case the units of the force F are those of the rate of change of momentum:

$$(\text{gr.cm./sec.})/\text{sec.},$$

usually, and more simply, written

$$\text{gr.cm./sec.}^2$$

This unit of force is defined, anew, as a dyne; i.e.,

$$1 \text{ dyne} = 1 \text{ gr.cm./sec.}^2$$

Stated more specifically, 1 dyne is the amount of force required to give a mass of 1 gram an acceleration of 1 cm./sec.² In geophysics, the unit gal is often used for acceleration. Thus 1 gal = 1 cm./sec.², and 1 dyne = 1 gr. gal. Gravity anomalies are stated in terms of milligals.

If one holds a 1-gram mass in his hand, the force exerted upward in this process is just enough to counterbalance the force of the earth pulling on this 1-gram mass. If allowed to fall, the mass will fall with an acceleration of 980 cm/sec.² The pull of the earth on this gram - the force exerted to hold it up - is thus

$$\begin{aligned} F &= (1 \text{ gr.}) \times 980 (\text{cm./sec.}^2) \\ &= 980 \text{ dynes.} \end{aligned}$$

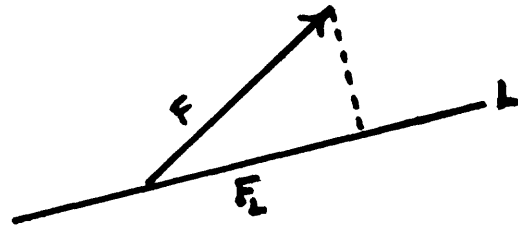
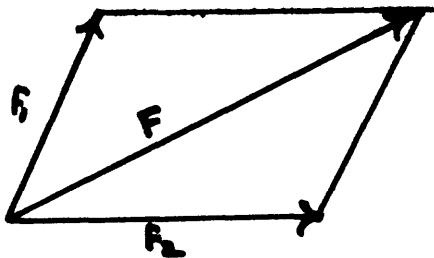
Roughly, then, a dyne is approximately 1/980 - or, in round numbers, 1/1000 of the force needed to hold up 1 gram of matter.

The second attribute of the concept of force, direction, is fundamental. In common with some other mechanical quantities, like velocity and acceleration, it is necessary to specify both the magnitude and direction

of a force for a complete definition. In this regard, then, it is called a vector as contrasted with a scalar quantity which is specified only by its magnitude.

Thus, one must not be content in saying, "A force of 10 dynes!"; the direction in which that force is applied must also be specified. Customarily, then, a force is indicated by an arrow, pointing in the direction of the force, the length of whose stem is equal to its magnitude.

Being a vectorial quantity, a force shares in common with other types of vector quantities the properties of combining with other forces into a resultant force; and of decomposition into components. The resultant of two forces and the component of a force are graphically illustrated in the figures below.



Gravitational Attraction--A force, as described above, is a push or a pull. In our daily life forces of many types are experienced. There are frictional forces and electrical forces; forces exerted in walking, in pushing, in pulling; forces which impel machinery and forces which slow things down.

One type of force which is completely all-pervading, ordinarily taken for granted and seldom considered extraordinary, is the universal force of gravitation. The fact that the universe pursues its orderly course, that individuals do not float about but are kept down to earth, all in response to universal gravitation: this usually fails to excite more than passing interest. In fact, only very young infants seem to be fascinated in noticing that an object, left free, will fall. Grown-ups have learned to expect the object to fall.

Until the beginning of quantitative and experimental science, a considerable amount of theological and other philosophical disputations persisted, naive in some respects and tragic in others, which dealt with falling bodies, orbits of planets and satellites and other celestial phenomena, all of which are known today to be moving in accordance with the single universal law of gravitational attraction. Empirical astronomical results made from observations - by the Egyptians, by the Greeks, and later by Kepler and others - were for a long time known, but only as individual items of considerable interest, curiosity and importance. The unification of these items under a single physical law and its consequences was one of the early triumphs of physical science and mathematics.

Newton, as is well known, first stated clearly the Law of Universal Gravitation and pursued its implications with what he called The Method of Fluxions, a mathematical tool he fashioned for his needs, and which, today, is called the calculus. A whole new vista of science was now opened in that experimental and observational science could make

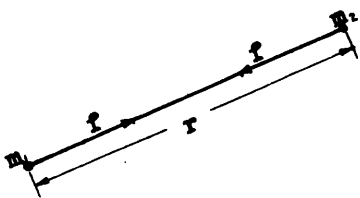
rapid progress with the help of mathematical analysis. In the physical sciences at least, it became possible to predict with certainty.

For simplicity, the universe can be considered to be made up of particles of masses which will not be defined except to say that the geometric dimensions of the particles are small. Indeed, they may be considered as tiny spheres. Between every pair of such particles, a force of attraction exists whose direction is along the straight line joining those particles. That is, each particle in the universe "pulls" on every other particle.

How big is this pull existing between a pair of particles? Intuitively, it would appear that this force should increase as the masses of the particles increase. In fact, one property of this universal force of gravitational attraction between two particles is that, in magnitude, it is proportional to the masses of the two particles. It should appear intuitively also that the farther removed these particles are from one another, the smaller this force should be. For various reasons the "inverse" square law" suggests itself and becomes justified in later developments by observation and measurement, terrestrial and celestial.

Combining all these arguments, we now state the basic law of universal gravitational attraction in this manner:

There exists a force of attraction between each two particles in the universe whose magnitude is proportional directly to the masses of those particles and inversely to the square of the distance between those particles.



Specifically, let two particles whose masses are m_1 and m_2 be separated by a distance r .

The force f of attraction between them is

$$f = G \frac{m_1 \cdot m_2}{r^2} .$$

The numerical value of the proportionality factor G is a matter of the units of mass, distance and force employed and is the same throughout the universe.

In general, m_1 and m_2 are expressed in grams, r in centimetres, and f in dynes. Since

$$1 \text{ dyne} = 1 \text{ gr.cm./sec.}^2 ,$$

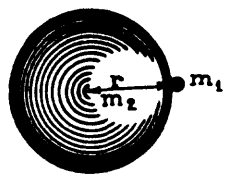
the relation above says, in dimensions, that

$$\text{gr.cm./sec.}^2 = G \frac{\text{gr.} \cdot \text{gr.}}{\text{cm}^2} .$$

It follows, then, that the "unit" of the universal gravitational constant G is

$$\frac{\text{cm.}^3}{\text{gr.sec.}^2}$$

At first, there appears to be a severe difficulty in the statement of the law of gravitation. It would seem that, as the distance between the two particles decreases to zero, the attracting force increases indefinitely because of the inverse-square relationship. The resolution of



this apparent paradox is, however, suggested by this argument. Suppose that a very minute particle of mass m_1 rests on a larger (spherical) particle of radius r and specific gravity δ . The mass of the second particle is

$$m_2 = \frac{4\pi r^3 \delta}{3} .$$

For the present, the assumption will be made that the larger particle attracts the first one as though all its matter were concentrated at its center (later this will be shown to be true for a homogeneous spherical mass). The magnitude of the force of attraction, since $m_2 = \frac{4\pi r^3 \delta}{3}$, is

$$f = G \cdot m_1 \cdot \frac{4\pi r^3 \delta}{3} \cdot \frac{1}{r^2} = G \frac{4\pi \delta m_1}{3} \cdot r$$

Thus, f will approach zero, rather than increase indefinitely, as r approaches zero.

The gravitational constant G is universal in the sense that for any particular set of units (the C.G.S. system, for example), it has the same value throughout all space. For the most part we shall use the C.G.S. system, in which the value is

$$G = 6.67 \times 10^{-8} \frac{\text{CM.}^3}{\text{GR. SEC.}^2} .$$

This value has been determined experimentally in the laboratory over many years by careful refinements of the Cavendish experiment.

Generally, for calculations, it is useful to use

$$G = \frac{20}{3} \times 10^{-8} \frac{\text{CM.}^3}{\text{GR. SEC.}^2}$$

Accepting as true this value for G , the assumption that the earth is a homogeneous sphere with a radius of 4000 miles and the principle stated above that a homogeneous spherical mass attracts as if all of its mass were concentrated at its center, the mean specific gravity of the earth can be calculated.

Recall that a gram of matter at the surface of the earth, and the earth attract each other with a force of about 980 dynes (the centrifugal effect of the earth's rotation may be neglected). Between two spheres the attraction is

$$F = G \frac{M_1 \cdot M_2}{R^2},$$

Substituting

$$F = 980 \text{ DYNES,}$$

$$G = \frac{20}{3} \times 10^{-8} \frac{\text{CM.}^3}{\text{GR. SEC.}^2},$$

$$M_1 = 1 \text{ GRAM,}$$

$$M_2 = E, \text{ THE MASS OF THE EARTH,}$$

and the radius of the earth r in centimetres is

$$r = (4000 \times 5280 \times 30) \\ \approx 6.4 \times 10^8 \text{ centimeters.}$$

Now, if the specific gravity of the earth is D , then

$$m_2 = E = \frac{4\pi r^3 D}{3}$$

and the formula becomes:

$$980 = \frac{20}{3} \times 10^{-8} \times \frac{1 \times 4\pi \times r^3}{3r^3} D$$

$$980 = \frac{20}{3} \times \frac{10^{-8} \times 12.5 \times 6.4 \times 10^8}{3} D$$

hence

$$D \approx 5.5.$$

That is to say, there is 5.5 times as much mass in the earth as there would be if it were composed entirely of water. The "weight" of the earth is 5.5 times as great as it would be if composed entirely of water.

Continuously Distributed Matter - The Gravitational "Field"--

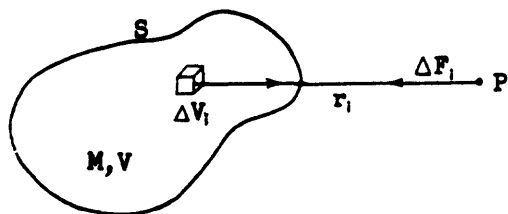
The statement of the Law of Universal Gravitation postulates the existence of a specific force of attraction between every pair of particles. To develop the consequences of this principle for masses as distinguished from particles raises certain philosophical difficulties which are of considerable practical importance. As in all physical science, the

resolution of these difficulties rests in observation and experimentation. These, in turn, lead to refinement of theory, further analysis and prediction, until a course is determined which best fits the "real" universe as we sense it.

In studying the gravitational attraction between two arbitrary masses, one must come to a definite decision as to whether to consider each of the masses as consisting of separate and discrete particles, or to idealize the conception mathematically and consider each mass as consisting of "continuously distributed" matter. Although a case may be logically built for the first possibility, the second alternative--that of continuously distributed matter--has the decided advantages of mathematical tractability. It avoids the necessity of defining a particle, and takes advantage of the close agreement of the results with observation and experimentation.

To introduce the concept of the gravitational force "field" due to a body, consider, a mass M of volume V enclosed by a (smooth) surface S . Let there be a particle of unit mass (1 gr., in the CGC system),

which will be called a unit particle, at an arbitrary point P .



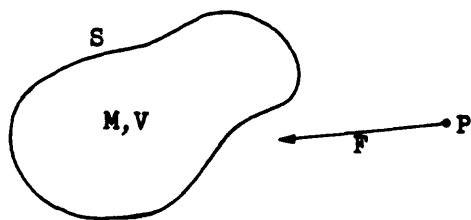
Think of the volume V as subdivided into a large number, n , of small pieces, the volume of the i th piece being ΔV_i , its mass ΔM_i , and its distance (say from its center of gravity) to P , r_i . If the mean

density of this little volume, ΔV_i is ρ_i , the force of attraction between the unit particle and P and this little volume is, to a high degree of accuracy (if ΔV_i is small enough and r_i large enough) equal in magnitude to

$$\Delta F_i = \frac{G \cdot 1 \cdot \rho_i \Delta V_i}{r_i^2},$$

and its direction lies along the line joining P to the "center" of ΔV_i .

Now, utilizing the principles of the integral calculus, each V_i is allowed to approach zero in such a way that its maximum diameter, too, is allowed to approach zero. The number of subdivisions n of V increases indefinitely and, in the limit, assuming this implied continuity of matter constituting M , there will be a force of attraction F between the unit particle at P and the mass M , definite in both magnitude and direction.



This force F is the limit of the vectorial sum of these N forces, ΔF_i .

It is evident from this definition of the force F that its value (in magnitude and direction) will depend on the position of P (which, at least for the present, is assumed outside of V). In other

words, at each point of space a vector can be drawn representing in direction and magnitude the force of attraction between a unit particle at that point

and the mass M . This is schematically illustrated in the next figure, which one should visualize in its three-dimensional aspect.

A number of facts should be obvious, intuitively, at least, about these vectors. In the first place, the magnitude of the force F decreases with increasing distance of P from M . Also, as this distance gets larger, the vector representing the value of the force F tends to point to a common position of M (its center of gravity) since M becomes relatively at least, a particle for greatly removed positions of P . Finally, and most importantly, these vectors vary continuously in space. By this we mean that as the point P moves continuously in space, the corresponding vector F changes both in magnitude and direction in a continuous manner. Each vector flows smoothly from one position to another.

These facts give rise to the concept of the field of force of M . The field of force for M consists of the totality of these vectors in space. It may become clear, from the figure, that as a result of the magnitudes and dispositions of these vectors, there will be a system of curves in space such that each vector will be tangent to one of these. It is natural to call these curves the lines of force of this field, and it becomes apparent that if a finite number of these lines of force is drawn, the spacing of these lines will, in some way, depend on the magnitude of the force in the neighborhood. Where the force is small - as in regions remote from M , the spacing of the lines becomes sparse; and as the force increases, on approaching M , the spacing becomes thick.

By considering the unit particle at P as a probe, moving it through space and noting the attraction between it and the mass M , we have an

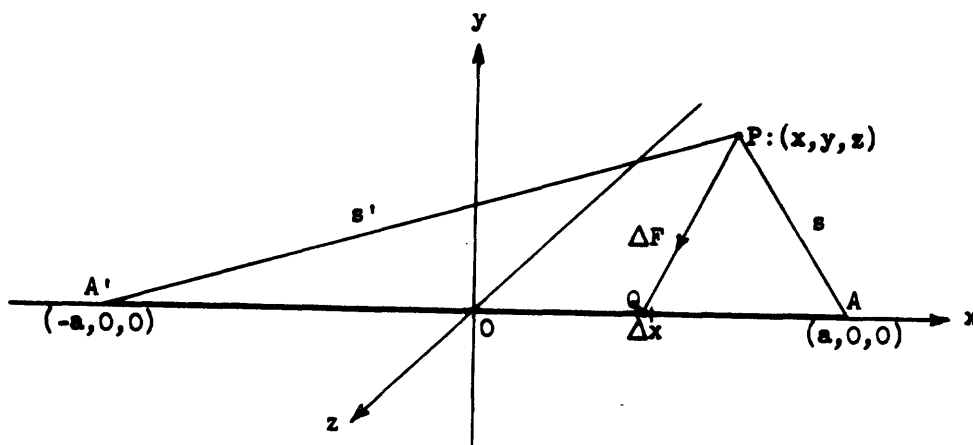
effective way of studying the field of force due to M.

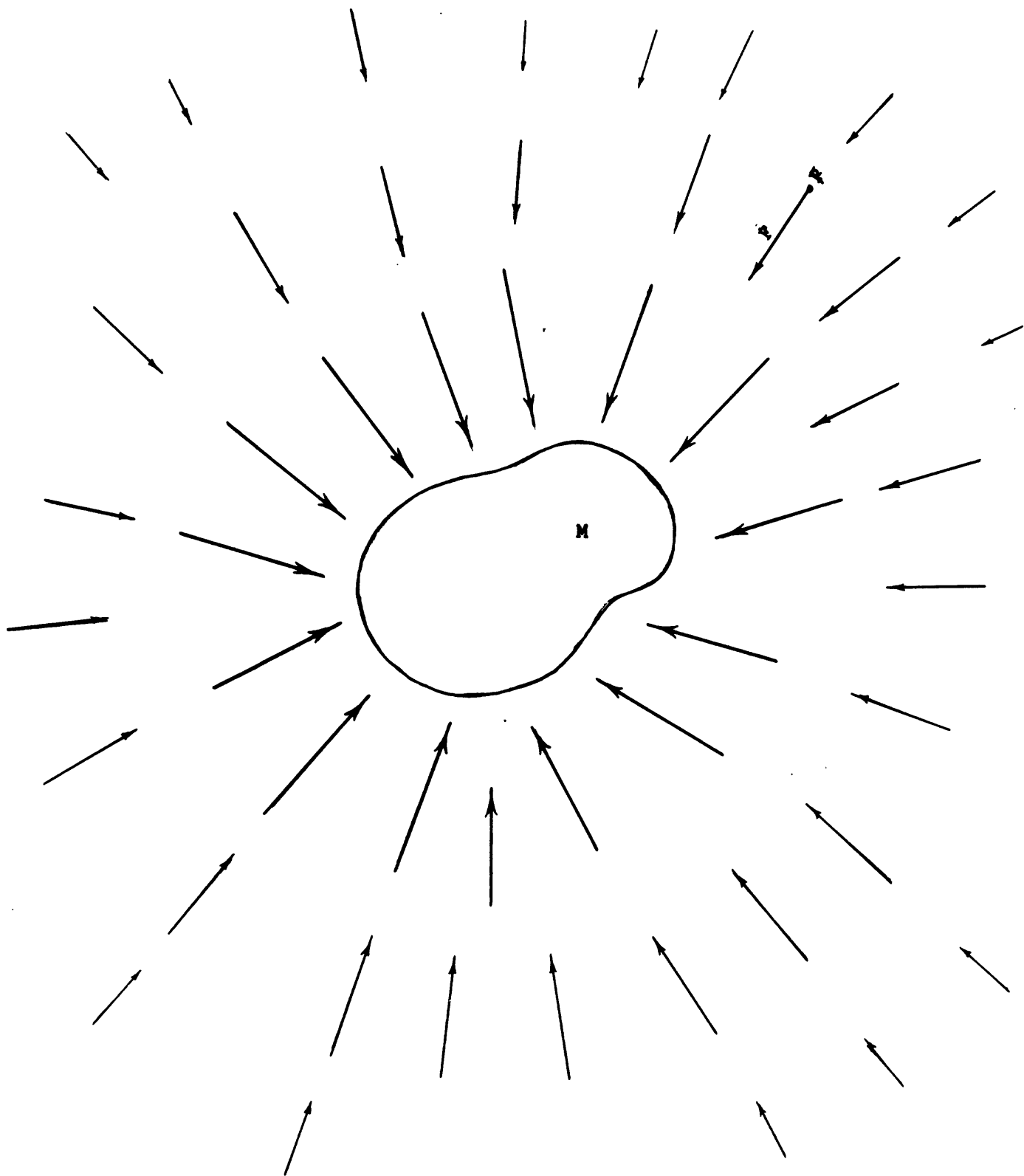
The essence of most interpretations of gravity data having scientific merit ultimately rests on the study of these gravitational fields. That is, the gravitational field due to various types of masses, are studied. The conclusions derived therefrom form the physical basis for going in the reverse direction from gravity data to the geologic model.

GRAVITY EFFECTS OF CERTAIN GEOMETRICAL FORMS

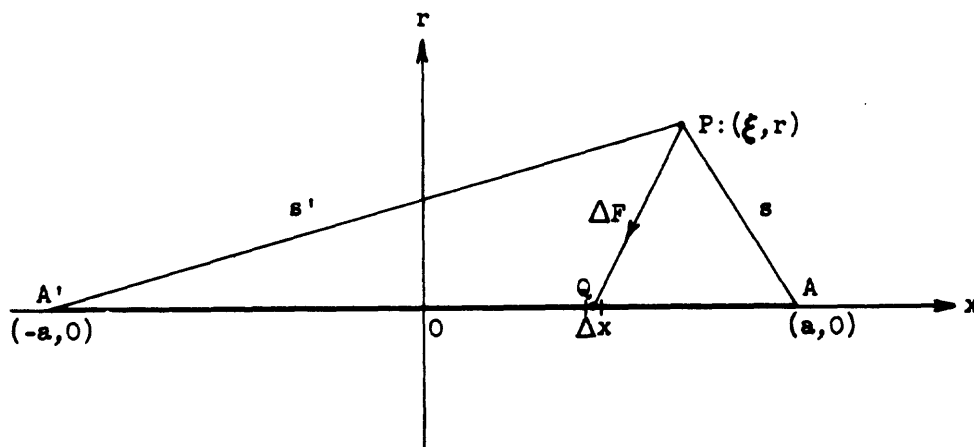
The Field of Force of a Straight Rod--At this point it is instructive to examine a few specific examples of fields of force in order that the physical ideas may be made sharper. The base of a thin homogeneous rod; so thin that it may be considered as a linear rather than a solid object, will be considered first.

Let the x-axis of a coordinate system be laid out along the (linear) rod, with the origin 0 at its center. The y- and z-axes are then arbitrarily set up through 0, mutually perpendicular and each perpendicular, of course, to the x-axis.





If the length of the rod is $2a$, the coordinates of the end-points, A' and A , become $(-a,0,0)$ and $(a,0,0)$. Let $P:(x,y,z)$ be an arbitrary point in space. It should be intuitively apparent that the field of force is cylindrically symmetric with respect to $A'A$. Hence all we need study is a plane meridian section of this field, as indicated below. R is chosen as the radial coordinate in an arbitrary plane section through $A'A$ and the coordinates of P are given by (ξ, r) . Let the linear density (gr./cm.) of



The rod be ρ , so that the mass of an element of length Δx of the rod will be $\rho\Delta x$. (The x -coordinate has been retained along the rod.) In order to keep the proper dimensions in mind, a unit particle at P will be indicated by its mass $\mathbf{1}$ ($= 1$ gr.) for didactic purposes.

The magnitude of the force between the mass I at P and the mass of the element Δx of which $Q:(x,0,)$ is some point, is

$$\Delta F \approx \frac{G \cdot I \cdot \rho \Delta x}{(PQ)^2} .$$

Its component in the x -direction is therefore

$$\begin{aligned} \Delta F_x &\approx - \frac{G I \rho \Delta x}{PQ^2} \cdot \cos (PQA) \\ &\approx - \frac{G I \rho \Delta x}{(\xi - x)^2 + r^2} \cdot \frac{(\xi - x)}{\sqrt{(\xi - x)^2 + r^2}} \\ &\approx - \frac{G I \rho (\xi - x) \Delta x}{[(\xi - x)^2 + r^2]^{\frac{3}{2}}} . \end{aligned}$$

Similarly, the component of ΔF in the r -direction is

$$\Delta F_r \approx - \frac{G I \rho \cdot r \cdot \Delta x}{[(\xi - x)^2 + r^2]^{\frac{3}{2}}} .$$

From these elementary considerations we pass to the limit by dividing $A'A$ into a large number of these x -subdivisions, and then letting this number increase indefinitely while at the same time requiring all the Δx 's to approach zero in length. We thus get, as the x -component, the resultant force of attraction F between P and the rod:

$$\begin{aligned}
 F_x &= - G I \rho \int_{-a}^a \frac{(\xi - x) dx}{[(\xi - x)^2 + r^2]^{\frac{3}{2}}} \\
 &= - G I \rho \left\{ \frac{1}{\sqrt{(\xi - a)^2 + r^2}} - \frac{1}{\sqrt{(\xi + a)^2 + r^2}} \right\}.
 \end{aligned}$$

Similarly, the r -component of the force of attraction F between P and the rod is

$$\begin{aligned}
 F_r &= - G I \rho r \int_{-a}^a \frac{dx}{[(\xi - x)^2 + r^2]^{\frac{3}{2}}} \\
 &= - \frac{G I \rho}{r} \left\{ \frac{\xi + a}{\sqrt{(\xi + a)^2 + r^2}} - \frac{\xi - a}{\sqrt{(\xi - a)^2 + r^2}} \right\}.
 \end{aligned}$$

The force of attraction F of a unit particle at P toward the rod is, then, indicated by the vector lying in the plane of the rod and the point P (from the cylindrical symmetry of the situation) and has a component parallel to the rod of

$$\begin{aligned}
 F_x &= G I \rho \left[\frac{1}{\sqrt{(\xi + a)^2 + r^2}} - \frac{1}{\sqrt{(\xi - a)^2 + r^2}} \right] \\
 &= \frac{G I M}{2a} \left[\frac{1}{\sqrt{(\xi + a)^2 + r^2}} - \frac{1}{\sqrt{(\xi - a)^2 + r^2}} \right],
 \end{aligned}$$

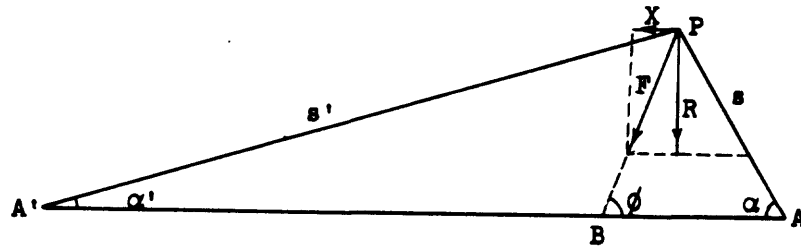
since the mass of the rod is $M = 2a\rho$.

The component of F in the orthogonal direction is

$$F_r = \frac{G I \rho}{r} \left[\frac{\xi - a}{\sqrt{(\xi - a)^2 + r^2}} - \frac{\xi + a}{\sqrt{(\xi + a)^2 + r^2}} \right]$$

$$= \frac{GIM}{2ar} \left[\frac{\xi - a}{\sqrt{(\xi - a)^2 + r^2}} - \frac{\xi + a}{\sqrt{(\xi + a)^2 + r^2}} \right].$$

A physical meaning can be given to these last two results so that the field of force can be studied. First the results will be separated from the coordinate system. Referring to the previous equations and to the figure below,



the component of the force of attraction F parallel to the rod $A'A$ may be written as

$$F_x = \frac{GIM}{2a} \left(\frac{1}{s'} - \frac{1}{s} \right).$$

having arbitrarily designated the orientation $A'A$ as positive in the indicated direction. Similarly, the component at right angles to the rod $A'A$ in a meridian plane may be written as

$$F_r = - \frac{GIM}{2a} \left[\frac{\cos \alpha}{s \sin \alpha} + \frac{\cos \alpha'}{s' \sin \alpha'} \right].$$

With the minus-sign, a positive direction in the meridian plane at right angles to the rod direction A'A has been chosen.

Let the angle between the force F and A'A be indicated by ϕ .

Then

$$\begin{aligned} \tan \phi &= \frac{R}{X} \\ &= - \frac{s' \cos \alpha \sin \alpha' + s \sin \alpha \cos \alpha'}{(s - s') \sin \alpha \sin \alpha'}. \end{aligned}$$

Since

$$s \sin \alpha = s' \sin \alpha' = H,$$

the length of the altitude of the triangle A'PA on A'A, one concludes that

$$\tan \phi = \frac{\cos \alpha + \cos \alpha'}{\sin \alpha - \sin \alpha'}.$$

The trigonometric manipulations follow, using the identity:

$$\begin{aligned} \tan (\phi + \alpha) &= \frac{\tan \phi + \tan \alpha}{1 - \tan \phi \tan \alpha} \\ &= \frac{\frac{\cos \alpha + \cos \alpha'}{\sin \alpha - \sin \alpha'} + \frac{\sin \alpha}{\cos \alpha}}{1 - \frac{\cos \alpha + \cos \alpha'}{\sin \alpha - \sin \alpha'} \cdot \frac{\sin \alpha}{\cos \alpha}} \\ &= \frac{\cos^2 \alpha + \cos \alpha \cos \alpha' + \sin^2 \alpha - \sin \alpha \sin \alpha'}{\sin \alpha \cos \alpha - \sin \alpha' \cos \alpha - \sin \alpha \cos \alpha - \sin \alpha \cos \alpha'} \\ &= \frac{1 + \cos (\alpha + \alpha')}{- \sin (\alpha + \alpha')} \\ &= \frac{1 - \cos [\pi - (\alpha + \alpha')]}{- \sin [\pi - (\alpha + \alpha')]} \\ &= \frac{1 - \cos \gamma}{- \sin \gamma} = - \tan \frac{\gamma}{2} \end{aligned}$$

$$= \tan \left(\pi - \frac{\gamma}{2} \right)$$

where $\gamma = \angle A'PA$.

This means that

$$\phi + \alpha + \frac{\gamma}{2} = \pi ;$$

and that, in fact, PB bisects $\angle A'PA$. The force of attraction F, therefore, between the unit particle at P and the rod A'A lies on the bisector at P of the angle subtending the rod.

How large is this force F? It can be shown that the magnitude of F is

$$\frac{GIM}{c^2},$$

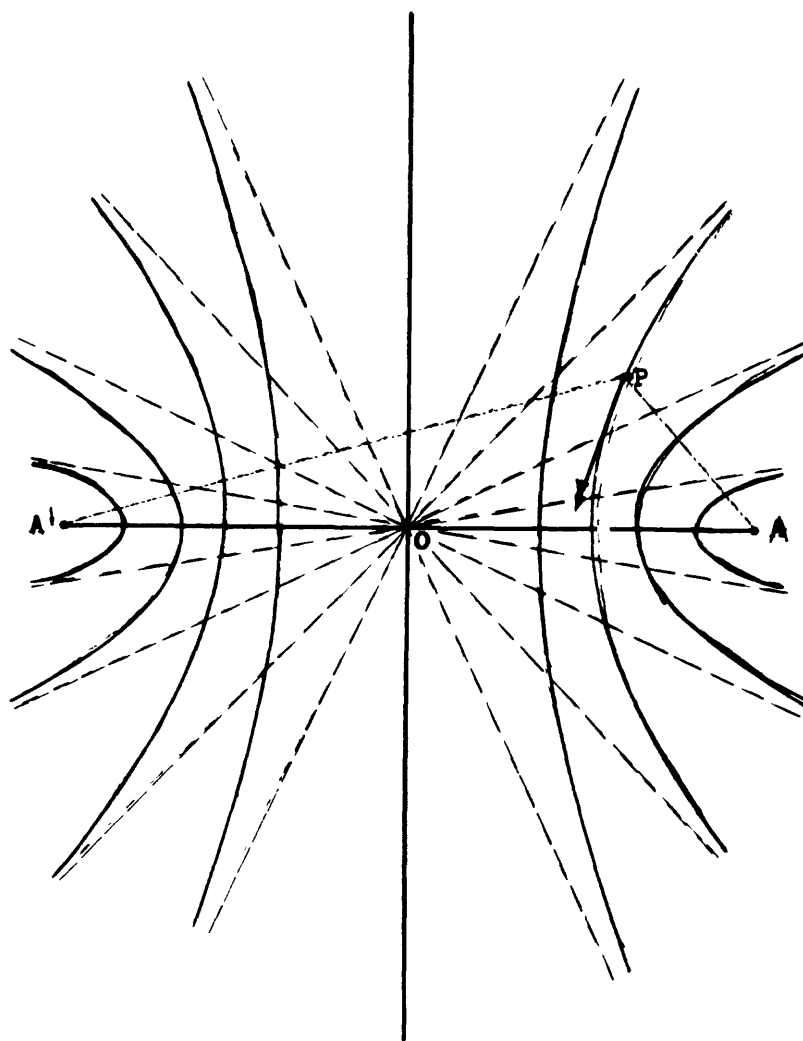
where

$$c^2 = \frac{s + s'}{2} \cdot b,$$

b being the length of the bisector PB from P to the rod.

From this information, the field of force of the rod can be constructed. At each point P of an arbitrary plane through the rod A'A draw the bisector of the angle A'PA. Specifying a direction at each point P of the plane in this manner, it can be shown that all these directions do in fact define a family of curves in the plane. First, it can be shown that the curve which is such that its tangent at any point

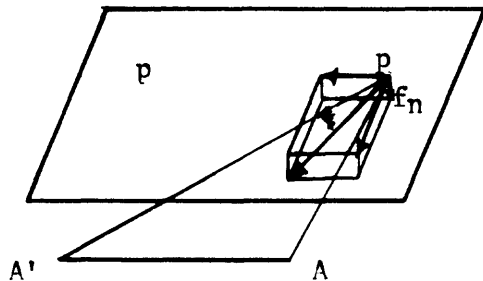
bisects the angle at that point which subtends a linear segment ($A'A$), is a hyperbola with the end points of the segment as its foci. It will follow then that the vector at any point indicating the attraction of a unit particle there to the rod $A'A$ will be tangent to the hyperbola through that point whose foci are A' and A . It will also follow that all these vectors will align themselves so that their envelopes form a family of hyperbolas whose foci are at A' and A .



A few of these hyperbolas (with their asymptotes sketched in lightly) are shown in the accompanying figure. Consider, then, the totality of these hyperbolas in this plane, and then consider the totality of hyperbolas of this sort in "all" the other plane sections through A'A. All these hyperbolas constitute the field of force of the linear rod. The hyperbolas are called the lines of force.

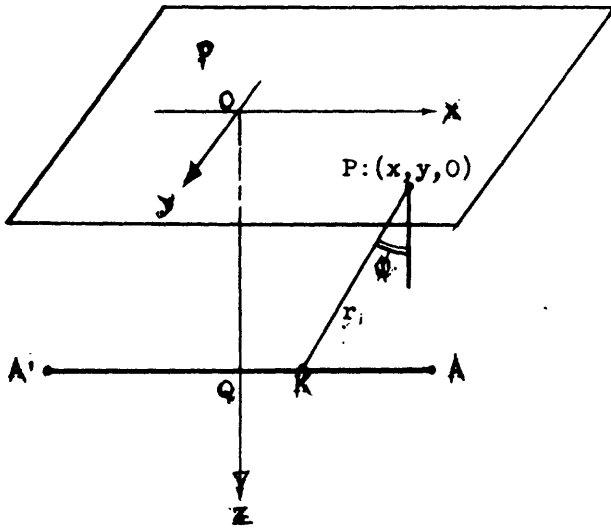
If it is desired to find the vector representing the force of attraction of a unit particle at any point of space toward the rod, one need only draw the tangent to the only hyperbola of this system of hyperbolas passing through that point. The magnitude of the vector will depend on the "density" of lines of force.

It is instructive to consider a problem of practical concern in gravimetric surveying. Suppose a plane P is parallel to the rod, A'A.



Suppose, further, that at an arbitrary point P in this plane P, it is desired to find the component F_n of the force of attraction F between a unit particle at P and the rod A'A, which is normal to p. To find F_n , there is a choice of mathematical approaches, one of which would be a direct calculation using the

results obtained previously. This approach looks rather forbidding; so another approach will be considered because of its relative simplicity and for the sake of introducing further tools and concepts.



Suppose that, from the midpoint Q of A'A, a perpendicular is dropped to the plane p and the foot of it is designated O, as the origin of a coordinate system. The line in p parallel to A'A is the x-axis, the y-axis is in p perpendicular thereto. The line OQ, oriented from O towards A'A will then be the z-axis. As before, the length of A'A is taken as $2a$; and $OQ = h$. Thus, the coordinates of the various points in the figure are

$$O: (0,0,0)$$

$$A': (-a,0,h)$$

$$A: (a,0,h)$$

$$Q: (0,0,h)$$

Let $P:(x,y,0)$ be a point of p where the unit particle is located. If the linear density of the rod is ρ , the element of mass contained in an element of length $\Delta\xi$ surrounding the point

$$K: (\xi, 0, h)$$

of A'A is

$$\rho \Delta \xi_i$$

and the force of attraction between P and the element at K is approximately

$$\Delta F_i = \frac{GI\rho\Delta\xi_i}{r_i^2} = \frac{GI\rho\Delta\xi_i}{(x - \xi_i)^2 + y^2 + h^2}$$

where $r_i = PK$, and I represents the unit mass at P. If the angle between PK and the direction OQ is indicated by ϕ_i , the components of the force ΔF_n normal to p is, then,

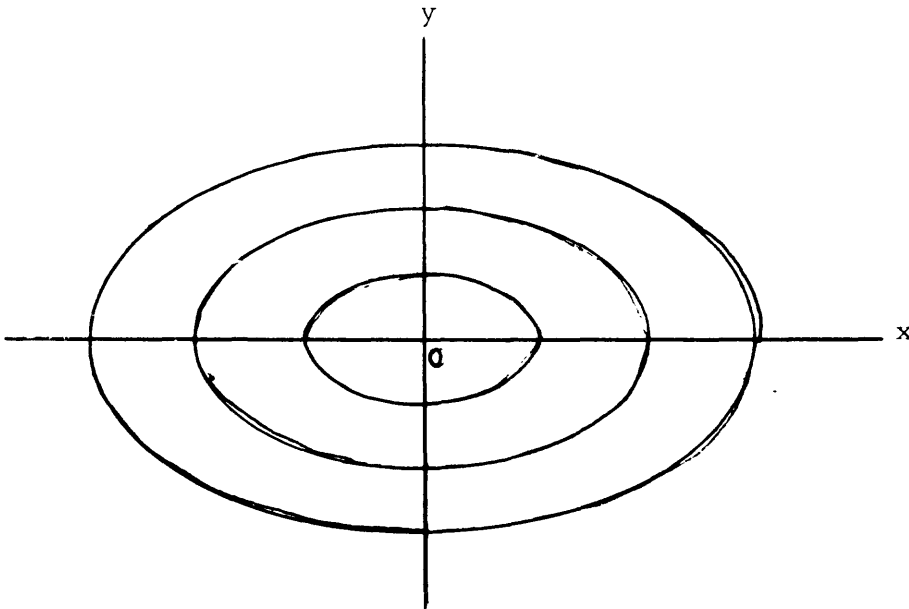
$$\begin{aligned}\Delta F_n &= \frac{GI\rho\Delta\xi_i}{(x - \xi_i)^2 + y^2 + h^2} \cos \phi_i \\ &= \frac{GI\rho\Delta\xi_i \cdot h}{[(x - \xi_i)^2 + y^2 + h^2]^{\frac{3}{2}}}\end{aligned}$$

It is now a simple step to get the component of force we are seeking by setting up and integrating the proper integral; namely,

$$\begin{aligned}F_n &= GI\rho h \int_{-a}^a \frac{d\xi}{[(x - \xi)^2 + y^2 + h^2]^{\frac{3}{2}}} \\ &= GI\rho h \left. \frac{\xi - x}{(\xi^2 + h^2)[\xi^2 - 2\xi x + (x^2 + y^2 + h^2)]^{\frac{1}{2}}} \right|_{-a}^a \\ &= GI\rho h \left\{ \frac{a - x}{(a^2 + h^2)[a^2 - 2ax + x^2 + y^2 + h^2]^{\frac{1}{2}}} \right. \\ &\quad \left. + \frac{a + x}{(a^2 + h^2)[a^2 + 2ax + x^2 + y^2 + h^2]^{\frac{1}{2}}} \right\}\end{aligned}$$

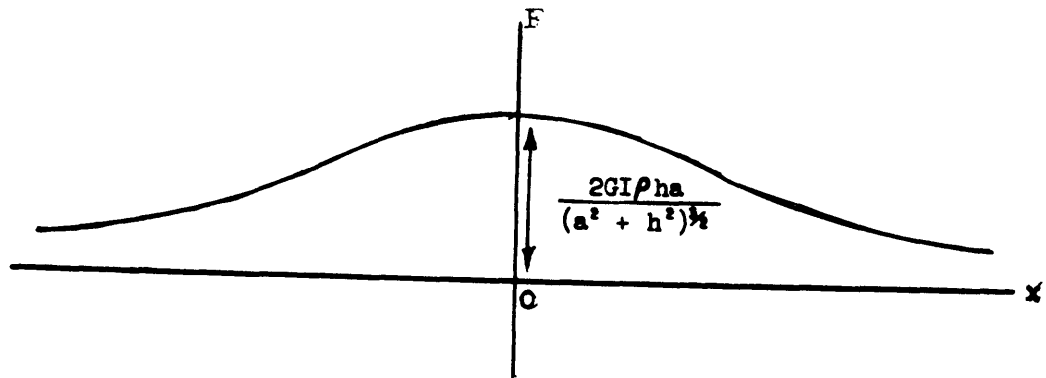
$$\begin{aligned}
&= \frac{GI\rho h}{a^2 + h^2} \left\{ \frac{a+x}{\sqrt{(a+x)^2 + y^2 + h^2}} + \frac{a-x}{\sqrt{(a-x)^2 + y^2 + h^2}} \right\} \\
&= \frac{GI\rho h}{OA^2} \left\{ \cos \angle PA'A + \cos \angle PAA' \right\}
\end{aligned}$$

These curves in the plane p assume an appearance of this sort:



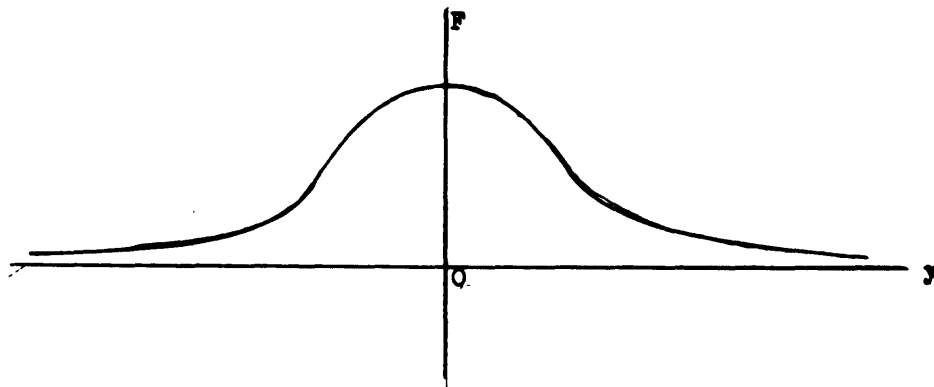
It is also instructive to plot the "vertical gravity" section immediately over the rod ($y = 0$); namely

$$F \Big|_{\substack{y=0 \\ z=0}} = \frac{GI\rho h}{a^2 + h^2} \left\{ \frac{a+x}{\sqrt{(a+x)^2 + h^2}} + \frac{a-x}{\sqrt{(a-x)^2 + h^2}} \right\}$$



The "vertical gravity" section along Oy, ($x = 0$), similarly, is:

$$F_y \Big|_{x=0} = \frac{2GI\rho ha}{(a^2 + h^2)} \left\{ \frac{1}{\sqrt{a^2 + y^2 + h^2}} \right\}$$



One final remark, which will be of some practical importance later, should be made concerning the attraction between a unit particle and a long rod.

Refer to the result at the bottom of page 20. If P is on the perpendicular bisector of the rod ($\mathcal{C} - 0$), the attracting force R , oriented positively toward the rod, is

$$F_r = \frac{2GI\rho a}{r\sqrt{a^2 + r^2}} .$$

If the length of the rod is allowed to increase indefinitely; i.e., if we let a increase without limit, we have

$$\lim_{a \rightarrow \infty} F_r = \frac{2GI\rho}{r} ;$$

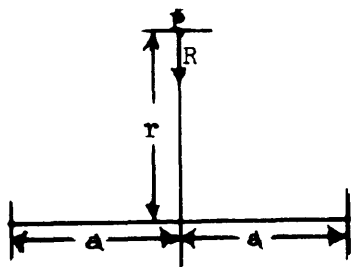
that is, the force of attraction F_r does not increase indefinitely. In fact, the force of attraction between an infinite rod and a unit mass at a distance r varies inversely with the distance r .

In practice, this result will be of importance in many problems because (for practical purposes) "infinite" extension of the mass in one direction can often be assumed. In addition, it is assumed that the mass is built up of rods of infinite length in the same direction. How "big" a dimension must be to be considered "infinite" is, of course, a matter of sensitivity of the measuring devices and the accuracy of the measurement desired or attained.

The Circular Disc--The result at the bottom of page 20 which expresses the force of gravitational attraction F_r between a unit mass I at a point P on the perpendicular bisector of a rod of length $2a$ and at a distance r is

$$F_r = \frac{2GI\rho a}{r\sqrt{a^2 + r^2}}$$

$$= \frac{GMI}{r\sqrt{a^2 + r^2}},$$



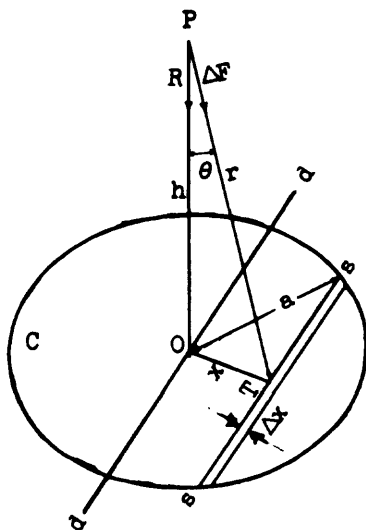
where ρ is the linear density of rod (assumed constant) and M is its mass. The force F_r is oriented positively toward the rod. From the symmetry of the situation, arising from the fact that P is

taken on the perpendicular bisector of the rod, it follows that F_r is the total force of attraction; that is, that there is no component at right angles to R .

Consider, now, a point P , at which there is a unit mass I which lies on the axis of a circular disc C . If this disc is of uniform laminar density, what is the force of gravitational attraction between I and C ? Since P is on the axis of C it follows immediately that the force will be along this axis directed toward C . Through O , the center of C , choose any diameter dd of C . At distances x and $x+\Delta x$ from O , draw two chords parallel to dd , the first being indicated by ss . These two chords substantially (to within infinitesimal corrections of high order) define a rod of length ss and width Δx , if Δx is small enough.

Now

$$\overline{ss} = 2\sqrt{a^2 - x^2},$$



in which a is the radius of C ,
and if we denote the surface
density of C by δ , then the mass,
 M , of this "rod" is, approximately,

$$\Delta M = \delta \cdot 2 \sqrt{a^2 - x^2} \cdot \Delta x .$$

Between I at P and this rod there
is an attractive force ΔF equal to

$$\Delta F = \frac{G \cdot \Delta M \cdot I}{r \sqrt{(a^2 - x^2) + r^2}} ,$$

where r is the distance PT , and T the midpoint of ss . This, of course,
comes from the second of the equations of page 31, with the symbols
replaced appropriately for our figure. This last form, in turn becomes

$$\begin{aligned} \Delta F &= \frac{2GI\delta \sqrt{a^2 - x^2} \Delta x}{\sqrt{x^2 + h^2} \sqrt{(a^2 - x^2) + (x^2 + h^2)}} \\ &= \frac{2GI\delta \sqrt{a^2 - x^2} \Delta x}{\sqrt{a^2 + h^2} \sqrt{x^2 + h^2}} , \end{aligned}$$

in which h is the distance from P to O .

The component of ΔF along PO is evidently

$$\Delta R = \Delta F \cos \theta$$

$$\begin{aligned} &= \frac{2GI\delta \sqrt{a^2 - x^2} \Delta x}{\sqrt{a^2 + h^2} \sqrt{x^2 + h^2}} \left(\frac{h}{\sqrt{x^2 + h^2}} \right) \\ &= \frac{2GI\delta h \sqrt{a^2 - x^2} \Delta x}{\sqrt{a^2 + h^2} (x^2 + h^2)} . \end{aligned}$$

Accordingly, the attraction of I for the disc C is, then,

$$\begin{aligned}
 F &= \int_{-a}^a \frac{2GI\delta h}{\sqrt{a^2 + h^2}} \cdot \frac{\sqrt{a^2 - x^2} dx}{x^2 + h^2} \\
 &= \frac{4GI\delta h}{\sqrt{a^2 + h^2}} \int_0^a \frac{\sqrt{a^2 - x^2} dx}{x^2 + h^2} \\
 &= \frac{4GI\delta h}{\sqrt{a^2 + h^2}} \left[\frac{\sqrt{a^2 + h^2}}{h} \tan^{-1} \frac{x \sqrt{a^2 + h^2}}{h \sqrt{a^2 - x^2}} - \sin^{-1} \frac{x}{a} \right]_0^a * \\
 &= \frac{4GI\delta h}{\sqrt{a^2 + h^2}} \frac{\sqrt{a^2 + h^2}}{h} \cdot \frac{\pi}{2} - \frac{\pi}{2} \\
 F &= 2GI\delta\pi \left[1 - \frac{h}{\sqrt{a^2 + h^2}} \right] .
 \end{aligned}$$

* This integration is performed by rewriting the integrand:

$$\frac{\sqrt{a^2 - x^2}}{x^2 + h^2} = \frac{1}{\sqrt{a^2 - x^2}} \left[\frac{a^2 + h^2}{x^2 + h^2} - 1 \right]$$

and using Formulas 229 and 127 of B. O. Peirce's "A Short Table of Integrals".

The last result, which has an important bearing on what shall be later referred to as the terrain correction, shows that the total force of attraction between a unit particle I at a point P in the axis of a disc and at a distance h from the disc, the radius of which is a, is directed along the axis toward the disc and in magnitude is equal to

$$F = 2GI\delta\pi \left[1 - \frac{h}{\sqrt{a^2 + h^2}} \right].$$

Recalling that δ is the surface density of the disc, then the mass of the disc is

$$M = \pi a^2 \delta$$

and the result may be rewritten as

$$F = \frac{2GIM}{a^2} \left[1 - \frac{h}{\sqrt{a^2 + h^2}} \right].$$

Returning now to the first form of the result, note that as the radius a of the disc grows larger and larger; that is, as $a \rightarrow \infty$, the force of attraction approaches a limiting value

$$\lim_{a \rightarrow \infty} F = 2GI\delta\pi,$$

a value independent of h . That is, the attraction of a particle to an infinitely extended thin plane sheet is independent of the distance of the particle (h) from that sheet.

In practical terms, this means that the gravitational field over the central area of a horizontally "very extended" thin bed consists of parallel lines, at right angles to the bed, so that the force of attraction is constant in magnitude and vertical at great distances from the bed. In fact, as we see, the ratio between the actual value of this force and this limiting (constant) force is

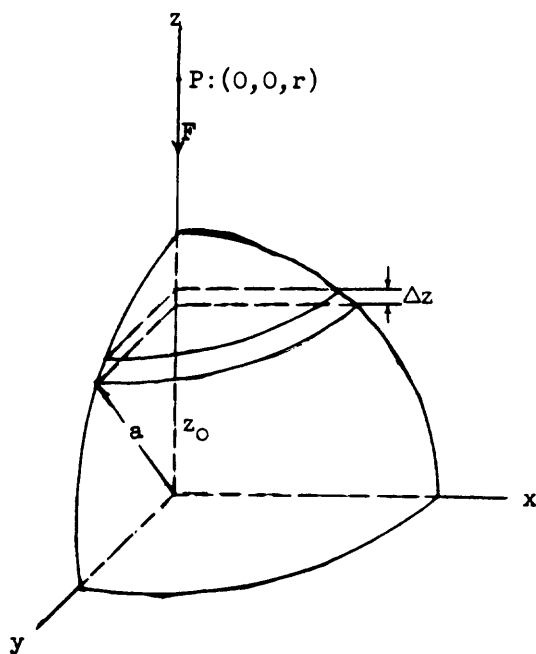
$$1 - \frac{h}{\sqrt{a^2 + h^2}} .$$

This result will form the basis of some numerical calculations for terrain corrections which will be discussed later.

Homogeneous sphere--

Let us now consider the

attraction between a unit particle and a homogeneous sphere. It is apparent, from considerations of symmetry, that the direction of the force lies along the line joining the particle to the center of the sphere. Let the radius of the sphere be a and choose the x-axis as the line which joins this center to the unit particle, as drawn.



If the sphere is sliced by the two parallel planes,

$$z = z_0$$

and

$$z = z_0 + \Delta z ,$$

when Δz is sufficiently small, we have a thin disc of mass

$$\Delta M = \pi(a^2 - z_0^2) \cdot \delta \cdot \Delta z ,$$

in which δ is the specific gravity of the material composing the sphere.

The attraction between the unit particle at P and this thin disc is, according to the result of page 34.

$$\begin{aligned} & \frac{2G \cdot \Delta M \cdot I}{a^2 - z_0^2} \left[1 - \frac{r - z_0}{\sqrt{(a^2 - z_0^2) + (r - z_0)^2}} \right] \\ &= \frac{2G \cdot I \cdot \delta \cdot \pi(a^2 - z_0^2) \Delta z}{(a^2 - z_0^2)} \left[1 - \frac{r - z_0}{\sqrt{a^2 + r^2 - 2rz_0}} \right], \end{aligned}$$

where r is the distance between the unit particle and the center of the sphere.

Thus, the required force is

$$\begin{aligned} F &= 2GI\pi\delta \int_{-a}^a \left[1 - \frac{r - z}{\sqrt{a^2 + r^2 - 2rz}} \right] dz \\ &= 2GI\pi\delta \left[z + \left(\frac{2r^2 - a^2 - rz}{3r^2} \right) \sqrt{a^2 + r^2 - 2rz} \right]_{-a}^a \\ &= 2GI\pi\delta \left[a + \frac{(2r^2 - a^2 - ar)(r - a)}{3r^2} + a - \frac{(2r^2 - a^2 + ar)(r + a)}{3r^2} \right] \\ &= \frac{2GI\pi\delta}{3r^2} [6ar^2 + 2a^3 - 6ar^2] \\ &= \frac{4GI\pi a^3 \delta}{3r^2} = \frac{GIM}{r^2}, \end{aligned}$$

since the mass of the sphere, M , is equal to

$$\frac{4\pi a^3 \delta}{3} .$$

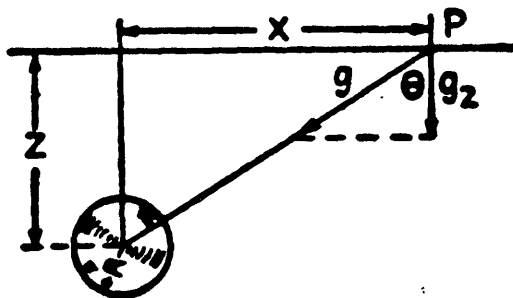
The result is well-known and of the utmost practical importance. It says that the gravitation field of a homogeneous sphere (outside the mass of that sphere) is the equivalent of the field of a particle of mass equal to that of the sphere and located at the center of the sphere.

Since a spherical shell is formed by removing from a complete sphere one that is concentric with it, it can be shown that the attraction between a homogeneous spherical shell and a unit particle outside the sphere is the same as though all the mass of the sphere were concentrated at its center.

It is apparent that the same result applies to a sphere, or a spherical shell, in which the density is a function of the radius alone.

The sphere is a useful model for approximating 3-dimensional geological structures whose horizontal dimensions are substantially less than the depth. Typical applications are for salt domes or igneous plugs and intrusives. The sphere attracts as if all its mass were concentrated

as a point at its center. Therefore, the gravity effect at



$$P(x,0,0,) \text{ is } g = \frac{Gm}{r^2} = \frac{4\pi R^3 G\rho}{3r^2}$$

The vertical component of gravity g_z is given by

$$\begin{aligned}
 g_z &= g \cos \theta \\
 &= \frac{Gm}{r^2} \cdot \frac{z}{r} = \frac{4\pi R^3 \rho G}{3} \cdot \frac{z}{(x^2 + z^2)^{3/2}} \\
 &= \frac{4\pi R^3 \rho G}{3z^2} \cdot \left[\frac{1}{(1 + \frac{x^2}{z^2})^{3/2}} \right] \\
 &= K \cdot f(x/z) \\
 &= \frac{8.52 \rho R^3}{z^2} \left[\frac{1}{(1 + \frac{x^2}{z^2})^{3/2}} \right]
 \end{aligned}$$

where R and z are in kilofeet and

g_z is in milligals

$$= \frac{27.94 \rho R^3}{z^2} \left[\frac{1}{(1 + \frac{x^2}{z^2})^{3/2}} \right]$$

where R and Z are in km

As an example, consider a sphere with radius $R = 3,000$ ft., depth to center $z = 5,000$ ft. and ρ (density contrast) = 0.25. Calculate a vertical gravity profile across the sphere.

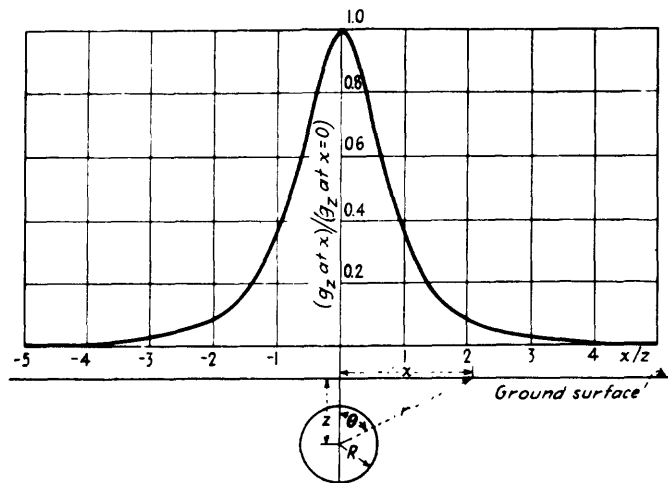
$$\begin{aligned}
 g_z &= \frac{8.52 \rho R^3}{z^2} \left[\frac{1}{(1 + \frac{x^2}{z^2})^{3/2}} \right] \\
 &= K \cdot f(x/z)
 \end{aligned}$$

Substituting,

$$K = \frac{(8.52) (0.25) (9)}{25} = 2.31$$

and

x/z	$f(x/z)$	g_z
0	1	2.31
1/2	0.71	1.62
1	0.35	0.81
2	0.09	0.21



A result of considerable significance that follows from the fact that the attraction of a homogeneous sphere, outside of the sphere, is the equivalent of that of a particle of equal mass located at the center of the sphere is that it would be impossible to differentiate between two such spheres (or spherical shells) of equal mass (of different densities and thus of unequal radii) by measuring their fields of attraction at points outside the spheres. This lack of uniqueness in the determination of the attracting bodies from their gravitational fields is one of the limitations of the gravity method.

Horizontal Cylinder--An infinite horizontal cylinder is a useful model when approximating 2-dimensional geological structures whose horizontal dimension is less than or not much greater than the depth to the center. A long anticline would be an example of a geological structure. The gravity effect from a horizontal line element of infinite length at $P(x, 0, 0)$ is (see page 30)

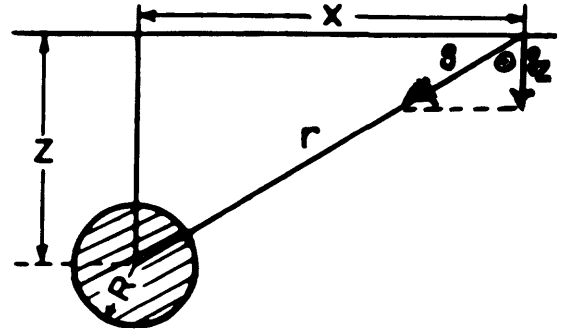
$$g = \frac{2 Gm}{r}$$

The vertical component of gravity g_z is given

by

$$g_z = g \cos \theta$$

$$g_z = g \cos \theta = \frac{2G m z}{r^2}$$



If the horizontal line element is replaced by a cylinder having mass per unit length of $\pi R^2 \rho$,

$$\begin{aligned} g_z &= 2\pi G \rho R^2 \frac{z}{r^2} = 2\pi G \rho R^2 \frac{z}{x^2 + z^2} \\ &= \frac{2\pi G \rho R^2}{z} \left[\frac{1}{\frac{x^2 + z^2}{z^2}} \right] \\ &= \frac{2\pi G \rho R^2}{z} \left[\frac{1}{1 + \frac{x^2}{z^2}} \right] = K \cdot f(x/z) \\ &= \frac{12.77 \rho R^2}{z} \cdot f(x/z) \quad \text{where } R \text{ and } z \text{ are in kilofeet and } g_z \text{ is in milligals.} \\ &= \frac{41.93 \rho R^2}{z} \cdot f(x/z) \quad \text{where } R \text{ and } Z \text{ are in km} \end{aligned}$$

Thus, a homogeneous infinite horizontal cylinder attracts as if all its mass were located at its axis. The depth z is the depth of an infinite line mass which has the same mass as the cylinder and produces the same gravity anomaly.

As an example, calculate the vertical gravity profile at right angles across an infinite horizontal cylinder with radius $R = 3,000$ feet,

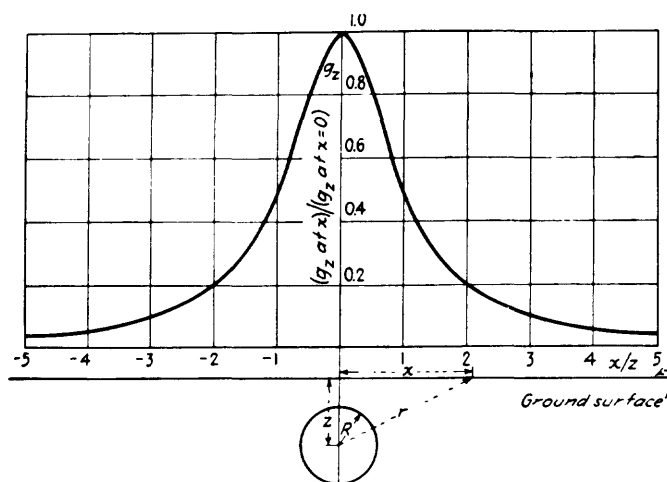
depth to the center $z = 5,000$ feet, and density contrast $\rho = 0.25$.

Substituting in $g_z = \frac{12.77 \rho R^2}{z} \cdot \left[\frac{1}{1 + \frac{x^2}{z^2}} \right]$

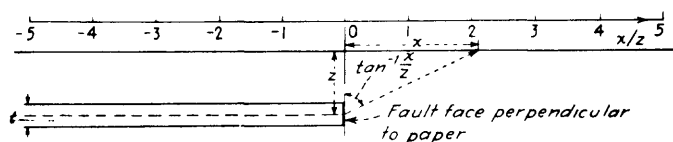
$$K = \frac{(12.77) (0.25) (9)}{5} = 5.72$$

and

x/z	$F(x/y)$	g_z
0	1	5.72
1/2	0.80	4.58
1	0.50	2.86
2	0.20	1.14
3	0.10	0.57



The Vertical Fault--The vertical fault can be approximated by the edge of a semi-infinite horizontal layer of finite thickness--a 1-dimensional model. The gravity effect of this body can be calculated on the assumption that the material is condensed into a thin sheet at the central plane



of the body. The vertical gravity effect is given by

$$g_z = 2G\rho t \left(\frac{\pi}{2} + \tan^{-1} \frac{x}{z} \right)$$

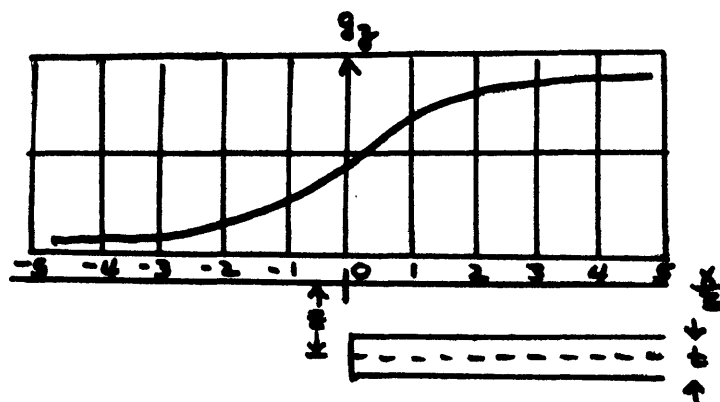
or

$$g_z = 2G\rho t \left[\frac{1}{2} + \frac{1}{\pi} \tan^{-1} \frac{x}{z} \right]$$

$$= K \cdot f(x/z) = 12.77 \rho t f(x/z) \text{ where } t \text{ is in kilofeet}$$

$$= 41.93 \rho t f(x/z) \text{ where } t \text{ is in km}$$

In both formulas g_z is in milligals. For a unit density contrast, a fault throw t of 2390 cm (or 78 feet) is needed to produce a gravity effect of 1 milligal. Thus, the thickness of faulted material of density contrast ρ required to cause a gravity effect of 1 mgal is about $80/\rho$ feet or $24/\rho$ metres.

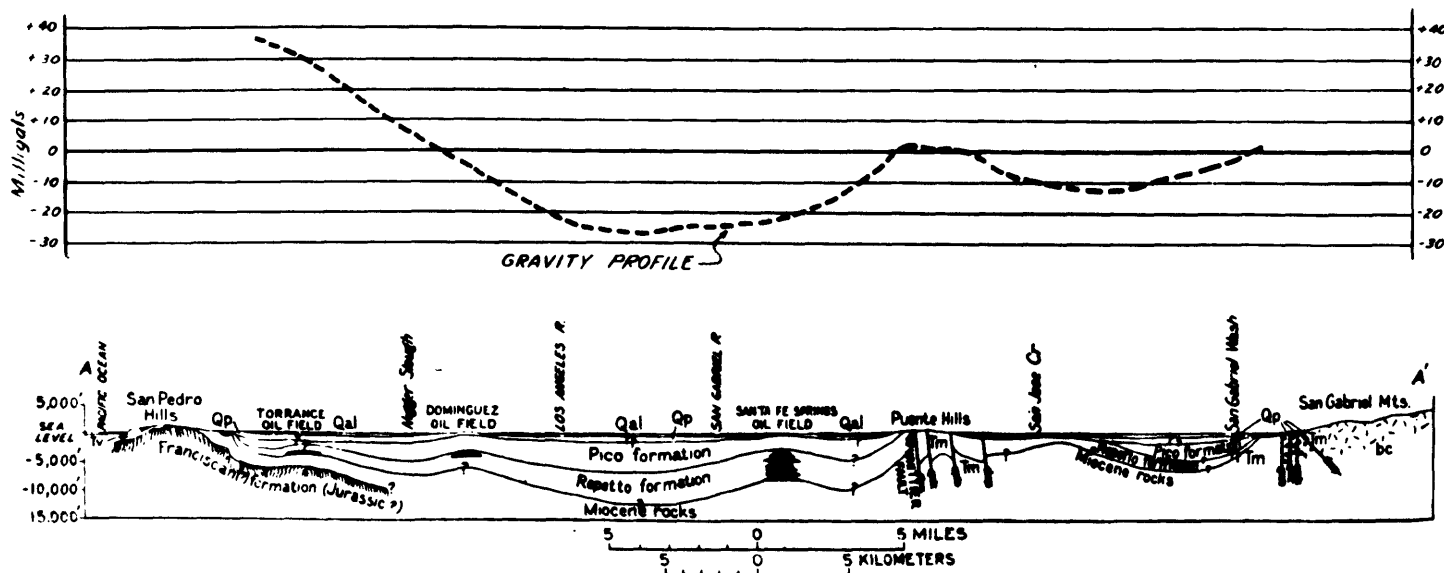


$\frac{x}{z}$	$F\left(\frac{x}{z}\right)$
0	$\pi/2$
$-\infty$	0
$+\infty$	π

This expression applies for a sheet whose horizontal extent is infinite compared with either the depth or thickness. From the accompanying gravity profile for the fault, it is evident that it takes a distance of about 6 times the depth (from $x = -3$ to $x = +3$) to reach about 80% (from 0.1 to 0.9) of the theoretical total magnitude for an infinite width sheet. Thus, it would require $\frac{78}{0.80} = 97$ feet of unit density contrast material to have a gravity effect of one milligal. Thus, for a given gravity effect and density contrast, the required thickness, in feet, is

$$t \approx (100/\rho) g_z \text{ max}$$

where t is in feet, ρ is the density contrast, and $g_z \text{ max}$ is the maximum gravity relief in milligals. An example of applying this general rule is shown in the attached figure of the gravity profile in the Los Angeles, CA Basin. From the gravity profile across the basin, the gravity relief

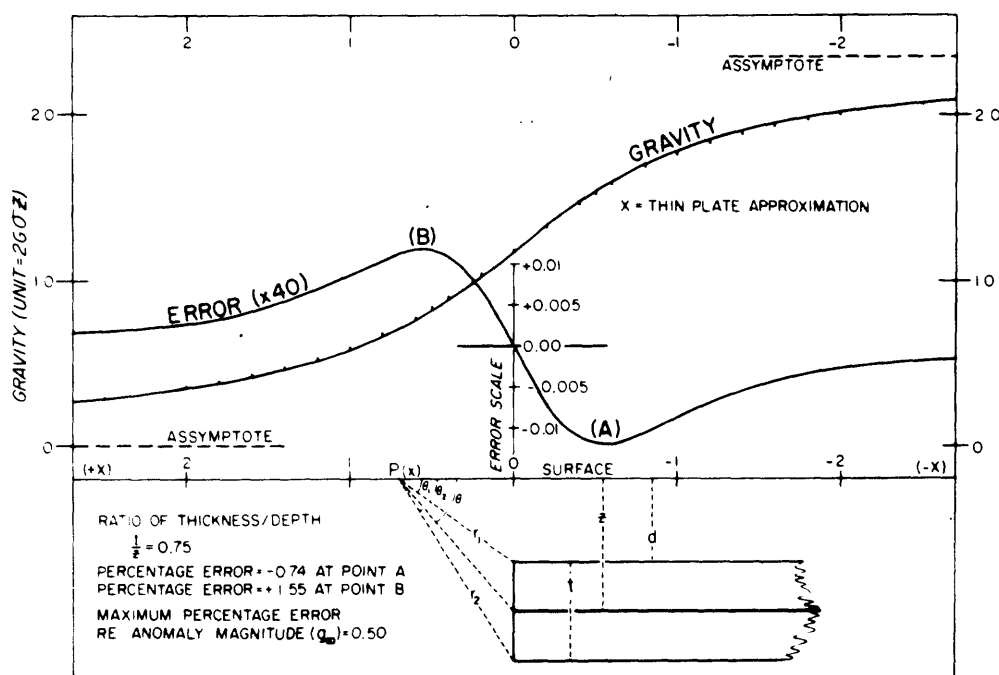


is seen to be approximately 60 mgal. The density contrast between the relatively recent Pliocene and Miocene sedimentary rocks and the Franciscan metamorphic basement rocks is not known precisely, but can be estimated to be between $(2.7 - 2.2) = 0.4$ and $(2.7 - 2.4) = 0.3$. Using a value of 0.35, we have a thickness of $\frac{100}{0.35}$ or 300 feet per miligal of gravity relief. Thus, the approximate thickness of the sediments in the basin causing the 60 mgal anomaly would be $(60) (300) = 18,000 \text{ ft.}$

ACCURACY OF SUBSURFACE MODEL APPROXIMATIONS

Calculation of the gravity effect for simple geometrical shapes is useful in practice because of the relative simplicity and reasonable accuracy. Commonly used approximations include: (1) equivalent sphere approximation for an infinitely long horizontal cylinder; (2) circular plate approximation for horizontal slabs of finite width; (3) vertical line element and thin horizontal plate approximations for vertical cylinders of variable radii and heights (domes, salt domes, igneous plugs); and (4) thin plate approximations for vertical dikes and horizontal faults blocks.

Fault Errors in some of the approximate calculations are remarkably small (Hammer, 1974).^{*} For example, the maximum error in the thin-plate approximation for an horizontal fault plate is less than 1% for a thickness/depth ratio ranging up to 0.75, a very substantial fault throw (see figure below).



^{*}Hammer, S., 1974, Approximations in Gravity Interpretation Calculations, Geophysics, v. 39, no. 2, pp. 205-222.

For the semi-infinite fault block of finite thickness (throw), the gravity effect is given by the general relation:

$$g_z = 2G\rho \left[\theta_2(t+d) - \theta_1 d - x \ln \frac{r_2}{r_1} \right]$$

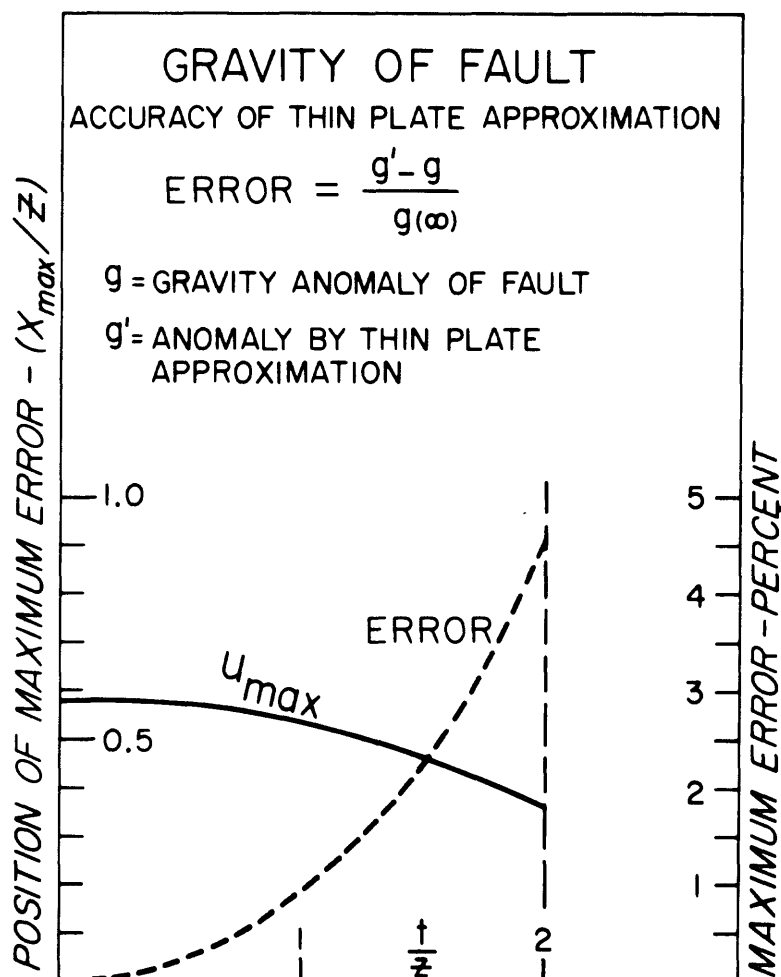
Compressing the mass of the fault block vertically onto its central plane given the thin-plate approximation:

$$g_z = 2Gt\theta = 2G\rho t \left[\frac{\pi}{2} + \arctan \frac{x}{z} \right]$$

The error in the approximate gravity value is

$$E(x) = g'(x) - g(x)$$

The error is zero directly above the fault and has equal maximum and minimum values on opposite flanks. The maximum error calculated relative



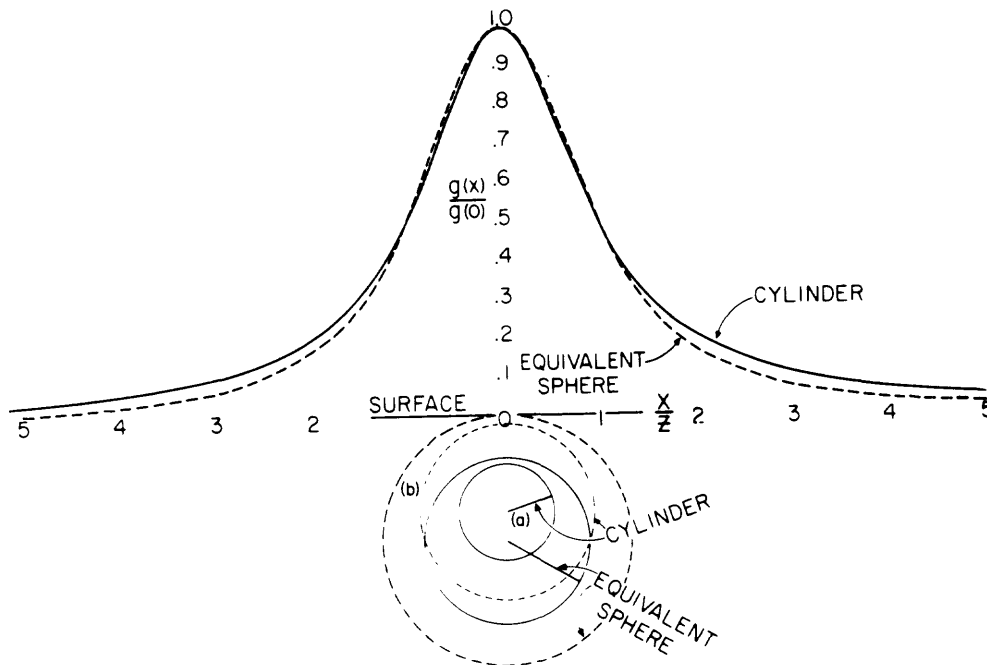
to the magnitude of the anomaly (at $x = \infty$) is less than 1/2%

A graph showing a summary plot of errors for a thin-plate approximation for a vertical 2-dimensional fault block is shown on the left. The error is plotted relative to plate thickness (t/z). It is apparent that the accuracy of the thin plate approximation is satisfactory for all but the most extreme cases.

For an error not exceeding 2%, t/z may be as large as 1.5, for which the fault throw is six times the depth to its top.

Equivalent Sphere Approximation--It is useful sometimes to assume that the observed anticlinal gravity anomaly is caused by an infinitely long horizontal cylinder and to calculate the interpreted structure in terms of an equivalent sphere. The gravitational attraction for the infinite horizontal cylinder is given by $g_z = 2GM \left[\frac{z}{x^2 + z^2} \right]$. When $x = 0$, $g(0) = \frac{2GM}{z}$ and the radius of the cylinder, R_c , can be defined as

$$R_c = \left[g(0)Z/2\pi G\rho \right]^{1/2}$$



The depth to the axis of the cylinder, z_c , is given by the "half-width" of the anomaly: $z_c = X^*$. The equivalent sphere defined to fit the gravity profile of the horizontal cylinder at $x = 0$ and $x = x^*$ has the following parameters.

$$\text{Depth: } Z_s = 1.305x^* = 1.305Z_c$$

$$\text{Radius: } R_s = \left[3g(o) \cdot Z_s^2 / 4\pi G\rho \right]^{1/3}$$

The calculated gravity profile for the equivalent sphere is obtained from

$$g'(x) = \frac{4 G\rho R_s^3}{3Z_s^2} \left[\frac{1}{1 + \frac{x^2}{Z_s^2}} \right]^{3/2}$$

Equating $g'(o)$ and $g(o)$, we obtain

$$R_s = 1.367 \left[\frac{\rho_c}{\rho_s} R_c^2 Z_c \right]^{1/3}$$

Comparison of the gravity profiles (see figure) shows that the approximation is very good. The difference is negligible except on the flanks where the effect of the sphere falls off more rapidly. Although the radius of the equivalent sphere is considerably larger than that of the cylinder, the depth to the top is reasonably close to that of the original cylinder. The error in the estimated depth depends on R_c which depends on the density contrast ρ . The radii in the figure were drawn assuming $\rho_s = \rho_c$ and for two cases: (a) $R_c = Z_c/2$ for which $R_s = 1.722 R_c$ (the depth error is -11.3%) and (b) $R_s = Z_s = 1.305Z_c$ for which the top of the interpreted sphere is at the surface. The depth error of the latter limiting case is 100%.

Vertical Cylinder and Approximation by Axial Line Element--An important class of geologic structures (e.g., igneous plugs, salt domes) can be

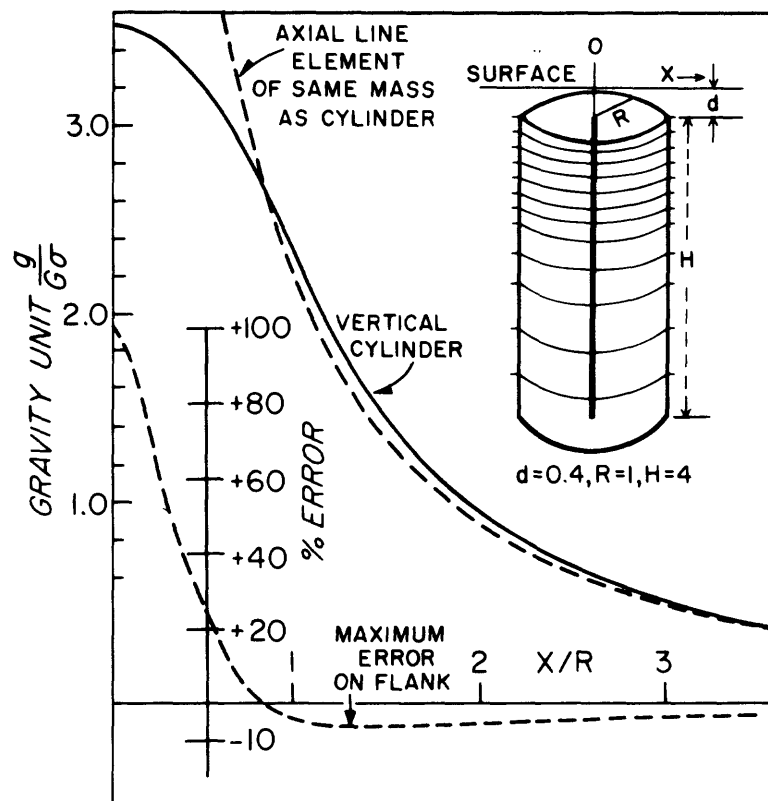
approximated by vertical right cylinders. Unfortunately, calculating the gravity effect of a vertical cylinder is easy only on the axis. At all other points, the calculation involves elliptical integrals or a series expansion of Legendre polynomials.

One approximation is to compress the mass of the vertical cylinder into an infinitesimal vertical line element along the axis. The vertical line approximation has a gravity effect which is given by

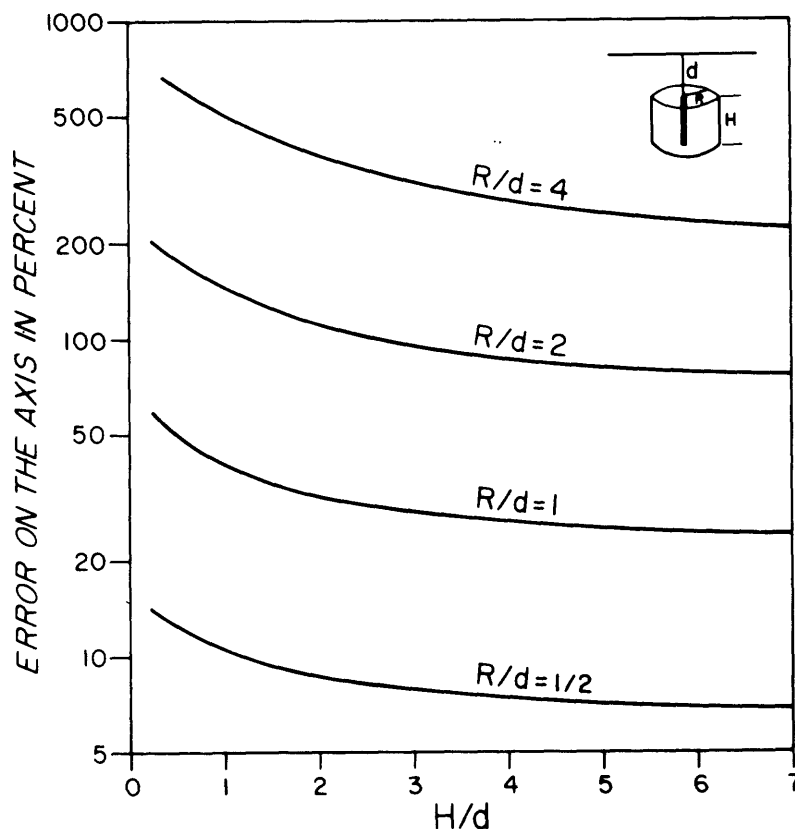
$$g_z = \pi G \rho R^2 \left[\frac{1}{S_1} - \frac{1}{S_2} \right]$$

where $S_1 = (x^2 + d^2)^{1/2}$ and $S_2 = (x^2 + (d+H)^2)^{1/2}$.

A comparison of the gravity profiles of the vertical cylinder and the vertical line element is shown in the top portion of the accompanying figure together with the error (gravity effect for line element minus gravity effect for cylinder). The range of maximum (axial) error is shown

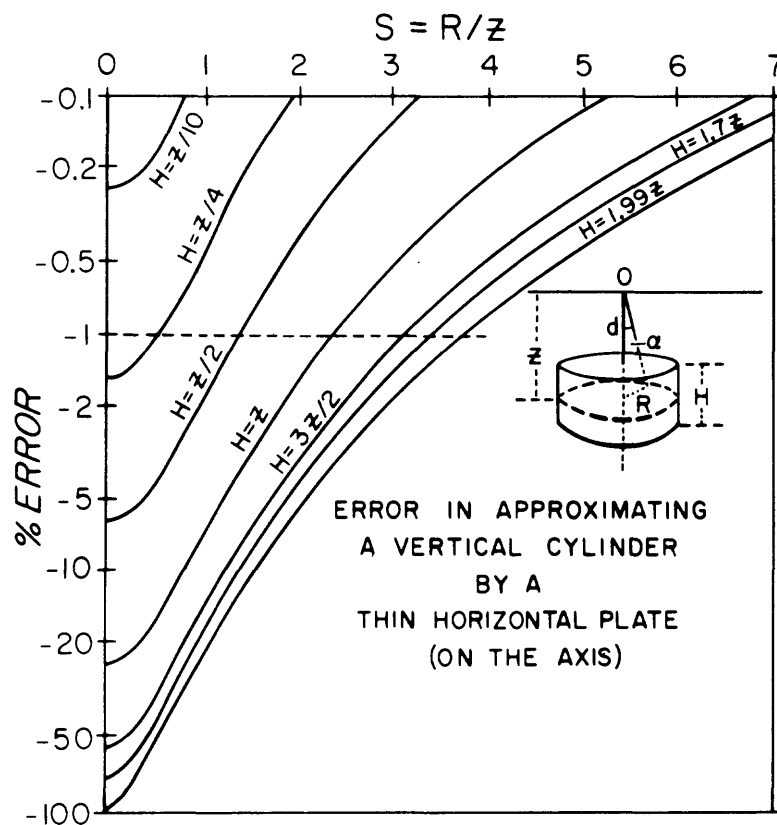


in the next figure. The curves are plotted in dimensionless unit H/d with dimensionless unit R/d as the variable parameter. It is clear from these curves that the axial line element is a poor approximation for a vertical cylinder of finite radius. A more useful approximation is a stack of thin horizontal discs.



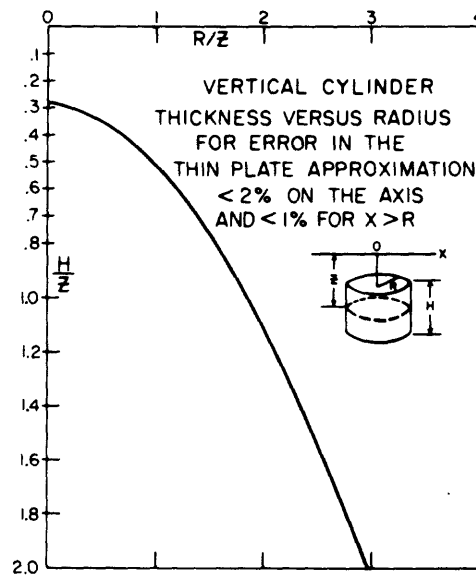
Vertical Cylinder Approximated by a Thin Horizontal Disc--Rapid

gravity profiles for a vertical cylinder can be obtained by using a thin horizontal disc of the same mass located at the central depth of the cylinder. Axial errors, expressed as a percentage of the central anomaly magnitude for the cylinder, are shown in the next figure. The abscissa R/Z

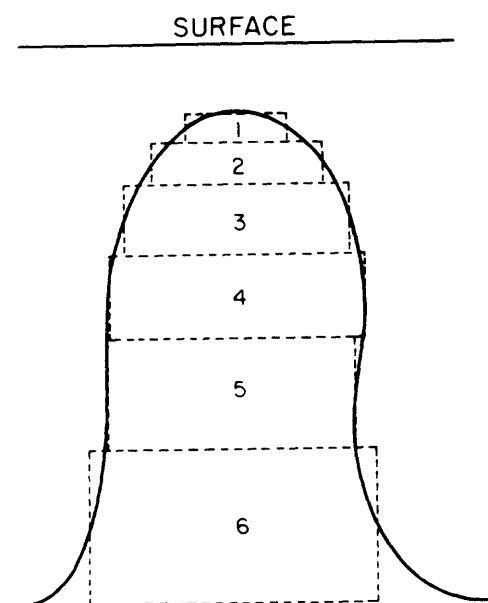


is the radius of the cylinder in units of depth, Z , to the center of the cylinder. The variable, H/Z , for the curves is the height of the cylinder also expressed in units of the depth. For any adopted tolerable maximum error, a horizontal line may be drawn to define the upper limits of the radius and height of the cylinder for which the stated precision can be achieved. The dashed line in the above figure corresponds to an allowable error of 1%.

An example of the practical application of this information can be described. The resultant curve of thickness (H/Z) versus radius (R/Z) for a maximum error of 2% on the axis (smaller on the flanks) is shown in the figure. This curve defines the minimum radius for a given height (or conversely a maximum height for a given radius) to satisfy the adopted precision criterion.



This information can be used to determine the layout of the minimum number



of slices required to approximate a salt dome, limiting the error of the thin plate approximation to 2%. The thickness of each disc is the maximum, corresponding to its radius, for which the largest incurred error is less than 2%. The number of discs is minimized to avoid unnecessary calculation.

FACTORS AFFECTING THE CHARACTER OF GRAVITY ANOMALIES

In calculating the gravity anomaly of a given structure, five principal variables are important. These are: volume, density contrast, depth, shape, and isolation. The magnitude of the gravity anomaly caused by a structure depends directly on its volume times its density contrast. The size of the anomaly and its sharpness decrease as a function of the depth. These relations hold, however, only as long as the structure has a concentrated shape. If the shape is diffuse, the observed anomaly will be reduced in magnitude and sharpness. If the structure is not sufficiently well isolated from other structures, similar or not, its own anomaly will not be resolved from that of the other structures.

The following table summarizes the formulae to determine the maximum gravitational attraction for the three anomaly classes: (1) 1-dimensional (slab); (2) 2-dimensional (horizontal cylinder); and (3) 3-dimensional (sphere).

In each formula, R , Z and t are expressed in units of kilofeet or km, g_z is in milligals and ρ , the density contrast, is in CGS units (see Appendix E for a conversion table to change R , Z and t to other units). The maximum value of gravitational attraction is given by g_z max.

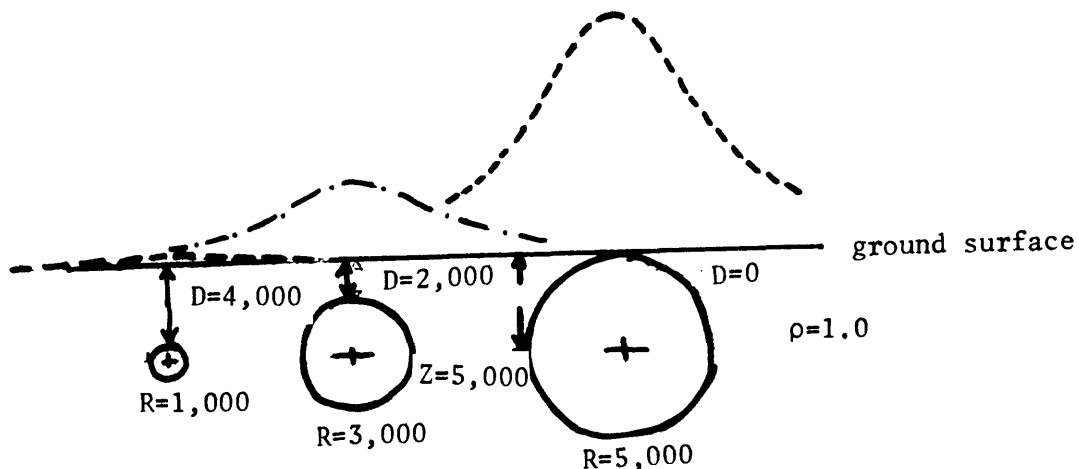
ANOMALY CLASS		FORMULA FOR MAXIMUM GRAVITY (g_z)		
		Shape Constant	Depth	Density Contrast
I.	Semi-infinite horizontal slab (fault) (one-dimensional)	12.77 (41.93)*		ρ
				t
	$g_z = 2G \rho t \left[\frac{\pi}{2} + \arctan \frac{x}{z} \right]$ $g_z = 12.77 \rho t \left[\frac{\pi}{2} + \arctan \frac{x}{z} \right]$			
	g_z max occurs as $x/z \rightarrow \infty$			
II.	Infinite horizontal cylinder (anticline) (two-dimensional)	12.77 (41.93)*	$1/z$	ρ
				R^2
	$g_z = 2GM \left[\frac{z}{x^2 + z^2} \right]$ $g_z = \frac{12.77 \rho R^2}{z} \left[\frac{1}{1 + \frac{x^2}{z^2}} \right]$			
	g_z max occurs at $x = 0$			
III.	Sphere (salt dome) (three dimensional, concentrated)	8.52 (27.94)*	$1/z^2$	ρ
				R^3
	$g_z = GM \left[\frac{z}{(x^2 + z^2)^{3/2}} \right]$ $g_z = \frac{8.52 \rho R^3}{z^2} \left[\frac{1}{1 + \frac{x^2}{z^2}} \right]^{3/2}$			
	g_z max occurs when $x = 0$			

Note: R, Z and t are in kilofeet, g_z in milligals, ρ is the density contrast (CGS Units), M is mass of the body.

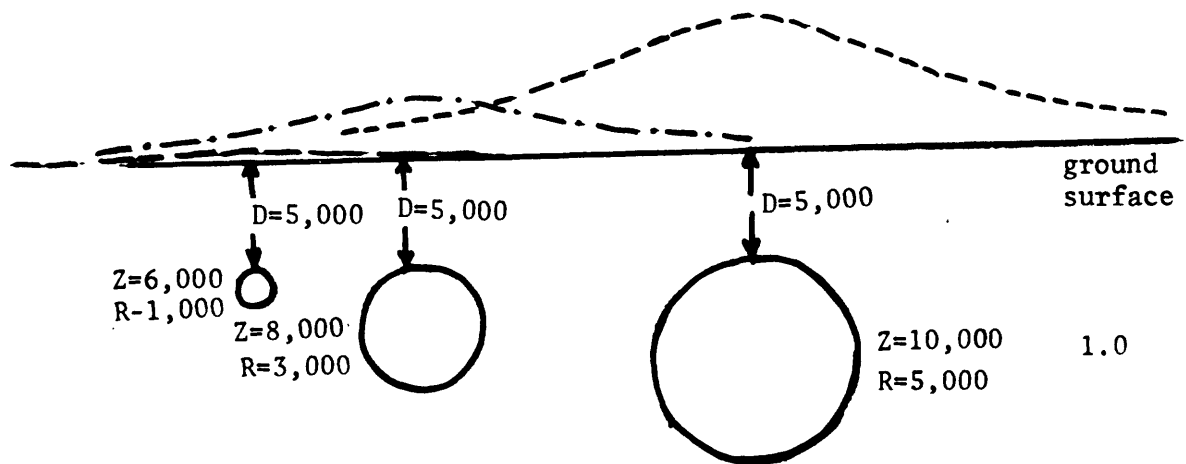
* Use this constant when R, Z, and t are in km.

Effect of Size of the Anomalous Mass on the Gravity Anomaly--

The most important variable in gravity anomalies is the size or amplitude of the anomaly. The volume of a structure is directly proportional to the size of the anomaly and can be computed if the depth and density contrast are known. From the preceding table, one can see that the size of a gravity anomaly due to a **concentrated 3-dimensional structure is inversely** proportional to the square of its depth. However, the gravity anomaly decreases linearly with depth for a 2-dimensional structure (such as an anticlinal ridge or a fold) and does not decrease with depth at all but remains constant for one-dimensional structures (slab, fault). The effect of size parameter changes are shown below for a buried infinite horizontal cylinder whose centers of mass are buried at the same depth.



Varying the size of the anomalous mass while holding the depth to the center of the mass constant causes the amplitude of the anomaly to vary, but the anomaly breadth remains constant. The next figure shows the



effect of size of simple anomalous masses whose "tops" are buried at the same depth. The conclusion is that--

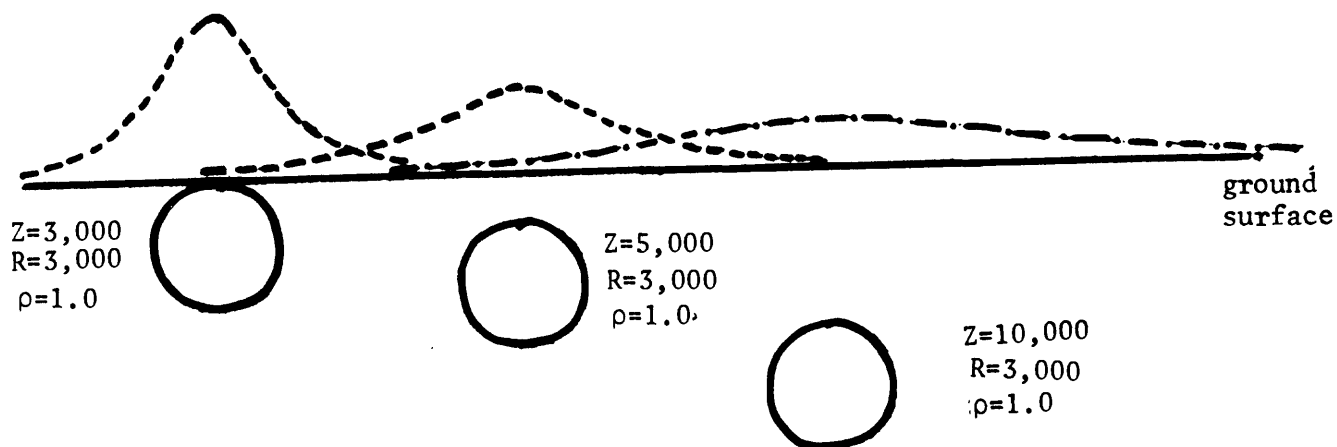
Varying the size while holding the depth to the "top" of the mass constant causes both the amplitude and breadth of the anomaly to vary.

These two results lead to the following conclusion:

As long as an anomalous mass is simple and it is buried at the same effective depth and deep enough so that its mass may be considered to be concentrated at a point, along a line, or a median plane, its gravity anomaly will change amplitude but not breadth as its size is varied.

Effect of Depth of the Anomalous Mass on the Gravity Anomaly--

If all the variables (shape, size, and density contrast) are held constant except depth to the center of a buried infinite horizontal cylinder, the effect of depth on the gravity anomaly can be assessed. The figure which follows shows that the breadth and amplitude of the anomalies vary as the



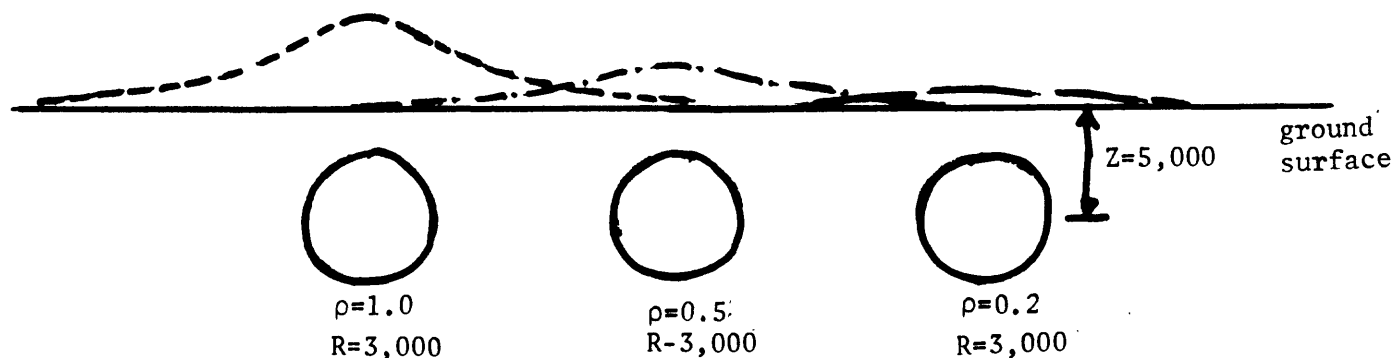
depth varies. The following conclusions can be made:

If all other factors are held constant, increasing the depth to the center of the mass of an anomalous body increases the breadth of the gravity anomaly and decreases the amplitude.

The breadth of a gravity anomaly is primarily a function of the shape and depth of the body.

Effect of Density Contrast of the Anomalous Mass on the Gravity

Anomaly-- If each of the anomalous masses have the same shape, size and depth to the center of mass, but the density contrast is allowed to vary, the effect of density contrast can be assessed.

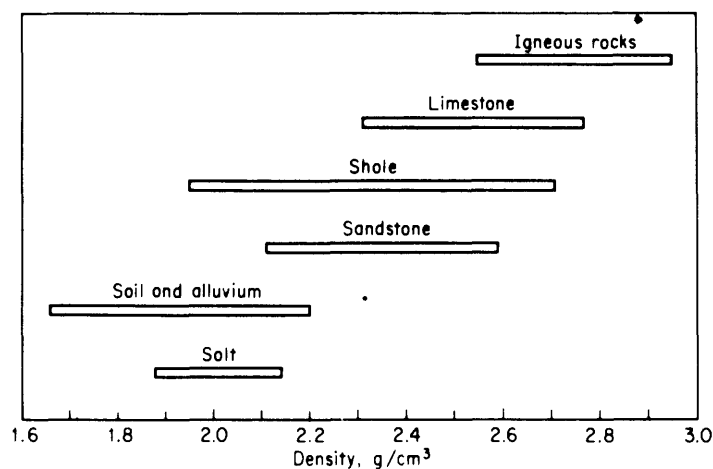


The preceding figure shows that the amplitude of the gravitation attraction varies as the density contrast varies, but the breadth of the anomaly remains constant. The conclusion which follows is:

If all other factors are held constant, increasing the density contrast increases the amplitude of the gravity anomaly, but does not influence its breadth.

The sign of the density contrast associated with an anomalous mass primarily determines the maximum or minimum nature of a gravity anomaly. An anomaly with maximum tendencies indicates a positive density contrast, whereas an anomaly with minimum tendencies indicates a negative density contrast.

A number of factors influence rock density. In the case of sedimentary rocks, the mineral composition and the age and depth of burial are the most important parameters. The general order of increasing density is: (1) soils and alluvium, (2) sandstones and conglomerates, (3) shales and clays, and (4) calcareous rocks (limestones and dolomites) (see



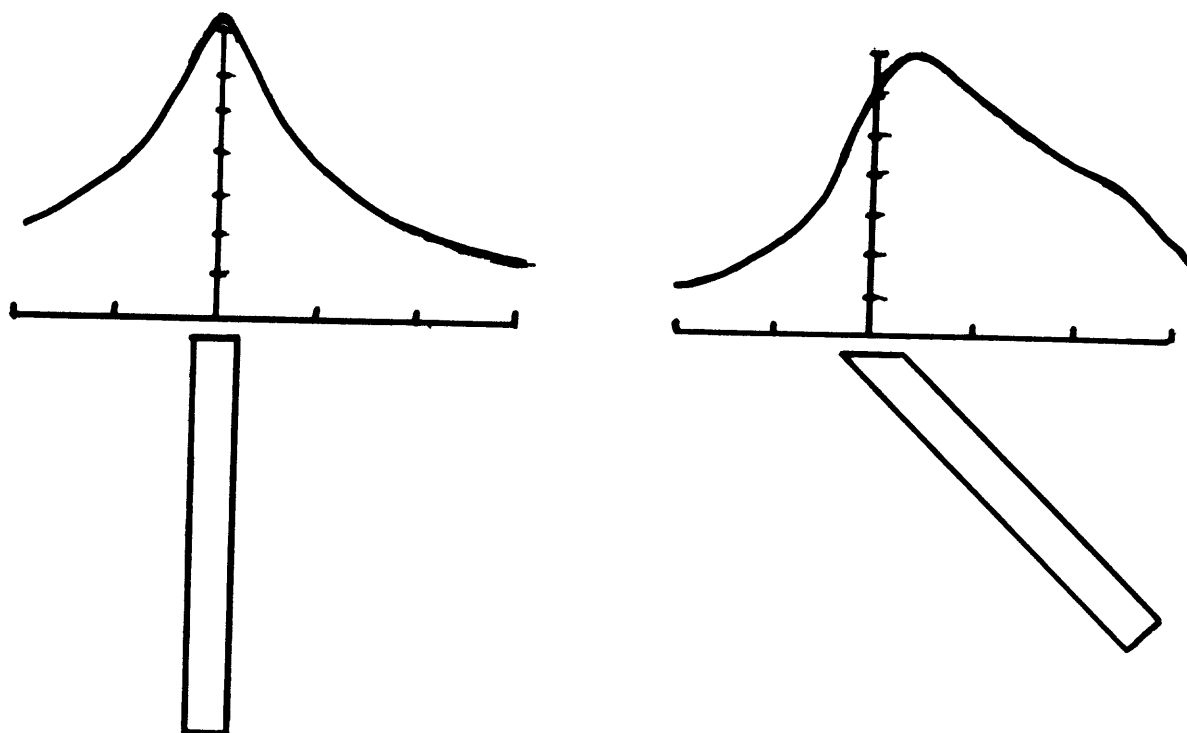
80% fiducial limits of bulk densities of various kinds of rocks

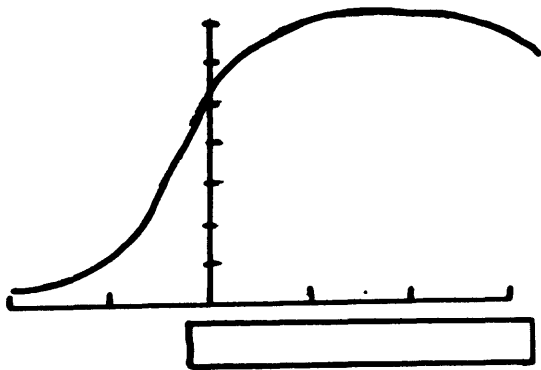
accompanying figure). Exceptions to this ordering do occur as a consequence of unusual porosities, the depth of the water table, and the age and depth of burial. Sediments buried for long periods of time tend to consolidate and to lithify, causing an increase in density. In the case of igneous rocks, the density usually increases

as the silica content decreases. Thus, gabbro is usually more dense than granite, diabase more dense than syenite, and basalt more dense than rhyolite. Metamorphic rocks are the least susceptible to rules of behavior, but, generally speaking, their density increases with degree of metamorphism.

Effect of Attitude of the Anomalous Mass on the Gravity Anomaly--

The attitude is a function of the depth or variation of the depth to different portions of an anomalous mass. The anomalous mass is a buried semi-infinite slab of finite depth extent (a dike). If all the anomalous masses have approximately the same mass and the ratio of the depth to the top of the anomalous mass to the thickness of the slab is 0.5, the effect of attitude of the mass on the gravity anomaly can be assessed. The accompanying illustrations show the effect.





These figures show that the same approximate mass buried with the same effective density contrast and a constant depth to the upper edge can produce very different gravity anomalies as the attitude of the anomalous mass is varied.

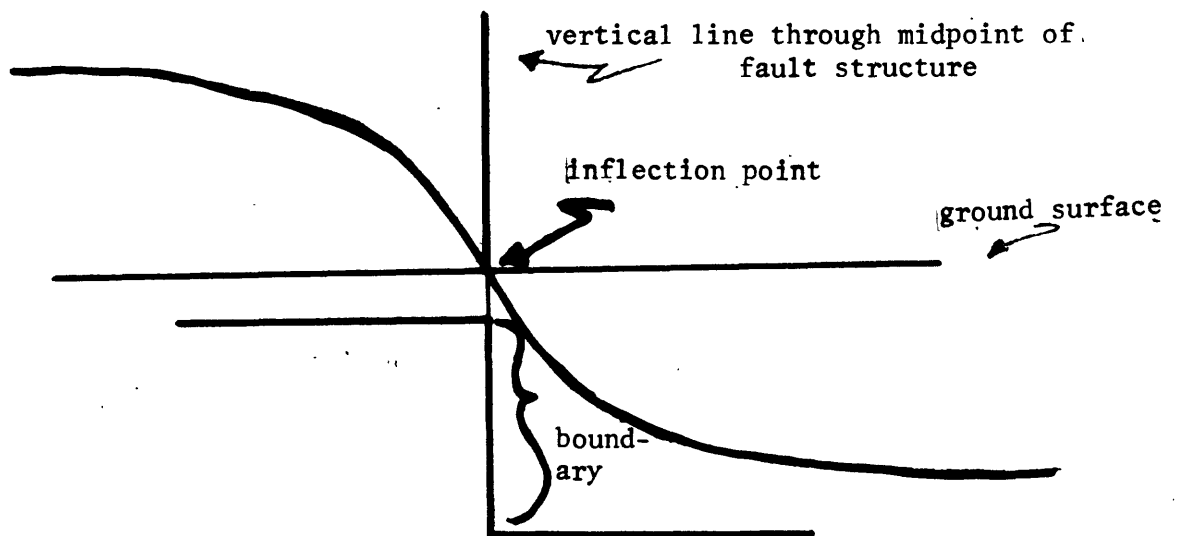
Effect of Boundary Conditions of the Anomalous Mass on the Gravity

Anomaly--The effect of varying the

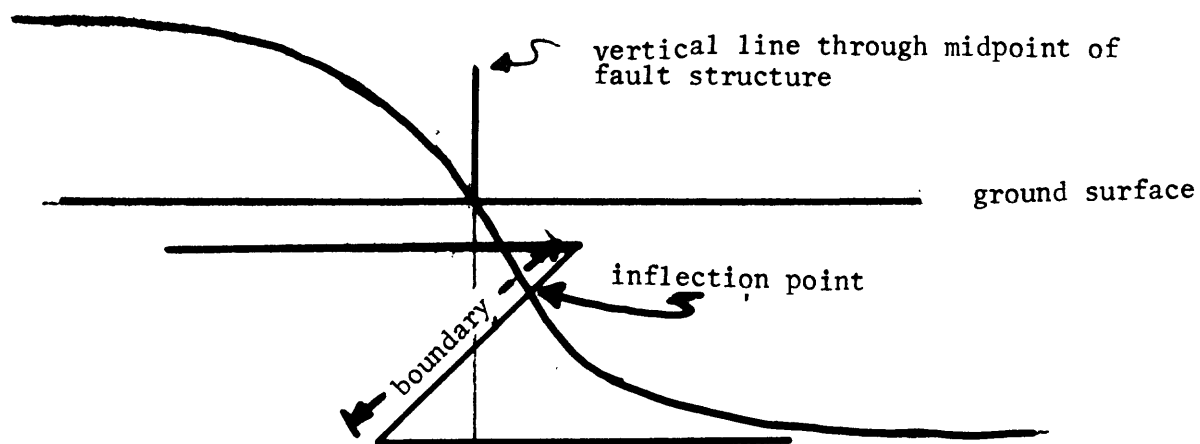
boundary conditions of a semi-infinite

horizontal slab (fault) is shown in the accompanying figures which illustrate the case of vertical thrust, and normal faults, respectively.

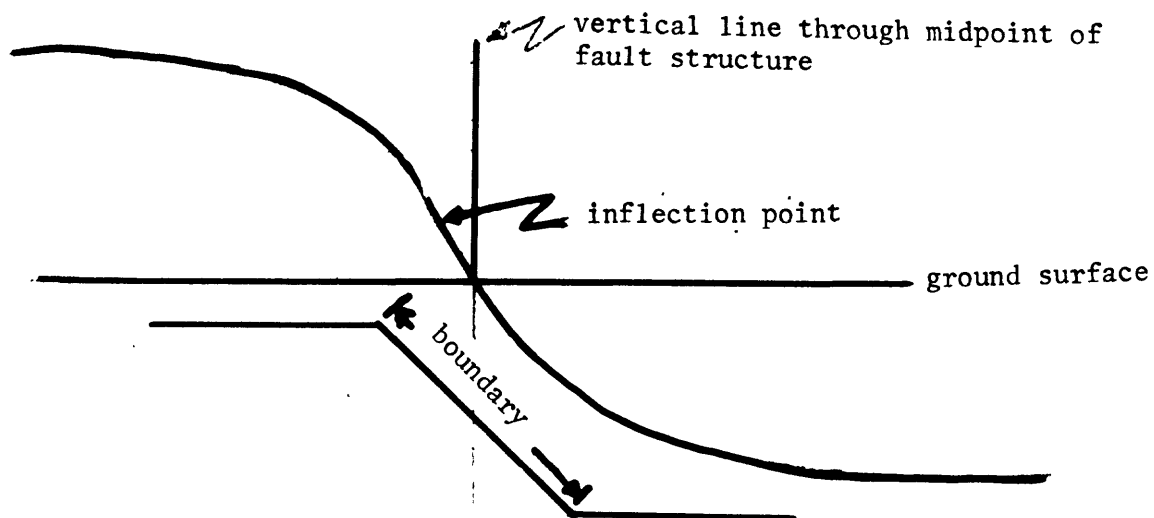
VERTICAL FAULT:



The gravity profile over a vertical fault has the steepest slope.

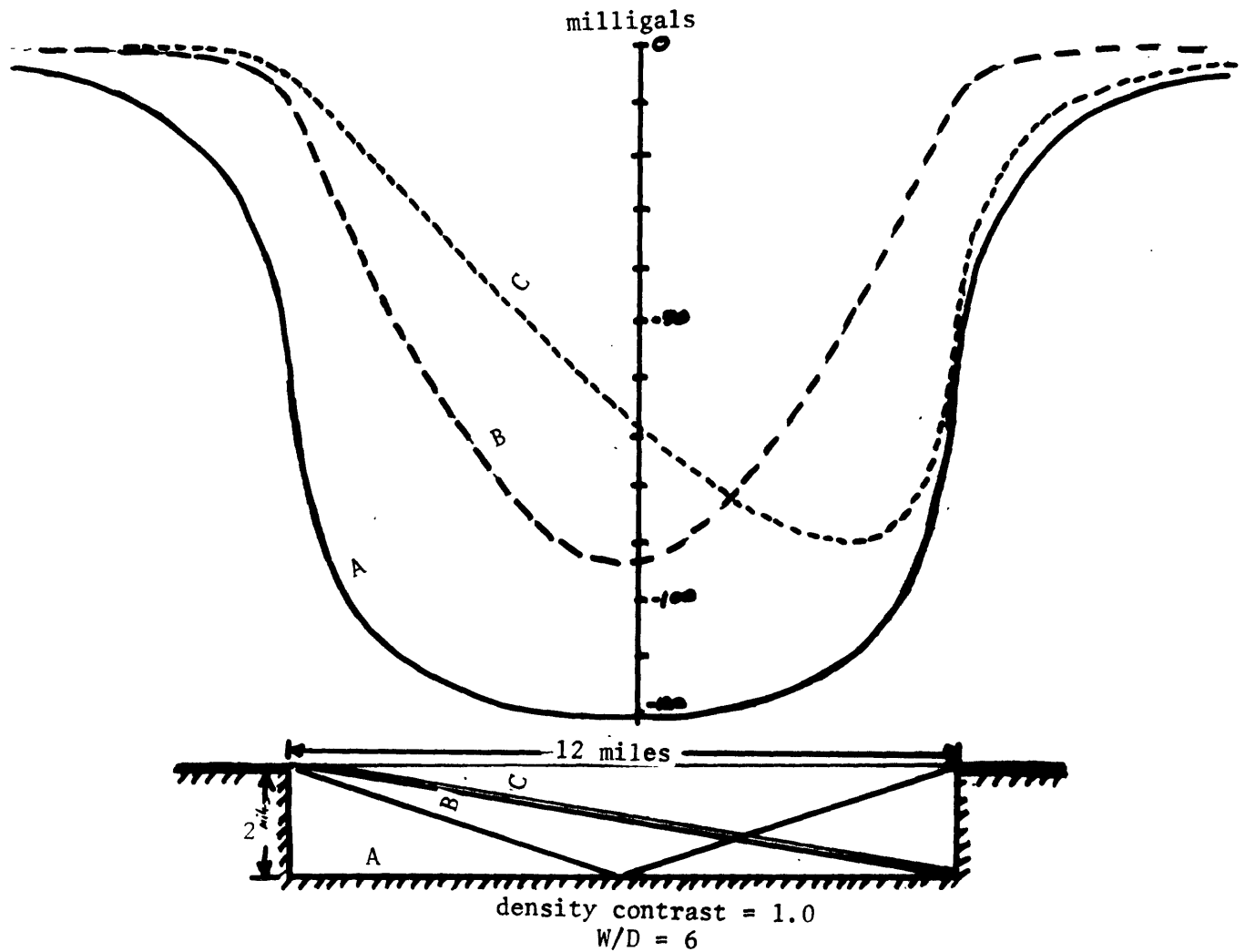
THRUST FAULT:

The gravity profile over the thrust fault shows the sharpest curvature concave upward.

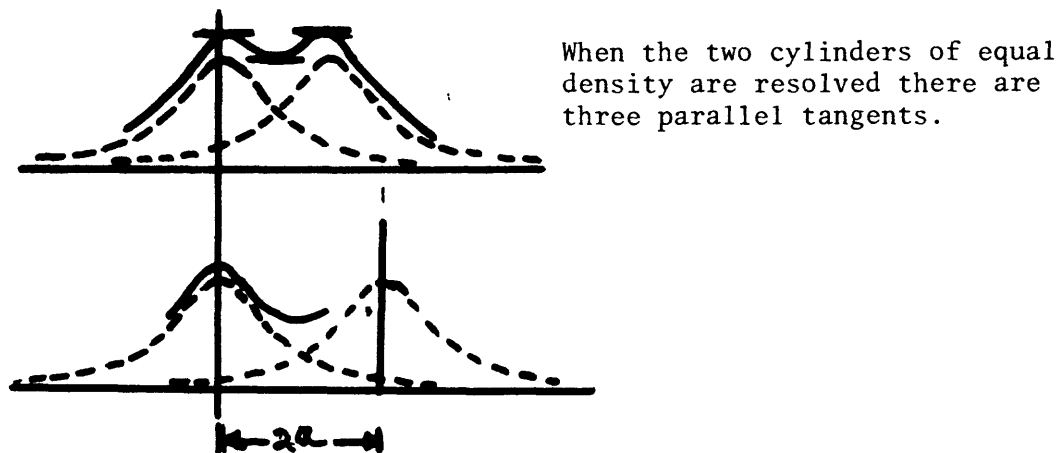
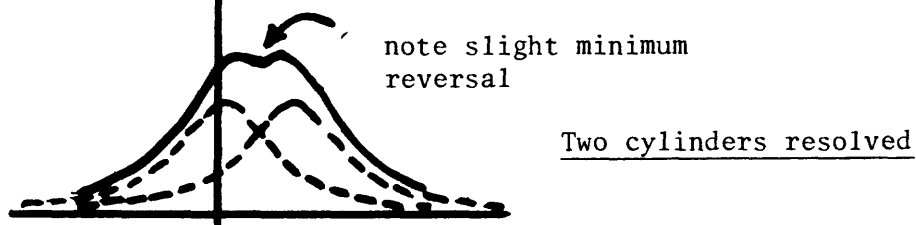
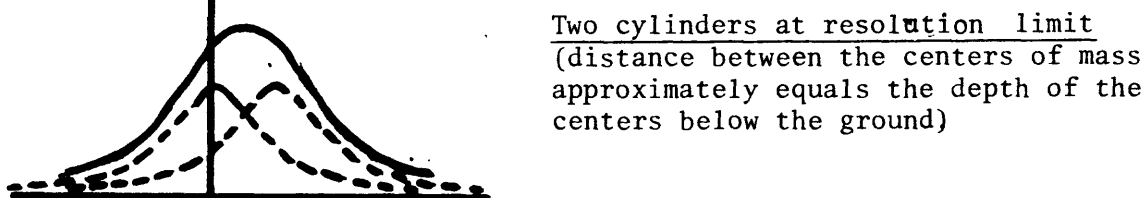
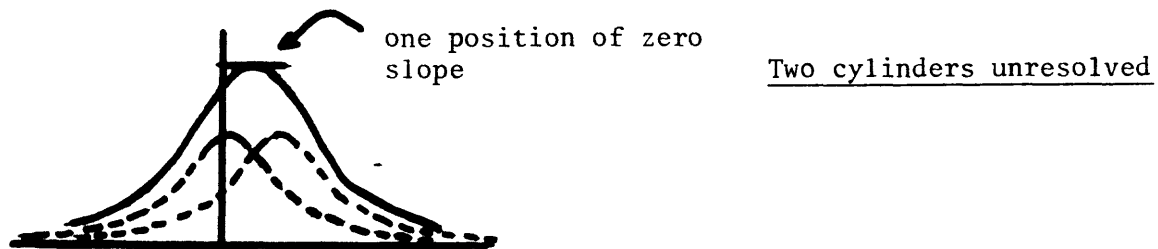
NORMAL FAULT:

Note: The gravity value over the midpoint of the fault increases as the fault changes from low angle normal to vertical to low angle thrust.

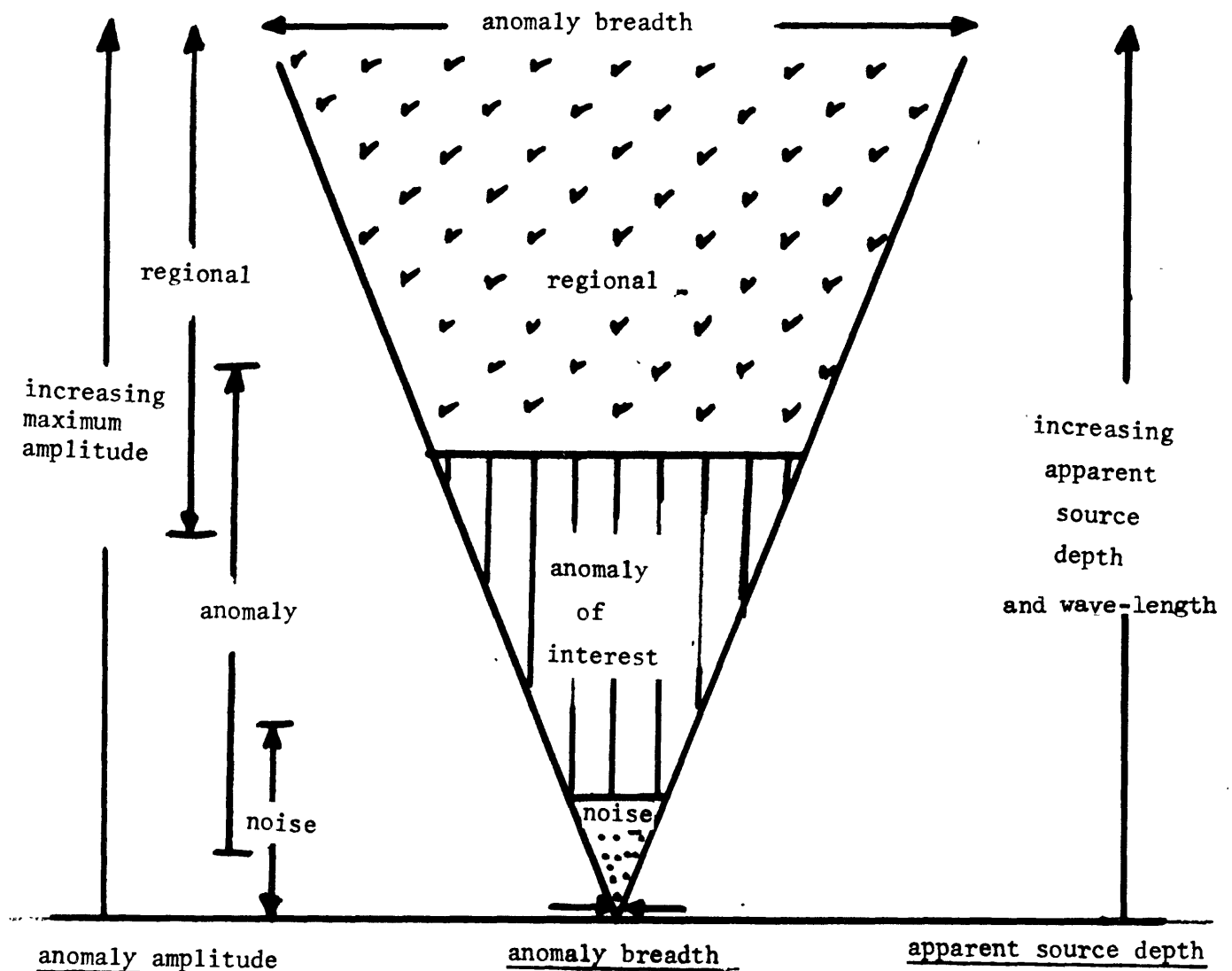
Effect of Shape of Sedimentary Basin on the Gravity Anomaly--The shape of the basin has an influence on the shape of the gravity profile obtained over it. As shown in the accompanying figure, the shape of the basin affects the amplitude of the gravity anomaly. All three basins contain the same maximum thickness, but a different volume of rock.



Isolation and Resolution--Two gravity anomalies are said to be resolved if they can be recognized as belonging to separate structures. The basic rule is that two must be separated by a distance of between two and three times their depth to produce a total anomaly which can be identified as a double instead of a single anomaly. The accompanying figures are for two infinite horizontal cylinders of equal effective densities and equal depths.

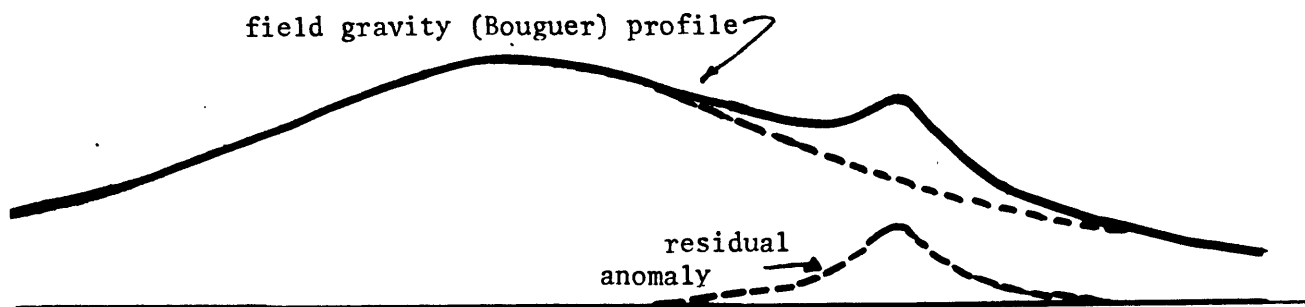


Isolation refers primarily to the separation of an anomaly of interest from regional gradients and noise. The accompanying figure shows the relative difference between noise, anomalies of interest, and the regional trend. The regional effect is a gradual and rather smooth change of gravity in a certain direction. Noise consists of shallow features of little immediate interest. Thus, the interpretation of gravity data requires isolation of the anomaly of interest from the regional trend and the noise.



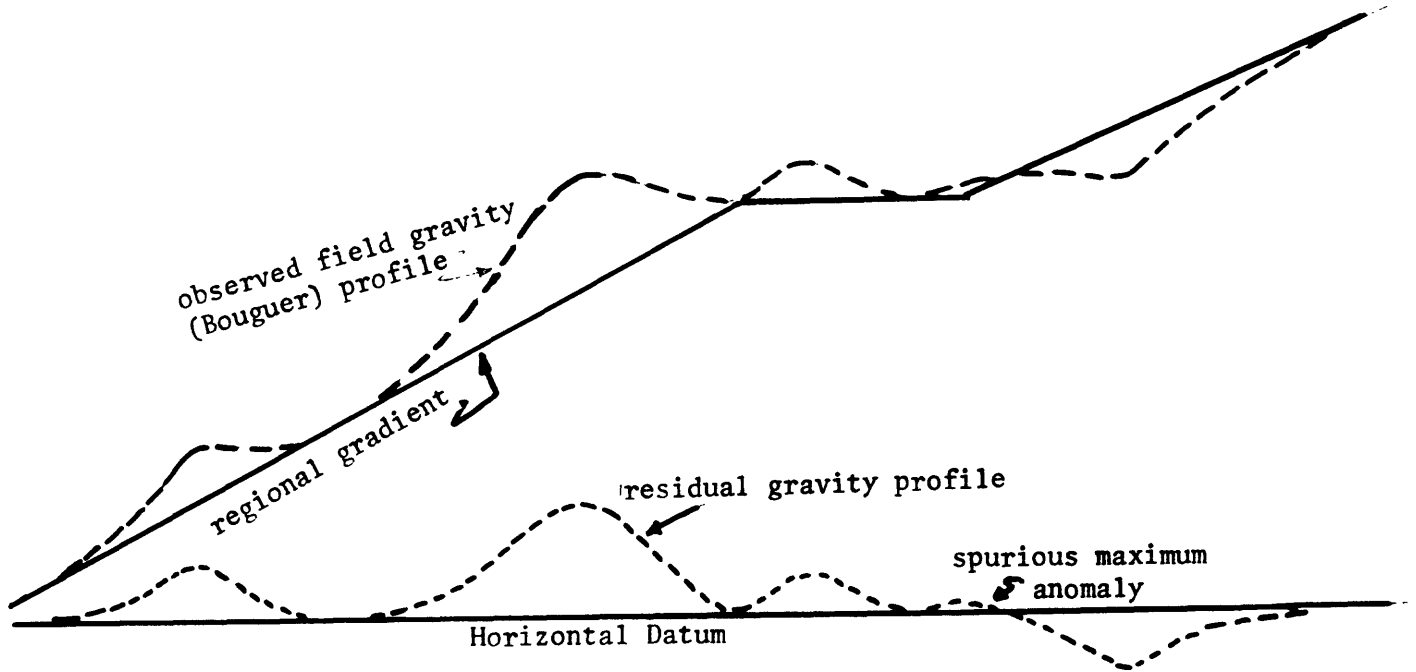
It is instructive to consider the source of the earth's gravity field in discussing the regional trend. All materials in the earth influence the earth's gravity field, g , but because of the inverse distance behavior, rocks which lie close to the point of observation will have a much greater effect than rocks located farther away. The bulk of the gravitational pull of the earth has little to do with the rocks of the earth's crust; it is caused by the enormous mass of the mantle and core. Because the mantle and core are regular in shape and smoothly varying in density, the earth's gravitational field is regular and smoothly varying also. Only about 0.3% of g are due to the materials contained within the earth's crust and of this small amount, about 15% (0.05% g) is accounted for by the uppermost 5 km of rock, that region of the crust generally thought of as being the source of "geological" phenomena. Changes in the densities of rocks within the upper 5 km will produce variations in g which generally do not exceed 0.01% of g anywhere. Thus, geological structures contribute very little to the total earth's gravitational field. They cause a point-by-point variation which can be mapped and interpreted.

The problem of isolation is shown schematically in the figure below.

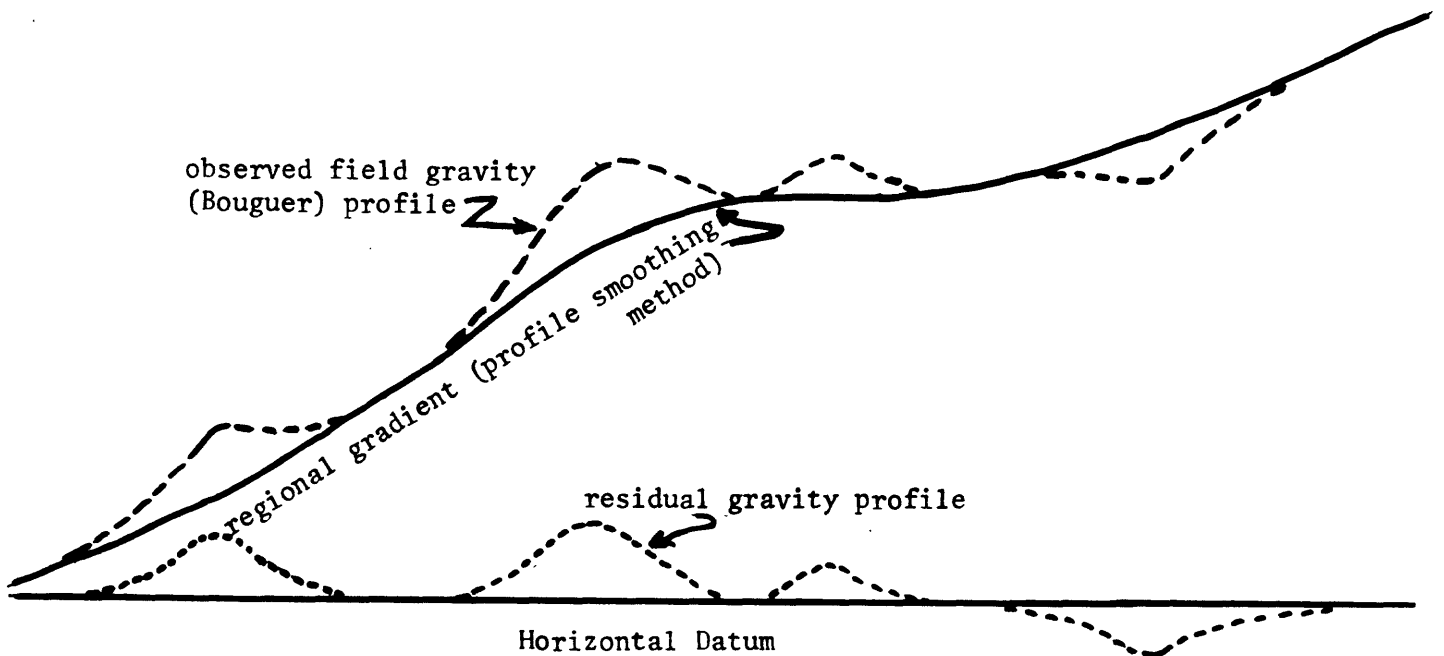


The average gradient and profile smoothing methods are used to remove the regional gradient. Each method is illustrated below.

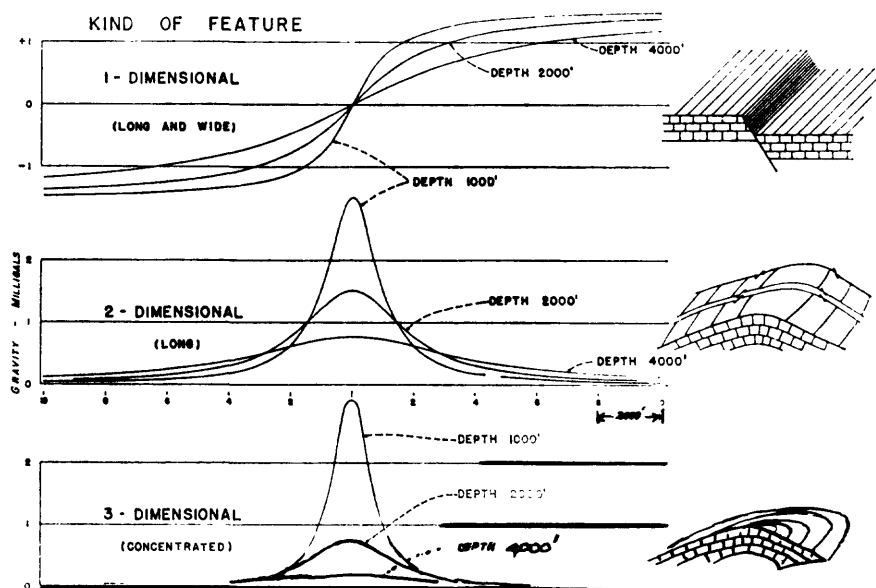
A AVERAGE GRADIENT METHOD OF REGIONAL REMOVAL



B PROFILE SMOOTHING METHOD OF REGIONAL REMOVAL



Horizontal Attenuation of Fault Anomalies--Sharp gravity anomalies are easy to identify, but the broad anomalies tend to merge into the regional trend and are difficult to identify. For a fault-type feature the sharpness of its gravity anomaly decreases with depth; for a long anomaly, sharpness decreases with the square of depth; and for a concentrated anomaly sharpness decreases as the cube of depth. In each case, the sharpness decreases with depth one power faster than the maximum amplitude of the anomaly.



Variation in Amplitude and Sharpness of Gravity Anomaly with Depth

For a fault of given throw, the maximum amplitude is maintained (in the limit as $x/z \rightarrow \infty$) regardless of the depth of burial. However, with increasing depth of burial, its gravity anomaly suffers horizontal attenuation. This will cause the deep-seated fault anomaly to become eventually lost in the regional trend.

DERIVATIVE METHODS OF DATA ENHANCEMENT

Derivative methods, of which the most popular one is the second vertical derivative, have both advantages and disadvantages. The principal advantage is that second derivative maps show changes in a steep gravity slope which are difficult to see with graphical techniques. They emphasize the effects of shallow geologic features and reduce the effects of deep structures. Composite gravity anomalies which cannot be easily resolved on the Bouguer gravity map may show up as separate components on a second derivative map. The disadvantages include: (1) the observations must be of high accuracy to offset the fact that the second derivative is sensitive to small errors; (2) unless the gravity stations are evenly and closely spaced, the second derivative tends to be an interpretation of the contours instead of the observed gravity values, (3) whereas it is reasonably easy for the interpreter to understand the physical relation between milligals of gravity and a rock mass, it is much harder to understand the relation between the rock mass and the second derivative, and (4) information (i.e., the amplitude of the anomaly) is lost in the process of finding the second derivative.

It is instructive to evaluate the second vertical derivative for the standard geometrical bodies and compare it with the g_z versus X profile obtained earlier.

Sphere--The vertical component of gravitational attraction for a buried spherical mass is given by

$$g_z = GM \left[\frac{Z}{(X^2 + Z^2)^{3/2}} \right]$$

To calculate maximum value of g_z , take the first vertical derivative,

$$\frac{\partial g_z}{\partial z} = \frac{GM (x^2 - 2z^2)}{(x^2 + z^2)^{5/2}}$$

The inflection points of the g_z versus x/z curve occur when the second vertical derivative is zero;

$$\frac{\partial^2 g_z}{\partial z^2} = \frac{3GM(2z^2 - 3x^2) z}{(x^2 + z^2)^{7/2}}$$

$$\frac{\partial^2 g_z}{\partial z^2} = 0 \text{ when } 2z^2 - 3x^2 = 0$$

or when $\frac{x}{z} = \sqrt{\frac{2}{3}}$, or $x \approx 0.82z$

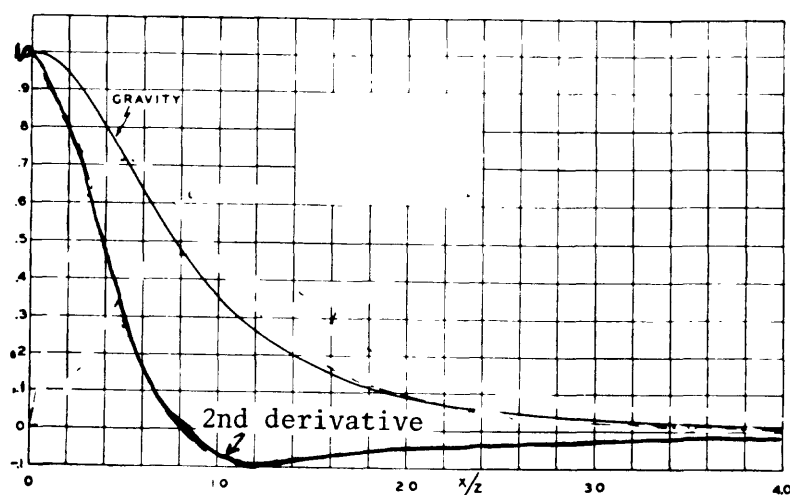
Thus, the second vertical derivative is zero when x equals about 0.82 the depth of burial of the sphere.

The second derivative has a maximum value

when $x = 0$.

It is negative when $3x^2 > 2z^2$ or when $\frac{x}{z} > 0.82$. It is positive when $\frac{x}{z} < 0.82$. The second derivative has a minimum value when $\frac{x}{z} = \pm \frac{2}{\sqrt{3}}$

or $x = \pm 1.18z$.



Note that the second horizontal derivative is

$$\frac{\partial^2 g_z}{\partial x^2} = \frac{3GMZ(4x^2 - z^2)}{(x^2 + z^2)^{7/2}}$$

and the inflection point of the g_z vs x curve occurs when $x = \pm \frac{z}{2}$

Infinite Horizontal Cylinder--The vertical component of gravitational attraction for a buried infinite horizontal cylinder is given by

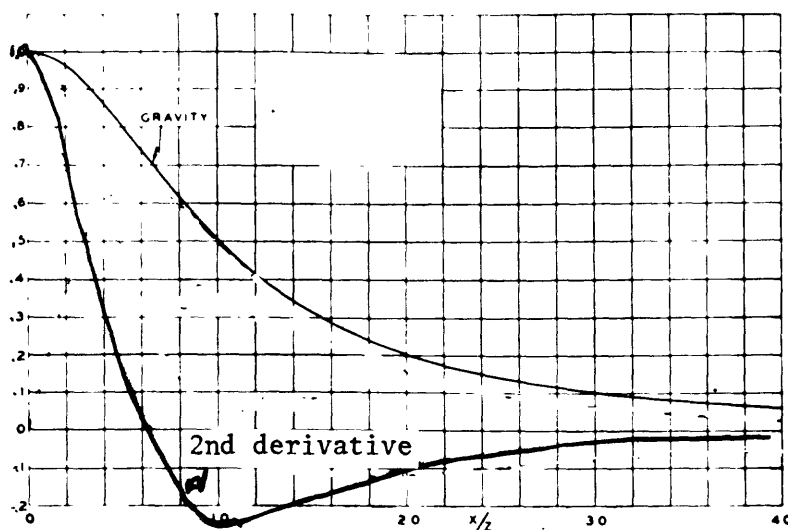
$$g_z = 2GM \left[\frac{z}{x^2 + z^2} \right]$$

$$\frac{\partial g_z}{\partial z} = - \frac{4G \cdot M \cdot x \cdot z}{(x^2 + z^2)^2}$$

So g_z max occurs when $x = 0$

$$\frac{\partial^2 g_z}{\partial z^2} = \frac{4GM Z (Z^2 - 3X^2)}{(X^2 + Z^2)^3}$$

The second vertical derivative of g_z is zero when $Z^2 - 3X^2 = 0$ or when $X = \pm \frac{Z}{\sqrt{3}}$. Therefore, the g_z versus x/z curve over a buried infinite horizontal cylinder has an inflection point when $x = \pm \frac{Z}{\sqrt{3}}$ or $X = 0.58Z$. The second derivative has its maximum value when $X = 0$; it is negative when $|X| > 0.58Z$. It has a minimum value at $X = \pm Z$.



Note that

$$\frac{\partial^2 g_z}{\partial x^2} = \frac{4GM (3X^2 - Z^2)}{(X^2 + Z^2)^3} = 0 \text{ when } x = \pm \frac{Z}{\sqrt{3}}$$

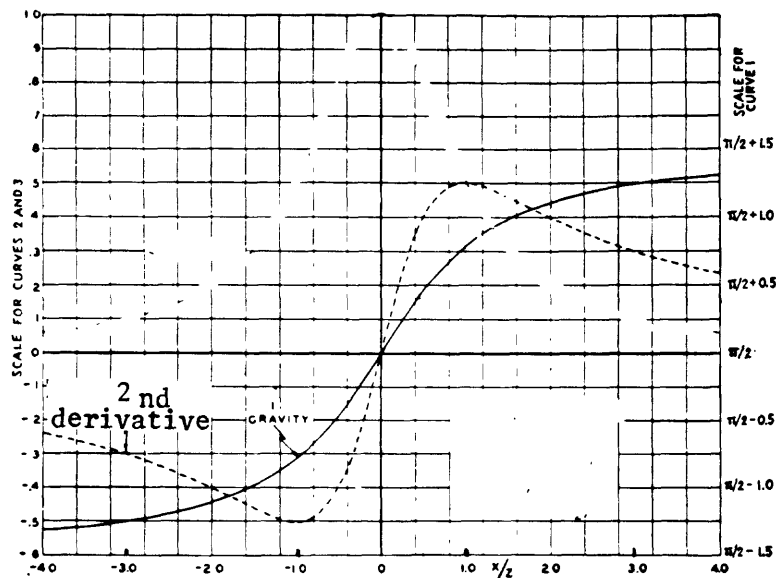
Infinite Horizontal Slab--The vertical component of gravitational attraction for a buried infinite horizontal slab (faulted slab) is given by

$$g_z = 2G\rho t \left[\frac{\pi}{2} + \arctan \frac{x}{z} \right]$$

$$\frac{\partial g_z}{\partial z} = - \frac{2G\rho t x}{x^2 + z^2}$$

$$\frac{\partial^2 g_z}{\partial z^2} = \frac{4G \rho t x z}{(x^2 + z^2)^2}$$

The second derivative of g_z is zero when $x = 0$. Therefore the g_z versus x/z curve for the faulted slab has an inflection point over the edge of the slab. The second derivative is positive when $x > 0$ and negative when $x < 0$. It has a maximum value when $x = + \frac{z}{\sqrt{3}} = 0.57z$ and a minimum value when $x = - 0.57z$. The second derivative anomaly over a faulted slab is very distinctive.



Numerical Calculation of 2nd Vertical Derivative from Potential

Field Data--If the values $G(x,y)$ which are contoured on the map are from a gravimeter or magnetometer survey, they represent a harmonic function on a plane for which the third coordinate, z , is constant. They therefore satisfy Laplace's equation

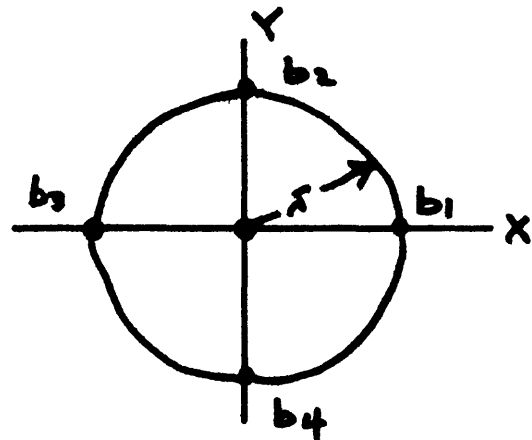
$$\frac{\partial^2 G}{\partial x^2} + \frac{\partial^2 G}{\partial y^2} + \frac{\partial^2 G}{\partial z^2} = 0$$

or

$$\frac{\partial^2 G}{\partial z^2} = - \left(\frac{\partial^2 G}{\partial x^2} + \frac{\partial^2 G}{\partial y^2} \right)$$

where the term on the left is the second vertical derivative of G in the vertical direction and the terms on the right are second horizontal derivatives in the x and y directions. If the data are sufficiently accurate and if the control is close enough, the two horizontal derivatives can be measured directly from the contour map. The equation above then provides a means for calculating the vertical second derivative. Thus, the second vertical derivative is a technique for isolating smaller shallower geologic anomalies from the deep-seated regional trend.

Referring to the accompanying figure, we can write down, from simple geometrical considerations, approximate expressions for the two horizontal derivatives $\frac{\partial^2 G}{\partial x^2}$ and $\frac{\partial^2 G}{\partial y^2}$. In this figure b_1 , b_2 , b_3 , and b_4 are four points on the original contour map which lie on the



circumference of a small circle of radius r whose center is at C . Let the line segments b_3b_1 and b_4b_2 be parallel to the x and y axes respectively. We can use divided differences as follows:

$$\frac{\partial^2 G}{\partial x^2} \approx \frac{1}{r} \left[\frac{b_1 - C}{r} - \frac{(C - b_3)}{r} \right] = \frac{b_1 + b_3 - 2C}{r^2}$$

Likewise, parallel to the y axis

$$\frac{\partial^2 G}{\partial y^2} \approx \frac{1}{r} \left[\frac{b_2 - C}{r} - \frac{(C - b_4)}{r} \right] = \frac{b_2 + b_4 - 2C}{r^2}$$

Hence,

$$\frac{\partial^2 G}{\partial x^2} = - \left(\frac{\partial^2 G}{\partial x^2} + \frac{\partial^2 G}{\partial y^2} \right) \approx \frac{4}{r^2} \left[C - \frac{(b_1 + b_2 + b_3 + b_4)}{4} \right]$$

The term inside the bracket is the value at the center point C minus the average of the four values on a circle of radius r . In the limit, as the radius of the averaging circle approaches zero, we can write the equation as:

$$\frac{\partial^2 G}{\partial z^2} = \lim_{r \rightarrow 0} \frac{4}{r^2} \left[C - \frac{(b_1 + b_2 + b_3 + b_4)}{4} \right]$$

In other words, the true mathematical second derivative is, except for the constant factor $4/r^2$, the limiting case of a very simple type of grid computing process which is in common use to produce so-called residual maps.

If values could be interpolated, or read, from the original contour map with absolute accuracy, four would theoretically be sufficient. Such precision is seldom inherent in the data from geophysical surveys. Therefore, eight or ten values, or more, are usually employed in order to give a better average on the circle.

On actual gravity or magnetic maps it is not possible to reduce the radius of the circle indefinitely. The practical limit, for the type of control usually obtained in most surveys, is of the order of one half to one mile. In areas where the anomalies are not too sharp, this will often give a close approximation to the second derivative. Regardless of the radius of the circles, however, the procedure always retains its simple physical significance as being a measure of the departure of the value of the central point from its neighborhood average.

All second derivative calculational systems used in practice are of the form:

$$D = \frac{C^2}{S^2} (W_0 H_0 + W_1 \bar{H}_1 + W_2 \bar{H}_2 + \dots + W_n \bar{H}_n)$$

where D is the derivative value, \bar{H}_0 is the centerpoint value, $\bar{H}_1, \bar{H}_2, \dots, \bar{H}_n$ are average values on the n circles used in the approximation, W_1, W_2, \dots, W_n are weighting factors, C is a numerical constant, and S is the distance of the unit grid spacing. A representative example, due to Henderson and Zietz (Geophysics, v. 14, p. 528, 1949) is

$$\frac{\partial^2 \Delta T}{\partial Z^2} = 2 \left[3\Delta T_0 - 4\bar{\Delta T}_1 + \bar{\Delta T}_2 \right]$$

where $\bar{\Delta T}_1$ and $\bar{\Delta T}_2$ are rings at distances of S, \sqrt{S} , respectively.

DEPTH ESTIMATES

Sphere--The half-width anomaly for a sphere can be defined as follows.

Let X^* be the value of X for which $g_z = 1/2 g_z \text{ max}$, thus,

$$\frac{GM \cdot Z}{[X^{*2} + Z^2]^{3/2}} = 1/2 \left(\frac{GM}{Z^2} \right)$$

$$2Z^3 = [X^{*2} + Z^2]^{3/2}$$

$$(4Z^2)^3 = [X^{*2} + Z^2]^3$$

$$4Z^2 = [X^{*2} + Z^2]$$

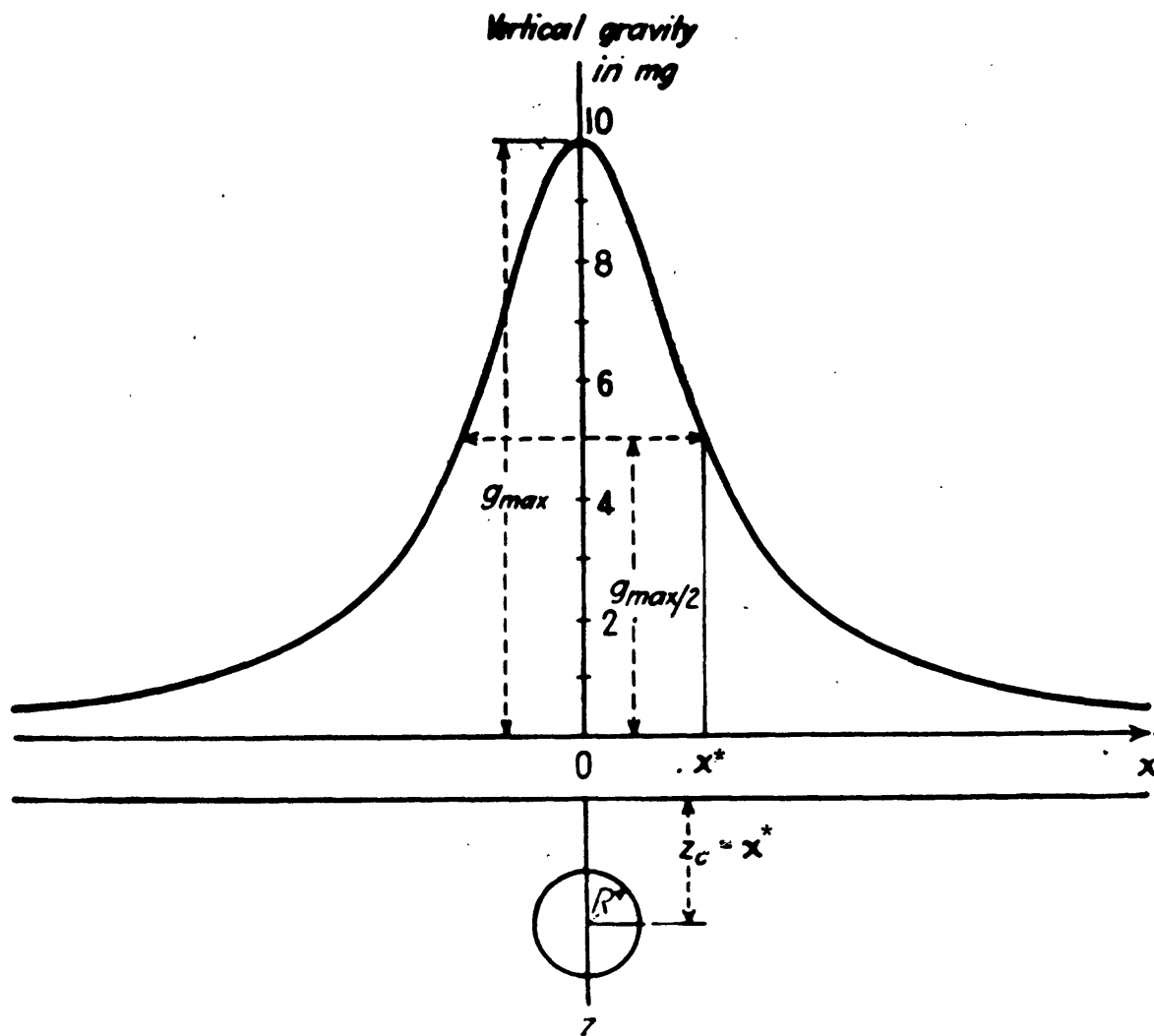
$$\text{so} \quad Z = 1.305X^* \quad \text{or } X^* = 0.766Z$$

Thus, in the ideal case, a gravimeter would record 1/2 the maximum value of the vertical gravity effect for a buried spherical mass at a distance X^* which is equal to 0.766 times the depth to the center of the mass. Alternatively, knowing the horizontal distance X^* where the g_z profile is 1/2 its maximum value enables one to estimate the depth to the center of the buried mass as 1.305 times the value of X^* .

Cylinder--The half-width anomaly for an infinite horizontal cylindrical mass is defined as follows (see figure). Let X^* be the value of X for which $g_z = 1/2 g_z \text{ max}$,

Thus

$$\frac{2GM}{[X^{*2} + Z^2]} = \frac{1}{2} \left(\frac{2GM}{Z} \right)$$



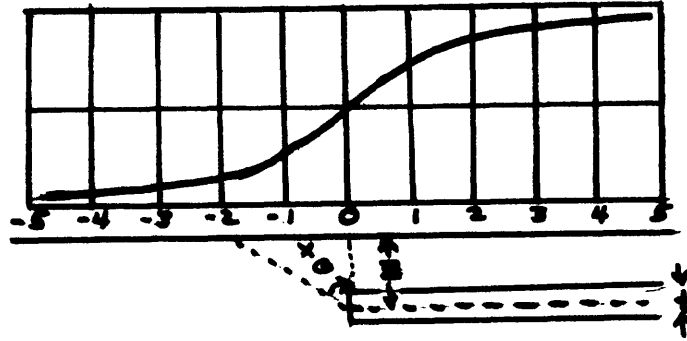
$$2Z^2 = x^{*2} + Z^2$$

$$Z^2 = x^{*2}$$

or $Z = x^*$

Thus, the horizontal distance x^* where the g_z profile is 1/2 of its maximum value is equivalent to the depth Z of the infinite horizontal line along which the mass of the cylinder is concentrated.

The half-width anomaly for the faulted slab is determined as follows. Let X^* be the



horizontal (map) distance from the vertical projection of the fault trace to the point on the g_z versus X curve where the gravity change is $1/2$ the amplitude of the curve from the trace of the fault (inflection point) to the maximum value which it asymptotically approaches as $x \rightarrow \infty$

Let $A = \text{total amplitude} = 2\pi G \rho t$

X^* is the distance at which $g_z = 1/4 A$.

Thus X^* is the point where $g_z = 1/2 (G_z(\infty) - G_z(0))$

$$X^* = 1/2 (2\pi G \rho t - \pi G \rho t)$$

Thus

$$2\pi G \rho t + 2G \rho t \arctan \frac{X^*}{Z} = \frac{1}{2} (\pi G \rho t)$$

$$2G \rho t \arctan \frac{X^*}{Z} = -\frac{3\pi}{2} G \rho t$$

$$\arctan \frac{X^*}{Z} = -\frac{3\pi}{4} \quad (-135^\circ \text{ or } 45^\circ)$$

$$\frac{X^*}{Z} = 1 \text{ or } X^* = Z$$

Thus, the half width of the gravity anomaly over a fault is equal to the depth to the median plane of the faulted slab.

Depth estimates can be made from either the corrected gravity data or from the second derivative data. The depth estimation parameters are listed in the table below.

Data	Mass Anomaly Form	Inflection Point	1/2 Width Point
Basic Gravity Data	1. Faulted slab	$\frac{X}{Z} = 0$	$\frac{X}{Z} = 1$
	2. Infinite horizontal cylinder	$\frac{X}{Z} = 0.577$	$\frac{X}{Z} = 1$
	3. Sphere	$\frac{X}{Z} = 0.82$	$\frac{X}{Z} = 0.766$
	Mass Anomaly Form	X max	X zero
Second Vertical Derivative	1. Faulted slab	$Z = X \text{ max}$	
	2. Infinite horizontal cylinder		$Z = X \text{ zero}$
	3. Sphere	$Z = 1.225 X \text{ Max}$	

X max = horizontal distance between max and min values

on $\frac{\partial^2 g_z}{\partial z^2}$ vs x profile

x zero = horizontal distance from max value to zero point

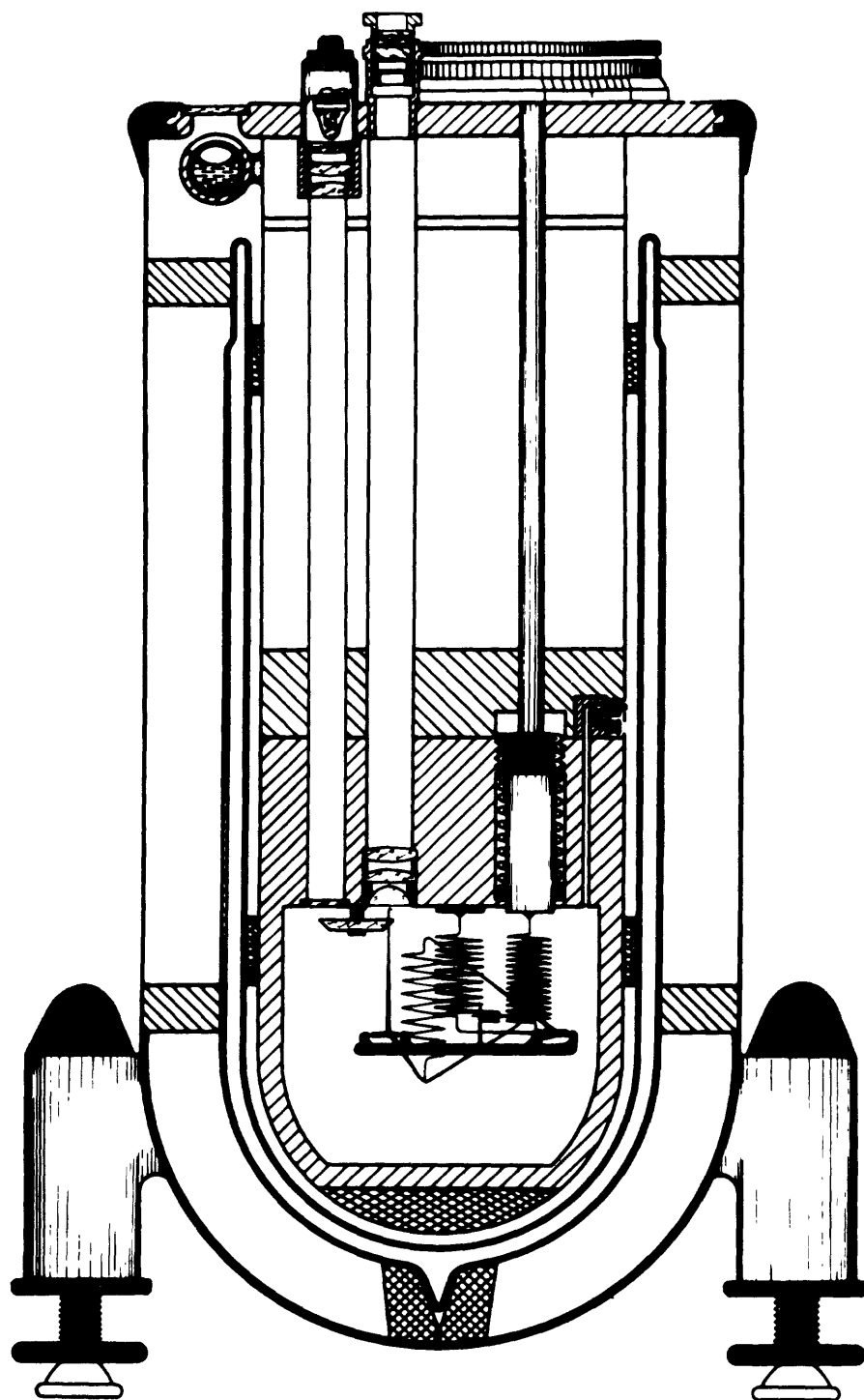
on $\frac{\partial^2 g_z}{\partial z^2}$ vs x profile

Two problems are in Appendix F to illustrate the application of the depth estimation principles.

CORRECTIONS APPLICABLE TO GRAVITY DATA

Two requirements must be fulfilled in order to produce useful gravity maps. First, the measuring apparatus must be sufficiently sensitive to detect the effects of local geologic structures on the gravitational field g of the earth. Second, methods must be used to correct the data for all sources of variation caused by other than the local geology.

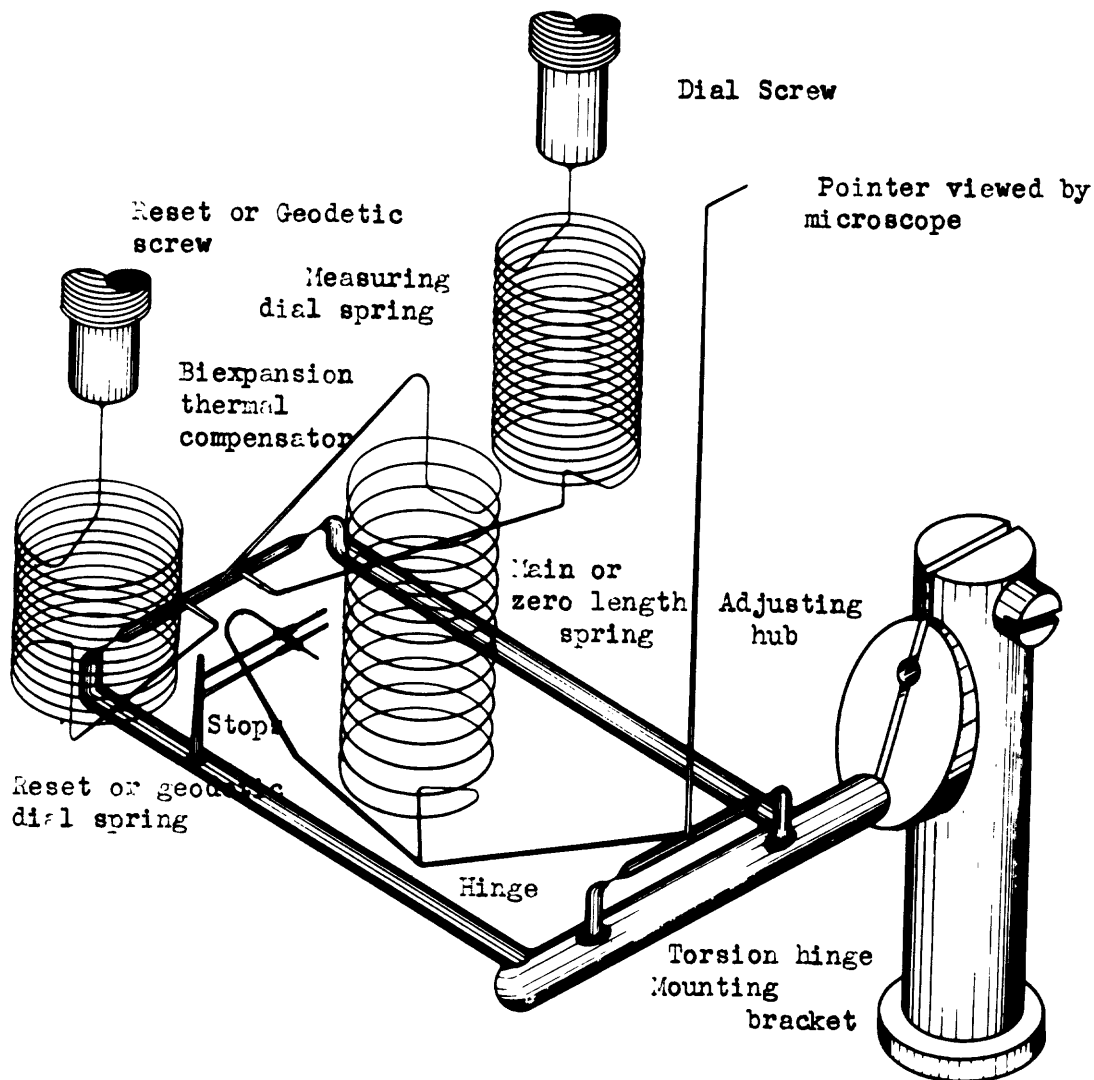
Gravimeters--The gravitational field of the earth has a world-wide average of about 980 gals with a total range of variation of about 5 gals, or $\pm 0.5\%$. Mineral ore bodies and geologic structures of interest seldom produce fluctuations in g exceeding a few milligals, or about 1 part in 10^6 of g . To calculate details of the size and shape of these structures requires a precision of 0.01 milligals, or about 1 part in 10^8 of the gravitational field of the earth. Modern gravimeters (see figures) are essentially an extremely sensitive spring balance and have reading sensitivities of 0.01 milligals. They respond to variations in g instead of measuring g directly. The development of gravimeters has now reached the point at which the limitation on the accuracy of interpretations is determined, not by the reading of data, but by the corrections which are applied to the data.



Worden Gravity Meter

SPRING SYSTEM OF WORDEN

GRAVIMETER



The gravity method depends on the location of anomalies in the earth's gravitational field and relating these anomalies to subsurface structures or features. If the earth were an isolated, perfectly smooth, spherical body of constant density with respect to its concentric composition shells and not rotating, the problem of interpreting the gravity data obtained would be greatly simplified. In this case, the geoid (the imaginary surface that has the same potential at every point such as the surface of the ocean) would be a perfect sphere. Local density variations or structural irregularities would then yield readily interpretable anomalies in the geoid. Unfortunately, the earth is far from being a perfect surface; it is far from being spherical and smooth, the density changes considerably from continental material to ocean basin material, and the effects of the sun and moon cannot be overlooked. In order to obtain results that are not misleading, one must mathematically isolate, stretch, and compress the earth until it conforms to the perfect model. The following corrections do this.

The earth tide or drift correction smooths the effects of the sun and the moon as well as correcting for the natural drift of the instrument. This is easily done by establishing a base station and making periodic readings at this station while the rest of the survey is being carried out. All stations may be corrected to one arbitrarily chosen reading of the base station, a procedure that may be done simply by plotting the variation of gravity at the base station against time and recording the time at which other station readings were taken. **For sensitive modern instruments, tidal charts are used to make the correction.**

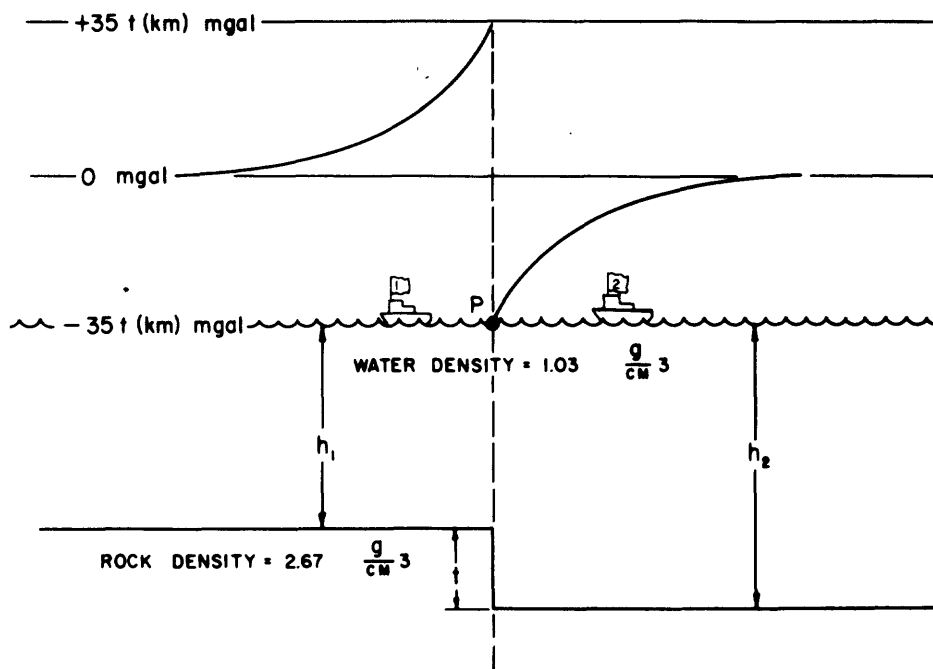
Corrections to reduce the earth to a smooth body can be split into three groups: (1) corrections involving differences in elevation above sea level, (2) corrections involving the material between the actual ground surface and the lower hypothetical smooth surface, (3) corrections for nearby topographic highs and lows. The free air correction essentially corrects all readings to an equal elevation above sea level. Based on the assumption that the earth is a sphere (a fact that will be corrected for later) this correction in effect corrects the data to a surface which is everywhere an equal distance from the earth's gravitational center. It can be shown from the inverse square law that gravity changes at a rate of 0.094 milligal/foot (0.3086 milligal/m) change in elevation; therefore, if a station is to be corrected downward to a datum, the correction would be plus $0.094h$ where h is the difference in elevation from the station to the datum. If by chance, a reading were taken below the arbitrarily chosen datum, the correction would be negative.

In the preceding free air correction, a new, smooth surface has been established at some distance below (or above) the irregular surface on which the original readings were made. It is still assumed that this new datum is at the surface of the earth, an invalid assumption until the material which is on top of the datum has been removed mathematically. This correction (Bouguer) is subtracted because it is mathematically removing material from the earth, except when the station is below the datum, in which case it would be added. The Bouguer correction is 0.4193ρ milligal/m, is opposite in sign and directly related to the free air correction. For this reason, the two corrections are often combined to give one correction,

$$F = 0.3086 - 0.04193 \rho \text{ milligal/m.}$$

The Bouguer correction has reduced the data to a smooth surface by removing the material between this new surface and the surface upon which the original measurements were made. The material was removed by slabs which assumes that the original surface terrain was essentially smooth and flat. Obviously, the lack of smoothness may be significant when dealing with small gravitational anomalies. The effect of the terrain is as follows. Hills will make the Bouguer correction too small, because less material than is actually there is being removed; whereas, valleys will make the Bouguer correction too large due to removing material that never was there. Also, hills surrounding a station will exert a gravitational pull that will be opposite to that of the normal pull of the earth. Because of all of this, corrections for the hills and the valleys are always added to the station value for land surveys. To compute the effect that each hill and valley surrounding a station has on the gravity at that point is a tedious process. The corrections can be made with an accuracy of 0.1 to 1.0 mgal by the use of templates and graphical methods (Appendix A contains terrain correction tables.) The topographic features closest to the station will have by far the greatest effect on the gravity reading whereas the topographic effect decreases rapidly with distance from the station.

When the gravitational attraction is measured on the ocean surface above the level of the ocean bottom, the Bouguer and terrain effects are calculated as if the water were replaced by rock. The terrain effect for a simple vertical cliff can be positive and negative. For a measurement



Terrain correction for gravity measurement at sea surface.

at position 1, the Bouguer effect is calculated as if the depth h , extended continuously and does not take into account the deeper water to the right of the cliff. Therefore, the calculated Bouguer effect is too small and the terrain correction is positive. At point 2, the Bouguer correction does not see the higher topography to the left of P, the calculated effect is too large and the terrain correction is negative. In the ideal case shown, the change increases to the point P and then suddenly reverses, as shown by the terrain correction curve in the upper part of the figure. In actual topography, the cliff would not be vertical and the two sharp peaks would be smoothed out. Because the instrument is above the topography in ocean measurements, the effects are much larger than for land measurements. For a survey off-shore California, terrain corrections of the order of ± 25 mgals were calculated. For gravity measurements made in the air, the effects are even larger than for marine measurements, because the density

contrast is rock relative to air rather than rock relative to water.

The latitude correction is a correction which mathematically corrects for the earth's rotation and makes it a sphere instead of an oblate spheroid. Also, the rotation of the earth and the associated centrifugal force causes an increase of gravity at the poles relative to the equator. This correction utilizes the international gravity formula to obtain the rate of change along a north-south line. The radius of the sphere is arbitrarily chosen by selecting any one station as being on the sphere and correcting the other stations so that all of the points now lie on the spherical surface.

Summary--The earth is isolated in space by means of the earth tide or drift correction, its surface is smoothed by means of free-air, Bouguer, and the terrain corrections, and its rotation stopped and reshaped into a sphere by means of the latitude corrections. If all of the corrections have been done correctly and carefully, the remaining anomaly should be due only to density contrasts caused by the replacement of a heavier or lighter material (ore body or salt dome) or due to structural features such as faults, anticlines, domes, etc. (see chart on next page).

Every correction need not be used in all cases. Those which are essential and should always be used are the earth tide or drift, free air, and Bouguer corrections. The terrain correction need not be used where the ground is exceptionally flat or where a large anomaly is being dealt with. The latitude correction need only be applied where the survey covers considerable distances in the north-south direction. The gravity map after the application of latitude, free-air, Bouguer, and terrain corrections (if used) is called a Bouguer map. The largest single source of error in land gravity maps is due to elevation errors.

Correcting gravity measurements made at sea aboard a moving ship is more complex than correcting land measurements. The horizontal and vertical accelerations due to the movements of the ship can be $0.1g$ (100,000 milligals) or more. The vertical motional accelerations are in the same direction as the gravity being measured and must be eliminated by damping and filtering operations. Any cross-coupling of horizontal forces to the vertical forces must be eliminated or measured and removed. The cross-coupling correction is a function of the particular gravimeter used in the gravity survey and is normally effected by direct measurement and subsequent vectoral subtraction or by mounting the gravimeter on a gyroscopically stable platform and developing a cross-coupling correction in the instrument.

The Eötvös correction is required to remove the accelerational effect experienced by a body moving over a curved, rotating earth instead of being stationary on the earth's surface. The Eötvös effect, which includes the vertical component of the Coriolis force, can be quite large even for moderate ship speeds. For example, at a speed of 10 knots on an eastward course at the equator, there is a 75 milligal positive correction and on a westward course, a 75 milligal negative correction. To make the Eötvös correction to an accuracy of 1 milligal or less for nearly east-west courses, the ship's speed must be known to about 0.1 knot; for nearly north-south courses, the azimuth (heading angle relative to astronomic north) must be known to about 1° .

The greatest single source of uncertainty in sea gravity maps is location. If a gravity value is to be determined at a closely defined point, its precision is low because the short-time value near that point is strongly influenced by short-period motional components. The higher the precision, the greater the time over which the average must be taken and, depending on the speed of the ship, the greater the distance over which the average is applicable.

MATHEMATICAL BACKGROUND FOR CORRECTING GRAVITY DATA

- A. Free air correction-- considers the change in gravity with change of distance from the center of the earth.



The gravity at sea level is $g_0 = \frac{kM}{r^2}$

where G = gravitational constant

M = mass of the earth

r = radius of curvature of the earth

The gravity g at a point "P," " h " metres above sea level is

$$g = \frac{GM}{(r+h)^2} = GM (r+h)^{-2} \quad \text{which can be expanded}$$

$$= GM \left[r^{-2} - 2r^{-3}h + \frac{(-2)(-3)}{2} r^{-4}h^2 + \frac{(-2)(-3)(-4)}{(3)(2)} r^{-5}h^3 + \dots \right]$$

$$g = \frac{GM}{r^2} \left(1 - \frac{2h}{r} + \frac{3h^2}{r^2} - \frac{4h^3}{r^3} + \dots \right) \quad \text{or}$$

$$g = g_0 \left(1 - \frac{2h}{r} + \frac{3h^2}{r^2} - \frac{4h^3}{r^3} + \dots \right)$$

The free air correction, " g_f " is $g_0 - g$

$$g_f = g_0 - g = \frac{2gmh}{r_0} \left(1 - \frac{3h}{2r_0} + \frac{4h^2}{r_0^2} - 0.000 \right)$$

where g_m is the average gravity value = $g_0/2$ and r_0 is the average radius of the earth.

The factor $\frac{2g_m}{r_0}$ is a constant at any gravity station. The second and third terms vanish except in very high altitudes. For example, if $h = 5000$ metres, the influence of the second term is 1.7 mgal, but for $h = 2,000$ metres, it is only 0.3 mgal. For $h = 1000$ m, the contribution is only 0.07 mgal.

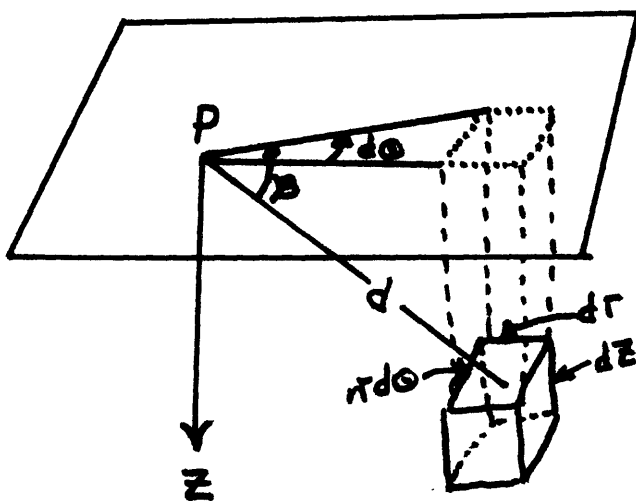
$$g_f = 0.3086 h \text{ milligals where } h \text{ is in metres}$$

$$g_f = 0.09406 h \text{ milligals where } h \text{ is in feet}$$

The Free Air correction is positive for areas above sea level and negative for areas below sea level.

B. Bouguer Correction--In addition to the attraction of the Earth's mass below the geoid's surface, the mass between the geoid and the observation point exerts an attraction. This attraction must be removed from the observed gravity.

Imagine a horizontal plane through the point "P" so that there is a plate of mass between the point "P" and the geoid. The attraction of the mass element "dm" on "P" can be found as follows:



$$dg = \frac{G dM}{d^2} \quad \text{but}$$

$$dM = \rho r dr d\theta dz$$

in cylindrical coordinates

$$d = \sqrt{r^2 + z^2}$$

$$\text{so } dg = G\rho \frac{r dr d\theta dz}{d^2}$$

$$\text{but } g_z = g \cos \beta$$

$$\text{so } dg_z = \frac{G\rho d\theta z dz r dr}{d^3}$$

$$g_z = G\rho \int_0^{2\pi} d\theta \int_{h_1}^{h_2} z dz \int_{r_1}^{r_2} \frac{r dr}{(z^2 + r^2)^{3/2}}, \quad \text{the vertical}$$

attraction of a cylindrical ring at the point "P." If we let $r_1=0, r_2=\infty, h_1=0$ we have the attraction of an infinite rock layer of thickness h .

The vertical attraction of the infinite rock layer of thickness h is

$$g_2 = 2\pi G \rho h \quad \text{where } h \text{ is the height above mean sea level (the surface of the geoid)}$$

So

$\frac{g_{\text{Bouguer}}}{h} = 2\pi k \rho_m = 0.04185 \rho_{\text{mean}} \text{ milligals/metre}$ <p>or</p> $\frac{g_{\text{Bouguer}}}{h} = 0.01276 \rho_m \text{ milligals/foot}$ <p style="text-align: right;">$\rho_m = \text{mean density of earth}$</p>

Using the relations

$$g = G \frac{m}{r^2} = \frac{4}{3} \pi G \rho_m r, \text{ we have } G = \frac{3g}{4\pi \rho_m r}$$

Substituting in the equation

$$g_{\text{Bouguer}} = 2\pi G \rho h, \text{ we have}$$

$$g_{\text{Bouguer}} = 2\pi \rho h \left(\frac{3g}{4\pi \rho_m r} \right) = \frac{3g \rho h}{2 \rho_m r}$$

The value of g_{Bouguer} must be subtracted from the observed gravity value at "P" if the gravity station is above the datum (always opposite to g_f).

Combining the free air and Bouguer corrections, we have

$$\begin{aligned} G_f + G_b &= \frac{2gh}{r} - \frac{3}{2} \frac{g \rho h}{\rho_m r} \\ &= \frac{2gh}{r} \left(1 - \frac{3r}{4\rho_m} \right) = \left(1 - \frac{3r}{4\rho_g} \right) f \end{aligned}$$

The effect of the Bouguer correction is to diminish the effect of the free air correction by about 1/3. We obtain different values for the combined correction according to values for ρ and ρ_m .

$$\text{If } \rho = 2.67 \text{ gm/cm}^3, \quad g_B = 0.034 \text{ mgal/foot}$$

or the combined correction becomes

$$(0.094 - 0.034)h \text{ or } 0.060h \text{ mgal where } h \text{ is in feet}$$

Table of combined correction values

Density (ρ)	mgal/metre	mgal/foot
1.6	0.2416	0.07364
1.7	0.2375	0.07237
1.8	0.2333	0.07109
1.9	0.2291	0.06982
2.0	0.2249	0.06854
2.1	0.2207	0.06726
2.2	0.2165	0.06599
2.3	0.2123	0.06471
2.4	0.2082	0.06344
2.5	0.2040	0.06216
2.6	0.1998	0.06088
2.7	0.1956	0.05960

Elevations must be known to about 1 foot (0.3 metre) if the combined correction ($g_f \pm g_b$) is to be accurate to less than 0.1 m gal.

C. Terrain correction: This correction is made through the use of charts and tables devised by S. Hammer (Geophysics, Vol. 4, pp. 184-194, 1939).

This correction is always positive for land measurements (see Appendix A).

D. Latitude correction: Because of the ellipticity of the earth and its rotation, the acceleration of gravity on its surface is not constant, but is a function of the latitude. We can make some calculations in order to obtain an approximate value of the difference in the acceleration of gravity at the poles and at the equator. Consider first the effect of the polar flattening. If we assume that the earth attracts as if all its mass were located at the center, the gravitational attraction at the poles would be

$$g_{\text{pole}} = GM / (6.3569 \times 10^8 \text{ cm})^2$$

At the equator, the gravitational attraction would be $GM / (6.3784 \times 10^8 \text{ cm})^2$

Their ratio is

$$g_p / g_e = (6.3784 \times 10^8)^2 / (6.3569 \times 10^8)^2 \text{ equals } 1.0043$$

Since g_p is approximately 1000 gal, g_p exceeds g_e by about 4 gals. However, this assumes that the earth attracts as if all its mass were located at its center which is not an entirely valid assumption. We must also take account of the centrifugal acceleration.

The centrifugal acceleration is perpendicular to the axis of rotation of the earth and is proportional to the distance from its axis. It is zero at the poles and attains its maximum at the equator. Its value at the equator is $\omega^2 r$ where ω is the angular acceleration and r is the equatorial radius of the earth. Thus we have

$$\omega^2 r \text{ equals } (7.29211 \times 10^{-5})^2 \times 6.3784 \times 10^8 \text{ equals } 3.4 \text{ gal.}$$

At the equator, the centrifugal force is directed opposite to the gravitational attraction. Thus, we would expect the acceleration of gravity at the poles to be about 7 or 8 gals greater than at the equator, a difference which is slightly greater than the actual observed value of about 5 gal.

In most cases, we wish to eliminate the differences in gravity due to latitude variations because they tend to mask or confuse the anomaly of interest.

The latitude correction takes into account the increase of gravity from the equator to the pole and is usually made relative to an arbitrary base latitude within the survey. To make the correction, the international gravity formula is used. It is as follows:

$$g_0 = 978.049 (1 + 0.005288 \sin^2 \phi - 0.0000059 \sin^2 2\phi)$$

We can use this formula directly or differentiate and obtain the rate of change of gravity in a north - south direction.

$$\frac{1}{R} \frac{dg_0}{d\phi} = 0.8119 \sin 2\phi \text{ mgal/km or}$$

$$\frac{1}{R} \frac{dg_0}{d\phi} = 1.307 \sin 2\phi \text{ mgal/mile or}$$

$$\frac{1}{R} \frac{dg_0}{d\phi} = 0.0002475 \sin 2\phi \text{ mgal/ft}$$

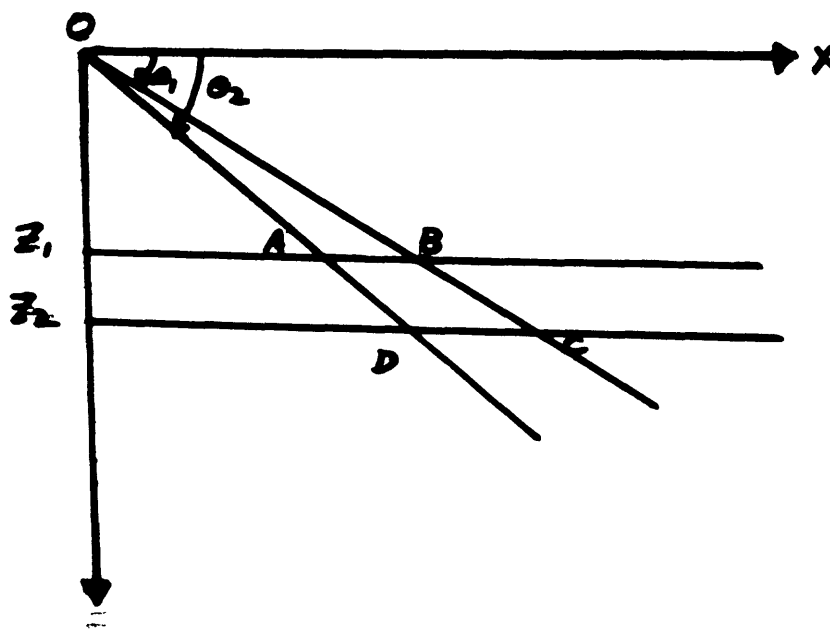
where R is the radius of curvature of the mean sphere (6371 km). In making the correction in the northern hemisphere, the correction is subtracted for points north of the reference latitude and added for points south of the reference latitude. (The opposite is true for the southern hemisphere).

E. Earth Tide or Drift Correction: This correction corrects for the attractive effects of the sun and the moon as well as correcting for the natural drift of the instrument. This correction is made by establishing a base station and making periodic readings at this station at frequent intervals of time while the rest of the survey is being made. All stations are then corrected to the first reading at the base station by plotting a graph of the variation of gravity at the base station vs time, recording the times at which other station readings were taken, and interpolating the magnitude of the correction for each station from the graph. Earth tide charts are also used.

SPECIAL INTERPRETATIONAL AIDS

The simple formulas for spheres, cylinders, and faults can serve very well as models to calculate the approximate magnitudes of gravity effects for comparison with observed values. There are, however, many interpretational problems in which the simple calculational models are inadequate. When more detailed calculations are needed, graticules, dot charts, solid angle charts, and other schemes are used. Each of these will be discussed in the following pages.

Skeel's Graticule



The vertical component of gravitational attraction at origin "o" of prism or solenoid ABCD (extending to infinity in direction normal to paper) is

$$\Delta g_z = 2G\rho (\theta_2 - \theta_1) (Z_2 - Z_1)$$

If we substitute $\rho = 1.0$ cgs units and $t = 100$ metres (or 328.1 feet) in the formula for an infinite slab: (Note: 328.1 ft = .3281 kilo ft)

$$\Delta g_z = (12.77) (1) (0.3281) = 4.19 \text{ milligals}$$

Thus, an infinite plate of 100 metre thickness has a Δg_z of almost 42 gravity units per 1.0 cgs density contrast.

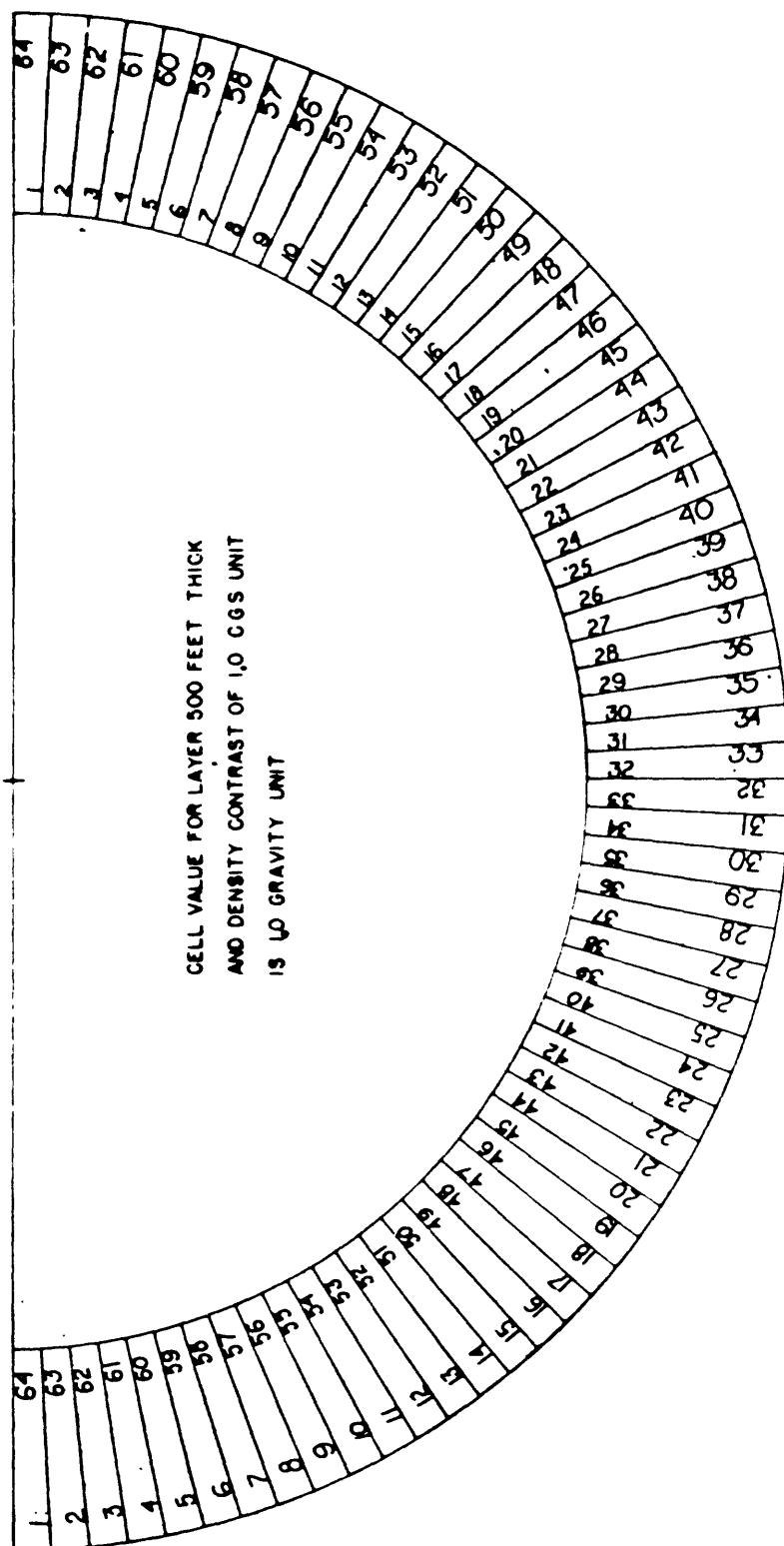
For $(Z_2 - Z_1) = 100$ metres and for $(\theta_2 - \theta_1) = 2\pi$, we then have the attraction of an infinite sheet 100 metres thick of density contrast 1.0 cgs. By constructing a graticule or template with 42 equal angles, the gravity effect of any one compartment defined by the angles and boundaries of the horizontal slab is 1/42 of the total effect or 1 gravity unit.

If $t = 500$ feet, then

$$\begin{aligned} \Delta g_z &= (12.77) (1.0) (0.5) \\ &\approx 64 \text{ gravity units} \end{aligned}$$

So 64 equal angles form the graticule

Skeel's has designed such a template to graphically determine the Δg_z of irregularly shaped 2-dimensional bodies. (See figure on next page.)



Dot Chart--In a dot chart, units of area are proportioned so that they represent elements of mass having equal effects at the origin of the chart. Thus, these units increase in size with their distance from the origin. If these elements of area are made small enough, each such area can be represented by a single dot at its center. To determine the

FOR 2-DIMENSIONAL CASE:

$$\Delta g = \frac{0.5 \times 10^{-3}}{S} \times \Delta \rho \times N \quad (\text{milligals})$$

where
 N = number of unit cross-section summed over the body
 $\Delta \rho$ = density contrast (gm/cm^3)
 S = scale factor

NOTE:

Each compartment (Δ) is 5 units of cross-section
 Each cell (\rightarrow) is 1 unit of cross-section
 Each circle (---) is 1/5 unit of cross-section

FOR 3-DIMENSIONAL CASE

$$\Delta g = \frac{0.5 \times 10^{-3}}{S} \times \Delta \rho \times \sum_{i=1}^n n_i F_i \quad (\text{milligals})$$

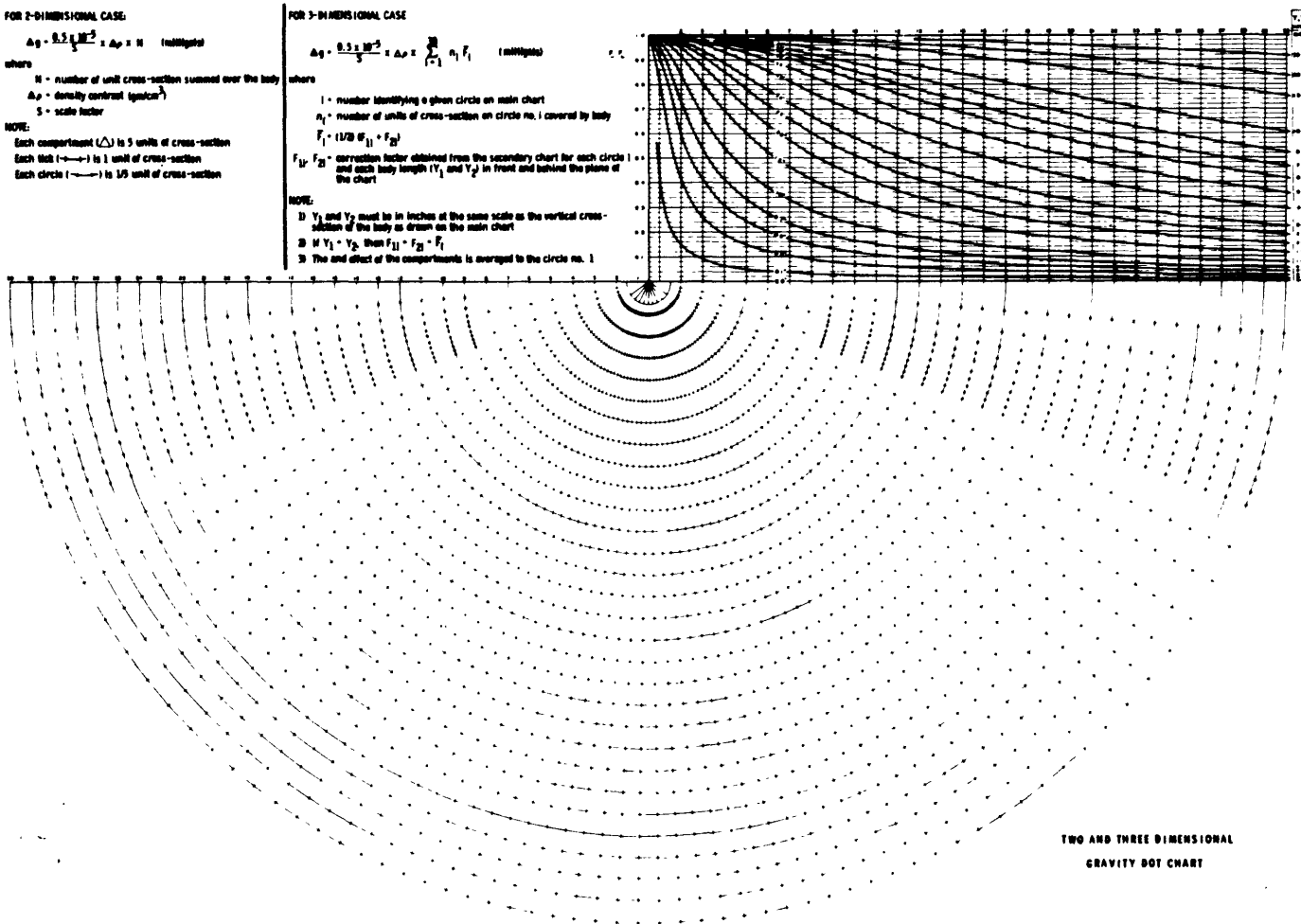
where

i = number identifying a given circle on main chart
 n_i = number of units of cross-section on circle no. i covered by body
 $F_i = (1/20) (V_{1i} + V_{2i})$

F_{1i}, F_{2i} = correction factor obtained from the secondary chart for each circle i and each body length (V_1 and V_2) in front and behind the plane of the chart

NOTE:

- 1) V_1 and V_2 must be in inches at the same scale as the vertical cross-section of the body as drawn on the main chart
- 2) If $V_1 = V_2$, then $F_{1i} = F_{2i} = F_i$
- 3) The end effect of the compartments is averaged to the circle no. 1

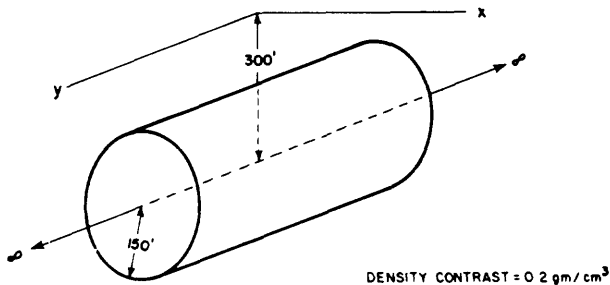


gravity effect of a 2-dimensional mass, it is necessary only to draw an outline to the scale of the dot chart for the body being considered and to count the number of dots lying within the area. The number of dots at each point is multiplied by a factor which depends on the design of the chart, the scale of the cross-section, and the density contrast. By repeating the operation for a number of points along a profile, the calculated gravity effect can be obtained in a straight forward manner.

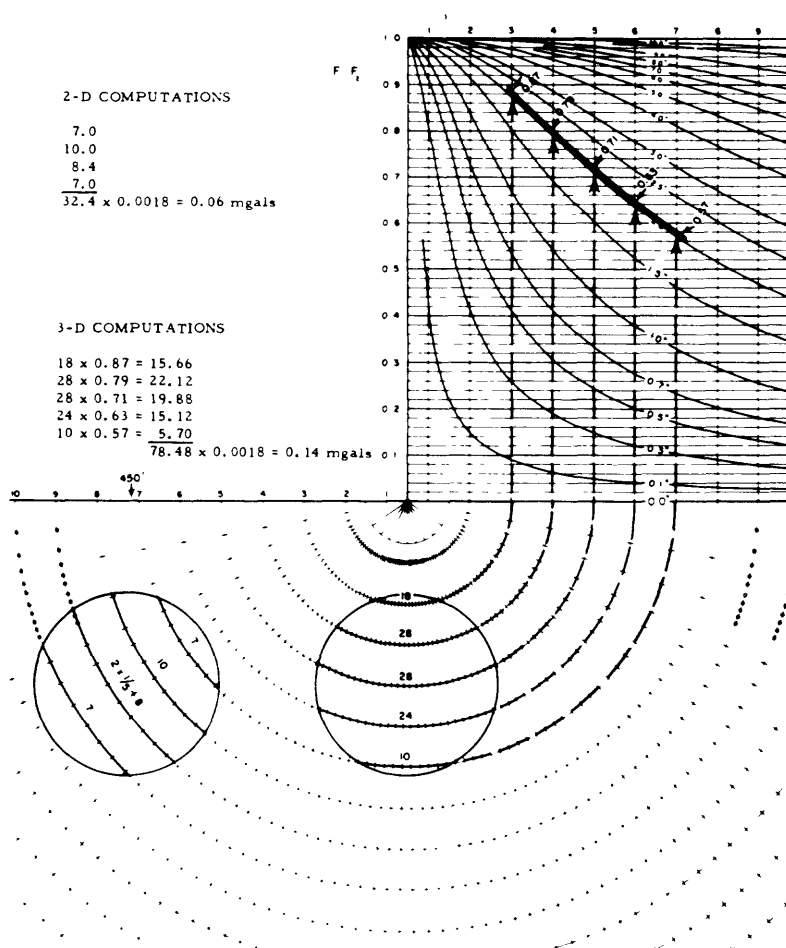
The dot chart developed by Morgan and Faessler (1972)* (shown above) is applicable for 2 and 3-dimensional problems. End corrections are made for 3-dimensional masses.

The following example will illustrate the use of the dot chart. The application is for a horizontal cylinder having infinite strike extent - a 2-D application. The cylinder's cross section is drawn at the scale of 1:1800 (1 inch to 150 feet) and is overlaid on the chart at an offset of 137.16 m (450 ft.) Being a 2-D case, it is sufficient to count the number of units covered by the body's cross section and substitute in the equation $G = C \cdot \rho \cdot S \cdot N$ where $C = 0.05 = \text{constant}$, $\rho = \text{density contrast} = 0.2 \text{ gm/cm}^3$, $S = \text{scale factor} = 1800$, and $N = \text{number of compartments or dots covered by the}$

*Morgan, N. A. and C. W. Faessler, 1972, A Two and Three Dimensional Gravity Dot Chart, Geophysical Prospecting, v. 20, no. 2, pp. 363-374.



Horizontal cylinder.



cross-section of the body = 32.4. This gives a gravity effect of 0.06 mgals. The cross-section of the body is shifted to different locations and the procedure is repeated, giving the values, in the table below, which compare very well with theory.

If the same cylindrical model is considered, but with a finite strike length of 183.88 m (600 ft), the dot chart can still be used. The central profile anomaly would have the same strike length (91.44 m or 300 ft) both in front and behind the plane of the chart. The scale of the cross-section of the body is the same as before, 1:1800 or 1 inch = 150 ft. The proper end correction curve for $x = \text{zero}$ is the 2 inch curve. Also $F_1 = F_2 = \bar{F}$. The computation is made using

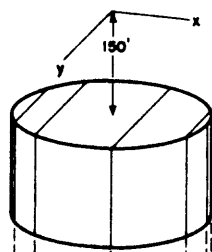
$$G - C \sum_{n_i} \bar{F}_n$$

Station (ft)	G (Chart value) mgal	G (theoretical value mgal)
0	0.19	0.19
150	0.16	0.15
300	0.10	0.10
450	0.06	0.06
600	0.04	0.04
750	0.02	0.03
900	0.02	0.02

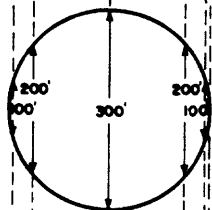
The gravity response at $x = 0 = 0.14$ mgals. The procedure is repeated for other locations, giving the values.

<u>Station (ft.)</u>	<u>g (chart value), mgal</u>	<u>g (computer), mgal</u>
0	0.14	0.14
150	0.11	0.10
300	0.06	0.06
450	0.03	0.03
600	0.02	0.02
750	0.01	0.01
900	0.01	0.01

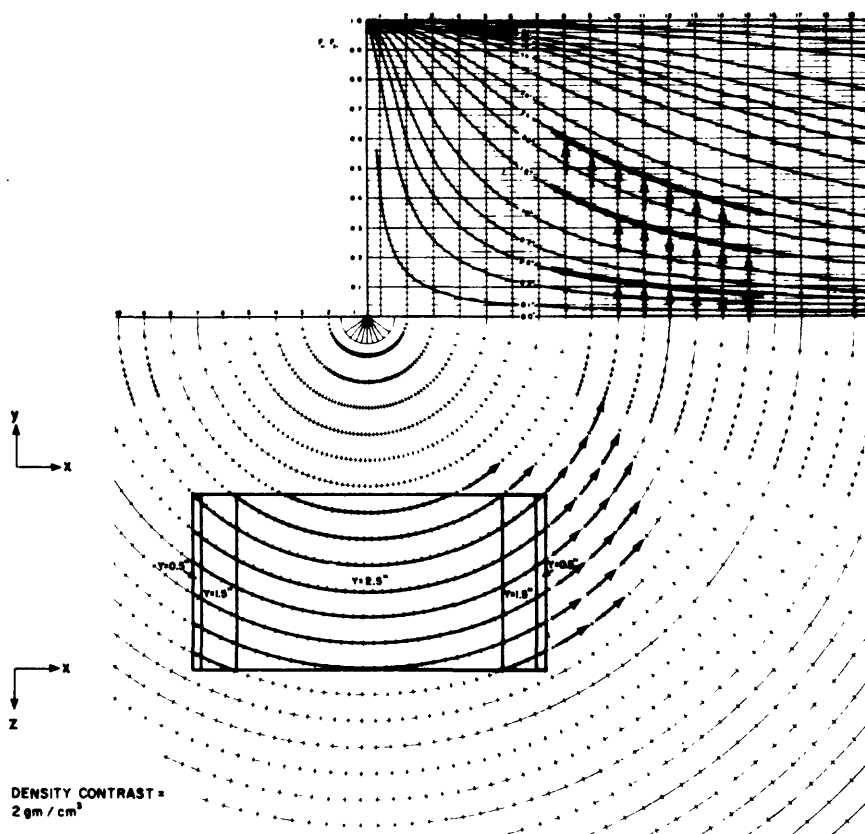
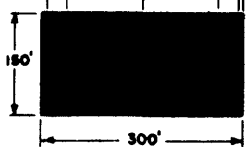
A. 3-D VIEW



B. PLAN VIEW



C. CROSS SECTION



The more complex case of a vertical cylinder may also be considered. The plan and cross-section views of the mass are shown in the preceding figure. The gravity effect on the vertical axis is to be calculated. The strike length varies from zero to 91.44 m (300 feet) and may be divided into an arbitrary number of blocks, each having an approximately constant strike length. In this example, five blocks are considered with a strike length increment of 30.48 m (100 ft). Thus the central block will have a strike length between 60.96 and 91.44 m (200-300 ft) or an average of 76.20 m (250 ft). Each of the two blocks on either side has an average strike length of 45.72 m (150 ft) while each of the outer ones has an average strike length of 15.24 m (50 ft). The cross-section of the body is drawn at a scale of 1:600 (1 inch to 50 ft). The procedure is as before for the second model, but with the correction factor applied to each block according to its average strike length. The calculation is shown in the table below.

<u>Circle No.</u>	<u>Y = 125 ft (2.5 in) no. \bar{F}</u>	<u>Y = 75 ft (1.5 in) no. \bar{F}</u>	<u>Y = 25 ft (0.5 in) no. \bar{F}</u>	<u>SUM</u>
8	(26) (0.605)	(0) (0.410)	(0) (0.150)	15.73
9	(36) (0.550)	(0) (0.370)	(0) (0.130)	19.80
10	(32) (0.510)	(8) (0.335)	(2) (0.115)	19.23
11	(28) (0.470)	(8) (0.310)	(2) (0.105)	15.85
12	(26) (0.440)	(8) (0.285)	(2) (0.100)	13.92
13	(24) (0.410)	(6) (0.260)	(2) (0.090)	11.58
14	(22) (0.385)	(6) (0.245)	(2) (0.085)	10.11
15	(0) (0.360)	(4) (0.230)	(2) (0.080)	<u>1.08</u>
				173.30

$$g = C.S.\rho.\Sigma ni \bar{F}_i =$$

$$= (0.5 \times 10^{-5}) (600) (0.2 \text{ gm/cm}^3) (173.30)$$

$$= 0.64 \text{ mgals}$$

The principal error in using dot charts comes from the interpolation of partially covered compartments.

Solid Angle Chart--For horizontal lamina, the vertical gravity effect at a point 0 is directly proportional to the solid angle ω = omega subtended by the lamina from that point. Thus, if the mass of an irregular body of thickness t and density contrast ρ is considered condensed onto a thin sheet or lamina at its midpoint, its gravity effect is given by

$$g_z = G\omega\rho t$$

or

$$g_z = 2.03\omega\rho t \quad (= 6.65 \omega\rho t \text{ if } t \text{ is in km})$$

where g_z is in mgals, t is in kilofeet, and ω is in steradians.

The approximation of condensing the body of thickness t onto a density sheet is quite good even for a thickness equal to half the depth.

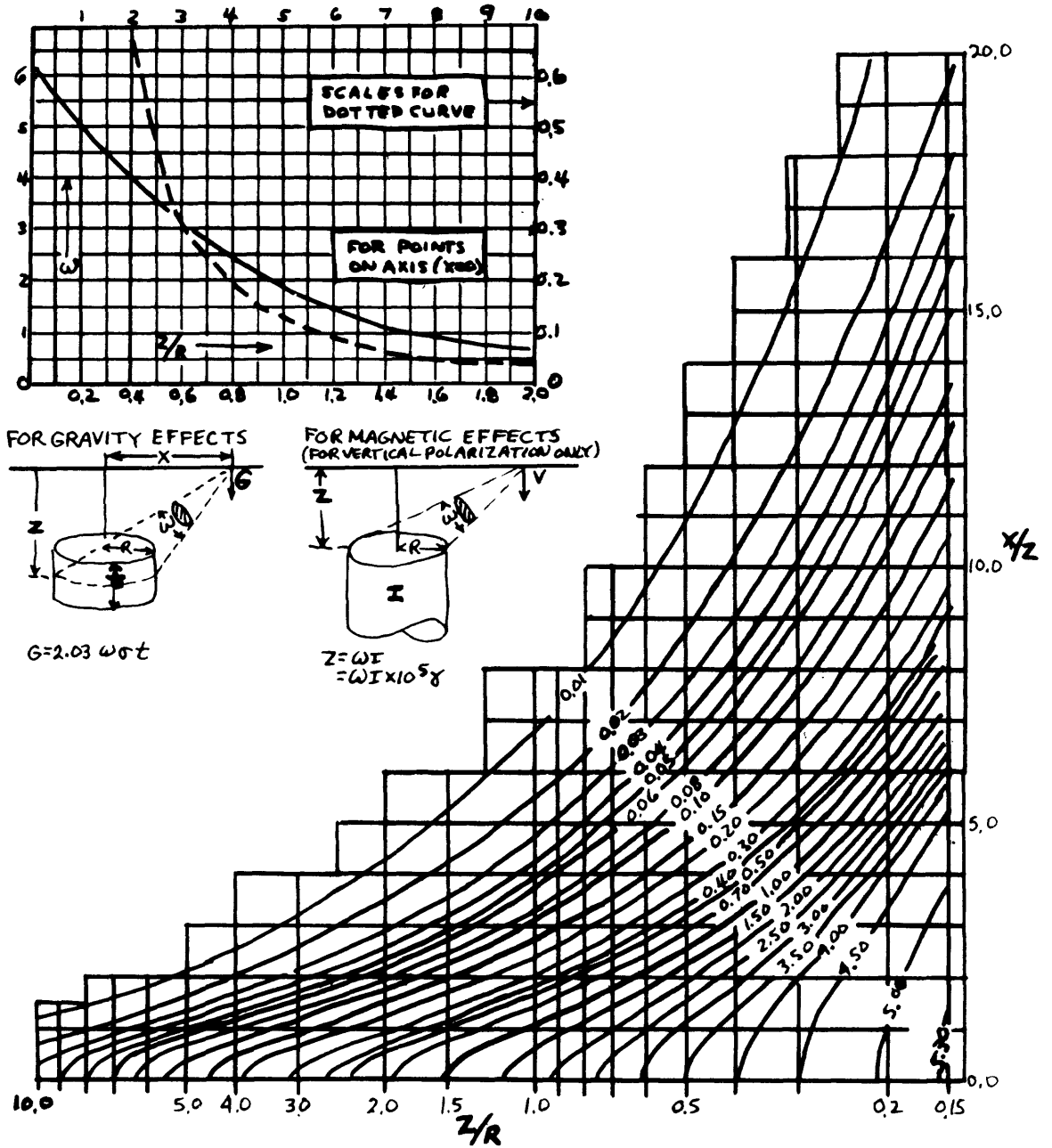
A relatively simple chart can be constructed (see accompanying figure) which will give the solid angles of circular lamina. If the body has relatively great vertical dimensions and is roughly circular in section, it can be approximated by circles representing contours of various depths. The gravity effects for each layer, with its appropriate depth, density contrast, and radius are computed for each point along a profile and added.

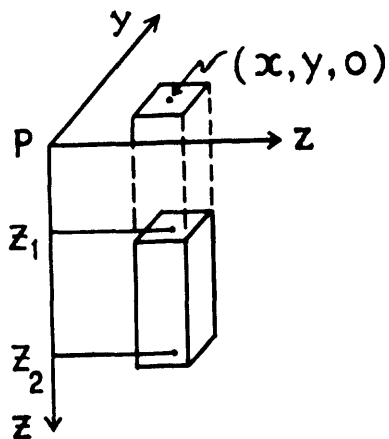
Computation for Irregularly Shaped 3-D Bodies--It is not possible in general to obtain an analytical expression for an irregularly shaped 3-D body. Roy* has published a simple scheme for estimating the effects

*Roy, A., 1961, Rapid Computation of Gravity Anomalies for Irregularly Shaped 3-Dimensional Bodies, Geophysics, v. 26, pp. 645-646.

SOLID ANGLES FOR HORIZONTAL CIRCULAR DISCS

105



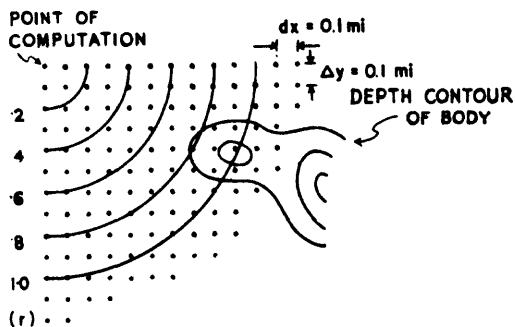


of such bodies. The body is divided into vertical elementary prisms of small cross sections, each of which contributes

$$G\rho dx dy \left(\frac{1}{(x^2 + y^2 + z_1^2)^{1/2}} - \frac{1}{(x^2 + y^2 + z_2^2)^{1/2}} \right)$$

to the gravitational effect at the origin. This is numerically equal to

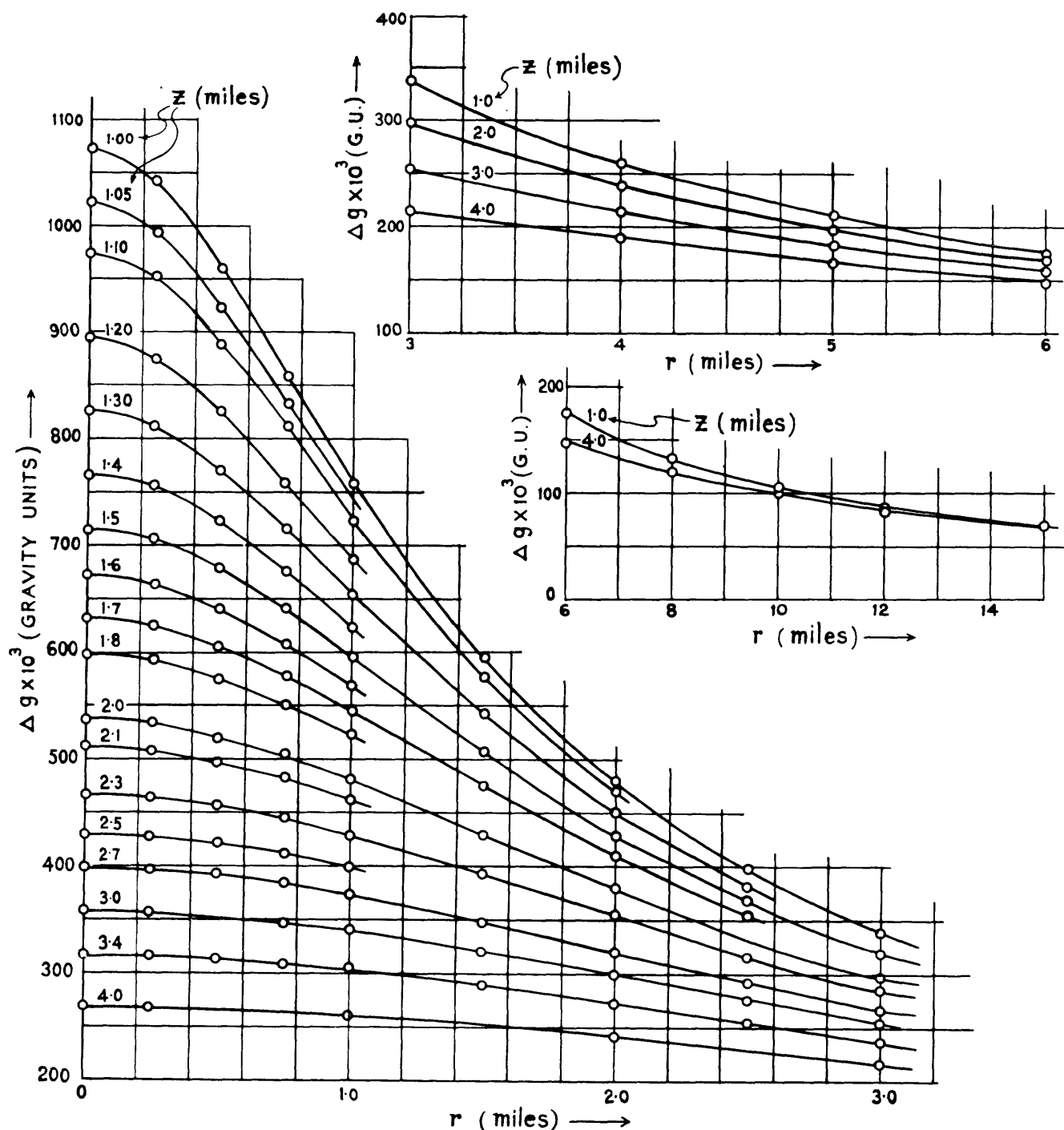
the difference in gravitational potential due to surface distributions of matter, $\rho \text{ gm/cm}^2$ on the two ends of the prism. Thus, one has to compute only one term like $\frac{1.073}{(r^2 + z^2)^{1/2}}$ where $dx(\Delta x) = dy(\Delta y) = 0.1 \text{ mile}$, $\rho = \text{density contrast} = 1 \text{ cgs unit}$, and r and z are expressed in miles. The constant 1.073 includes the gravitational constant, changes units from cm to miles, specifically for $\Delta x = \Delta y = 0.1 \text{ mile}$, and for effects in gravity units ($10 \text{ gravity units} = 1 \text{ mgal}$).



Portion of computation template. To be drawn to the scale of available map with one dot for every $\Delta x \Delta y$. Circles are for different values of r (miles).

The adjoining figure shows part of a transparent template drawn to the scale of the available map, with one dot for every elementary area, $\Delta x \Delta y$. For every dot enclosed by the depth contours of the body, one value of r and two values of z (the deeper value usually being constant for all dots) are read off from the template (properly positioned) and the contours, respectively.

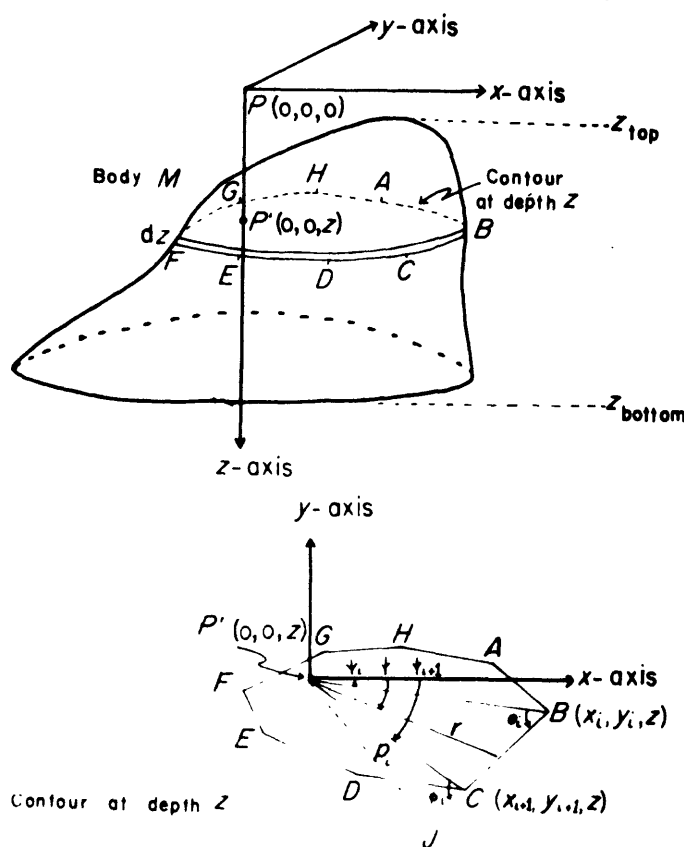
Their gravitational contributions are determined from the chart below, added and multiplied by the actual density contrast. The chart below



... Chart for rapid computation of gravitational anomalies. Gives the vertical component of attraction due to vertical columns of square cross-section (0.01 square mile). r is the horizontal distance of the prism from the point of computation and z is the depth of the prism top. The lower end extends to infinity.

is valid for $Z \gg \Delta x$ or Δy . When shallow depths are involved, Δx and Δy must be smaller. A correction factor is used with the chart. For example, if $\Delta x \Delta y = 0.0025$ instead of 0.01 square miles, the anomaly is divided by 4.

Talwani and Ewing* proposed a technique for calculating the gravitational effect of a 3-dimensional body of arbitrary shape.



Geometrical elements involved in the computation of the gravity anomaly caused by a three-dimensional body.

In this technique, the 3-D body is represented by contours. Each contour is replaced by a horizontal irregular n-sided polygonal lamina. By making the number of sides, n , sufficiently large, the polygons can be made to approximate the contour lines as closely as desired. The gravity anomaly

*Talwani, M., and Ewing, M., 1960, Rapid Computation of Gravitational Attraction of Three-Dimensional Bodies of Arbitrary Shape, *Geophysics*, v. 25, pp. 203-225.

caused by each lamina can be determined analytically at any external point and is plotted as a function of the height of the lamina (i.e., contour elevation). A continuous curve can be obtained relating the heights of the lamina with their gravity anomalies. The total area under this curve gives the gravity anomaly caused by the entire body.

In the figure above, the point P is the point at which the gravity anomaly of the body M is being evaluated. A contour on the surface of the body at depth Z below P is replaced by the polygonal lamina ABCDEF . . . of infinitesimal thickness dZ. The vertical component of gravitational attraction caused by ABCDEF . . . at P is

$$g_z = VdZ$$

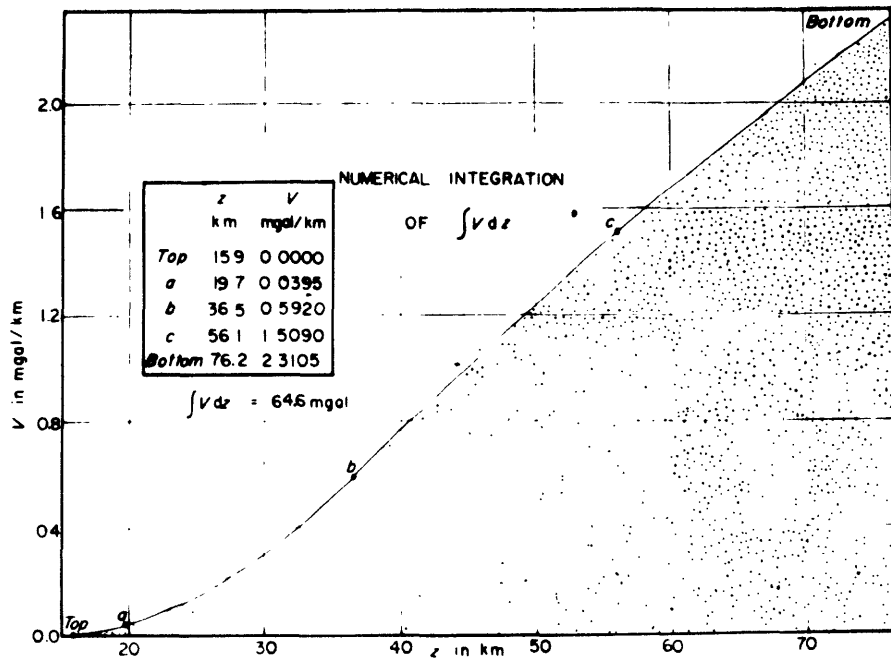
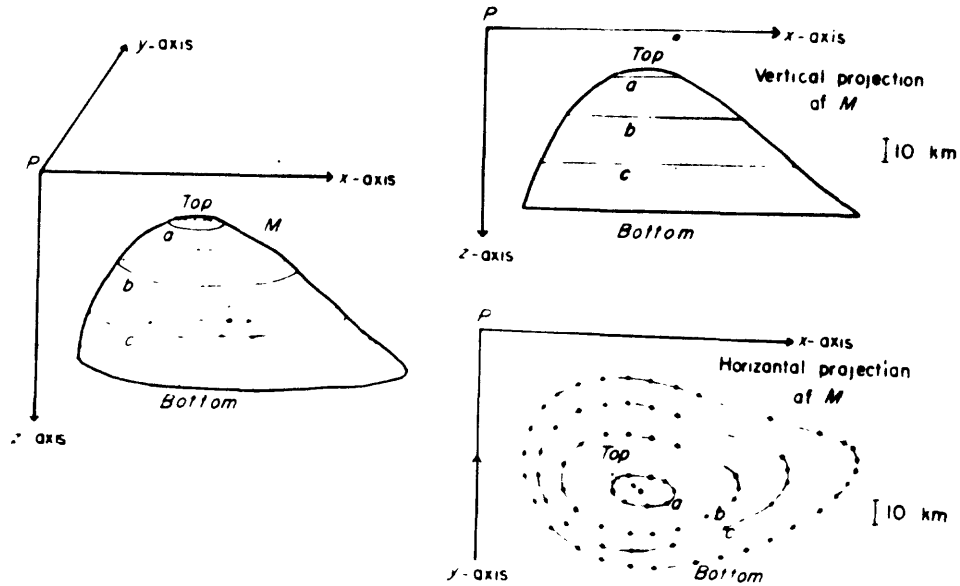
where V is the anomaly caused by ABCDEF . . ., which is given by

$$V = k\rho \left[\sum_{i=1}^n \left\{ \psi_{i+1} - \psi_i - \arcsin \frac{z \cos \theta_i}{(p_i^2 + z^2)^{1/2}} + \arcsin \frac{z \cos \phi_i}{(p_i^2 + z^2)^{1/2}} \right\} \right].$$

The total anomaly caused by the entire body is given by

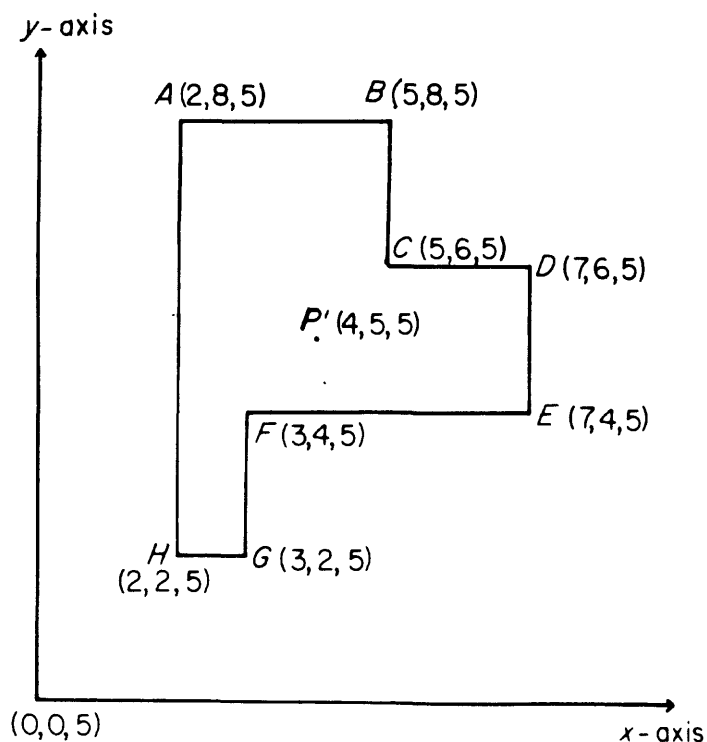
$$g_z \text{ total} = \int_{Z_{\text{bottom}}}^{Z_{\text{top}}} VdZ$$

As an example, evaluate the gravity anomaly of the body M shown in the next figure. The first step is to pick out points on each of the contours in such a way that when they are joined in order, the resulting irregular polygon fits the contour closely. The coordinates of these points are determined. The Z coordinate is the depth of the contour below P. The x and y coordinates are determined by placing a sheet of transparent graph paper on the drawing of the contours.

Numerical integration of the integral $\int V dz$.

The function V is calculated for each contour. The value of V versus Z is plotted and the area under the continuous curve through the points top, a, b, c, and bottom is determined analytically. This value (64.6 mgal) gives the vertical component of the gravitational attraction of M at point P .

For hand computation, a good approximation for the value of V can be obtained by replacing the polygon by another one which fits it closely, but whose sides are alternately parallel to the x and y



Polygon used for "hand computation."

axes. The value of the function V is then given by

$$V = G\rho \left[T - \sum QRU \right]$$

where G is the gravitational constant, ρ is the density contrast, and $T = 2\pi$ when the projection of the point at which the anomaly is being evaluated on the plane of the polygon lies within the polygon; $T = 0$ when the projection lies

outside the polygon. When the point lies on the boundary of the polygon, $T =$ value of the angle subtended at this point by the adjacent sides of the polygon boundary. The summation is carried out over all the

vertices of the polygon, the values of Q , R_L and U being determined from the relations

where

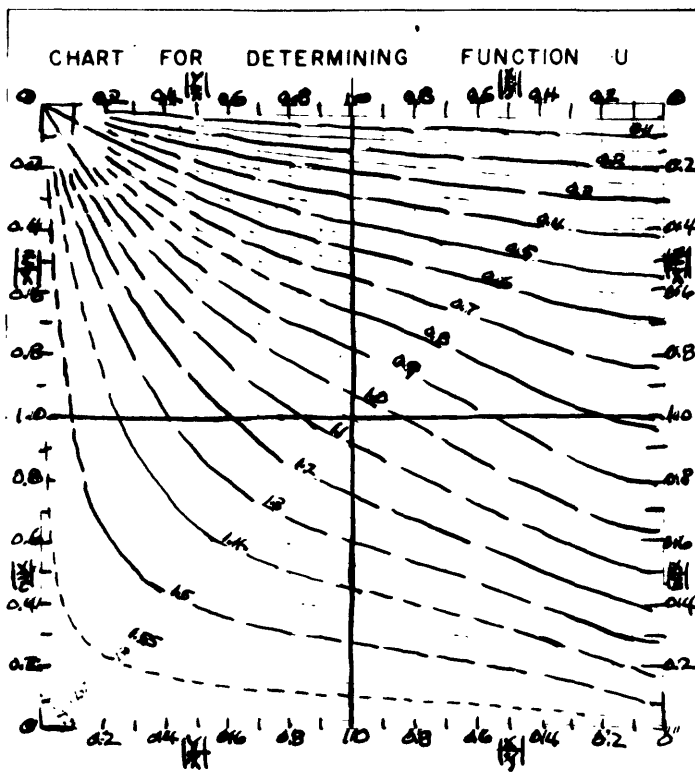
$$U = \left[\arcsin \frac{z}{(x^2 + z^2)^{1/2}} \frac{y}{(x^2 + y^2)^{1/2}} + \arcsin \frac{z}{(y^2 + z^2)^{1/2}} \frac{x}{(x^2 + y^2)^{1/2}} \right],$$

$R = +1$ if the product $xyz > 0$

$R = -1$ if $xyz < 0$.

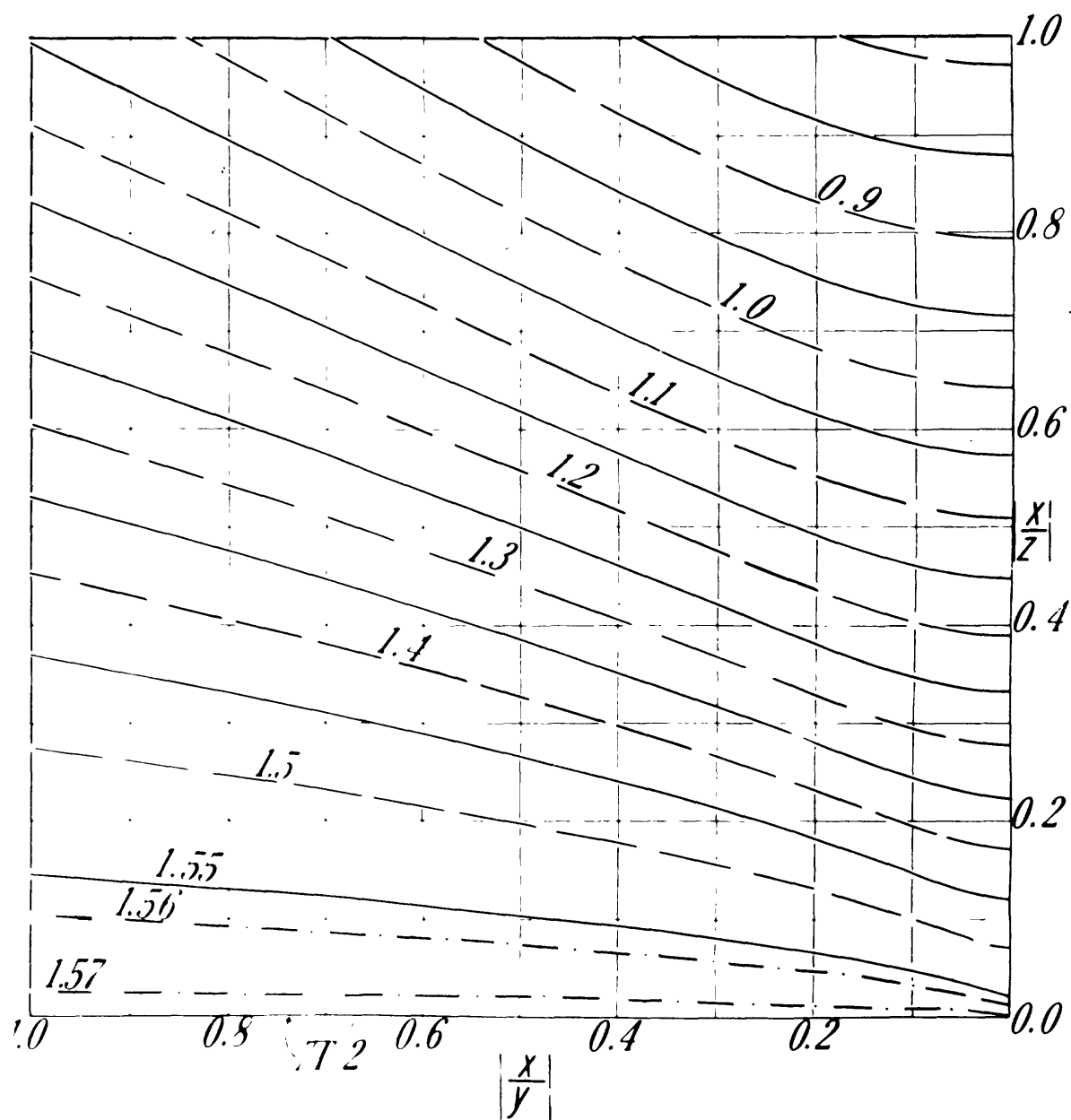
x , y , z being the coordinates of the polygon referred to the point at which the anomaly is being determined, as origin.

$Q = +1$ and -1 for successive vertices of the polygon. For vertices B, D, F in the above figure, $Q = -1$.

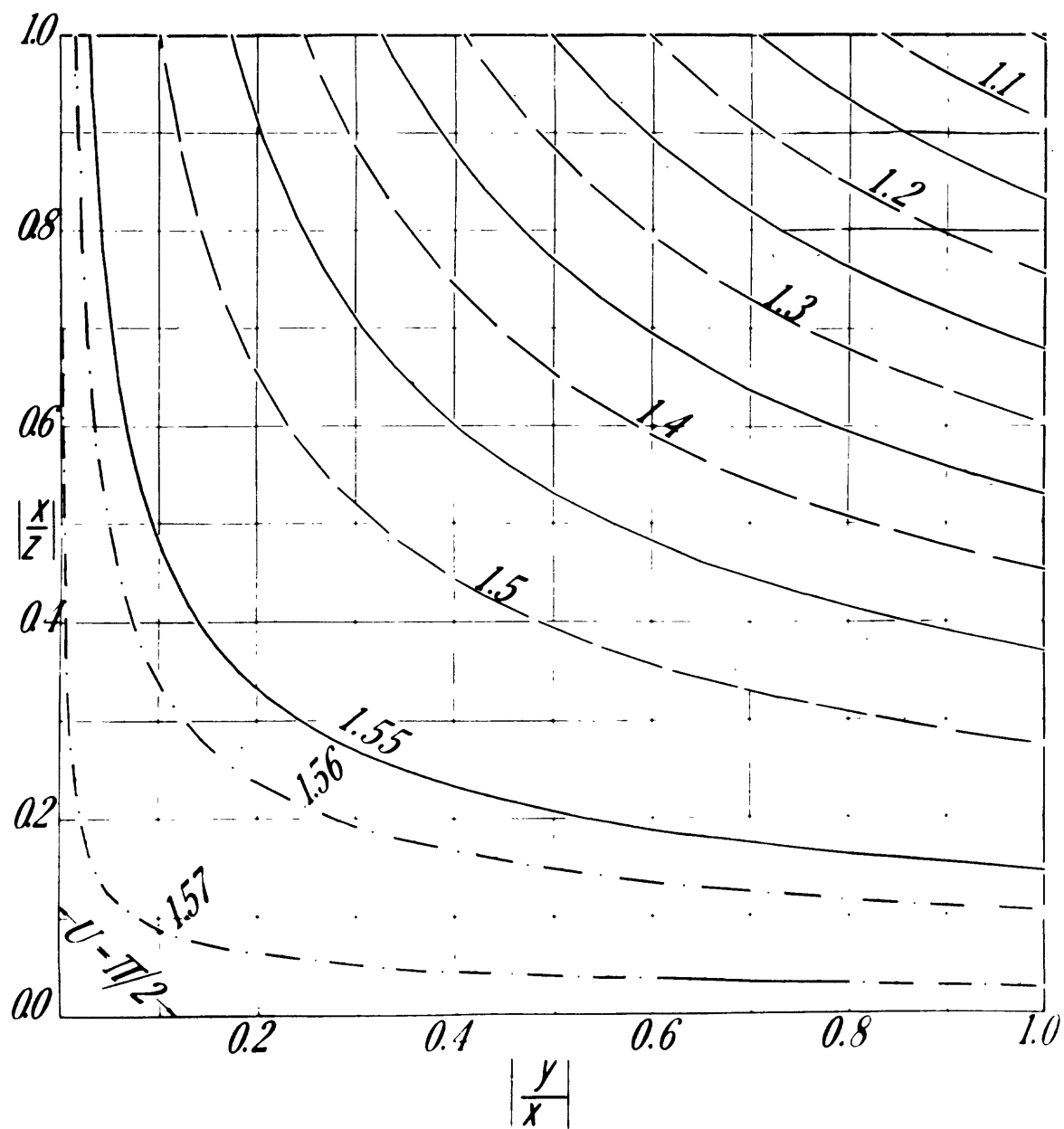


NOTE: The four quadrants of the chart are expanded in the following pages.

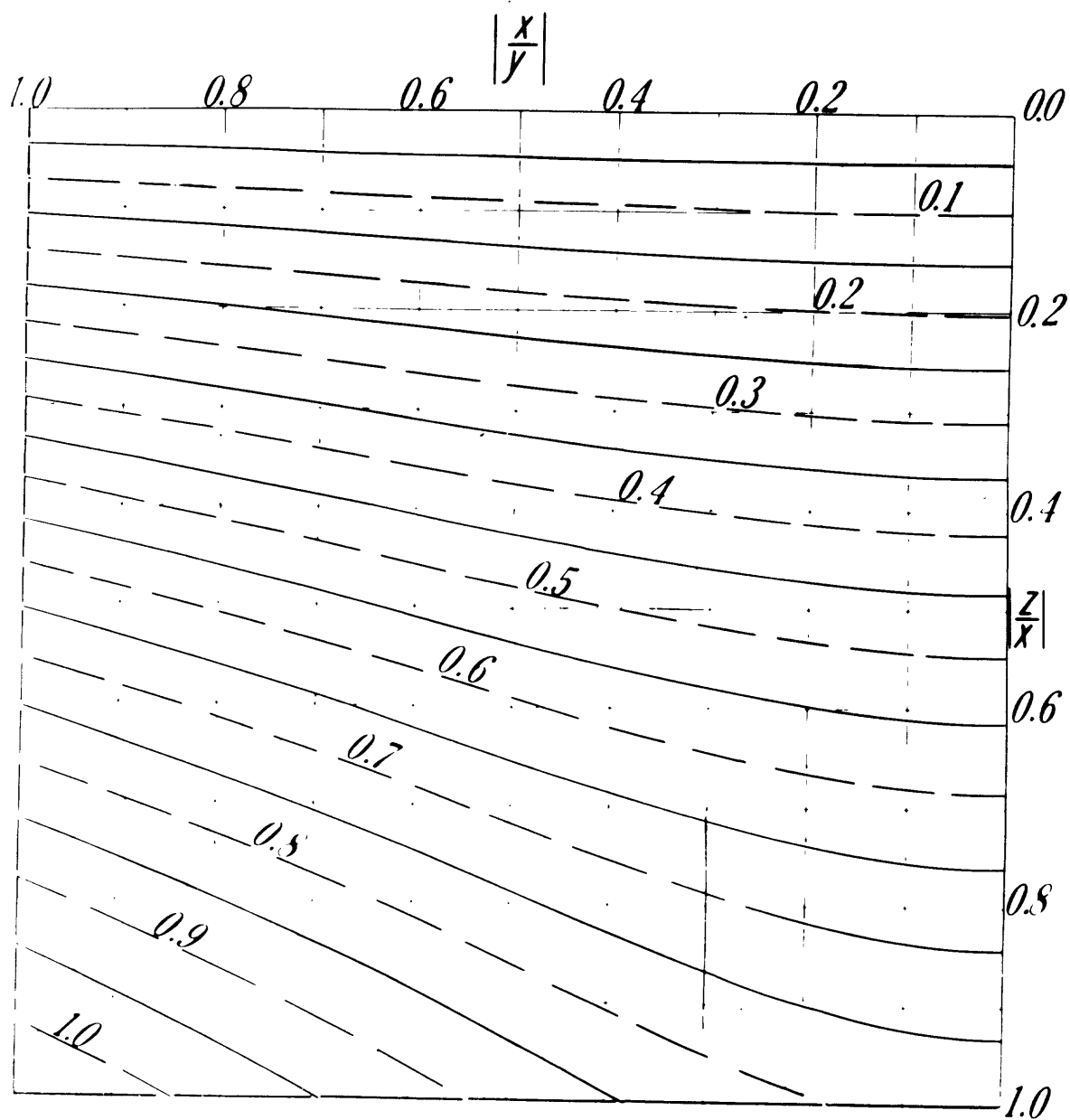
The value of U can be obtained from the chart for any set of values of x , y , z . Since the choice of the x and y axes is arbitrary, they can be interchanged to facilitate computation. For example, to determine U at a point where the x , y , and z coordinates are 50 km, 5 km, and 2.5 km, $\left| \frac{z}{x} \right| = 0.05$ and $\left| \frac{y}{x} \right| = 0.1$. From the chart, U is



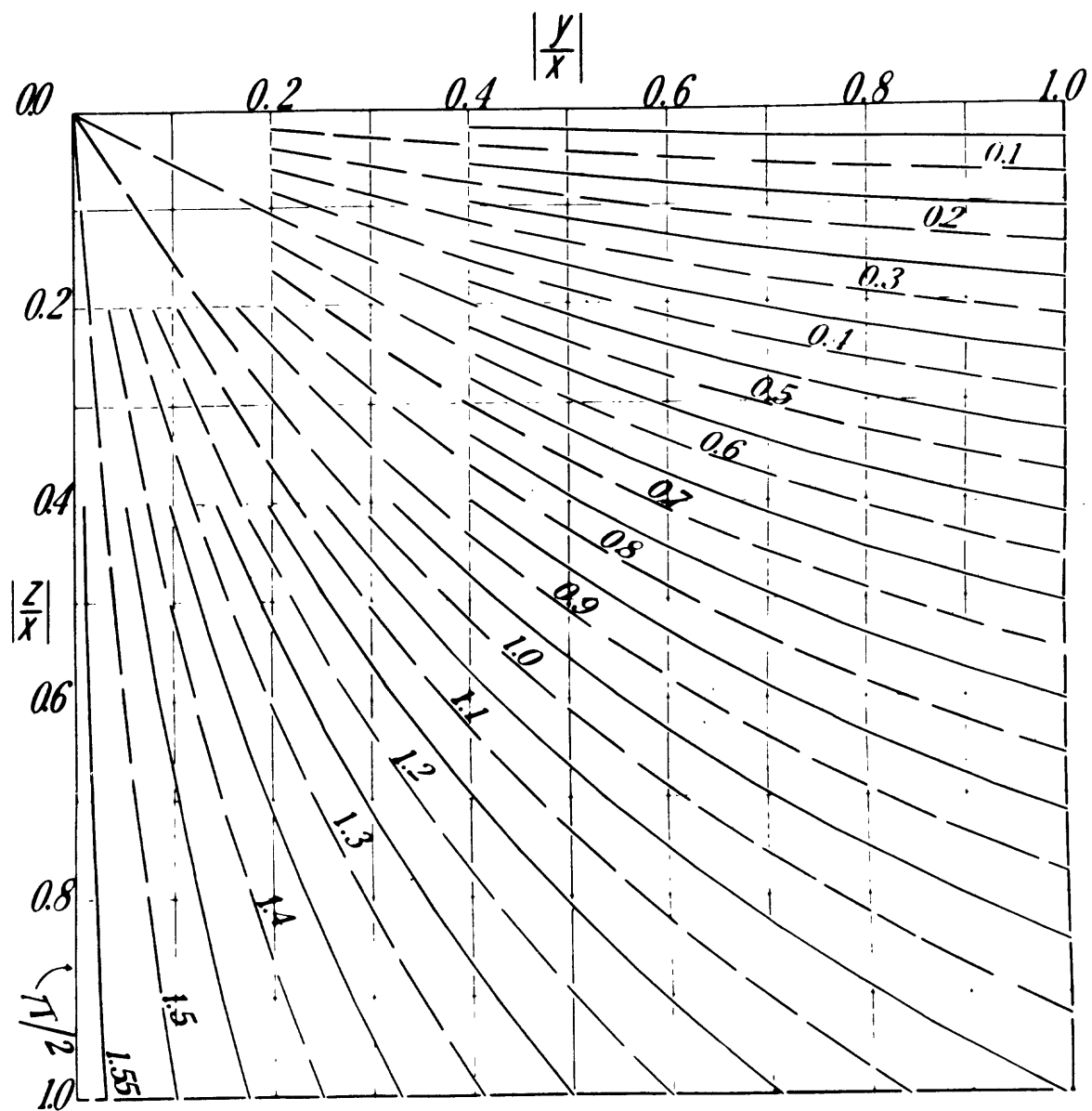
Lower right quarter of Fig.



Lower left quarter of Fig. 1



Upper right quarter of Fig. .



Upper left quarter of Fig. .

determined to be 0.45, but the precision is small. Interchanging the x and y coordinates gives $x = 5$ km, $y = 50$ km, and $Z = 2.5$ km. This gives $|\frac{z}{x}| = 0.5$ and $|\frac{x}{y}| = 0.1$. From the chart, a value for U of 0.466 is obtained. The correct value is 0.4661. When $|x| = \infty$ with a finite value of y, U cannot be determined without interchanging coordinates.

The physical meaning of U is as follows. $(\frac{\pi}{2} - U)$ represents the solid angle subtended at a point by a horizontal rectangle at a distance Z below it, the sides of the rectangle having lengths x and y and one of the corners of the rectangle lying directly below the point.

Once the value of U is obtained from the chart, the value of V is determined. V is plotted as a function of Z, the depth of the polygonal lamina. This is repeated for lamina representing all the contours. A smooth curve is then drawn through the (V, Z) plots and the area bounded by this curve, the Z-axis, and the two lines parallel to the V axis (corresponding to the values of Z which give the top and bottom of the irregularly shaped body) is determined. This area gives the total anomaly caused by the body. If Z is in km, ρ in gm/cm³, and a value of 6.67 is chosen for G, the result is obtained directly in mgals.

The following example illustrates the calculational procedure. Referring to the polygon shown earlier, the coordinates of the vertices are noted on the figure and in the table which follows. The point

at which the calculation is to be made is at (4, 5, 0). In the figure, P' is the projection of point P on the plane of the polygon. In the table, column 3 lists the coordinates of the vertices of the polygon with respect to P. In column 4, the ratios $|\frac{x}{y}|$ or $|\frac{y}{x}|$ and $|\frac{x}{z}|$ or $|\frac{z}{x}|$ are evaluated. The curves shown earlier for the evaluation of the function U are constructed only for coordinate ratios less than unit. Next, a point is located on the chart whose coordinates are given by the ratios determined in the table. For A, $|\frac{x}{y}| = 0.667$ and $|\frac{x}{z}| = 0.4$, so this point is located in the bottom right quadrant of the chart. This point lies between the curves for U having the values 1.35 and 1.40. By interpolation, a value of 1.300 is obtained and is entered in column 5 of the table. As a check for this value, the x and y coordinates of A are interchanged. For the interchanged coordinates, $x = 3$, $y = -2$ and $|\frac{y}{x}| = 0.667$ and $|\frac{x}{z}| = 0.6$; these ratios are noted in column 6.

TABLE
VARIOUS STEPS INVOLVED IN THE "HAND-COMPUTATION" OF FUNCTION V

(1) Vertex	(2) Coordinates of Vertex	(3) Coordinates of Vertex referred to point of computation	(4) Coordinate Ratios				(5) U	(6) Interchanged Coordinate Ratios				(7) U After Interchange	(8) Mean Value of U	(9) R	(10) Q	(11) QRU
		x y z	x/y	y/x	x/z	z/x		x/y	y/x	x/z	z/x					
A	2 8 5	-2 3 5	0.667		0.400		1.380		0.667	0.600		1.378	1.379	-1	-1	+1.379
B	5 8 5	1 3 5	0.333		0.200		1.471		0.333	0.600		1.469	1.470	+1	+1	+1.470
C	5 6 5	1 1 5	1.000		0.200		1.530	1.000		0.200		1.530	1.530	+1	-1	-1.530
D	7 6 5	3 1 5		0.333	0.600		1.469	0.333		0.200		1.471	1.470	+1	+1	+1.470
E	7 4 5	3 -1 5		0.333	0.600		1.469	0.333		0.200		1.471	1.470	-1	-1	+1.470
F	3 4 5	-1 -1 5	1.000		0.200		1.530	1.000		0.200		1.530	1.530	+1	+1	+1.530
G	3 2 5	-1 -3 5	0.333		0.200		1.471		0.333	0.600		1.469	1.470	+1	-1	-1.470
H	2 2 5	-2 -3 5	0.667		0.400		1.380		0.667	0.600		1.378	1.379	+1	+1	+1.379

$$\Sigma(QRU) = +5.698$$

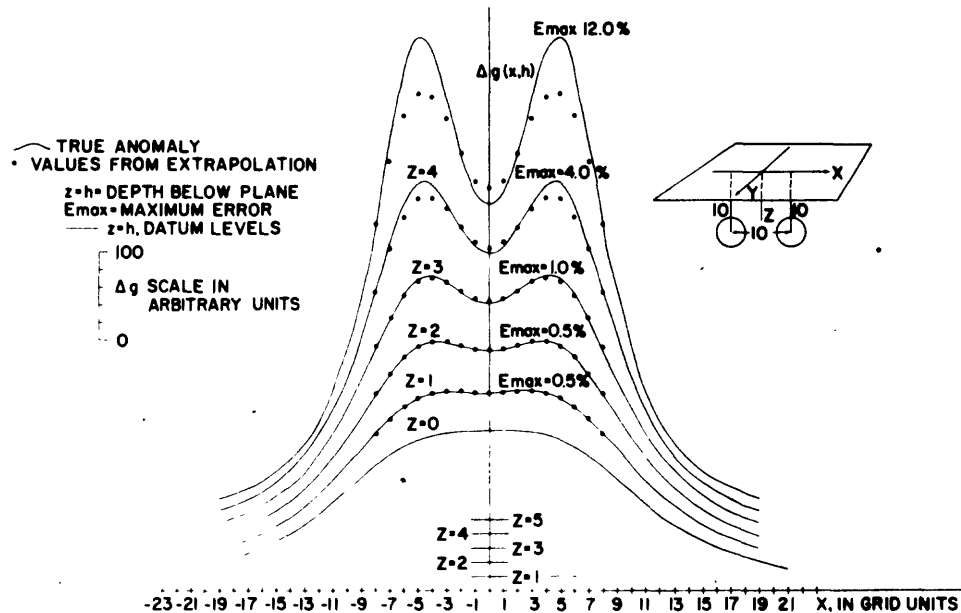
Again a point with these coordinates is located in the bottom left quadrant of the chart. By interpolation, a value of 1.378 is obtained for U at this point and is listed in column 7. The two values obtained for U should be identical; the difference denotes the errors made in the interpolations. For evaluating V, a mean value of 1.379 is adopted for U and entered in column 8. The product xyz at A is -30. Since it is negative, R = -1 (column 9). The value of the y-coordinate at A equals the value of the y-coordinate at B, thus Q = -1 (column 10). The product QRU = 1.379 and is entered in column 11. In a similar manner the product QRU is evaluated at all the other vertices of the polygon and $\Sigma(QRU)$ is evaluated by adding all the terms, giving 5.698. The value of T is 2π since the polygon subtends this total angle at P'. Thus

$$V = G\rho \left[2\pi - 5.698 \right]$$

If a density of 1 gm/cm^3 is assumed for ρ and a value of 6.67 for G, a value of 3.90 mgal/km is obtained for V.

Analytical Continuation of Potential Field Data--If the gravity or magnetic intensity is known on the surface of the earth or on a plane above the earth, the intensity can be projected upwards to higher levels (upward continuation) or downwards (downward continuation) to levels closer to the source of the anomaly. Upward continuation gives a smoother field, downward continuation a sharper field than at the surface of the measurement.

Downward continuation is applied for anomaly separation. The technique is particularly useful for resolving the overlapping effects of sources which are close together. An example is two spheres buried



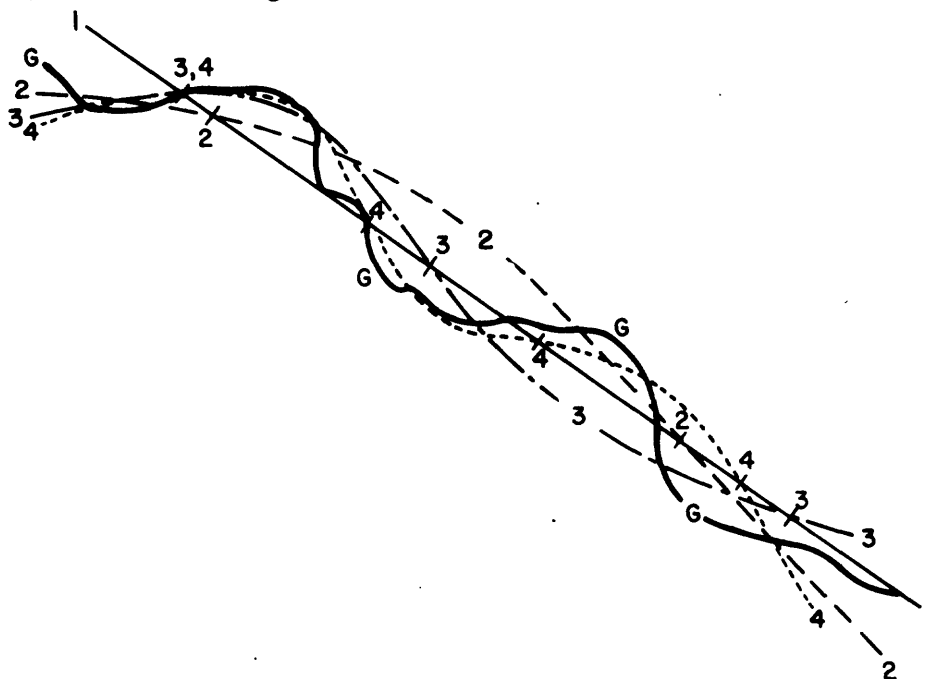
Downward continuation of composite gravity anomaly of two spheres.

at 10 depth units below the surface. The gravity anomaly at $Z = 0$ (surface) does not show the separate sources, but, when continued downward clearly shows the effects of the separate sources. Because aeromagnetic measurements are made at substantial elevations above the ground, downward continuation has considerable application in magnetic data interpretation.

Upward continuation always gives a smoother map than the original map. Therefore, the technique has been used as a form of smoothing as a basis for anomaly separation.

The computational scheme is similar to that used for the second derivative--arrays of values and circles of different radii. The continuation formulas usually involve values over a wider area than second derivative schemes. The continuation schemes proposed by Henderson* are widely used. They are described in Appendix B along with a Fortran listing of a digital computer program used to implement them.

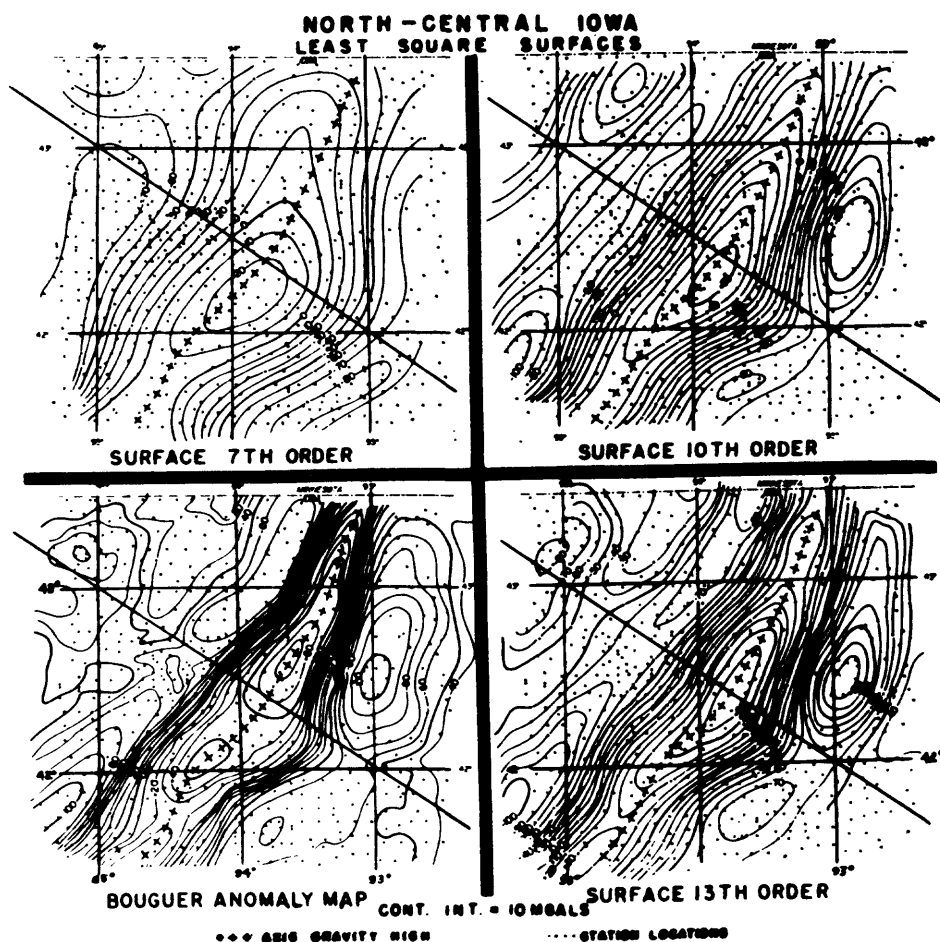
Surface Fitting Methods--An approach to anomaly separation involves two-dimensional surface fitting to the Bouguer gravity data. The general concept is illustrated in the accompanying figure, using a profile rather than a 2-dimensional array of data. Observed gravity is represented by curve G. A first degree least squares fit would be a straight line (curve 1). A second degree fit could have one reversal and two line



Schematic curves illustrating least squares surface fit technique. Curve G represents an observed gravity profile. Curves 1, 2, 3, and 4 represent fits of successively higher degrees. The "residual" for a given order is the difference of the observed from the corresponding surface fit.

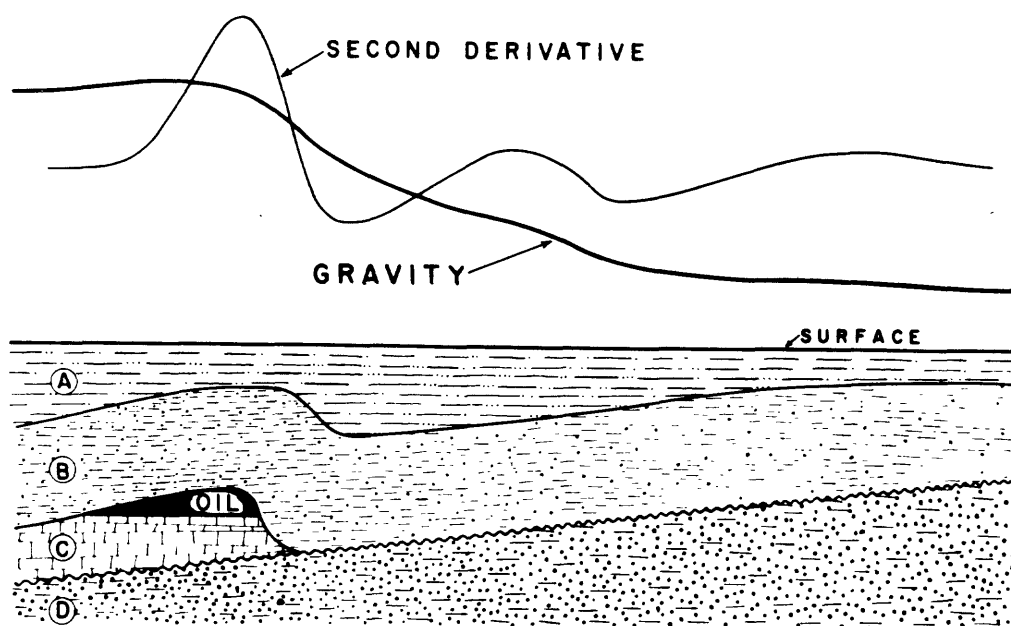
*Henderson, R., 1960, A Comprehensive System of Automatic Computation in Magnetic and Gravity Interpretation, Geophysics, v. 25, p. 569.

crossings (curve 2). A third degree curve could have two reversals and three line crossings (curve 3) and so on. In each case, the sum of the squares of the differences between the calculated curve and the observed gravity (G) is a minimum. The differences between the calculated and observed values are the residuals. As the order of the approximation increases, the residuals decrease. An example of surface fitting and the comparison with the Bouguer map is shown below.



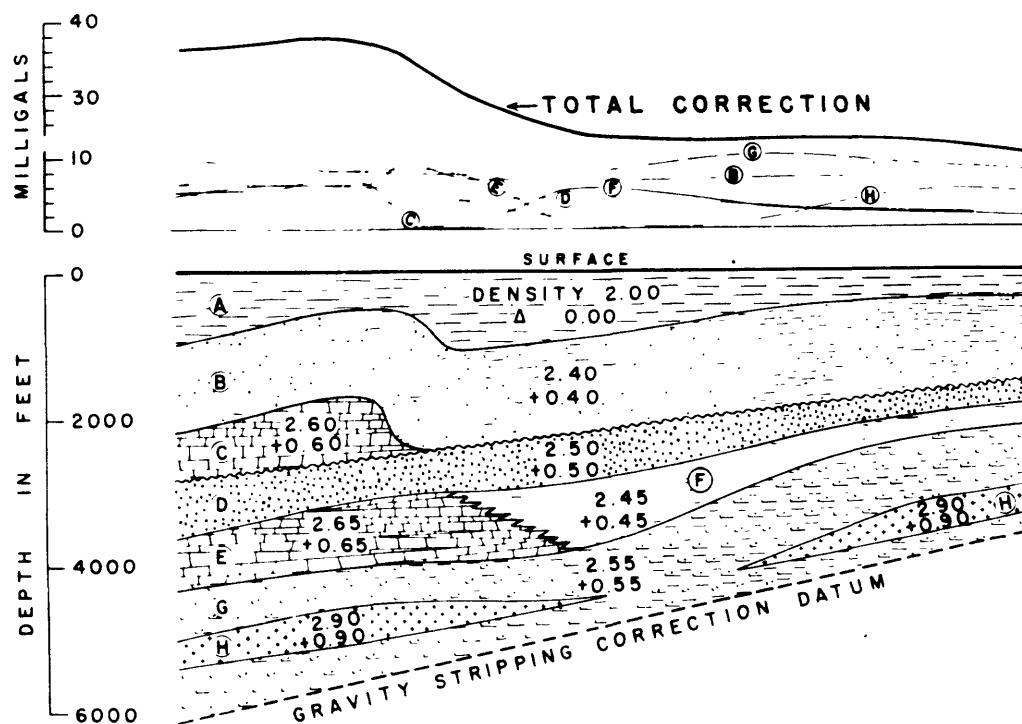
Example of least square surface fit; lower left map is Bouguer gravity. Other maps show gravity calculated with successively higher orders of fit (Coons et al, 1967).

Stripping--A gravity survey may be reinterpreted many times in the light of new evidence and knowledge. An interpretational technique called "stripping" was proposed by Hammer* in 1963. This technique enables the interpreter to look at the effect of deep structures after subtracting the effect of known shallow subsurface features. The deep gravity effect originates below the stripping datum. The stripping technique will be described below, using hypothetical gravity survey results. The shallow

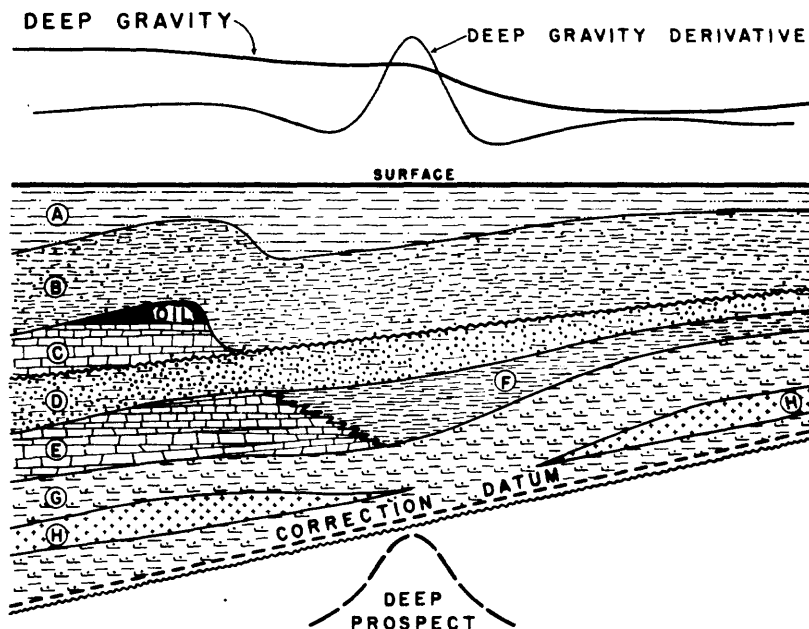
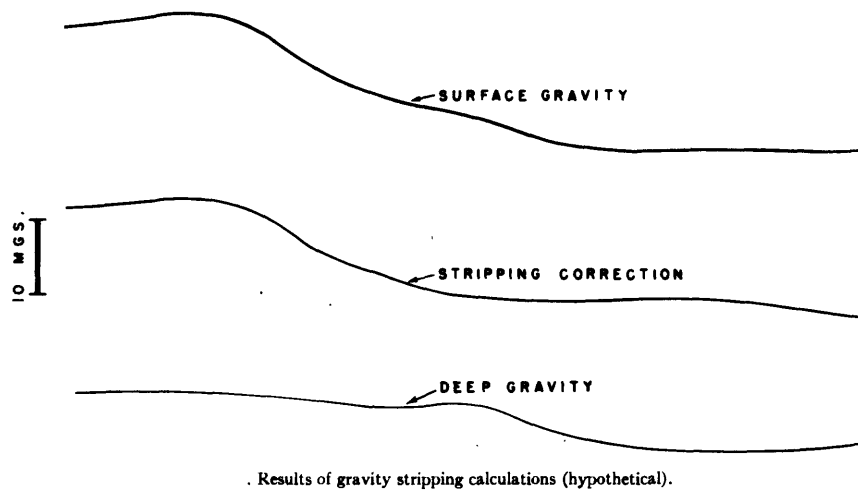


subsurface structure and formation properties are defined through drilling and logging. These data provide a basis for calculating and subtracting (stripping) gravity effects of the known subsurface section down to the depth of the well control. The correction datum is selected as a sloping plane in order to avoid having the datum cut more than one density stratum. The regional gravity effect of the sloping datum does not complicate the interpretation of the results.

*Hammer, S., 1963, Deep Gravity Interpretation by Stripping, *Geophysics*, v. 28, pp. 369-378.



Calculations of the gravity effects of the various density strata are carried out separately by standard techniques. The infinite flat plate approximation is adequate. The calculated gravity effects of strata B to H are shown in the above figure. The calculations give gravity differences in terms of density contrasts referred to stratum A. The sum of the contributions is of the order of 15 mgal and is the total stripping correction. Subtracting the stripping correction from the surface gravity values gives the gravity effect of the deep structure (see figure on next page). Note that the large anomaly on the left is completely eliminated in the deep gravity, but the central anomaly is enhanced. This means that the central anomaly originates below the stripping datum.

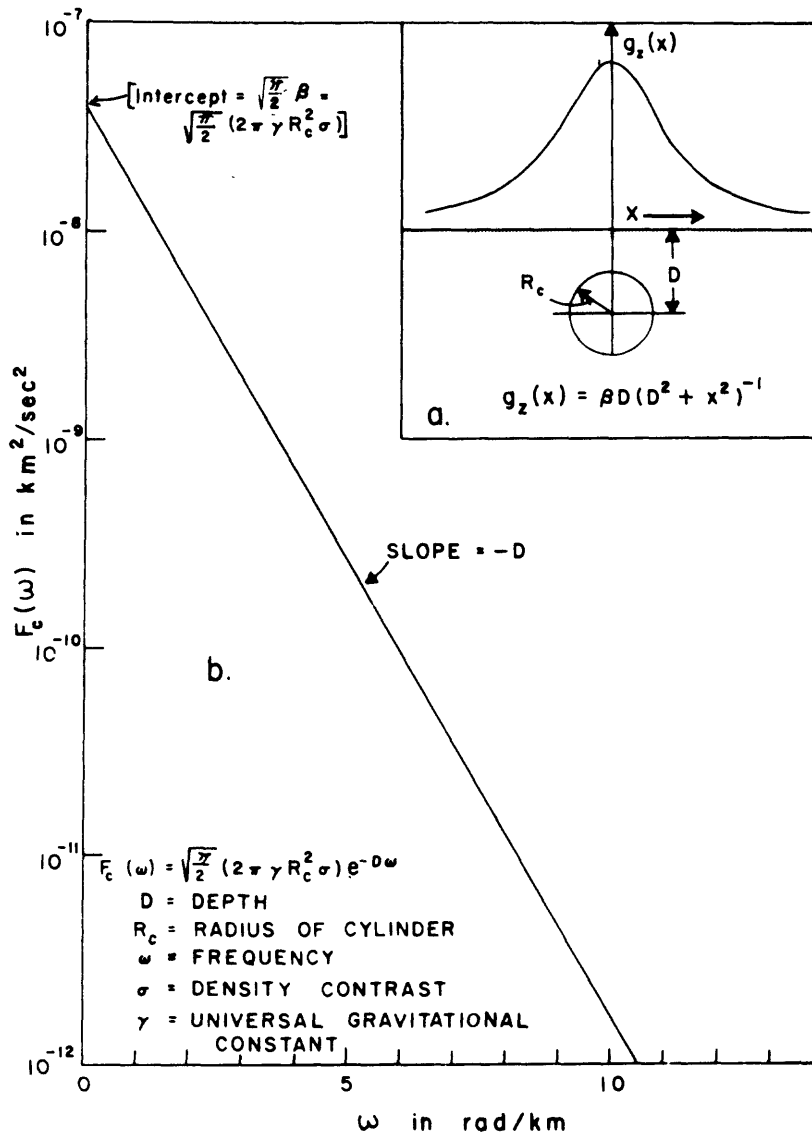


Frequency Analysis of Gravity Data--A gravity map can be transformed into the wave number* domain using the Fourier transform. By this technique, the observed gravity map is approximated by the sum of a series of harmonic waves in the x-y plane that have different spatial frequencies, azimuths, amplitudes, and phase relations. This set of waves is called a spectrum. Thus, a filtering system can be devised which will enhance

*Wave number = 1/wavelength

certain components and eliminate others in a manner that is quite analogous to an ordinary electrical filter which will pass certain frequencies and will reject others. (see appendix C)

It is instructive to analyze the frequency spectrum for simple bodies*-cylinder, sphere, and fault. Because the character of an anomaly of a regular body is determined by depth, density, and size, the frequency spectrum of such a body should contain information regarding the same variables.



Cylinder--The

vertical gravity effect at each point along a profile perpendicular to a buried cylinder is given by (see figure)

$$g_z(x) = \frac{\beta D}{D^2 + x^2}$$

$$(\beta = 2\pi R^2 \sigma)$$

Because $g_z(x)$ is an even function, the Fourier transform is given by

$$F(\omega) = \frac{2\beta D}{\sqrt{2\pi}} \int_0^{\infty} \frac{\cos(\omega x)}{D^2 + x^2} dx$$

Solving:

$$F(\omega) = \sqrt{\frac{\pi}{2}} \beta e^{-D\omega}$$

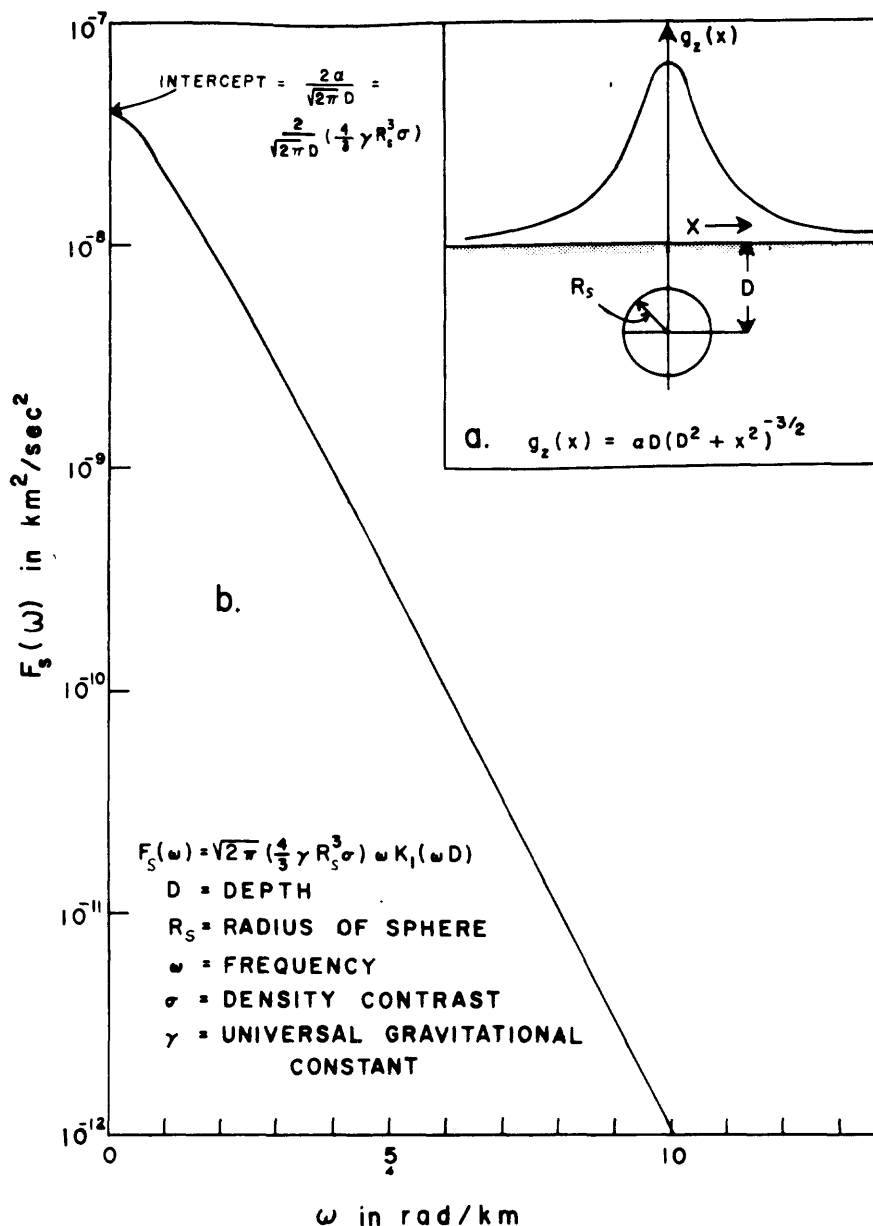
* Odegard, M. E. and Berg, J. W. Jr., 1965, Gravity Interpretation using the Fourier Integral, Geophysics, v 30, pp 424-438.

A plot of the exact integral versus ω on a semilogarithmic scale depicts

$$\ln (F(\omega)) = \ln \left(\sqrt{\frac{\pi}{2}} \beta \right) - D\omega$$

and is linear with a slope equal to the negative of the depth and an intercept related to the density and size of the cylinder.

Sphere--The Fourier transform for the gravitational attraction of a sphere is more complicated and involves a zero-order modified Bessel function of the second kind. The spectrum is similar to that for the cylinder and approaches an exponential as ω becomes large. (see figure)



Two-Dimensional Filtering of Gravity Data-- A 2-dimensional set of data, such as that obtained in a gravity or magnetic survey, can be thought of as a superposition of potential fields due to a subsurface distribution of sources. Consequently, linear-methods of 2-dimensional filtering (e.g., the second derivative, downward continuation) can be used to separate the various components according to their wave number spectrum. The concept of the application of two-dimensional Fourier transforms to two-dimensional data sets, such as gravity and magnetic survey data, is well established. A set of two dimensional data, $f(x,y)$, in the space domain can be represented in the wave number domain by the 2-D Fourier transform

$$F(u, v) = \int_{-\infty}^{\infty} \int_{-\infty}^{\infty} f(x, y) e^{-i2\pi(ux + vy)} dx dy$$

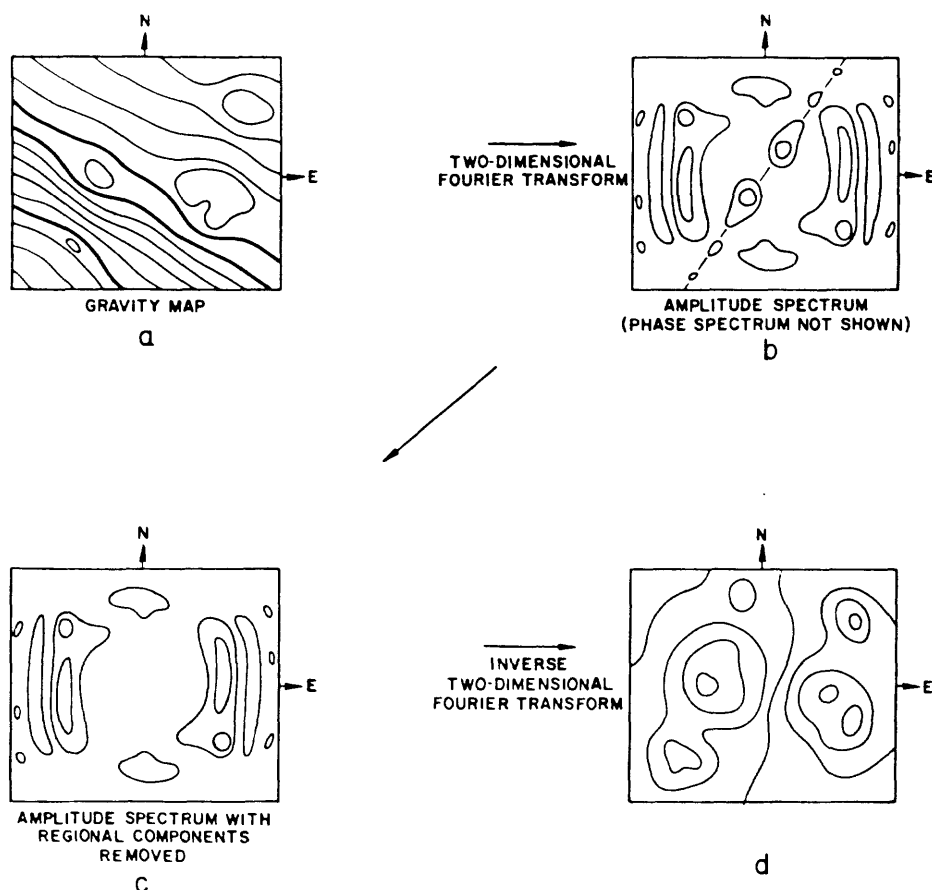
where u, v are the wave numbers. The inverse Fourier transform is given by

$$f(x,y) = \int_{-\infty}^{\infty} \int_{-\infty}^{\infty} F(u,v) e^{i2\pi(ux + vy)} du dv$$

These equations describe an analysis of the 2-D function $f(x,y)$ into components of the form $\exp \left[i2\pi(ux+vy) \right]$, which are sinusoids.

The process of using spatial frequency domain characteristics for separating gravity anomalies is illustrated with the idealized gravity map*

*Nettleton, L. L., (1976), Interpretation of Gravity Data, McGraw-Hill Publishing Co., New York, p 162.



Idealized separation of regional and anomalies using frequency-domain characteristics. Long wavelengths, i.e., small wave numbers, are plotted at the center of the diagram; hence the data involving the regional appear near the center of the amplitude-spectrum plot; recomposing the spatial-data map from the wavelength (or wave number) requires phase information.

shown in the accompanying figure. The low-wave number (regional) trend is associated with an east-southeasterly orientation. The higher-wave number anomalies show no preferential direction. In the spatial frequency (wave number) domain, the data components corresponding to the regional trend and the anomalies of interest exhibit distinctive characteristics. The basic analysis procedure is as follows: (1) use the 2-D Fourier transform to calculate the wave number amplitude and phase spectra, (2) Filter or remove those elements in the spatial frequency domain that correspond to the regional effect, (3) apply the inverse Fourier transform to obtain a gravity map that shows primarily the anomalies of interest. Perfect separation of gravity anomalies cannot be accomplished. The particular distribution of spatial frequencies will vary as a function of distance to the source and the source characteristics; it will never consist of a single-frequency component or even a small number of components unless the source is infinite in extent

Convolution of 2-dimensional data with a 2-dimensional operator or filter is an important concept. This process is represented in the spatial domain by the expression

$$G(x,y) = \int_{-\infty}^{\infty} \int_{-\infty}^{\infty} h(x-\lambda, y-\rho) k(\lambda, \rho) d\lambda d\rho$$

where $G(x,y)$ = output of the convolution process

$h(x,y)$ = input data

$k(\lambda, \rho)$ = linear operator or filter,

and in the wave number domain by

$$G(u,v) = H(u,v) \cdot K(u,v)$$

Symbolically, the filtering of any arbitrary input function is represented as follows in the (x,y) domain.

$$G_{\text{out}}(x,y) = h_{\text{in}}(x,y) * k(x,y)$$

and in wave number (u,v) domain:

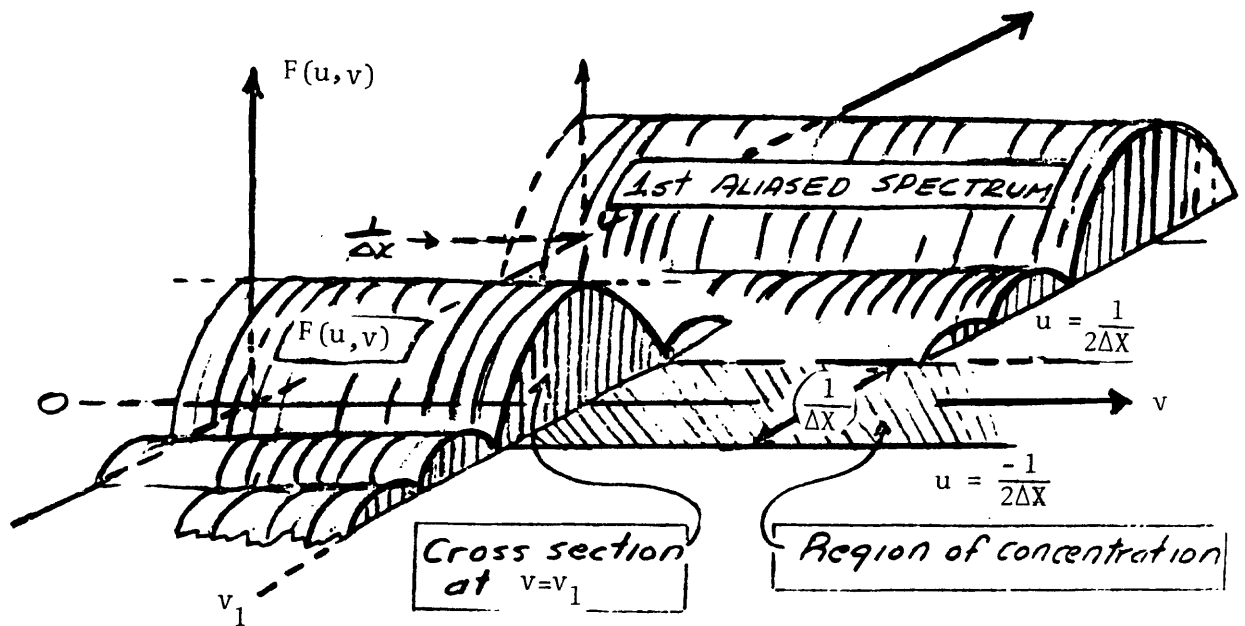
$$G_{\text{out}}(u,v) = H_{\text{in}}(u,v) \cdot K(u,v)$$

Thus, convolution in the (x,y) domain is equivalent to multiplication of the individual transforms in the wave number domain.

If the data are sampled on a square grid, then the equations take the form:

$$\begin{aligned} F(u,v) &= \Delta x \Delta y \sum_n \sum_m f(n\Delta x, m\Delta y) e^{-i2\pi(un\Delta x + vm\Delta y)} \\ f(x,y) &= \Delta u \Delta v \sum_k \sum_l F(k\Delta u, l\Delta v) e^{i2\pi(k\Delta u x + l\Delta v y)} \\ g(x,y) &= \Delta x \Delta y \sum_{\lambda=-\infty}^{\infty} \sum_{\rho=-\infty}^{\infty} h(x-\lambda\Delta x, y-\rho\Delta y) k(\lambda\Delta x, \rho\Delta y) \end{aligned}$$

There is an aliasing effect which is introduced by the 2-dimensional discrete sampling of the data. In aliasing, high wave number components are made to appear as erroneous low wave number components. The spectrum folds over about the wave number points $\left(\frac{\pm n}{2\Delta x}, \frac{\pm m}{2\Delta y} \right)$



For data representing a potential field, the second vertical derivative is obtained from Laplace's equation

$$\frac{\partial^2 f(x,y)}{\partial z^2} = - \frac{\partial^2}{\partial x^2} + \frac{\partial^2}{\partial y^2} f(x,y)$$

By taking the Fourier transform of both sides of the equation, one obtains

$$F_{ZZ}(u,v) = 4\pi^2 (u^2 + v^2) F(u,v)$$

Thus, the second derivative operation can be thought of as a filtering operation using a filter with a response function

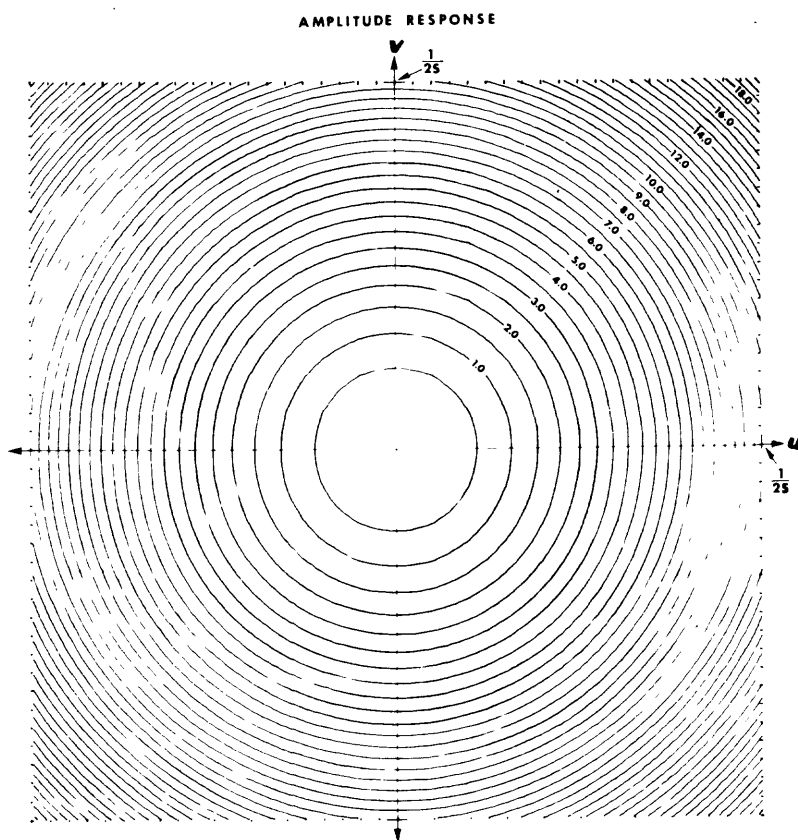
$$Y(u,v) = 4\pi^2 (u^2 + v^2), \text{ which is}$$

a purely real function; so the phase spectrum is identically zero.

If the data are on a square grid with station spacing s , $= \Delta x = \Delta y$, it is convenient to scale the (u,v) domain in terms of $1/s$. Thus, we have

$$Y\left(\frac{k}{s}, \frac{l}{s}\right) = \frac{4\pi^2}{s^2} (k^2 + l^2)$$

The figure below shows the amplitude response of the second derivative filter for the case where the operator points in the space domain are located on a square grid with grid spacing s . The response is shown as a plot of the gain out to the first set of wave number "fold over" points. The aliased components of this response appear throughout the wave number domain, being centered about the point $(m/s, n/s)$ where $m, n = 0, 1, 2, \dots$



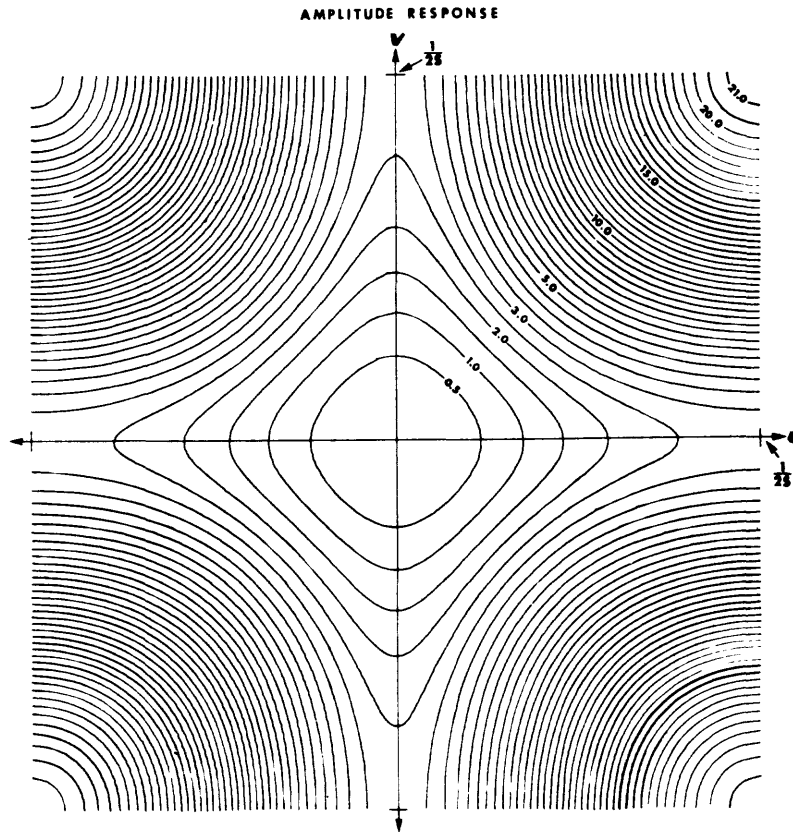
THEORETICAL SECOND DERIVATIVE AMPLITUDE RESPONSE

CONTOUR INTERVAL 0.50/s²

Darby and Davies* have calculated the two-dimensional amplitude response function for several second derivative calculational schemes.

*Darby, E. K., and Davies, E. B., 1967, The Analysis and Design of Two-Dimensional Filters for Two-Dimensional Data, *Geophysical Prospecting*, v. 15, pp. 383-406.

The one for Henderson and Zietz (Geophysics, v. 14, pp. 508-516, 1949) is shown below. It has pronounced directional properties and approximates the theoretical response only in the 45° directions.



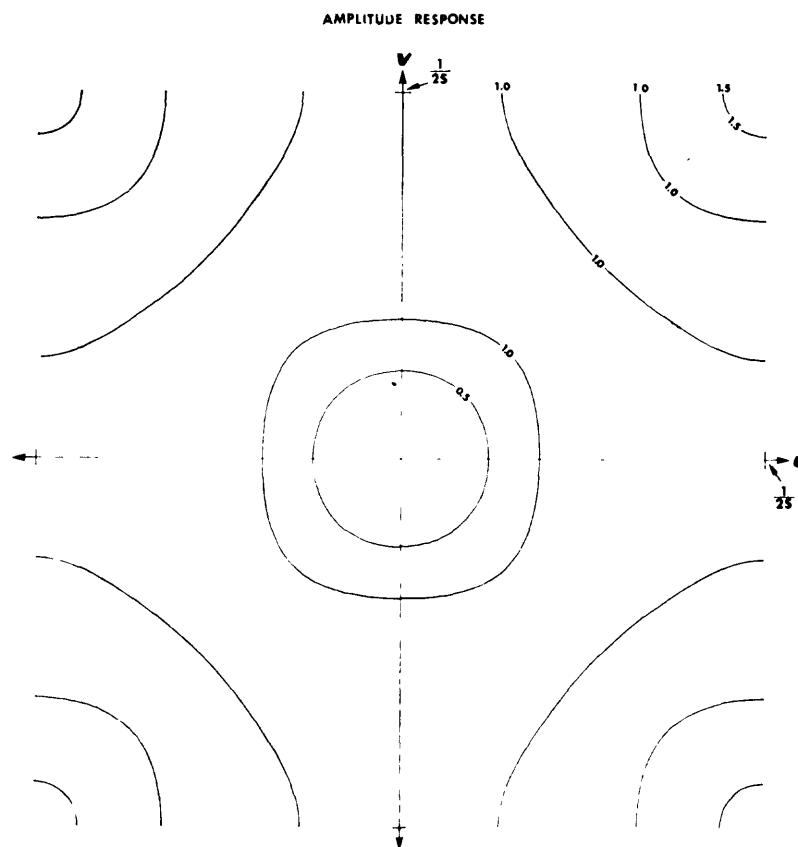
IMPULSE RESPONSE

0	0	-0.0838	0	0
0	+1.0000	-2.6667	+1.0000	0
-0.0838	-2.6667	+7.0000	-2.6667	-0.0838
0	+1.0000	-2.6667	+1.0000	0
0	0	-0.0838	0	0

|-----|
5

HENDERSON AND ZIETZ (1949) EQUATION (15)
SECOND DERIVATIVE FILTER IMPULSE AND AMPLITUDE RESPONSE
CONTOUR INTERVAL 0.50/s²

The amplitude response function for the second derivative scheme proposed by Elkins (Geophysics, v. 16, pp. 29-50, 1951) is shown below. It is a poor approximation to the theoretical function, both in gain and circular symmetry.



IMPULSE RESPONSE

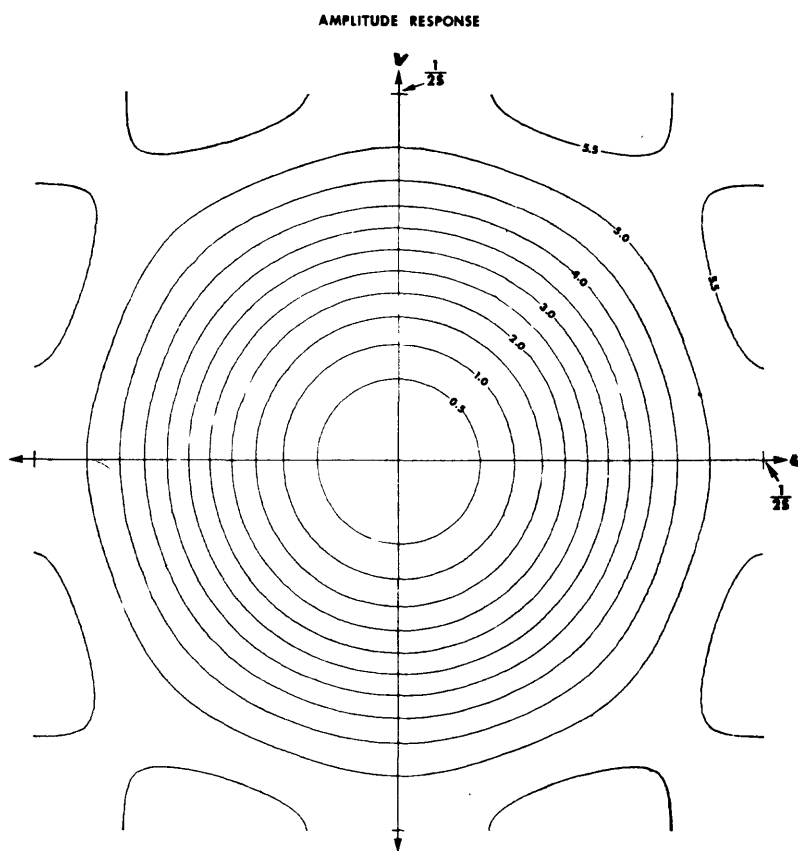
0	-0.0833	0	-0.0833	0
-0.0833	-0.0667	-0.0334	-0.0667	-0.0833
0	-0.0334	+1.0468	-0.0334	0
-0.0833	-0.0667	-0.0334	-0.0667	-0.0833
0	-0.0833	0	-0.0833	0

ELKINS 1951 EQUATION 13

SECOND DERIVATIVE FILTER IMPULSE AND AMPLITUDE RESPONSE

CONTOUR INTERVAL 0.50/s²

The amplitude response for the second derivative scheme suggested by Rosenbach (Geophysics, v. 18, pp. 894-912, 1953) is shown below. This 5 x 5 coefficient set gives a fairly good approximation to the theoretical second derivative amplitude response and has reasonably good circular symmetry.



IMPULSE RESPONSE

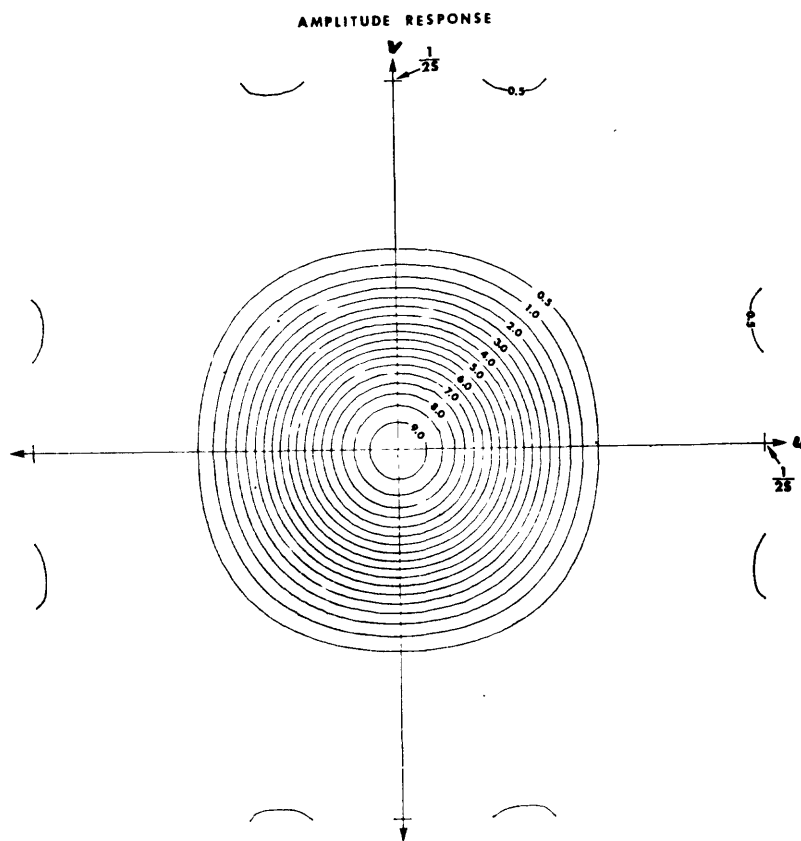
0	+0.0416	0	+0.0416	0
+0.0416	-0.3332	-0.7500	-0.3332	+0.0416
0	-0.7500	+4.0000	-0.7500	0
+0.0416	-0.3332	-0.7500	-0.3332	+0.0416
0	+0.0416	0	+0.0416	0

← 5 →

ROSENBAACH (1953) EQUATION (16)
SECOND DERIVATIVE FILTER IMPULSE AND AMPLITUDE RESPONSE
CONTOUR INTERVAL 0.50/s²

In the one-dimensional case, the Fourier transform of many simple functions (e.g., the ramp function, may be used to design filters which have desired amplitude response characteristics in the wave number domain. This concept can be carried forward in two-dimensions. However, a desirable property of two-dimensional filters is that they have circular symmetry in both the space and wave number domains. Some fairly simple functions can be used for filter design.

$$f(r) = \frac{\lambda - r}{\lambda} \quad r \leq \lambda$$



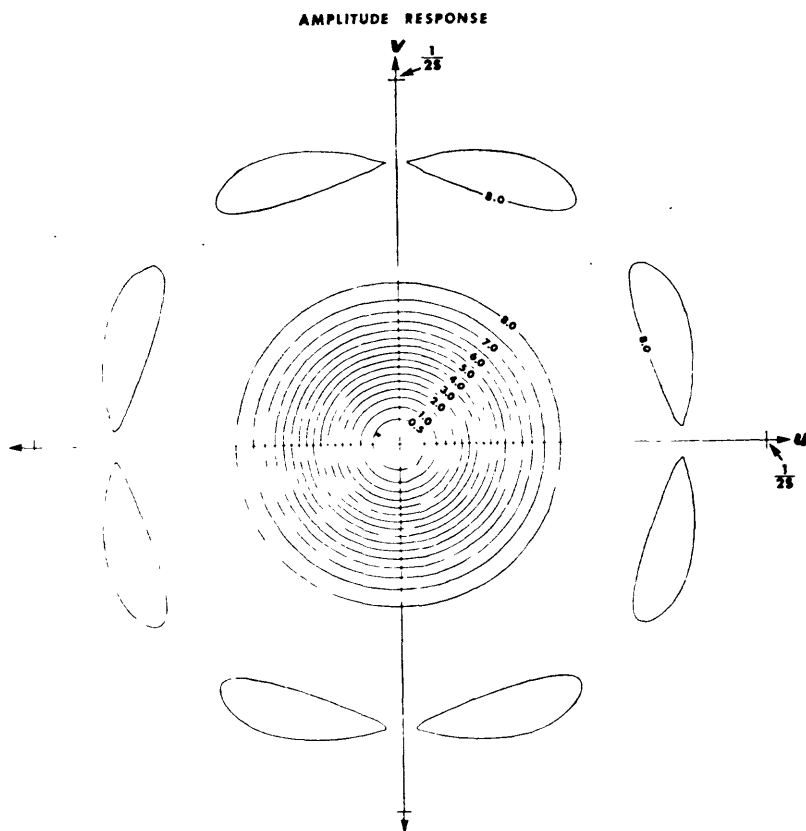
where r is the radial component in the space domain and λ is a constant. The impulse response for a 5×5 square array which results from sampling a circular ramp function when $\lambda = 3$ is shown in the next figure. The amplitude response shows that the ramp function is a low-pass filter having fairly good circular symmetry and a reasonably good correspondence to the theoretical second derivative. This filter is a regional pass filter.

IMPULSE RESPONSE

+0.0572	+0.2546	+0.3333	+0.2546	+0.0572
+0.2546	+0.5286	+0.6667	+0.5286	+0.2546
+0.3333	+0.6667	+1.0000	+0.6667	+0.3333
+0.2546	+0.5286	+0.6667	+0.5286	+0.2546
+0.0572	+0.2546	+0.3333	+0.2546	+0.0572

IMPULSE AND AMPLITUDE RESPONSE FOR
TWO DIMENSIONAL RAMP FILTER

CONTOUR INTERVAL 0.50



IMPULSE RESPONSE

+0.0000	-0.0370	-0.1000	-0.1220	-0.1000	-0.0370	+0.0000
-0.0370	-0.1450	-0.2200	-0.2480	-0.2200	-0.1450	-0.0370
-0.1000	-0.2200	-0.3230	-0.3750	-0.3230	-0.2200	-0.1000
-0.1220	-0.2480	-0.3750	+7.7080	-0.3750	-0.2480	-0.1220
-0.1000	-0.2200	-0.3230	-0.3750	-0.3230	-0.2200	-0.1000
-0.0370	-0.1450	-0.2200	-0.2480	-0.2200	-0.1450	-0.0370
+0.0000	-0.0370	-0.1000	-0.1220	-0.1000	-0.0370	+0.0000

IMPULSE AND AMPLITUDE RESPONSE FOR
TWO DIMENSIONAL SPIKE - RAMP FILTER
CONTOUR INTERVAL 0.50

By forming the
function (spike-
ramp)

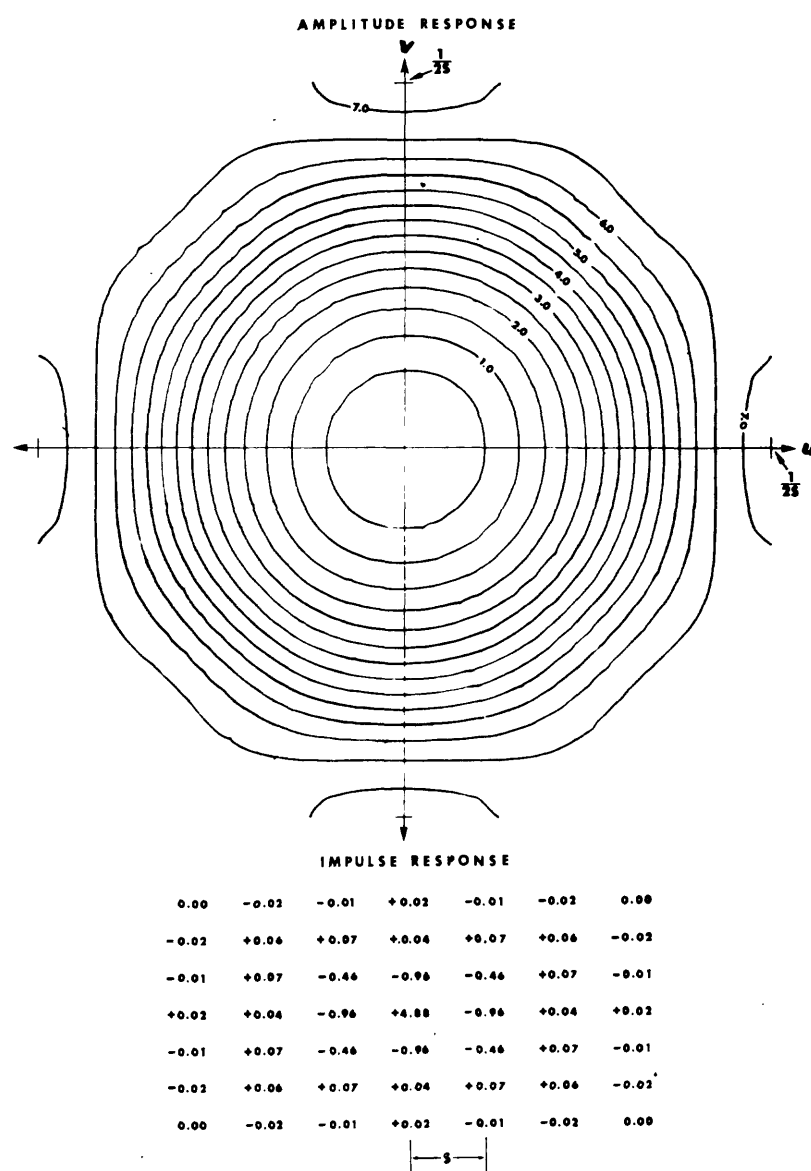
$$f(r) = A\delta(r) - \left(\frac{\lambda-r}{\lambda} \right)$$

where the A value
has been chosen so that
the array value has zero
response at the origin
in the wave number
domain, a low-wave
number reject filter
is formed. Such a fil-
ter would reject many of

the wavelengths which
make up the regional
components of a gravity
(or magnetic) field.

This filter is not a
good approximation to
the theoretical second
derivative.

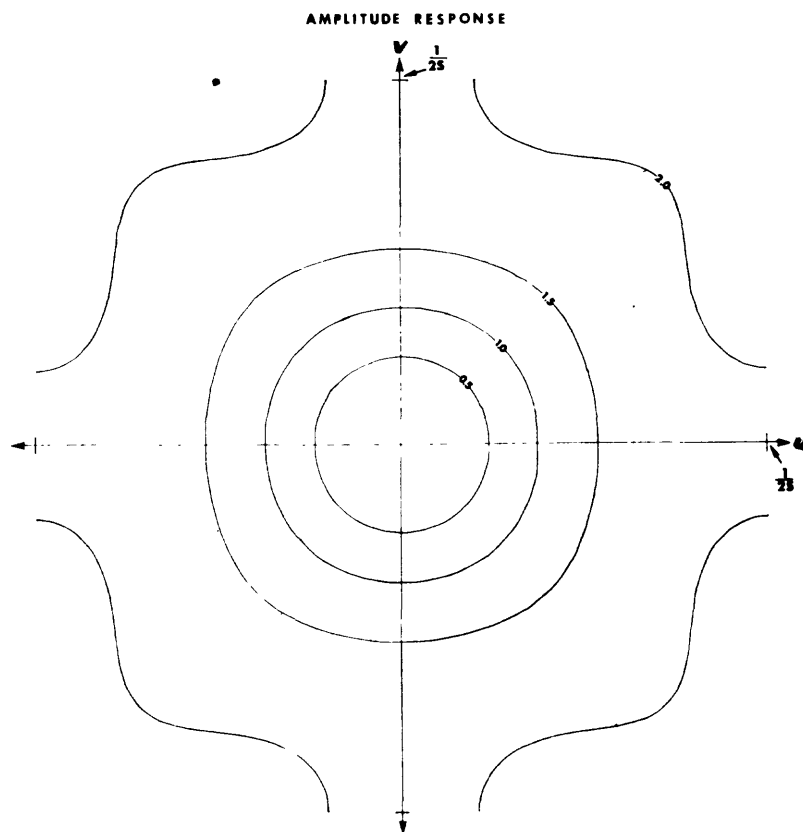
The most direct method of designing two-dimensional filters is to specify the response in the wave number domain and then perform the inverse Fourier transform to obtain the impulse response in the space domain. The figure below shows a filter designed to provide a close approximation to the theoretical second derivative. It would be a regional reject filter.



IMPULSE AND AMPLITUDE RESPONSE OF A SECOND DERIVATIVE
FILTER DESIGNED BY THE INVERSE TRANSFORM METHOD

CONTOUR INTERVAL 0.50/s²

In many cases, high gain at large wave number values is undesirable since it tends to emphasize the high frequency noise content (instrumental error, faulty corrections, gridding errors, etc.) in the data. Therefore, it may be useful to design a second derivative filter which approximates the second derivative amplitude response only at low wave number values and then has a constant gain for higher wave number values. Such a filter is shown below.



IMPULSE RESPONSE

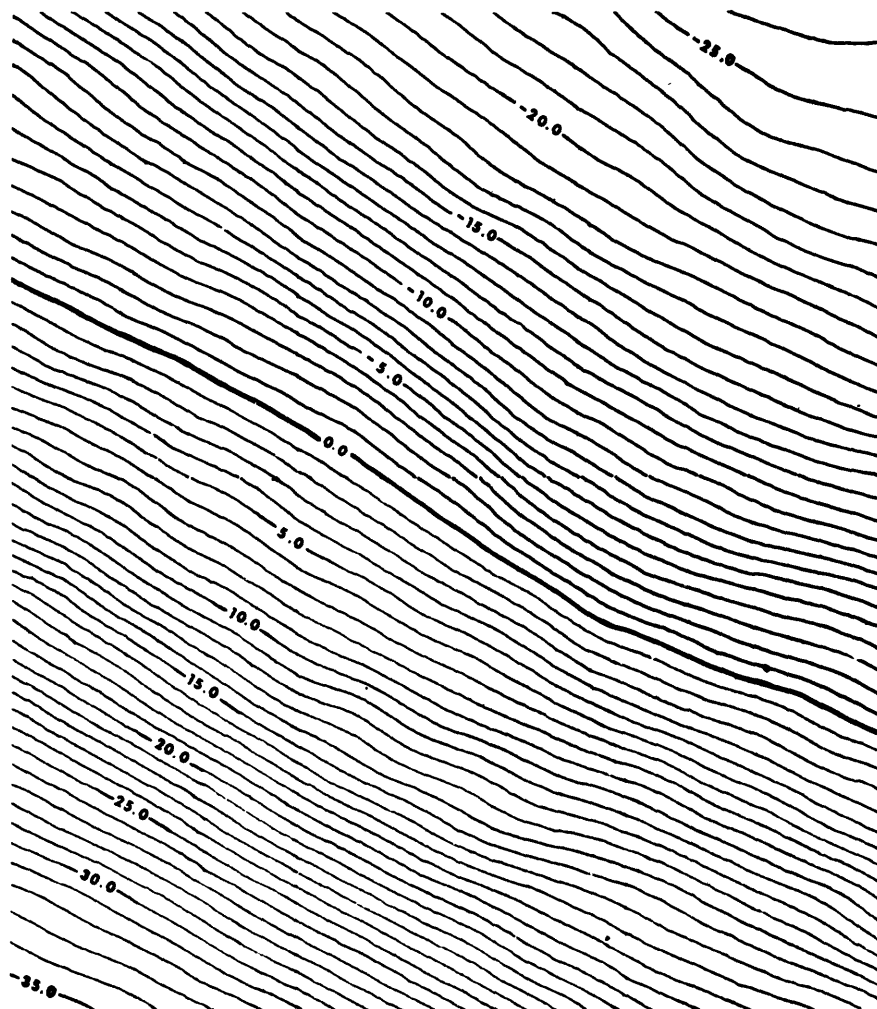
0	0	0	-0.01	0	0	0
0	-0.02	-0.02	-0.03	-0.02	-0.02	0
0	-0.02	-0.11	-0.21	-0.11	-0.02	0
-0.01	-0.03	-0.21	+1.68	-0.21	-0.03	-0.01
0	-0.02	-0.11	-0.21	-0.11	-0.02	0
0	-0.02	-0.02	-0.03	-0.02	-0.02	0
0	0	0	-0.01	0	0	0

|— 5 —|

IMPULSE AND AMPLITUDE RESPONSE OF A SECOND DERIVATIVE
FILTER DESIGNED BY THE INVERSE TRANSFORM METHOD

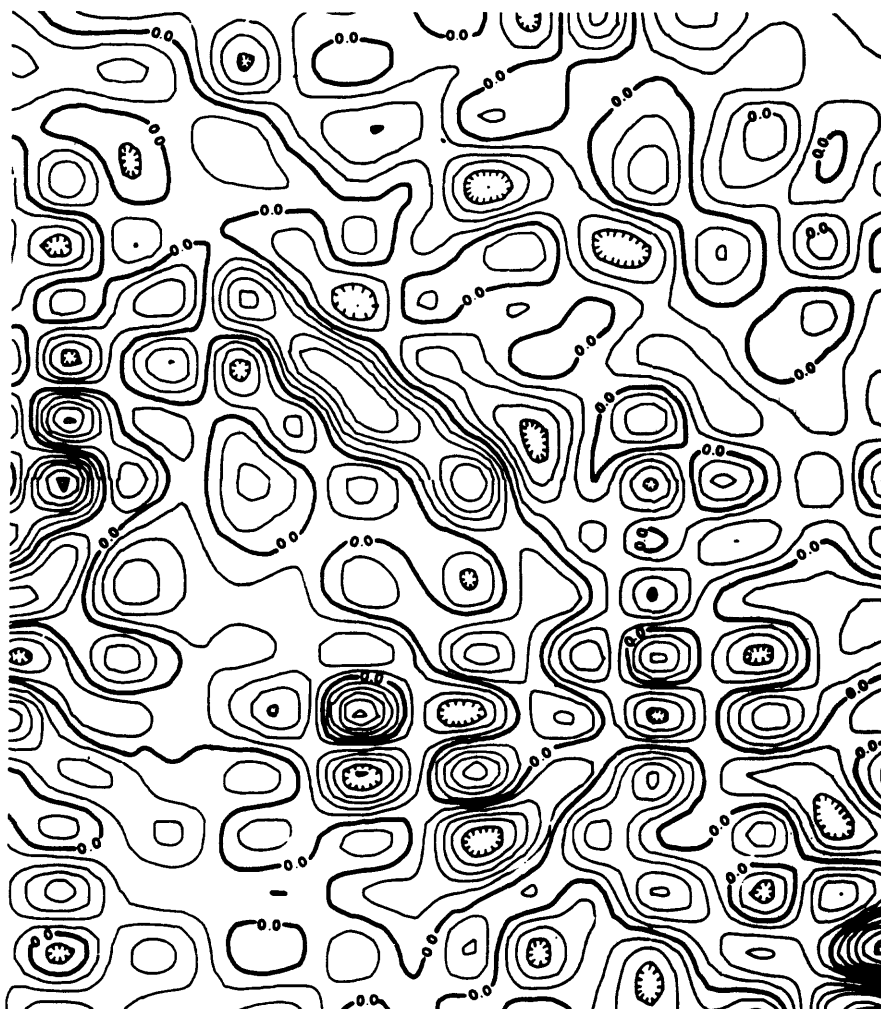
CONTOUR INTERVAL $0.50/s^2$

Example of Application to Gravity Data--A set of observed (corrected) gravity data interpolated to a square grid is shown in the figure below. These data are used as input to the two-dimensional filters discussed earlier.



OBSERVED GRAVITY DATA
CONTOUR INTERVAL - 1.0 MGALS

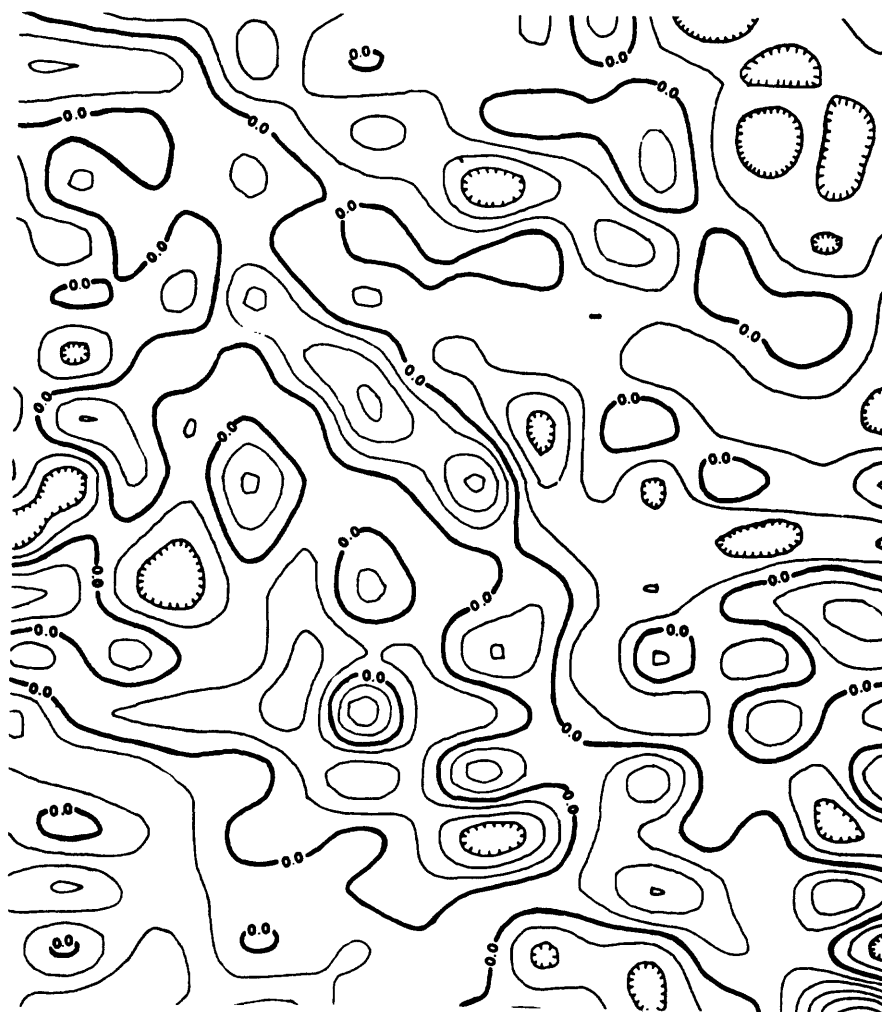
The convolution results using the second derivative filter of Henderson and Zietz are shown below. The high gain of this filter at large wave numbers has resulted in many high wave number events being passed; these are probably not structurally significant. Also, the strong directional properties of the filter has resulted in some exaggerated trends in the output data.



SECOND DERIVATIVE FILTER
HENDERSON AND ZIETZ EQUATION (15).
CONTOUR INTERVAL - 0.50 MGALS./G²

CONVOLUTION OF SECOND DERIVATIVE COEFFICIENT
SET WITH OBSERVED GRAVITY DATA

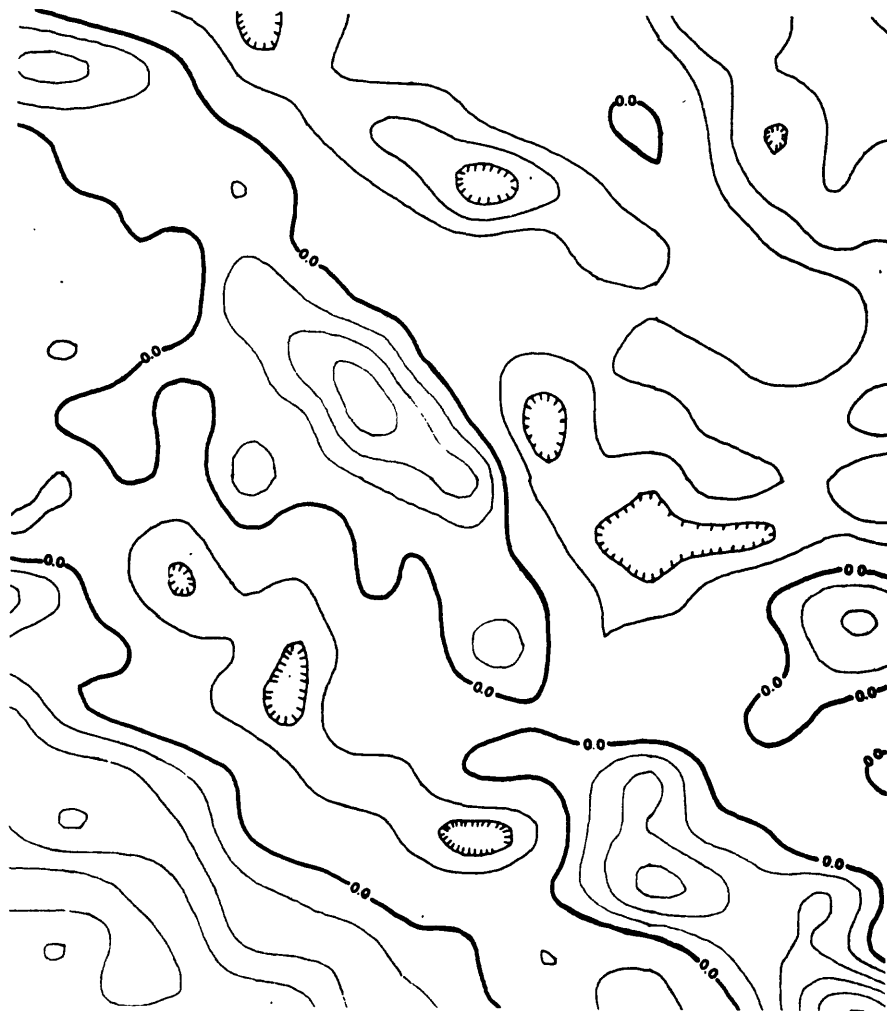
Using the second derivative scheme proposed by Rosenbach yields the map shown below. This map contains some high frequency components, but does not show the strong trends contained in the map representing the output of the Henderson and Zietz filter.



SECOND DERIVATIVE FILTER
ROSENBAUGH EQUATION (16)
CONTOUR INTERVAL - 0.50 MGALS/S²

CONVOLUTION OF SECOND DERIVATIVE COEFFICIENT
SET WITH OBSERVED GRAVITY DATA

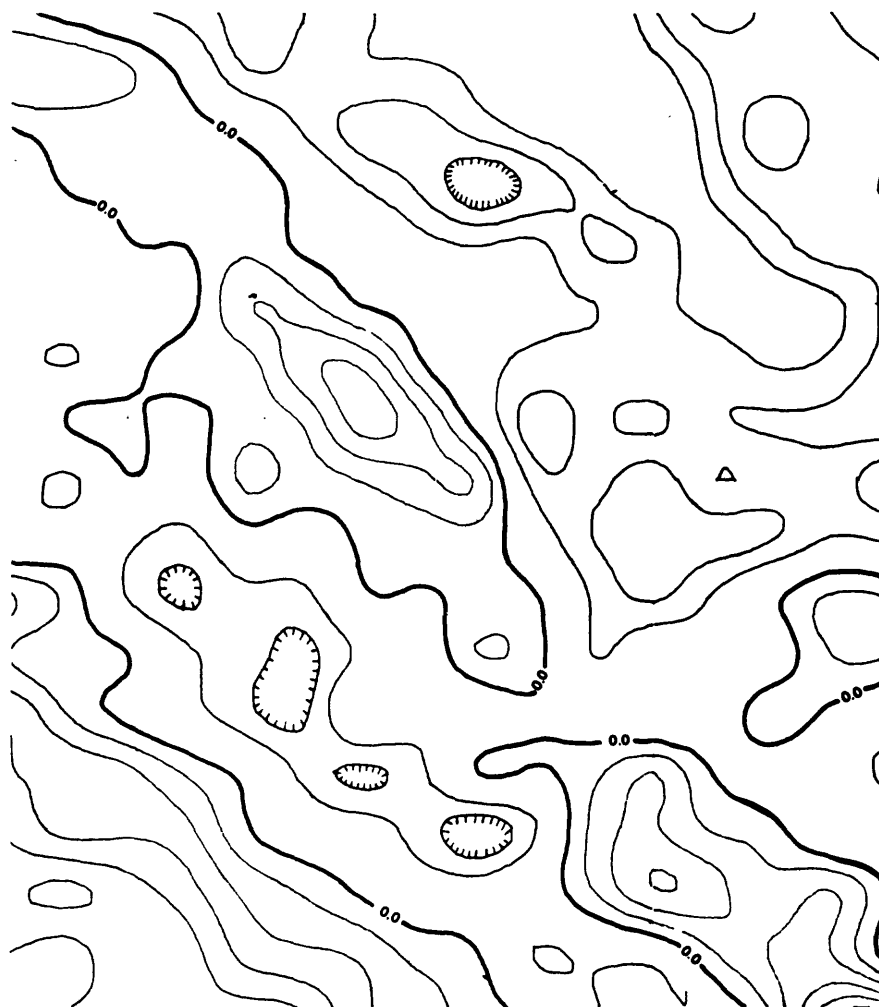
The second derivative scheme proposed by Elkins produces the output data shown below. The low and theoretically incorrect gain of this filter for large wave numbers yields data which more closely resemble a residual gravity map.



SECOND DERIVATIVE FILTER
ELKINS EQUATION (13)
CONTOUR INTERVAL - 0.20 MGALS/S²

CONVOLUTION OF SECOND DERIVATIVE COEFFICIENT
SET WITH OBSERVED GRAVITY DATA

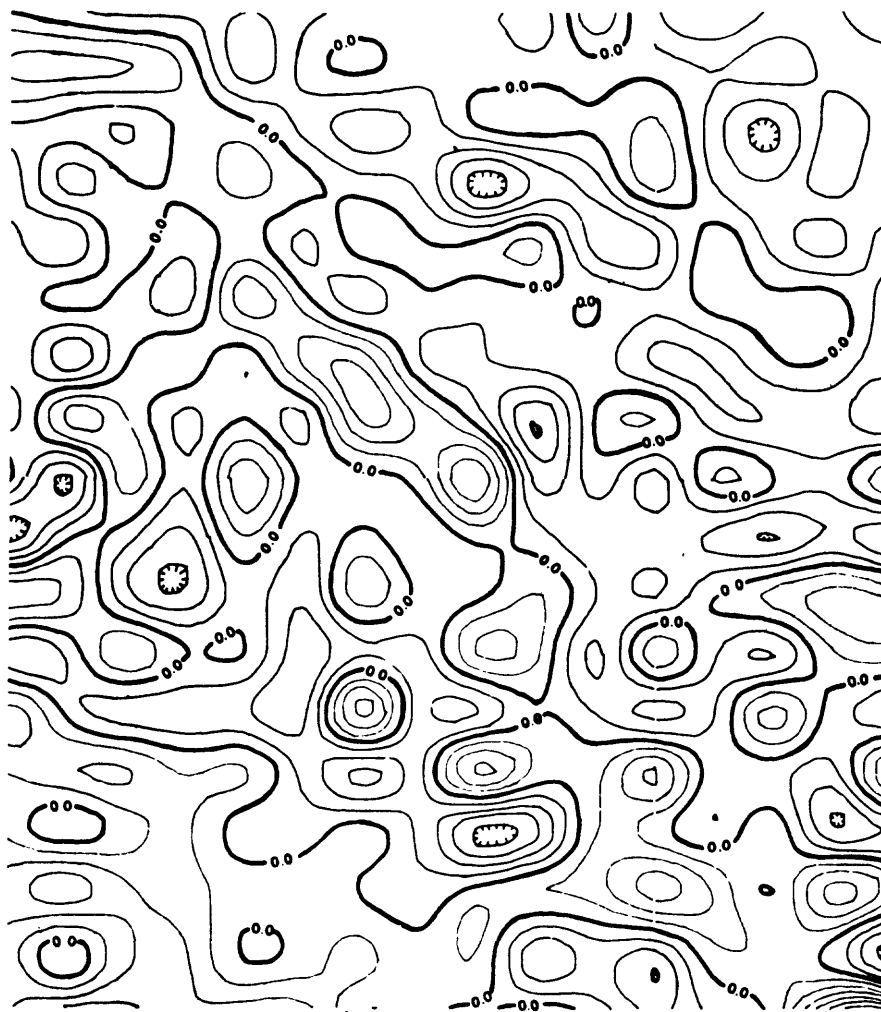
Using the low-wave number reject filter (spike-ramp), (normalized so that the maximum gain of the filter is near unity) gives the map shown below. The low wave number components have been suppressed and the output data resemble a residual map. Many features present on the second derivative maps are also evident on this map, but the anomalies are less sharply defined due to the presence of many intermediate wave-length components.



SPIKE-RAMP FILTER OF FIGURE 6
CONTOUR 0.20 MGALS.

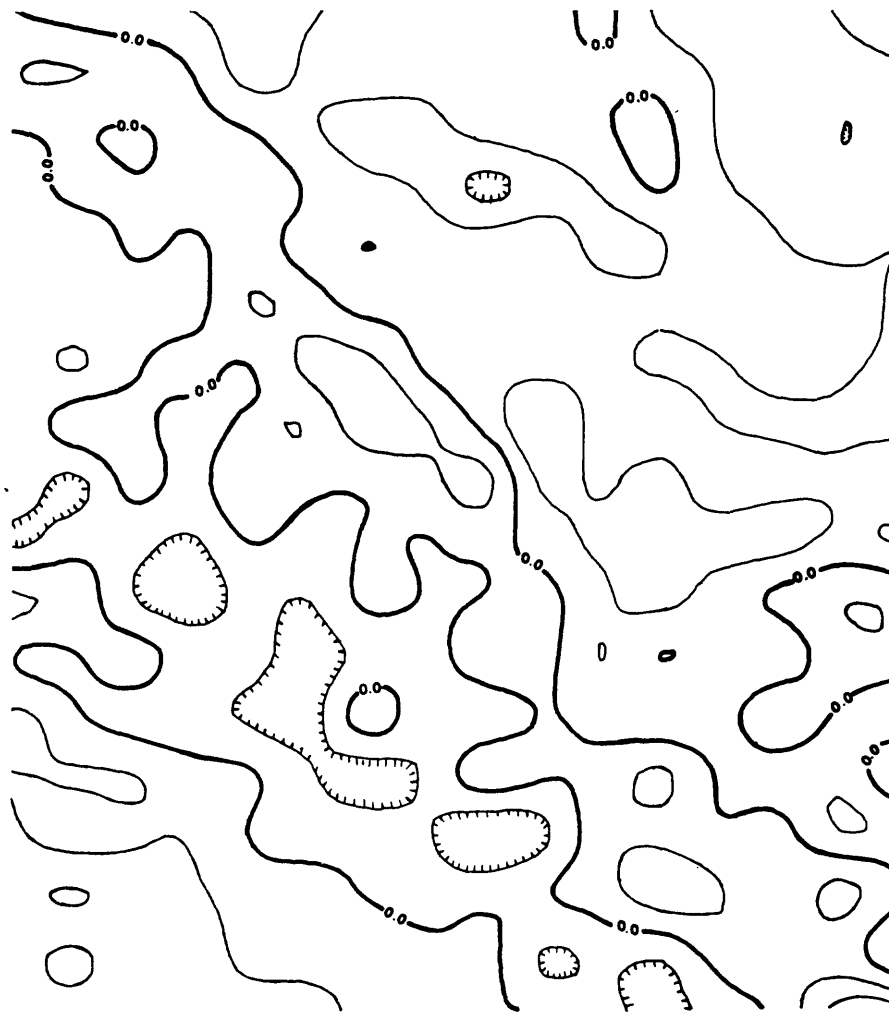
**CONVOLUTION OF SPIKE-RAMP FILTER WITH
OBSERVED GRAVITY DATA**

The map representing the convolution of the high gain second derivative filter designed by the inverse transform with the observed gravity data is shown below. The high wave number information is enhanced, as evidenced by the large number of small sharp anomalies.



HIGH GAIN SECOND DERIVATIVE FILTER OF FIGURE 7
CONTOUR INTERVAL—0.50 MGALS/S²
CONVOLUTION OF SECOND DERIVATIVE FILTERS
WITH OBSERVED GRAVITY DATA

The convolution of the low gain second derivative filter designed by the inverse Fourier transform and the observed gravity data produces the map shown below. The high wave number components are relatively suppressed and smooth anomalies result.



LOW GAIN SECOND DERIVATIVE FILTER OF FIGURE 8
CONTOUR INTERVAL - 0.50 MGALS/S²

CONVOLUTION OF SECOND DERIVATIVE FILTERS
WITH OBSERVED GRAVITY DATA

In summary, the prominent residual anomalies appear on all output maps obtained by convolving the input gravity data with the various second derivative, regional-reject and regional-pass filters. However, the slope and relief of these anomalies is dependent on the characteristics of the filter used. Thus, an understanding of the filtering operation used to emphasize the gravity anomaly is a very important factor in interpreting the source of the anomaly.

REFERENCES ON THE GRAVITY METHOD CONTAINED IN
EARLY GEOPHYSICAL PAPERS, GEOPHYSICS, AND GEOPHYSICAL PROSPECTING

The code for the following sample listing is explained below.

GE-18-1-003

EP = EARLY GEOPHYSICAL PAPERS, Society of Exploration Geophysicists
 Publication

GE = GEOPHYSICS, Society of Exploration Geophysicists Publication

GP = GEOPHYSICAL PROSPECTING, European Association of Exploration
 Geophysicists Publication

18 = Volume Number

1 = Issue Number (0=yearbook)

0003 = Page Number

Analysis of Some Torsion-Balance Results in California (Gravity Surveys)	EP 01 -0-0129
New Instruments for Measuring Very Small Differences in Gravity (Gravimeter)	EP 01 -0-0165
Effects of Heat Treatment on Fine Metallic Suspensions (Gravity)	EP 01 -0-0176
Accuracy of Determination of Relative Gravity by Torsion Balance	EP 01 -0-0395
Curvature of Equipotential Surfaces (Gravity)	EP 01 -0-0410
Recent Developments in Gravity Prospecting on Gulf Coast	EP 01 -0-0679
Prediction of Overhang at Barbers Hill Chambers County Texas-A Study in Quantitative Calculations from Torsion-Balance Data (Gravity Salt-Dome)	EP 01 -0-0685
The Amount and Distribution of Seismic and Gravity Exploration in the Gulf Coast through 1936 (Surveys Activity)	GE 02 -1-0001
Gravimeter Design and Operation (Gravity)	GE 02 -4-0301
An Introduction to the Second Derivative Contour Method of Interpreting Torsion Balance Data (Gravity)	GE 03 -3-0234
The Resolution of Combined Effects with Applications to Gravitational and Magnetic Data (Gravity)	GE 03 -4-0315
Relative Gravity Measurements Using Precision Pendulum Equipment	GE 05 -2-0176
A Brief History of the Gravity Method of Prospecting for Oil	GE 05 -3-0231
Tidal Force Observations (Corrections Gravity) *	GE 05 -4-0317
Network Adjustment of Least Squares Alternative Formulation and Solution by Iteration (Gravity Magnetic)	GE 06 -2-0168
The Calculation of Gravity Anomalies Due to Bodies of Finite Extent	GE 06 -2-0180
Gravity Meter Survey of the Wellington Field Larimer County Colorado (Case-History)	GE 06 -3-0264
Relation of Gravity to Structure in the Northern Appalachian Area	GE 06 -3-0270
Simplification of Tidal Corrections for Gravity Meter Surveys	GE 07 -1-0035
The Analytic Basis of Gravity Interpretation	GE 07 -2-0169
Gravity and Magnetic Calculations	GE 07 -3-0293
The Value of Quantitative Interpretation of Gravity Data	GE 07 -4-0345
A Mechanical Integrator for the Computation of Gravity Anomalies	GE 07 -4-0354
Gravity and Magnetic Observations on Iron Mountain Magnetite Deposit Llano County Texas (Surveys)	GE 08 -1-0032

REFERENCES ON THE GRAVITY METHOD CONTAINED IN
EARLY GEOPHYSICAL PAPERS, GEOPHYSICS, AND GEOPHYSICAL PROSPECTING--continued

Gravity Expression of the Hatchetigbee Anticline (Surveys)	GE 08 -1-0046
Notes on Earth Tides (Gravity)	GE 08 -1-0051
Note on the Variation from Equator to Pole of the Earths Gravity (Corrections Gravimeter Surveys Earth)	GE 08 -1-0057
A Rapid Method for Measuring the Profile Components of Horizontal and Vertical Gravity Gradients	GE 08 -2-0119
Nomograms for Computing Tidal Gravity (Corrections Gravity)	GE 08 -2-0134
Use of the Gravity Meter in Establishment of Gravity Bench Marks (Geodetic Measurements)	GE 08 -4-0379
Correlation of Gravity Observations with the Geology of the Smoothing-Iron Granite Mass Llano County Texas (Surveys)	GE 09 -1-0079
Estimating Ore Masses in Gravity Prospecting	GE 10 -1-0050
Gravity and Magnetic Investigations at the Grand-Saline Salt Dome Van-Zandt Co Texas (Surveys Case-History)	GE 10 -3-0376
Interpretation of Isostatic Anomalies South of Java Using Integral Equations and Crustal Deformation Theories (Gravity)	GE 11 -2-0183
Estimating Depth and Excess-Mass of Point-Sources and Horizontal Line-Sources in Gravity Prospecting (Mass)	GE 11 -2-0195
Geophysical History of Typical Mississippi Piercement Salt Domes (Gravity Surveys Case-History)	GE 12 -1-0030
Ambiguity in Gravity Interpretation	GE 12 -1-0043
A Line-Integral Method of Computing the Gravimetric Effects of Two-Dimensional Masses (Gravity)	GE 13 -2-0215
A Note on Terrain Corrections (Gravity)	GE 13 -2-0255
The Determination of an Infinite Inclined Dike from the Results of Gravity and Magnetic Surveys	GE 13 -3-0437
Residual Gravity in Theory and Practice (Regional Corrections)	GE 14 -1-0039
Correlation of Gravity Observations with the Geology of the Coal Creek Serpentine Mass Blanco and Gillespie Counties Texas (Surveys)	GE 14 -2-0151
Geophysics Geology and Oil Finding Presidential Address (Gravity Minimum Regional Gulf Coast)	GE 14 -3-0273
A Precision Detail Gravity Survey Jameson Area Coke County Texas	GE 14 -4-0535
The Gravity Meter as a Geodetic Instrument (Gravimeter Surveys)	GE 15 -1-0001
The Case for Gravity Data from Boreholes	GE 15 -4-0605
Density Determinations by Underground Gravity Measurements	GE 15 -4-0637
The Second Derivative Method of Gravity Interpretation	GE 16 -1-0029
Combined Analysis of Gravity and Magnetic Anomalies	GE 16 -1-0051
Least Squares Residual Anomaly Determination (Gravity)	GE 16 -4-0686
The World-Wide Gravity Program of the Mapping and Charting Research Laboratory of Ohio State University (Geodetic Surveys)	GE 16 -4-0697
The Effect of Random Errors in Gravity Data on Second Derivative Values*	GE 17 -1-0070
A Discussion on the Recent Progress of the Gravity Program of the Columbus Group	GE 17 -1-0156
Subsurface Gravity Measurements	GE 17 -2-0365
An Application of Punched Card Methods in Geophysical Interpretation (Gravity Magnetic)	GE 17 -4-0707
Use of the Wave Height Operational Index in Planning Offshore Gravity Meter Surveys	GE 17 -4-0924
A Least Square Method for Gravity Meter Base Stations	GE 18 -2-0394
Approximation to the Lateral Variation of Residual Gravity Due to a Frustum of a Vertical Cone (Salt-Domes)	GE 18 -2-0401

REFERENCES ON THE GRAVITY METHOD CONTAINED IN
EARLY GEOPHYSICAL PAPERS, GEOPHYSICS, AND GEOPHYSICAL PROSPECTING--continued

A Contribution to the Computation of the Second Derivative from Gravity Data	GE 18 -4-0894
Residual Anomalies and Depth Estimation (Gravity)	GE 18 -4-0913
Regional Residuals and Structures (Corrections Gravity Magnetic Second Derivatives)	GE 19 -1-0001
A Theory for the Regional Correction of Potential Field Data (Gravity Residual Anomalies)	GE 19 -1-0023
Some Geometrical Properties of Residual Maps (Second Derivatives Gravity Magnetic)	GE 19 -1-0046
A Note on Downward Continuation of Gravity	GE 19 -1-0071
The Correlation between Pre-Cambrian Rock Densities and Bouguer Gravity Anomalies Near Parry Sound Ontario (Surveys)	GE 19 -1-0076
Gravity Maxima Corresponding with Sedimentary Basins (Surveys Argentina Isostasy)	GE 19 -1-0089
Gravity Case-History Dawn No 156 Pool Ontario (Surveys Reefs)	GE 19 -1-0095
A Geological and Geophysical Study of Pilot Knob (South) Travis County Texas (Surveys Gravity Magnetic Serpentine Rock Densities Susceptibilities)	GE 19 -3-0438
The First Vertical Derivative of Gravity (Second-Derivative)	GE 20 -1-0148
Orthogonal Polynomials Their Use in Estimating the Regional Effect (Corrections Residual Gravity Anomalies Second Derivatives)	GE 20 -4-0807
Gravity Investigations in the Hockley Salt Dome Harris County Texas (Surveys)	GE 20 -4-0829
Geophysical Prospecting in the Union of South Africa (Water Gold Surveys Magnetic Gravity Resistivity Logging Dike)	GE 20 -4-0886
Regional Gravity Survey in Northeastern Oklahoma and Southeastern Kansas	GE 21 -1-0088
Minimum Variance in Gravity Analysis Part II-Two-Dimensional (Residual Second Derivative Orthogonal Polynomials)	GE 21 -1-0107
Review of Current Developments in Exploration Geophysics (Velocity Logging Magnetic Playback High-Frequency Recording Reynolds Plotter Weight Dropping Gravity Electromagnetic Radioactivity Magnetometer)	GE 21 -1-0142
Prospecting for Chromite with Gravimeter and Magnetometer Over Rugged Topography in East Turkey (Gravity Magnetic Surveys)	GE 21 -2-0433
Observation of the Vertical Gradient of Gravity in the Field	GE 21 -3-0771
Geophysical Studies in the Intermontane Basins in Southern California (Gravity Surveys Searles Lake)	GE 21 -3-0839
Bouguer Corrections with Varying Surface Density (Rocks Gravity)	GE 21 -4-1004
Regional Gravity Survey of Parts of Tooele Juab and Millard Counties Utah (Faulting Graben)	GE 22 -1-0048
A Gravity Maximum in the Great Valley of California Due to the Isostatic Effect of the Sierra-Nevada (Surveys)	GE 22 -1-0062
A Problem in the Analysis of Geophysical Data (Residual Polynomial Least-Squares Gravity Magnetic)	GE 22 -2-0309
Submarine Gravity Detailing San-Luis Pass Dome Brazoria County Texas (Surveys Salt-Domes)	GE 22 -2-0348
A New Method for Interpretation of Aeromagnetic Maps Pseudo-Gravimetric Anomalies (Magnetic Gravity)	GE 22 -2-0359
Gravity Survey Over a Gulf Coast Continental Shelf Mound (Salt-Domes)	GE 22 -3-0630
Chart to Check Elevation Factor Effects on Gravity Anomalies (Nomograms)	GE 22 -3-0643
Gravity Prospecting for Chromite Deposits in Camaguey Province Cuba (Surveys)	GE 22 -4-0848
Frequency Analysis for Gravity and Magnetic Interpretation (Filtering Second Derivatives Residual Downward Upward Continuation)	GE 23 -1-0097
Maximum Gravity Effect of Certain Solids of Revolution	GE 23 -3-0506
Results for a Gravity Control Network at Airports in the United States (Gravimeter Base Stations Calibration)	GE 23 -3-0520

REFERENCES ON THE GRAVITY METHOD CONTAINED IN
EARLY GEOPHYSICAL PAPERS, GEOPHYSICS, AND GEOPHYSICAL PROSPECTING--continued

Prize-Winning Essay on a Gravity Investigation of a Sulphide Deposit (Surveys Quebec Mass)	GE 23 -3-0606
Key Variables of Gravity (Fault Second Derivatives Resolution Salt-Domes)	GE 23 -4-0684
Terrain Corrections for an Inclined Plane in Gravity Computations (Tables)	GE 23 -4-0701
Letter on Residual and Second Derivative of Gravity and Magnetic Maps	GE 23 -4-0860
Reply to Letter on Residual and Second Derivative of Gravity and Magnetic Maps	GE 23 -4-0862
Surface Ship Gravity Measurements on the Texas A and M College Ship the Hidalgo (Marine Gravimeter)	GE 24 -2-0309
The Use of Cracovian Computation in Estimating the Regional Gravity (Least-Squares Polynomial Fitting Residual Digital)	GE 24 -3-0465
Standardization of Gravity Survey Procedures (Base Stations Gravimeter Calibration Corrections Map Scales)	GE 24 -3-0479
Tests of an Airborne Gravity Meter (Surveys Imperial Valley California)	GE 25 -1-0181
Photogrammetric Determination of Elevations for Gravity Surveys	GE 25 -2-0445
A Comprehensive System of Automatic Computation in Magnetic and Gravity Interpretation (Upward Downward Continuation Second Derivatives)	GE 25 -5-1023
Letter to the Editor on Horizontal Surveying Accuracy Required for Gravity Meter Projects	GE 25 -5-1150
On a Successive Approximation Method for Interpreting Gravity Anomalies (Digital Computer Salt-Dome Igneous Pipes)	GE 25 -6-1215
Geophysical Study of Subsurface Structure in Southern Owens Valley California (Gravity Refraction Surveys)	GE 26 -1-0012
Gravity Prospecting for Reefs Effects of Sedimentation and Differential Compaction (Rock Densities Case-History)	GE 26 -1-0045
An Evaluation of the Gravity Control Network in North America (Surveys Gravimeter Calibration)	GE 26 -1-0057
Underground and Surface Gravity Survey Leadwood Missouri (Mining Rock Densities)	GE 26 -2-0158
A Simple Integral Transform and Its Applications to Some Problems in Geophysical Interpretation (Gravity Magnetic Line Segment Dike Dipping Beds Electrical Resistivity)	GE 26 -2-0229
An Integration Technique for Airborne Gravity Gradient Measurements	GE 26 -4-0474
Terrain Corrections for Airborne Gravity Gradient Measurements (Charts)	GE 26 -4-0480
Gravity Surveys in Heavy Sand Dunes (Arabia Africa Terrain Corrections)	GE 26 -4-0490
Discussion on Rapid Computation of Gravity Anomalies for Irregularly Shaped Three-Dimensional Bodies (Charts)	GE 26 -5-0645
Gravity and Aeromagnetic Exploration in the Paradox Basin	GE 27 -1-0073
Geophysical Study of Cenozoic Geologic Structures of Northern Owens Valley California (Graben Basin Range Gravity Faulting)	GE 27 -3-0334
Aeromagnetic and Gravity Studies of the Precambrian in Northeastern New Mexico	GE 27 -3-0343
A Simple Criterion for Interpretating Negative Gravity Anomalies (Granites Sedimentary Basins)	GE 27 -3-0376
A Comprehensive System of Terrain Corrections Using a Digital Computer (Gravity)	GE 27 -4-0455
Eotvos Corrections for a Moving Gravity Meter (Airborne Marine Geodesy)	GE 27 -4-0531
An Analysis of Some Second Derivative Methods (Gravity Magnetic Harmonic Functions)	GE 27 -5-0611
Bouguer Gravity Corrections Using a Variable Density	GE 27 -5-0616
A Short Note on the Average Horizontal Gravity Gradient (Torsion Balance Terrain Effect)	GE 27 -5-0714
A Short Note on Terrain Correction Tables for Gravity	GE 27 -5-0715
Investigation of Upward Continuation Systems (Gravity Potential Theory Airborne Gravimeter)	GE 27 -6-0796

REFERENCES ON THE GRAVITY METHOD CONTAINED IN
EARLY GEOPHYSICAL PAPERS, GEOPHYSICS, AND GEOPHYSICAL PROSPECTING--continued

Deep Gravity Interpretation by Stripping	GE 28 -3-0369
Seismic and Gravity Studies at the South-Pole (Antarctic Ice Velocity)	GE 28 -4-0582
A Density Determination by Underground Gravity Measurements in Michigan	GE 28 -4-0663
An Approximate Solution of the Problem of Maximum Depth in Gravity Interpretation	GE 28 -5-0724
Preliminary Study of the Crustal Structure Across the Campeche Escarpment from Gravity Data	GE 28 -5-0736
Interpretation of Geophysical Profiles between Singapore and Labuan North Borneo (Aeromagnetic Orient Gravity)	GE 28 -5-0805
The Vertical Gravity Gradient in Borehole Exploration (Density Average-Gradients)	GE 28 -6-1072
Borehole Gravity Meter and Its Application (Logging Density)	GE 29 -5-0774
Free-Air Gravity Anomaly Map of the Gulf of Mexico and Its Tectonic Implications 1963 Edition (Ship Gravity-Meter)	GE 30 -1-0102
Theory of Gravity Instability with Variable Overburden and Compaction	GE 30 -2-0213
A Least-Squares Procedure for Gravity Interpretation (Two-Dimensional)	GE 30 -2-0228
A Short Note on Convolution Filtering of Gravity and Magnetic Maps (Residual Second Derivative Smoothing)	GE 30 -2-0281
Gravity Interpretation Using the Fourier Integral (Spectral Analysis)	GE 30 -3-0424
A Short Note on International Gravity Bureau (I G B) (Geodesy)	GE 30 -3-0444
A Short Note on Reconnaissance Survey Using Average Horizontal Gradients of Gravity (Simpson Desert Australia)	GE 30 -4-0661
A Geophysical Study of a Basement Anomaly in Indiana (Magnetics Gravity)	GE 30 -5-0740
Geophysical Investigations in the Area of the Perth Basin Western Australia (Marine Refraction Gravity)	GE 30 -6-1026
Crustal Structure from Converted Head Waves in Central Western Manitoba (Refraction Gravity)	GE 30 -6-1053
Fictitious Anomalies of Higher Vertical Derivatives of Gravity	GE 30 -6-1094
A Confirmation by Gravity Measurements of an Underground Density Profile Based on Core Densities (Porosity Logging Gradient)	GE 30 -6-1108
Density Determinations by Underground Gravity Measurements a Sequel	GE 30 -6-1133
A Short Note on Double-Track Profiling with the Gravity Meter (Horizontal Gradients)	GE 30 -6-1135
A Short Note on Correlating Vertical Magnetic Intensity and Average Horizontal Gradients of Gravity	GE 30 -6-1138
Three-Dimensional Gravity Instability Derived from Two-Dimensional Solutions (Salt-Domes Salt-Pillows Overburden Compaction)	GE 31 -1-0153
Short Note-Correlating Sea-Surface and Aerial Gravity Measurements	GE 31 -1-0264
Gravity Anomalies of Two-Dimensional Faults	GE 31 -2-0372
Application of Filter Theory and Information Theory to the Interpretation of Gravity Measurements (Newton Potential Wave-Number Power Spectral Target-Layer)	GE 31 -3-0570
Two-Dimensional Filtering and the Second Derivative Method (Gravity)	GE 31 -3-0606
Arctic Ocean Geophysical Studies-The Southern Half of the Siberia Basin (Reflection Gravity Magnetics Crustal Structure)	GE 31 -4-0683
Outlining of Shale Masses by Geophysical Methods (Diapiric Velocity Density Resistivity Gravity)	GE 31 -4-0711
The Development and Use of a High-Precision Downhole Gravity Meter (Density Porosity Acoustic Impedance)	GE 31 -4-0764
The Simulation of Magnetic and Gravity Profiles by Digital Computer (Two-Dimensional Potential Field)	GE 31 -4-0773
Short Note-Vertical Gradient of Gravity on Axis for Hollow and Solid Cylinders (Bore-Hole Meter)	GE 31 -4-0816

REFERENCES ON THE GRAVITY METHOD CONTAINED IN
EARLY GEOPHYSICAL PAPERS, GEOPHYSICS, AND GEOPHYSICAL PROSPECTING--continued

Direct Interpretation of Two-Dimensional Structural Faults from Gravity Data (Upward Continuation)	GE 31 -5-0940
In-Situ Determination of the Remanent Magnetic Vector of Two-Dimensional Tabular Bodies (Paleomagnetism Gravity Potential Dikes)	GE 31 -5-0949
Statistical Properties of Potential Fields Over a Random Medium (Magnetic Gravity)	GE 32 -1-0088
Lacoste and Romberg Stabilized Platform Shipboard Gravity Meter (Lacoste-Romberg)	GE 32 -1-0099
Quantitative Evaluation of a Stabilized Platform Shipboard Gravity Meter	GE 32 -1-0110
Short Note-Magnetic Survey of the Puget Sound Earthquake Zone (Geomagnetism Gravity Tectonics Fault)	GE 32 -1-0119
Short Note-Detail Gravity Profile Across San-Andreas Fault Zone	GE 32 -2-0297
A Geophysical History of the Lacq Field (Telluric Electrical Sounding Reflection Gravity Reef Case-History)	GE 32 -2-0311
Geophysical Exploration for Buried Valleys in an Area North of Two-Hills Alberta (Gravity Groundwater Hydrology)	GE 32 -2-0331
A Method of Computing Residual Anomalies from Bouguer Gravity Map by Applying Relaxation Technique (Least-Square Regional)	GE 32 -4-0708
An Electromagnetic Analog Method for Computing Gravity and Magnetic Effects of Two-Dimensional Bodies (Anomaly Simulation)	GE 32 -5-0833
Convergence and Divergence in Downward Continuation (Boundary Curve Gravity Magnetic Potential Theory Taylor Series)	GE 32 -5-0867
Short Note-What is residual Gravity (Regional Polynomial Least-Square Convolution)	GE 32 -5-0872
Spectrum of the Potential Field Due to Randomly Distributed Sources (Gravity Magnetic Covariance Continuation)	GE 33 -2-0337
Iterative Three-Dimensional Solution of Gravity Anomaly Data Using a Digital Computer (Model Automatic)	GE 33 -4-0596
Discovery Case-History of the Pyramid Ore Bodies Pine Point Northwest Territories Canada (Induced Polarization Gravity Lead Zinc)	GE 33 -4-0645
Effects of Structure on the Gravity Field of Wyoming (Isostasy Germano-Tectonics)	GE 33 -5-0781
Variations of Vertical Gravity Gradient in New York City and Alpine New Jersey (Upward Continuation)	GE 34 -2-0235
On the Interpretation of Gravity Data	GP 01 -2-0075
Gravity Effect on Earth Tides	GP 01 -2-0082
Beitrag Zur Interpretation Von Schwerebildern Mit Hilfe Hoherer Ableitungen (Gravity Derivatives)	GP 01 -4-0250
A Universal Table for the Prediction of the Lunar-Solar Correction in Gravimetry (Tidal Gravity Correction)	GP 02 -5-0002
Tidal Gravity Corrections for 1954	GP 02 -5-0006
Tidal Gravity Corrections for 1954	GP 02 -5-0032
A Comparison of the Second Derivative Method of Gravity Interpretation with Reflection Seismics and Geological Findings in the Offenburg Area	GP 02 -1-0001
Quantitative Studies Concerning the Vertical Gradient and Second Derivative Methods of Gravity Interpretation	GP 02 -2-0128
Some Remarks on the Errors in the Calculation of the Vertical Gradient of Gravity	GP 02 -4-0285
Tidal Gravity Corrections for 1955	GP 03 -5-0001
Tidal Gravity Corrections for 1955	GP 03 -5-0030
Three Dimensional Gravity Survey	GP 03 -1-0015
Relative Determination of the Density of Surface Rocks and the Mean Density of the Earth from Vertical Gravity Measurements	GP 03 -3-0212

REFERENCES ON THE GRAVITY METHOD CONTAINED IN
EARLY GEOPHYSICAL PAPERS, GEOPHYSICS, AND GEOPHYSICAL PROSPECTING--continued

Gravity Variations in Surveys Across Geological Boundaries	GP 03 -4-0403
Correlation of Rock Density Determinations for Gravity Survey Interpretation	GP 05 -1-0020
Some Depth Formulae for Local Magnetic and Gravity Anomalies	GP 07 -1-0055
Optical Analogue of Gravity and Magnetic Fields	GP 07 -4-0414
Some Formulae for Interpreting Local Gravity Anomalies	GP 08 -4-0607
Tidal Gravity Corrections for 1963	GP 10 -5-0001
Simplified Gravity Terrain Corrections	GP 10 -1-0019
The Detection of Caves by Gravity Measurements	GP 11 -1-0001
High Speed Calculation of Gravity and Magnetic Profiles Across Two-Dimensional Bodies Having an Arbitrary Cross-Section	GP 11 -1-0010
Surface-Ship Gravity Measurements in the North-Sea	GP 11 -4-0535
On the Correlation of Gravity with Tidal Anomalies	GP 12 -4-0434
Charts for Determining the Gravity Effect of Two and Three Dimensional Bodies Bounded by Arbitrary Polygons	GP 13 -1-0012
Some Notes Concerning the Frequency Analysis for Gravity Interpretation	GP 13 -3-0475
Topographic and Isostatic Corrections to Gravity Surveys in Mountainous Areas	GP 15 -1-0151
Graphical Evaluation of Magnetic and Gravity Attraction of Three-Dimensional Bodies	GP 15 -2-0167
Investigation of Tectonics by Gravity Detailing	GP 15 -3-0480
Analysis of Gravity Anomalies of Two Dimensional Faults Using Fourier Transforms	GP 16 -1-0077
Gravitational Surveying with the Gravity-Meter (Gravimeter)	GE 02 -1-0021
Gravity-Meter Survey of the Kettleman-Hills Lost Hills Trend California	GE 11 -2-0121
Free-Air Gravity Anomaly Map of the Gulf of Mexico and Its Tectonic Implications 1963 Edition (Ship Gravity-Meter)	GE 30 -1-0102
Short Note-Possible Application of the Anomalous Free-Air Vertical Gradient to Marine Exploration (Bore-Hole Gravity-Meter Densities)	GE 31 -1-0260
Time Variations of the Calibration of the Worden Gravity-Meter	GP 07 -2-0141
Some Pressure Effects on the Behaviour of Worden Gravity-Meters	GP 08 -1-0111
Gravity Studies Over Three Evaporite Piercement Domes in the Canadian Arctic	GE 35 -1-0057
Some Formulas Useful in the Interpretation of Gravitational and Magnetic Profiles	GE 35 -1-0066
The Anomalous Vertical Gradient of Gravity	GE 35 -1-0153
The Gradiational Density Contrast as a Gravity Interpretation Model	GE 35 -2-0270
Gravity Diagrams for Thickness Determination of Exposed Rock Bodies	GE 35 -3-0471
Gravity Anomalies of a Fault Cutting a Series of Beds	GE 35 -4-0708
Instrumental Arrangement to Measure Gravity with Gradients	GE 35 -4-0713
Discussion-Convergence and Divergence in Downward Continuation	GE 36 -1-0211
Discussion-The Anomalous Vertical Gradient of Gravity	GE 36 -1-0214
Automatic Trend Analysis and Interpretation of Potential Field Data	GE 36 -2-0339
A Filtering Technique for Interpreting the Gravity Anomaly Generated by a 2-D Fault	GE 36 -3-0554
Application of Rational Approximation in Calculation of the 2nd Derivative of the Gravity Field	GE 36 -3-0571
The Bouguer Correction for the Spherical Earth	GE 36 -4-0761
Linear Filters to Suppress Terrain Effects on Geophysical Maps	GE 36 -5-0963
The Use of Linear Filtering in Gravity Problems	GE 36 -6-1174
Extended Terrain Correction Tables for Gravity Reductions	GE 37 -2-0377
Review of Data Processing and Interpretation Methods in Gravity and Magnetics, 1964-1971	GE 37 -4-0647
Discussion-The Use of Linear Filtering in Gravity Problems	GE 37 -4-0704

REFERENCES ON THE GRAVITY METHOD CONTAINED IN
EARLY GEOPHYSICAL PAPERS, GEOPHYSICS AND GEOPHYSICAL PROSPECTING--continued

Technique for Improved Convergence in Iterative Analysis of Gravity Anomaly Problems	GE 38 -3-0500
Gravity Analysis Using an Exponential Density-Depth Function, San Jacinto, Graben, California	GE 38 -4-0684
Bouguer Gravity and Its Geologic Evaluation in the Western Part of the Bengal Basin and Adjoining Area, India	GE 38 -4-0691
Cross Correlation Method for Evaluating and Correcting Shipboard Gravity Data	GE 38 -4-0701
The Use of Nonlinear Functional Expansions in Calculation of the Terrain Effect in Airborne and Marine Gravimetry and Gradiometry	GE 39 -1-0033
Approximations in Gravity Interpretation Calculations	GE 39 -2-0205
The Inversion and Interpretation of Gravity Anomalies	GE 39 -4-0526
Topographics and Terrain Corrections for Airborne Gravity	GE 39 -4-0537
Best Bounds on Density and Depth from Gravity Data	GE 39 -5-0644
Gravity Profile Interpretation Using the Fourier Transform	GE 39 -6-0862
Distribution and Regional Variation of Density in the Western Canada Basin	GE 40 -1-0056
A Bouguer Gravity Anomaly Map of South America	GE 40 -1-0120
Exploring for Stratigraphic Traps with Gravity Gradients	GE 40 -2-0256
Discussion-Gravity Interpretation Using the Fourier Integral	GE 40 -2-0356
Inversion of Gravity Profiles by Use of a Backus-Gilbert Approach	GE 40 -5-0763
Digital Convolution for Computing Gravity and Magnetic Anomalies Due to Arbitrary Bodies	GE 40 -6-0981
Spectral Analysis of Gravity and Magnetic Anomalies Due to 2-Dimensional Structures	GE 40 -6-0993
Automatic 3-Dimensional Modeling for the Interpretation of Gravity or Magnetic Anomalies	GE 40 -6-1014
The Effect of Finite Data Length in the Spectral Analysis of Ideal Gravity Anomalies	GE 41 -1-0044
Remanent Magnetization from Comparison of Gravity and Magnetic Anomalies	GE 41 -1-0056

Geophysics (GE)

Geophysical Prospecting (GP)

<u>Vol.</u>	<u>Year</u>	<u>Vol.</u>	<u>Year</u>	<u>Vol.</u>	<u>Year</u>	<u>Vol.</u>	<u>Year</u>	<u>Vol.</u>	<u>Year</u>
1	1936	15	1950	29	1964	1	1953	13	1965
2	1937	16	1951	30	1965	2	1954	14	1966
3	1938	17	1952	31	1966	3	1955	15	1967
4	1939	18	1953	32	1967	4	1956	16	1968
5	1940	19	1954	33	1968	5	1957	17	1969
6	1941	20	1955	34	1969	6	1958	18	1970
7	1942	21	1956	35	1970	7	1959	19	1971
8	1943	22	1957	36	1971	8	1960	20	1972
9	1944	23	1958	37	1972	9	1961	21	1973
10	1945	24	1959	38	1973	10	1962	22	1974
11	1946	25	1960	39	1974	11	1963	23	1975
12	1947	26	1961	40	1975	12	1964	24	1976
13	1948	27	1962	41	1976				
14	1949	28	1963						

REFERENCES ON THE GRAVITY METHOD

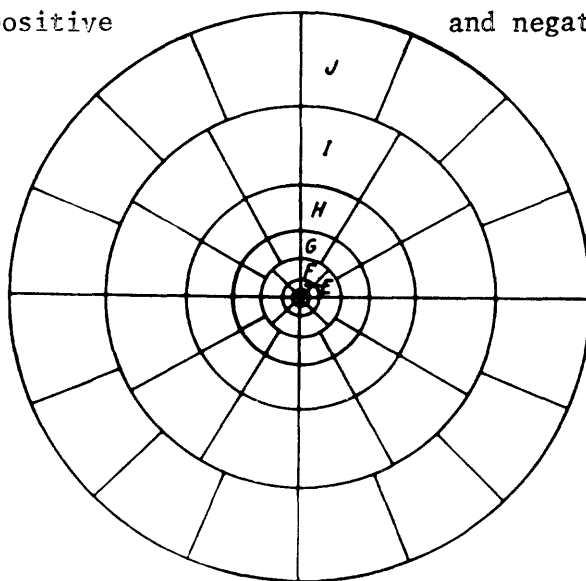
Books

- Dobrin, Milton B., 1975, Introduction to Geophysical Prospecting, 3rd Edition, McGraw-Hill Book Co., New York, New York.
- Grant, F. S., and West, G. F., 1965, Interpretation Theory in Applied Geophysics, McGraw-Hill Book Co., New York, New York.
- Nettleton, L. L., 1940, Geophysical Prospecting for Oil, McGraw-Hill Book Co., New York, New York.
- Nettleton, L. L., 1971, Elementary Gravity and Magnetism for Geologists and Seismologists, Society of Exploration Geophysicists Monograph Number 1, Tulsa, Oklahoma.
- Nettleton, L. L., 1976, Interpretation of Gravity Data, McGraw-Hill Book Co., New York, New York.

APPENDIX A

Tables for the Gravity Terrain Correction

Hammer* and Bible** have developed procedures for terrain corrections. The zones and their radii are as proposed by Hammer (see figure) but are extended by Bible. For simplicity the minimum correction is 0.005 mgal. As the elevation differences for zones B through D are usually estimated in the field, the number of compartments is reduced to 4 in zone C and increased to 8 in zone D. The number of compartments is increased to 16 in zones E through I, similarly for zones J through M. Each zone is a circular ring of indicated radii in feet, divided into 4, 8, or 16 equal compartments of arbitrary azimuth. h is the range of the difference of elevation in feet between the gravity station and the mean elevation of the compartment without regard to sign. The corrections are in milligals and have been computed for a specific gravity of 2.0 between the ground and air. The terrain correction is always positive for land measurements; positive and negative for sea measurements.



Terrain correction zone chart designed by Hammer, used in conjunction with Table

*Hammer, S., 1939, Terrain Corrections for Gravimeter Stations, Geophysics, v. 4, p. 184.

**Bible, J. L., 1962, Terrain Corrections for Gravity, Geophysics, v. 27, pp. 715-718.

Terrain Correction Table For Gravity.

Zones	B	C	D	E	F	G	H	I	J	K	L	M
Compartments	4	4	8	16	16	16	16	16	16	16	16	16
Inner radius	6.56	53.6	175	558	1,280	2,936	5,018	8,578	14,662	21,826	32,490	48,365
Outer radius	54.6	175	558	1,280	2,936	5,018	8,578	14,662	21,826	32,490	48,365	71,996
Correction in milligals	+ h (ft.)	+ h (ft.)	+ h (ft.)	+ h (ft.)	+ h (ft.)	+ h (ft.)	+ h (ft.)	+ h (ft.)	+ h (ft.)	+ h (ft.)	+ h (ft.)	+ h (ft.)
0	0.2	0.8	0.20	0.56	0.84	0.165	0.194	0.254	0.374	0.434	0.555	0.678
00.5	2.4	8.14	20.34	56.97	84.116	165.258	194.336	254.540	374.555	434.677	555.826	678.1,008
01	4.7	14.20	34.49	97.126	146.189	258.308	336.397	540.673	555.918	677.119	826.1,365	1,008.1,665
02	7.9	20.26	49.64	126.170	189.255	308.433	397.558	673.806	918.1185	1,119.1,445	1,365.1,763	1,665.2,150
03	9.12	26.32	64.76	150.206	235.408	333.532	558.719	806.938	1,185.1,403	1,445.1,711	1,763.2,086	2,150.2,545
04	12.14	32.36	76.87	206.238	308.353	552.632	719.810	918.1,056	1,403.1,592	1,711.1,941	2,086.2,366	2,545.2,886
05	14.16	36.40	87.97	238.266	353.394	632.760	810.901	1,056.1,174	1,592.1,762	1,941.2,146	2,366.2,617	2,886.3,191
06	16.19	40.44	97.107	268.293	394.431	700.764	901.992	1,174.1,292	1,762.1,917	2,146.2,335	2,617.2,846	3,191.3,470
07	19.21	44.48	107.116	298.318	431.466	744.823	992.1,074	1,292.1,385	1,917.2,060	2,335.2,509	2,846.3,056	3,470.3,728
08	21.23	48.52	116.126	318.342	466.498	823.860	1,074.1,146	1,385.1,478	2,060.2,195	2,509.2,672	3,058.3,257	3,728.3,970
09	24.25	52.56	126.135	342.366	498.529	880.933	1,146.1,209	1,478.1,571	2,195.2,322	2,672.2,826	3,257.3,444	3,970.4,198
10	27.30	56.60	135.143	366.388	529.559	933.982	1,209.1,270	1,571.1,650	2,322.2,442	2,826.2,973	3,444.3,622	4,198.4,414
11	30.34	60.64	143.151	388.410	559.587	982.1,031	1,270.1,331	1,650.1,729	2,442.2,558	2,973.3,115	3,622.3,780	4,414.4,620
12	34.38	64.68	151.159	410.432	587.614	1,031.1,079	1,331.1,392	1,729.1,807	2,558.2,669	3,115.3,250	3,780.3,935	4,620.4,820
13	38.42	68.72	159.167	432.454	614.641	1,079.1,123	1,392.1,447	1,807.1,878	2,669.2,776	3,250.3,375	3,935.4,090	4,820.5,010
14	42.46	72.76	167.174	454.476	641.668	1,123.1,167	1,447.1,502	1,878.1,949	2,776.2,879	3,375.3,500	4,090.4,243	5,010.5,190
15	46.51	76.80	174.181	476.498	668.694	1,167.1,210	1,502.1,557	1,949.2,020	2,879.2,978	3,500.3,620	4,245.4,390	5,190.5,365
16	51.57	80.84	181.189	498.518	694.719	1,210.1,251	1,557.1,607	2,020.2,081	2,987.3,075	3,620.3,730	4,390.4,570	5,365.5,540
17	57.63	84.87	189.196	518.538	719.743	1,251.1,291	1,607.1,656	2,081.2,142	3,075.3,170	3,730.3,840	4,530.4,670	5,540.5,700
18	63.70	88.90	196.204	538.558	743.767	1,292.1,333	1,656.1,704	2,142.2,204	3,170.3,263	3,840.3,950	4,670.4,800	5,700.5,860
19	70.78	90.94	204.212	558.578	767.791	1,333.1,372	1,704.1,753	2,204.2,265	3,263.3,353	3,950.4,060	4,800.4,930	5,860.6,030
20	78.88	94.98	212.220	578.598	791.815	1,372.1,411	1,753.1,802	2,265.2,326	3,353.3,440	4,060.4,170	4,930.5,060	6,030.6,180
21	88.100	98.102	220.227	598.619	815.839	1,411.1,450	1,802.1,850	2,326.2,387	3,440.3,518	4,170.4,270	5,060.5,180	6,180.6,330
22	100.114	102.106	227.234	619.640	839.863	1,450.1,488	1,850.1,896	2,387.2,444	3,518.3,606	4,270.4,370	5,180.5,300	6,330.6,470
23	114.132	106.110	234.242	640.661	863.885	1,488.1,526	1,896.1,942	2,444.2,501	3,596.3,674	4,370.4,470	5,300.5,420	6,470.6,620
24	132.156	110.114	242.249	661.683	885.907	1,526.1,564	1,942.1,987	2,501.2,557	3,674.3,752	4,470.4,570	5,420.5,530	6,620.6,760
25	156.189	114.119	249.257	683.704	907.929	1,564.1,602	1,987.2,030	2,557.2,610	3,752.3,830	4,570.4,660	5,530.5,640	6,760.6,900
26	189.236	119.124	257.265	704.725	929.951	1,602.1,639	2,030.2,073	2,610.2,663	3,830.3,908	4,660.4,750	5,640.5,750	6,900.7,030
27	236.312	124.128	265.273	725.746	951.973	1,639.1,676	2,073.2,115	2,663.2,715	3,908.3,986	4,750.4,840	5,750.5,860	7,030.7,160
28	312.455	128.133	273.281	746.767	973.995	1,676.1,711	2,115.2,158	2,715.2,768	3,986.4,064	4,840.4,930	5,860.5,965	7,160.7,290
29	455.812	133.138	281.289	767.788	995.1,016	1,711.1,745	2,158.2,201	2,768.2,821	4,064.4,142	4,930.5,020	5,965.6,070	7,290.7,420
30	812.3,560	138.143	289.297	788.809	1,016.1,037	1,745.1,779	2,201.2,243	2,821.2,873	4,142.4,220	5,020.5,110	6,070.6,175	7,420.7,550
31	3,560	143.148	297.305	809.832	1,037.1,058	1,779.1,812	2,243.2,282	2,873.2,922	4,220.4,298	5,110.5,200	6,175.6,280	7,550.7,667
32		148.153	305.314	832.855	1,058.1,079	1,812.1,844	2,282.2,321	2,922.2,971	4,288.4,356	5,200.5,280	6,280.6,380	7,667.7,784
33		153.159	314.322	855.878	1,079.1,100	1,844.1,876	2,321.2,361	2,971.3,017	4,356.4,424	5,280.5,360	6,380.6,480	7,784.7,901
34		159.165	322.331	878.901	1,100.1,121	1,876.1,908	2,361.2,400	3,019.3,067	4,424.4,492	5,360.5,440	6,480.6,580	7,901.8,018
35		165.171	331.339	901.924	1,121.1,142	1,908.1,940	2,400.2,439	3,067.3,115	4,492.4,560	5,440.5,520	6,580.6,680	8,018.8,135

Terrain Correction Table—(Continued)

Zones	B	C	D	E	F	G	H	I	J	K	L	M
Compartments	4	4	8	16	16	16	16	16	16	16	16	16
Inner radius	6.6	54.6	175	558	1,280	2,936	5,018	8,578	14,662	21,826	32,490	48,365
Outer radius	54.6	175	558	1,280	2,936	5,018	8,578	14,662	21,826	32,490	48,365	71,996
Correction in millicals	- h (ft.)	- h (ft.)	+ h (ft.)	+ h (ft.)	+ h (ft.)	+ h (ft.)	+ h (ft.)	+ h (ft.)	+ h (ft.)	+ h (ft.)	+ h (ft.)	+ h (ft.)
36	171 177	339 348	339 348	924 948	1,142 1,163	1,940 1,972	2,439 2,477	3,115 3,164	4,560 4,628	5,520 5,600	6,680 6,780	8,135 8,252
37	177 184	348 356	348 356	948 972	1,163 1,184	1,972 2,004	2,477 2,514	3,164 3,209	4,628 4,696	5,600 5,675	6,780 6,880	8,252 8,369
38	184 191	356 365	356 365	972 996	1,184 1,205	2,004 2,036	2,514 2,551	3,209 3,254	4,696 4,764	5,675 5,755	6,880 6,970	8,369 8,486
39	191 198	365 373	365 373	996 1,021	1,205 1,226	2,036 2,068	2,551 2,589	3,254 3,300	4,764 4,832	5,755 5,830	6,970 7,060	8,486 8,603
40	198 206	373 382	373 382	1,021 1,046	1,226 1,247	2,068 2,100	2,589 2,625	3,300 3,343	4,832 4,900	5,830 5,910	7,060 7,150	8,603 8,720
41	206 214	382 392	382 392	1,046 1,070	1,247 1,268	2,100 2,132	2,625 2,661	3,343 3,386	4,900 4,968	5,910 5,990	7,150 7,240	8,720 8,837
42	214 222	392 402	392 402	1,070 1,095	1,268 1,288	2,132 2,164	2,661 2,697	3,386 3,430	4,968 5,022	5,990 6,065	7,240 7,330	8,837 8,926
43	222 230	402 411	402 411	1,095 1,120	1,288 1,309	2,164 2,196	2,697 2,733	3,430 3,473	5,022 5,083	6,065 6,140	7,330 7,420	8,926 9,029
44	230 239	411 423	411 423	1,120 1,145	1,309 1,330	2,196 2,228	2,733 2,769	3,473 3,516	5,083 5,144	6,140 6,210	7,420 7,500	9,029 9,132
45	239 249	423 435	423 435	1,145 1,170	1,330 1,350	2,228 2,260	2,769 2,804	3,516 3,560	5,144 5,205	6,210 6,280	7,500 7,580	9,132 9,235
46	249 259	435 446	435 446	1,170 1,197	1,350 1,370	2,260 2,291	2,804 2,839	3,560 3,603	5,205 5,266	6,280 6,350	7,580 7,660	9,235 9,338
47	259 270	446 457	446 457	1,197 1,226	1,370 1,391	2,291 2,322	2,839 2,874	3,603 3,647	5,266 5,327	6,350 6,420	7,660 7,730	9,338 9,441
48	270 281	457 468	457 468	1,226 1,255	1,391 1,411	2,322 2,352	2,874 2,909	3,647 3,691	5,327 5,388	6,420 6,490	7,730 7,800	9,441 9,544
49	281 292	468 479	468 479	1,255 1,284	1,411 1,432	2,352 2,383	2,909 2,944	3,691 3,735	5,388 5,449	6,490 6,560	7,800 7,920	9,544 9,647
50	292 306	479 490	479 490	1,284 1,313	1,432 1,452	2,383 2,414	2,944 2,979	3,735 3,779	5,449 5,510	6,560 6,640	7,920 8,000	9,647 9,750
51	306 320	490 501	490 501	1,313 1,345	1,452 1,473	2,414 2,444	2,979 3,013	3,779 3,823	5,510 5,571	6,640 6,720	8,000 8,080	9,750 9,853
52	320 334	501 513	501 513	1,345 1,377	1,473 1,494	2,444 2,475	3,013 3,047	3,823 3,867	5,571 5,632	6,720 6,800	8,080 8,160	9,853 9,956
53	334 350	513 524	513 524	1,377 1,409	1,494 1,515	2,475 2,506	3,047 3,081	3,867 3,911	5,632 5,693	6,800 6,880	8,160 8,240	9,956 10,059
54	350 368	524 536	524 536	1,409 1,441	1,515 1,536	2,506 2,536	3,081 3,116	3,911 3,955	5,693 5,754	6,880 6,960	8,240 8,320	10,059 10,162
55	368 386	536 547	536 547	1,441 1,474	1,536 1,557	2,536 2,567	3,116 3,150	3,955 4,000	5,754 5,815	6,960 7,040	8,320 8,400	10,162 10,265
56	386 407	547 559	547 559	1,474 1,510	1,557 1,579	2,567 2,598	3,150 3,184	4,000 4,045	5,815 5,876	7,040 7,120	8,400 8,480	10,265 10,368
57	407 430	559 570	559 570	1,510 1,547	1,579 1,600	2,598 2,628	3,184 3,218	4,045 4,090	5,876 5,937	7,120 7,200	8,480 8,560	10,368 10,471
58	430 455	570 582	570 582	1,547 1,584	1,600 1,622	2,628 2,659	3,218 3,252	4,090 4,135	5,937 6,000	7,200 7,280	8,560 8,640	10,471 10,574
59	455 483	582 593	582 593	1,584 1,622	1,622 1,643	2,659 2,690	3,252 3,285	4,135 4,180	6,000 6,061	7,280 7,360	8,640 8,720	10,574 10,677
60	483 514	593 605	593 605	1,622 1,661	1,643 1,665	2,690 2,720	3,285 3,318	4,180 4,225	6,061 6,122	7,360 7,440	8,720 8,800	10,677 10,780
61	514 549	605 621	605 621	1,661 1,703	1,665 1,687	2,720 2,751	3,318 3,351	4,225 4,270	6,122 6,183	7,440 7,520	8,800 8,880	10,780 10,883
62	549 587	621 637	621 637	1,703 1,745	1,687 1,709	2,751 2,781	3,351 3,384	4,270 4,315	6,183 6,244	7,520 7,600	8,880 8,960	10,883 10,986
63	587 632	637 653	637 653	1,745 1,787	1,709 1,731	2,781 2,811	3,384 3,417	4,315 4,360	6,244 6,305	7,600 7,680	9,000 9,080	10,986 11,089
64	632 685	653 669	653 669	1,787 1,831	1,731 1,753	2,811 2,841	3,417 3,450	4,360 4,405	6,305 6,366	7,680 7,760	9,080 9,160	11,089 11,192
65	685 745	669 685	669 685	1,831 1,875	1,753 1,775	2,841 2,871	3,450 3,483	4,405 4,450	6,366 6,427	7,760 7,840	9,160 9,240	11,192 11,295
66	745 815	685 701	685 701	1,875 1,926	1,775 1,797	2,871 2,901	3,483 3,515	4,450 4,495	6,427 6,488	7,840 7,920	9,240 9,320	11,295 11,398
67	815 903	701 717	701 717	1,926 1,978	1,797 1,819	2,901 2,931	3,515 3,547	4,495 4,540	6,488 6,549	7,920 8,000	9,320 9,400	11,398 11,499
68	903 1,010	717 733	717 733	1,978 2,030	1,819 1,841	2,931 2,961	3,547 3,579	4,540 4,585	6,549 6,610	8,000 8,080	9,400 9,480	11,499 11,599
69	1,010 1,140	733 749	733 749	2,030 2,082	1,841 1,863	2,961 2,992	3,579 3,610	4,585 4,630	6,610 6,671	8,080 8,160	9,480 9,560	11,599 11,699
70	1,140 1,310	749 766	749 766	2,082 2,134	1,863 1,885	2,992 3,023	3,610 3,641	4,630 4,675	6,671 6,732	8,160 8,240	9,560 9,640	11,699 11,799
71	1,310 1,540	766 788	766 788	2,134 2,195	1,885 1,908	3,023 3,054	3,641 3,671	4,675 4,720	6,732 6,793	8,240 8,320	9,640 9,720	11,799 11,899
72	1,540 1,870	788 811	788 811	2,195 2,257	1,908 1,931	3,054 3,086	3,671 3,702	4,720 4,765	6,793 6,854	8,320 8,400	9,720 9,800	11,899 11,999
73	1,870 2,380	811 833	811 833	2,257 2,319	1,931 1,954	3,086 3,117	3,702 3,733	4,765 4,810	6,854 6,915	8,400 8,480	9,800 9,880	11,999 12,099
74	2,380 3,260	833 856	833 856	2,319 2,381	1,954 1,977	3,117 3,148	3,733 3,764	4,810 4,855	6,915 6,976	8,480 8,560	9,880 9,960	12,099 12,199
75	3,260 5,200	856 878	856 878	2,381 2,443	1,977 2,000	3,148 3,180	3,764 3,795	4,855 4,900	6,976 7,037	8,560 8,640	9,960 10,040	12,199 12,299

(Continued on next page)

Terrain Correction Table—(Continued)

Zones	B	C	D	E	F	G	H	I	J	K	L	M
Compartments	4	4	8	16	16	16	16	16	16	16	16	16
Inner radius	6.56	54.6	175	558	1,280	2,936	5,018	8,578	14,662	21,826	32,490	48,365
Outer radius	54.6	175	558	1,280	2,936	5,018	8,578	14,662	21,826	32,490	48,365	71,996
Correction in milligals	- h (ft.)	- h (ft.)	- h (ft.)	- h (ft.)	- h (ft.)	- h (ft.)	- h (ft.)	- h (ft.)	- h (ft.)	- h (ft.)	- h (ft.)	- h (ft.)
76		5,200	878 901	2,443 2,521	2,000 2,023	3,180 3,212	3,795 3,827	4,710 4,745				
77			901 923	2,521 2,599	2,023 2,046	3,212 3,244	3,827 3,860	4,745 4,780				
78			923 946	2,599 2,677	2,046 2,070	3,244 3,276	3,860 3,893	4,780 4,816				
79			946 968	2,677 2,756	2,070 2,093	3,276 3,308	3,893 3,925	4,816 4,851				
80			968 991	2,756 2,836	2,093 2,116	3,308 3,340	3,925 3,957	4,851 4,886				
81			991 1,027	2,836 2,915	2,116 2,140	3,340 3,372	3,957 3,990	4,886 4,922				
82			1,027 1,064	2,915 3,035	2,140 2,165	3,372 3,404	3,990 4,022	4,922 4,957				
83			1,064 1,101	3,035 3,135	2,165 2,190	3,404 3,437	4,022 4,054	4,957 4,992				
84			1,101 1,138	3,135 3,235	2,190 2,215	3,437 3,470	4,054 4,085	4,992 5,028				
85			1,138 1,175	3,235 3,335	2,215 2,240	3,470 3,503	4,085 4,116	5,028 5,063				
86			1,175 1,212	3,335 3,478	2,240 2,266	3,503 3,536	4,116 4,147	5,063 5,098				
87			1,212 1,249	3,478 3,621	2,266 2,291	3,536 3,570	4,147 4,179	5,098 5,133				
88			1,249 1,286	3,621 3,764	2,291 2,316	3,570 3,603	4,179 4,210	5,133 5,169				
89			1,286 1,323	3,764 3,907	2,316 2,341	3,603 3,636	4,210 4,241	5,169 5,204				
90			1,323 1,360	3,907 4,050	2,341 2,367	3,636 3,670	4,241 4,272	5,204 5,240				
91			1,360 1,424	4,050 4,260	2,367 2,393	3,670 3,703	4,272 4,303	5,240 5,272				
92			1,424 1,488	4,260 4,472	2,393 2,420	3,703 3,736	4,303 4,334	5,272 5,304				
93			1,488 1,552	4,472 4,684	2,420 2,447	3,736 3,770	4,334 4,366	5,304 5,336				
94			1,552 1,616	4,684 4,896	2,447 2,473	3,770 3,803	4,366 4,397	5,336 5,368				
95			1,616 1,680	4,896 5,108	2,473 2,500	3,803 3,836	4,397 4,428	5,368 5,400				
96			1,680 1,744	5,108 5,452	2,500 2,527	3,836 3,870	4,428 4,460	5,400 5,432				
97			1,744 1,808	5,452 5,796	2,527 2,554	3,870 3,903	4,460 4,491	5,432 5,464				
98			1,808 1,872	5,796 6,140	2,554 2,581	3,903 3,937	4,491 4,522	5,464 5,496				
99			1,872 1,936	6,140 6,484	2,581 2,608	3,937 3,971	4,522 4,553	5,496 5,528				
1 00			1,936 2,000	6,484 6,830	2,608 2,635	3,971 4,005	4,553 4,585	5,528 5,560				

Table 1. Terrain correction tables for gravity. h is the mean topographic elevation in ft (without for each compartment in units of 0.01 mgal for density (d) = 2.0 gm/cm³. This correction

Zone B 4 compartments 6.56 to 54.6*			Zone C 6 compartments 54.6 to 175			Zone D 6 compartments 175 to 358			Zone E 8 compartments 358 to 1280			Zone F 8 compartments 1280 to 2936			Zone G 12 compartments 2936 to 5018		
$\pm h$ (ft)	T		$\pm h$ (ft)	T		$\pm h$ (ft)	T		$\pm h$ (ft)	T		$\pm h$ (ft)	T		$\pm h$ (ft)	T	
0 to 1.1	0		0 to 4.3	0		0 to 7.8	0		0 to 18	0		0 to 27	0		0 to 58	0	
1.1- 1.9	0.1		4.3- 7.5	0.1		7.8- 13.4	0.1		18- 30	0.1		27- 46	0.1		58- 100	0.1	
1.9- 2.5	0.2		7.5- 9.7	0.2		13.4- 17.4	0.2		30- 39	0.2		46- 60	0.2		100- 129	0.2	
2.5- 2.9	0.3		9.7- 11.5	0.3		17.4- 20.5	0.3		39- 47	0.3		60- 71	0.3		129- 153	0.3	
2.9- 3.4	0.4		11.5- 13.1	0.4		20.5- 23.3	0.4		47- 53	0.4		71- 80	0.4		153- 173	0.4	
3.4- 3.7	0.5		13.1- 14.5	0.5		23.3- 25.8	0.5		53- 58	0.5		80- 88	0.5		173- 192	0.5	
3.7- 7	1		14.5- 24	1		25.8- 43	1		58- 97	1		88-147	1		192- 317	1	
7- 9	2		24- 32	2		43- 56	2		97-126	2		147-190	2		317- 410	2	
9- 12	3		32- 39	3		56- 66	3		126-149	3		190-224	3		410- 486	3	
12- 14	4		39- 45	4		66- 76	4		149-170	4		224-255	4		486- 552	4	
14- 16	5		45- 51	5		76- 84	5		170-189	5		255-282	5		552- 611	5	
16- 19	6		51- 57	6		84- 92	6		189-206	6		282-308	6		611- 666	6	
19- 21	7		57- 63	7		92-100	7		206-222	7		308-331	7		666- 716	7	
21- 24	8		63- 68	8		100-107	8		222-238	8		331-353	8		716- 764	8	
24- 27	9		68- 74	9		107-114	9		238-252	9		353-374	9		764- 809	9	
27- 30	10		74- 80	10		114-121	10		252-266	10		374-394	10		809- 852	10	
30- 33	11		80- 85	11		121-127	11		266-280	11		394-413	11		852- 894	11	
33- 37	12		85- 91	12		127-134	12		280-293	12		413-431	12		894- 933	12	
37- 41	13		91- 97	13		134-140	13		293-306	13		431-449	13		933- 972	13	
41- 45	14		97-103	14		140-146	14		306-318	14		449-466	14		972-1009	14	
45- 50	15		103-110	15		146-152	15		318-330	15		466-483	15		1009-1045	15	
50- 55	16		110-116	16		152-158	16		330-342	16		483-499	16		1045-1081	16	
55- 60	17		116-123	17		158-164	17		342-354	17		499-515	17		1081-1115	17	
60- 67	18		123-130	18		164-170	18		354-366	18		515-530	18		1115-1149	18	
67- 75	19		130-138	19		170-175	19		366-377	19		530-545	19		1149-1182	19	
75- 84	20		138-145	20		175-181	20		377-388	20		545-560	20		1182-1214	20	
84- 95	21		145-153	21		181-187	21		388-399	21		560-574	21		1214-1246	21	
95- 108	22		153-162	22		187-192	22		399-410	22		574-589	22		1246-1277	22	
108- 125	23		162-171	23		192-198	23		410-421	23		589-603	23		1277-1307	23	
125- 147	24		171-180	24		198-204	24		421-432	24		603-617	24		1307-1337	24	
147- 177	25		180-190	25		204-209	25		432-443	25		617-630	25		1337-1367	25	
177- 221	26		190-201	26		209-215	26		443-453	26		630-644	26		1367-1396	26	
221- 293	27		201-213	27		215-221	27		453-464	27		644-657	27		1396-1425	27	
293- 429	28		213-225	28		221-226	28		464-474	28		657-670	28		1425-1454	28	
429- 795	29		225-239	29		226-232	29		474-485	29		670-683	29		1454-1482	29	
795-5247	30		239-253	30		232-238	30		485-495	30		683-696	30		1482-1510	30	

* Radii of the zone in ft.

regard to sign) in each compartment with respect to the elevation of the station. T is the correction applied with the simple Bouguer correction for the Bouguer anomaly is always positive.

Zone H 12 compartments 5018 to 8578		Zone I 12 compartments 8578 to 14,662		Zone J 16 compartments 14,662 to 21,826		Zone K 16 compartments 21,826 to 32,490		Zone L 16 compartments 32,490 to 48,365		Zone M 16 compartments 48,365 to 71,996	
$\pm h$ (ft)	T	$\pm h$ (ft)	T	$\pm h$ (ft)	T	$\pm h$ (ft)	T	$\pm h$ (ft)	T	$\pm h$ (ft)	T
0 to 76	0	0 to 99	0	0 to 168	0	0 to 205	0	0 to 250	0	0 to 302	0
76-131	0.1	99-171	0.1	168-290	0.1	205-354	0.1	250-431	0.1	302-525	0.1
131-169	0.2	171-220	0.2	290-374	0.2	354-456	0.2	431-557	0.2	525-678	0.2
169-200	0.3	220-261	0.3	374-443	0.3	456-540	0.3	557-659	0.3	678-803	0.3
200-226	0.4	261-296	0.4	443-502	0.4	540-612	0.4	659-747	0.4	803-912	0.4
226-250	0.5	296-327	0.5	502-555	0.5	612-677	0.5	747-826	0.5	912-1007	0.5
250-414	1	327-541	1	555-918	1	677-1120	1	826-1366	1	1007-1666	1
414-535	2	541-698	2	918-1186	2	1120-1446	2	1366-1763	2	1666-2150	2
535-633	3	698-827	3	1186-1404	3	1446-1711	3	1763-2086	3	2150-2544	3
633-719	4	827-938	4	1404-1592	4	1711-1941	4	2086-2366	4	2544-2886	4
719-795	5	938-1037	5	1592-1762	5	1941-2147	5	2366-2617	5	2886-3191	5
795-866	6	1037-1128	6	1762-1916	6	2147-2334	6	2617-2845	6	3191-3469	6
866-931	7	1128-1213	7	1916-2060	7	2334-2509	7	2845-3057	7	3469-3727	7
931-992	8	1213-1292	8	2060-2194	8	2509-2672	8	3057-3256	8	3727-3969	8
992-1050	9	1292-1367	9	2194-2321	9	2672-2826	9	3256-3443	9	3969-4196	9
1050-1105	10	1367-1438	10	2321-2442	10	2826-2972	10	3443-3621	10	4196-4413	10
1105-1158	11	1438-1506	11	2442-2557	11	2972-3112	11	3621-3790	11	4413-4619	11
1158-1208	12	1506-1571	12	2557-2668	12	3112-3246	12	3790-3953	12	4619-4816	12
1208-1257	13	1571-1633	13	2668-2775	13	3246-3375	13	3953-4109	13	4816-5006	13
1257-1304	14	1633-1694	14	2775-2878	14	3375-3499	14	4109-4260	14	5006-5190	14
1304-1350	15	1694-1752	15	2878-2977	15	3499-3620	15	4260-4406	15	5190-5367	15
1350-1394	16	1752-1809	16	2977-3074	16	3620-3736	16	4406-4547	16	5367-5538	16
1394-1437	17	1809-1864	17	3074-3168	17	3736-3850	17	4547-4684	17	5538-5705	17
1437-1480	18	1864-1918	18	3168-3259	18	3850-3960	18	4684-4818	18	5705-5867	18
1480-1521	19	1918-1971	19	3259-3349	19	3960-4067	19	4818-4948	19	5867-6024	19
1521-1561	20	1971-2022	20	3349-3436	20	4067-4172	20	4948-5074	20	6024-6178	20
1561-1600	21	2022-2072	21	3436-3521	21	4172-4275	21	5074-5198	21	6178-6328	21
1600-1639	22	2072-2121	22	3521-3604	22	4275-4375	22	5198-5319	22	6328-6475	22
1639-1677	23	2121-2169	23	3604-3686	23	4375-4473	23	5319-5438	23	6475-6619	23
1677-1714	24	2169-2216	24	3686-3767	24	4473-4570	24	5438-5554	24	6619-6760	24
1714-1751	25	2216-2262	25	3767-3845	25	4570-4664	25	5554-5668	25	6760-6898	25
1751-1787	26	2262-2308	26	3845-3923	26	4664-4757	26	5668-5780	26	6898-7033	26
1787-1822	27	2308-2352	27	3923-3999	27	4757-4848	27	5780-5890	27	7033-7166	27
1822-1857	28	2352-2396	28	3999-4074	28	4848-4938	28	5890-5998	28	7166-7297	28
1857-1891	29	2396-2440	29	4074-4148	29	4938-5026	29	5998-6104	29	7297-7425	29
1891-1925	30	2440-2482	30	4148-4220	30	5026-5113	30	6104-6209	30	7425-7552	30

APPENDIX B

Fortran Program for the Upward and Downward Continuation and Derivatives of Potential Fields

By ALBERT J. RUDMAN and ROBERT F. BLAKELY¹

Abstract

In 1960 Roland G. Henderson, of the U.S. Geological Survey, published a comprehensive system for computation of first and second derivatives of potential fields and the continuation of fields to levels above or below the plane of observation. In our study a Fortran IV program (HNDRSN2), based on Henderson's algorithm, uses map data digitized at an equally spaced grid interval. Output from program HNDRSN2 includes maps of the field continued upward or downward from one to five grid units and first and second derivative maps on the surface and on selected downward continued levels. Test cases demonstrate the reliability of the program in standard analyses of gravity and magnetic fields.

Introduction

Measurements of the earth's gravity and magnetic field in geophysical exploration do not directly yield a unique geologic picture of the surveyed region. Usually, the first step in the analysis of such potential fields involves routine and well-understood procedures to reduce observed values to a datum. Interpretation of these data may then follow any of the numerous analytic and graphic methods that are described in standard texts (Dobrin, 1960; Nettleton, 1940). The most important of these interpretive methods are those that use first and second derivatives, but all attempt to isolate and sharpen the anomaly and relate the resulting field to its geologic source. Another approach involves continuation of the observed field upward or downward to a new level. A field measured at any level above a geologic source, for example, may be transformed downward to a selected level in relation to the source. "Seeing" the anomaly at close range is advantageous in the interpretation of the data, especially in delineating the edges of the source.

In 1960 Roland G. Henderson, of the U.S. Geological Survey, published a comprehensive system for the calculation of first and second vertical derivatives of potential

fields and the analytical continuation of fields to levels above and below the plane of observation. Although derivatives and continuation have long been recognized as a basic approach in the enhancement and analysis of gravity and magnetic fields, Henderson's method permits the geophysicist to implement this technique rapidly on the computer and has become one of the most popular approaches. The purpose of this paper is to present a Fortran IV program for computing the derivative and continued fields and to present a test case based on Henderson's algorithm.

One common application of the first derivative is to suppress the regional gradient and to increase the sharpness of an anomaly. The net effect of taking the first derivative is an isolation of the anomalous field. The second derivative also may be used to outline the shape of the source of an anomaly, especially in the magnetic case, provided the source is essentially a vertically sided, vertically polarized prism. In that case the cross section of the upper surface of the prism may be outlined by the zero contour of the second derivative (Vacquier and others, 1951). In the case of a gravitational field, the source is isolated but not outlined as definitively as in the magnetic case.

Upward continuation is used to smooth out irregularities in the observed field. As the field is continued upward, away from the source, sharp variations in the field are either eliminated or subdued. Thus prominent anomalies originating from shallow geologic sources are filtered out by the process of upward continuation. The opposite effects are observed in downward continuation. The effects of anomalies having shallow sources are emphasized, while regional variations originating from deeper sources are subdued. Recently, downward continuation also has been used to detect the top of the source of an anomaly (Rudman and others, 1971; LeMouel and others, 1974), although this application has not been tested widely.

The merit in Henderson's approach lies in its simplicity: a set of 11 values are computed once for each

¹Dr. Rudman is associate professor of geophysics at Indiana University. Dr. Blakely is a geophysicist of the Indiana Geological Survey and associate professor in the department of geology at Indiana University.

ALGORITHM FOR PROGRAM HNDRSN2

3

$$P(ka) \approx \sum_{i=0}^{10} \bar{P}(r_i) C(r_i, k) \quad (\text{Equation 3})$$

where a is the digitizing or grid interval and k is an integer. Tests of simple geometries show that k should not exceed 5 and that the field $P(0)$ is adequately sampled by the central point $r = 0$ and average \bar{P} values at radii of $r = a, a\sqrt{2}, a\sqrt{5}, a\sqrt{8}, a\sqrt{13}, a\sqrt{17}, a\sqrt{20}, a\sqrt{25}, a\sqrt{29}, a\sqrt{32}, a\sqrt{37}, a\sqrt{41}, a\sqrt{45}, a\sqrt{50}$. The coefficients $C(r_i, k)$ for upward continuation were given by Henderson from the assumption that a grid value of $a = \text{unity}$.

Equation 3 is also the fundamental working formula for calculation of downward continuation and first and second derivatives, with different coefficient sets specified for each quantity. Once the average field values are calculated for the 10 rings around a point, calculation of any quantity directly above or below that point depends only on multiplying these averages by the appropriate coefficients and summing them to obtain a final value. The method is efficient because the ring values need only be calculated once.

Reliability of the results depends on the grid interval selected, smoothness of the field, and the depth of continuation. For example, oscillations are generated if the sampling grid is too fine, if the original field is noisy, or if the field is continued downward to a depth too close to the source of the anomaly. Such oscillations are minimized if (1) a grid interval is selected equal to one-fourth the depth of the top of the anomalous source; (2) a filter is applied to smooth the original field; and (3) continuation does not extend below the source. Because downward continuation generally introduces some noise in the form of minor variations and oscillations in the field, differentiation of downward continued levels also presents special problems. The differentiation process emphasizes changes in the field and these are not always geologically meaningful on downward continued surfaces.

Underlying the basic computational formula (equation 3) is a generalized expression for the field fitted to a Lagrange interpolation formula

$$\bar{P}(z) = \sum_{k=0}^n \frac{(-1)^k z(z+a)(z+2a)\dots(z+ka)}{a^n (z+ka) (n-k)! k!} P(-ka) \quad (\text{Equation 4})$$

This equation may be modified to compute the field $\bar{P}(z)$ above and below the plane of observation. It can also be used to arrive at the derivative formula. Although Henderson's 1960 paper placed strong theo-

retical emphasis on equation 4, it does not play a role in the application of the algorithm in our report.

Algorithm for Program HNDRSN2 (See appendix 1)

1. Input Parameters (See appendix 2)

Read in identification card (HEADING); codes to select specified continuation levels and derivatives (ISELECT(L)); maximum x, y coordinate of the map input (IMAX, JMAX); base value to adjust original map data (BASE); and a scale factor (SCALE).

A generalized flow of program HNDRSN2 (appendix 1) is given in these sections. The first operation involves reading the parameters summarized above. The base value (selected by the user) is added to the original input data to adjust it for printing as a positive number on a map with format of F4.0. Program HNDRSN2 yields a compact map with each output map printed on one page. Because the F4.0 format accommodates only a three-digit positive number or a two-digit negative number, the scale factor (SCALE) is used to modify the output data to the map size. A second program with a larger output format is available in our files and does not need the scale factor. It is called HNDRSN1 and its output is printed on four separate line printer sheets with an F10.2 format. The user must assemble (clip or tape) these four sheets into one map. Details of the identification card, the code to select a specified operation on the data, and the exact map size for HNDRSN2 are given in appendices 2-5 for a test case of a gravitational field over a vertical prism. (HNDRSN1 will not be discussed.)

2. Input Map Data (See appendix 2)

Read in map data ($P(I, J)$); adjust to base value and appropriate scale factor; and print results in map form.

Map data ($P(I, J)$), one per card, is read in row by row, with the x coordinate (horizontal) governed by the I index and the y coordinate by the J index. (For orientation details see fig. 2.) Row length and number of rows are designated by IMAX, JMAX parameters. A maximum number of 25×25 map values can be read in for program HNDRSN2. (As the program is written, simply increasing the "dimensions" of the array will not increase the input capacity.) Map values are next modified by the base value and then multiplied by the scale factor and values stored in a two-dimensional array.

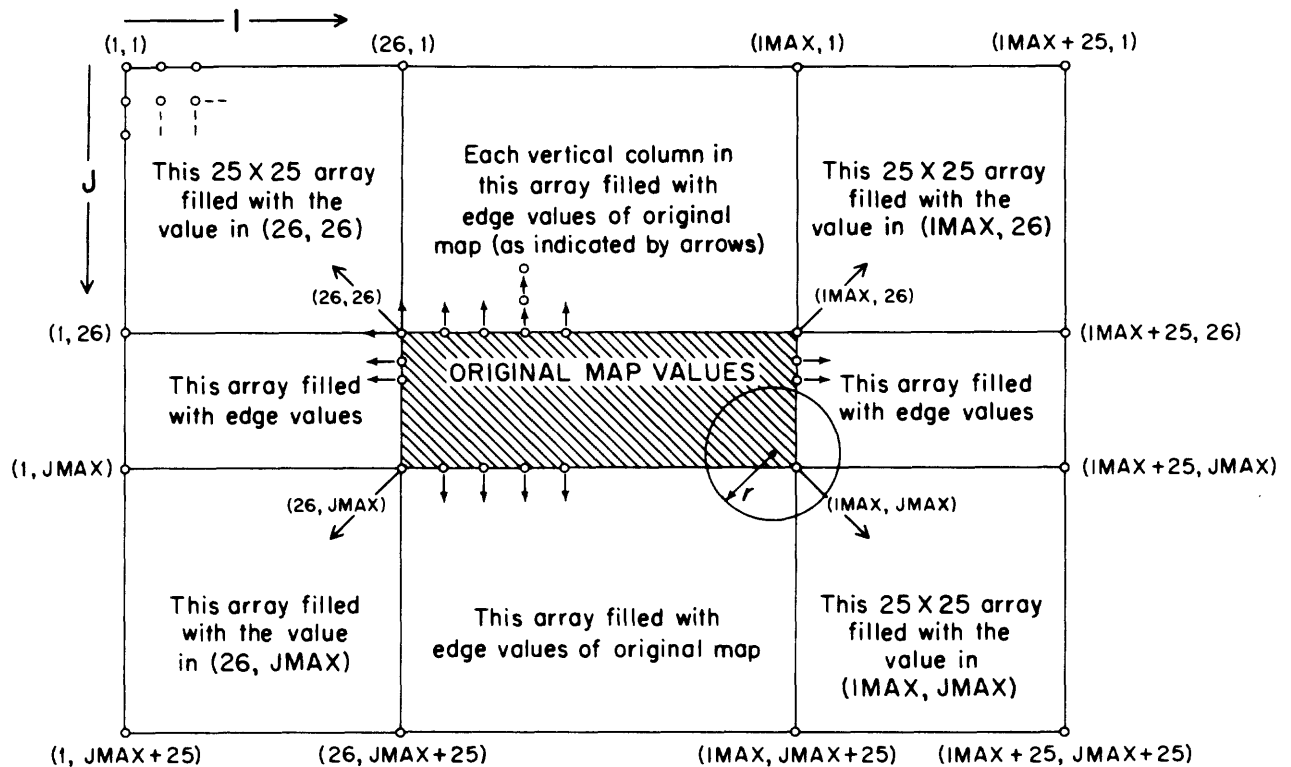


Figure 2. Sketch of original data and adjacent blocks filled with pseudo-map values. The average value around a circle of radius r may involve data from more than one adjacent block. Data in the adjacent blocks are obtained by extending edge values of the original data in the manner shown. Output maps are always the size of the input map.

3. Calculate Ring Averages (See fig. 2)

Generate pseudo-map data in regions adjacent to the original map. (See fig. 2.) Average values ($R(I, J, K)$) are calculated for 10 rings surrounding each map point.

Each map point has associated with it 11 values ($R(I, J, K)$): the original map value ($K = 1$) and average ring values calculated for 10 circles of varying radii surrounding the point ($K = 2, 3, \dots, 11$). These 11 values are stored in a three-dimensional array for later calculations to obtain the derivative and continued fields at that point. Circles surrounding a point near the edge of the map may extend beyond the original map. Figure 2 shows a circle that intercepts three adjacent "blocklike" areas. Rather than use "zero" values in these adjacent blocks, values along the edge of the original map are extended outward. Because the largest circle is 25 grid units in radius, adjacent areas are a maximum of 25×25 . (Computations depend on the average value of each ring; this figure demonstrates why data near the edge of the original map is sometimes unreliable.)

4. Calculate and Print Output (See appendices 3-5)

The 11 values ($R(I, J, K)$) associated with each point (I, J) are multiplied by 11 coefficients ($C(K, L)$) and then summed to yield 11 numbers (equation 3). The sum of these yield one value appropriate to the continuation and (or) derivative designated by the L code. Output maps are printed to present the final results.

Because the 11 $R(I, J, K)$ values for each point are stored, computation for each continuation level and derivative requires only one step: multiplication by the appropriate coefficient and summing the 11 numbers. Output maps include (1) the original map data (modified by the base and scale factors) and (2) all the maps specified by the L code. Each map is identified by the identification parameter and a statement describing the derivative and (or) the continuation level.

LITERATURE CITED

5. Possible Modifications of the Algorithm

Every programmer knows that there are always better ways to write a program. So, too, with HNDRSN2. Some of the possible modifications are desirable enough that a few comments are in order. In our original approach, both map and computational data were stored in either two- or three-dimensional arrays. Programming for data displayed in this manner is simple to visualize and manipulate, but both space and computer time could be saved if data were handled in smaller arrays. For example, once the 11 ring values around a point are calculated, it would be possible to compute all the desired values at that point and then discard the ring values. Instead, we store these ring values in a three-dimensional array $R(I, J, K)$ and make all computations separately.

Similarly, the pseudo-map values in adjacent map areas are created by extending the edge values. Because potential fields are smooth functions, a polynomial trend surface fit to the real map data might be used to predict better adjacent values. Writing such a program and the fitting process are time consuming and the advantages of the system have not been investigated. Moreover, as now programmed, these larger 25×25 arrays are all stored for use during the "ring" computations. A program could be written to assign the appropriate values (without stored arrays) by using the (I, J) value as an identifier of the current ring calculation.

Coefficients for each derivative and continuation operation are presently incorporated into the Fortran program. For each calculation, all the coefficients need to be repeatedly read in. A rewriting of the program should include these coefficients as part of the initialization process under the Fortran command:

```
DATA CC (1, 1), CC (2, 2), . . . /0.11193, 0.32193, . . . /
```

The experienced programmer will find numerous other major and minor changes to make; however, we leave the program in its present state for expediency. It is a working program!

Concluding Statement

Appendices 1-5 discuss the operating procedures and present a test case. In our discussion of the output maps (appendices 3, 4, and 5), little mention has been made of the reliability of the results. The input data was a field computed over a cylinder. All the param-

eters of this model are known, and selected analytic calculations were made by hand for the exact values and derivatives of the field at various levels. The computer derived values compared favorably with the predicted results, demonstrating the validity of the program and supporting the reliability of Henderson's basic algorithm.

Special acknowledgments are extended to Indiana University's Wrubel Computing Center for the generous use of its facilities and expertise of its personnel.

Literature Cited

- Dobrin, M. B.
1960 - Introduction to geophysical prospecting: New York, McGraw-Hill Book Co., Inc., 446 p.
- Grant, F. S., and West, G. F.
1965 - Interpretation theory in applied geophysics: New York, McGraw-Hill Book Co., Inc., 583 p.
- Henderson, R. G.
1960 - A comprehensive system of automatic computation in magnetic and gravity interpretation: *Geophysics*, v. 25, p. 569-585.
- LeMouel, J. L., and others
1974 - A simple formalism for the study of transformed aeromagnetic profiles and source location problems: *Jour. Geophys. Research*, v. 79, p. 324-331.
- Nettleton, L. L.
1940 - Geophysical prospecting for oil: New York, McGraw-Hill Book Co., Inc., 442 p.
- Peters, L. J.
1949 - The direct approach to magnetic interpretation and its practical application: *Geophysics*, v. 14, p. 290-320.
- Rudman, A. J., and others
1971 - Geophysical analysis in central Indiana using potential field continuation: *Geophysics*, v. 36, p. 878-890.
- Talwani, Manik, and Ewing, Maurice
1960 - Rapid computation of gravitational attraction of three-dimensional bodies of arbitrary shape: *Geophysics*, v. 25, p. 203-225.
- Vacquier, V., and others
1951 - Interpretation of aeromagnetic maps: *Geol. Soc. America Mem.* 47, 151 p.

map point. From them all derivative or continued fields at that point can be approximated by a multiplication process, wherein coefficients may be selected to calculate first or second derivatives on any upward or downward continued surface. Multiplication by the coefficients is essentially a filtering process. Results of the calculations are not unique in that they approximate the analytic solution. Although recent papers have explored other methods for calculating derivatives and continuation (especially filtering in the frequency domain), Henderson's 1960 paper continues to be the classic approach and it remains one of the more popular procedures.

Theory

The following discussion of the continuation and derivative processes is intended only to introduce the basic equations used in the algorithm. For an extensive presentation the reader is referred to Henderson's 1960 paper, to the text by Grant and West (1965), or to numerous articles cross indexed in the "S.E.G. Cumulative Index of Geophysics" under the key words CONTINUATION and DERIVATIVE. Peters' (1949) article is a basic reference and is a good starting point for any comprehensive review.

Given the field $P(0)$ on a surface $z = 0$ (fig. 1), the field at a point $-z$ above the surface can be computed from the classic solution of the Dirichlet problem for a half space

$$P(-z) = \int_0^\infty \frac{\bar{P}(r) dr}{(r^2 + z^2)^{3/2}} \quad (\text{Equation 1})$$

where r is the radius of a circle about the central point. $\bar{P}(r)$ is the average value of the field on a circle of radius r and is given by

$$\bar{P}(r) = \frac{1}{2\pi} \int_0^{2\pi} \bar{P}(r, \vartheta) d\vartheta \quad (\text{Equation 2})$$

In routine calculations, $\bar{P}(r)$ is the arithmetic average of values intercepted by the digitizing grid on a circle of specified radius r . For example, in figure 1 $\bar{P}(r_3)$ is the average of the eight values at the intersections of the grid system.

Henderson used a heuristic approach to obtain a working formula to compute the field at a specified height $z = ka$

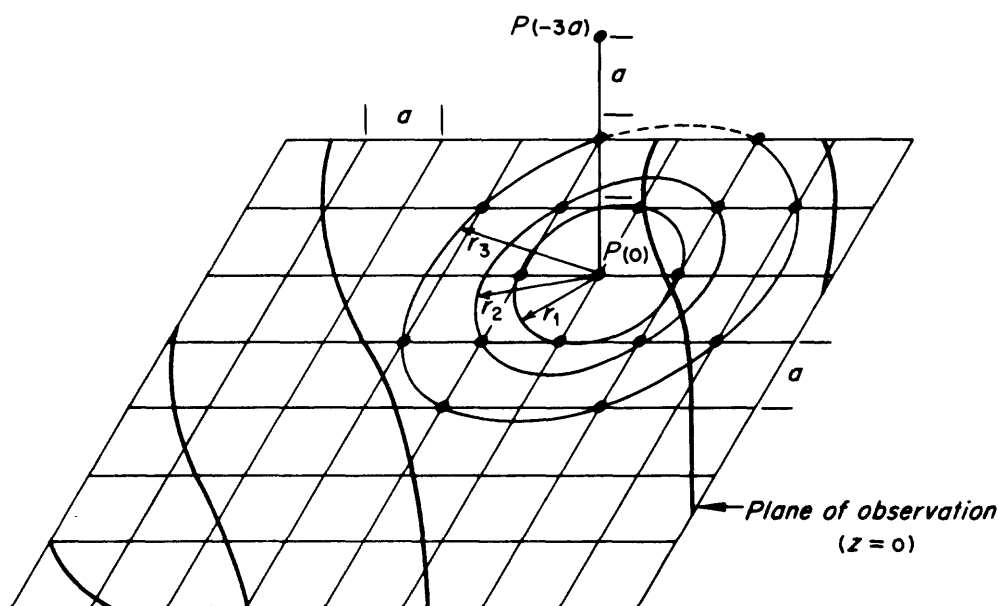


Figure 1. Diagram showing field at the surface ($z = 0$), a point on the surface $P(0)$, the point $P(-3a)$ at which the upward continued field is to be calculated, the grid system used to digitize the field at a spacing of a , and three of the 10 circles of radius r_i used to sample the field. Note that a value of $r_1 = a$ has four grid (field) points, that $r_2 = a\sqrt{2}$ also has four, and that $r_3 = a\sqrt{5}$ has eight. In some examples circles with large radii may extend into adjacent regions where the field is not defined. (See fig. 2 for additional discussion.) In our example circles with large radii would intersect grid points beyond the edge of the original map.

Appendix 1. Fortran IV Program HNDRSN2

The program, as written, contains numerous comment routines are used.
cards identifying the purpose of each section. No sub-

```

PROGRAM HNDRSN2 (INPUT,OUTPUT,TAPE1=INPUT,TAPE2=OUTPUT)
C
C *****
C      THIS PROGRAM FOLLOWS HENDERSONS TECHNIQUE FOR UPWARD
C      AND DOWNWARD CONTINUATION AND FIRST AND SECOND
C      DERIVATIVES (SEE HENDERSON,1960,GEOPHYSICS,VOL.25,
C      NOS.3,P.569-585.). WRITTEN FOR FORTRAN IV USE ON
C      CDC 6600 SERIES COMPUTER. OUTPUT MAPS ARE THE SIZE OF
C      INPUT MAPS. UP TO A MAXIMUM OF 25 X 25.
C *****
C
C *****
C      DIMENSION STATEMENTS FOR DATA UP TO 25 X 25
C *****
C
C      DIMENSION HEADING (10)
C      DIMENSION ISELECT (20), P(75,75), C(11,19),R(25,25,11)
C      COMMON P, C, R
C
C *****
C      READ IN IDENTIFICATION CARD(HEADING) AND ISELECT
C      CARD WHICH CONTAINS CODES FOR LIST OF MAPS DESIRED.
C      CODES ARE IDENTIFIED LATER IN THIS PROGRAM.
C *****
C
C      READ(1,1)(HEADING(I),I=1,10)
C      1 FORMAT (10A8)
C      READ(1,2)(ISELECT(L),L=1,19)
C      2 FORMAT (19I1)
C
C *****
C      READ IN MAXIMUM VALUE OF I(=IMAX). I BEGINS AT 26 AND
C      IMAX MUST BE 50 OR LESS. SIMILARLY FOR JMAX. READ IN
C      ON SAME CARD THE VALUE (BASE) TO BE SUBTRACTED FROM
C      MAP VALUES P(I,J).NEXT READ A SCALE VALUE TO MODIFY
C      DATA TO FIT THE LIMITED SIZE MAP FORMAT OF F4.0.
C      P(I,J) DATA IS MULTIPLIED BY THIS SCALE FACTOR.
C *****
C
C      READ(1,3) IMAX, JMAX, BASE
C      3 FORMAT (2I2,F6.2)
C      READ(1,501) SCALE
C      501 FORMAT(F10.4)
C
C *****
C      READ IN P(I,J) DATA.SUBTRACT BASE. MULTIPLY BY SCALE.
C      PRINT HEADING AND PLOT ON MAP TYPE OUTPUT.
C      MAP IS PRINTED FROM P(26,26) TO P(IMAX,JMAX)
C      IF DATA IS LESS THAN 25 X25 , A BLANK
C      IS PRINTED IN THE SPACES TO FILL OUT THE MAP

```


GEOPHYSICAL COMPUTER PROGRAM 1

```

8
C *****
C
  READ(1,4) ((P(I,J), I=26, IMAX), J=26, JMAX)
4  FORMAT(17X,F7.2)
  DO 6 I=26, IMAX
  DO 5 J = 26, JMAX
5  P(I,J)=(P(I,J)-BASE)*SCALE
6  CONTINUE
  WRITE(2,7)
7  FORMAT (1H1)
  WRITE(2,101)(HEADING(I),I=1,10)
101 FORMAT(20X,10A8/)
  WRITE(2,8) BASE,SCALE
8  FORMAT( 20X,*INPUT DATA LESS BASE OF *F6.2,3X,*MULTIPLIED BY SCALE
1  OF *F5.2/)
  DO 9 J=26,JMAX
  WRITE(2,222)
222 FORMAT(4X,24(1H*,4X),1H*)
  WRITE(2,10)(P(I,J),I=26,IMAX)
10 FORMAT(2X,25(F4.0,1X)/)
  IF(IMAX.LT.50) 600, 9
600 WRITE(2,601)
601 FORMAT(1H )
9  CONTINUE
  IF(JMAX.LT.50) 602, 605
602 LMAX=(50-JMAX)
  DO 603 LL=1,LMAX
603 WRITE(2,604)
604 FORMAT(4X,24(1H*,4X),1H*//)
605 CONTINUE
C *****
C
C      NEXT SECTION PREPARES REGIONS BEYOND EDGE OF MAP TO
C      BE USED IN ANALYSIS. APPROACH IS TO FILL THE SURROUNDING
C      SPACE BY EXTENDING EACH EDGE VALUE NORMAL TO THE MAP
C      FOR 25 UNITS.
C *****
C
  IMAX1 = IMAX + 1
  IMAX25 = IMAX + 25
  JMAX1 = JMAX + 1
  JMAX25 = JMAX + 25
  DO 14 J=26,JMAX
  DO 15 I=1,25
15  P(I,J)=P(26,J)
  DO 16 I = IMAX1, IMAX25
16  P(I,J)=P(IMAX,J)
14  CONTINUE
C
C
  DO 17 I=26,IMAX
  DO 18 J=1,25
18  P(I,J)=P(I,26)
  DO 19 J = JMAX1, JMAX25
19  P(I,J)=P(I,JMAX)
17  CONTINUE

```

APPENDIX 1

```

C
C
      DO 20 I=1,25
      DO 21 J=1,25
21  P(I,J)=P(26,26)
20  CONTINUE
C
C
      DO 22 I = IMAX1, IMAX25
      DO 23 J=1,25
23  P(I,J)=P(IMAX,26)
22  CONTINUE
C
C
      DO 24 I=1,25
      DO 25 J = JMAX1, JMAX25
25  P(I,J)=P(26,JMAX)
24  CONTINUE
C
C
      DO 26 I = IMAX1,IMAX25
      DO 27 J = JMAX1, JMAX25
27  P(I,J)=P(IMAX,JMAX)
26  CONTINUE
C
C
      *****
      CALCULATION OF AVERAGE VALUE OF DATA ON RINGS CENTERED
      AT EACH MAP POINT. CALL THESE R (I,J,K), WHERE
      K=1 TO 11
      *****
C
      M=0
      DO 28 I=26,IMAX
      M=M+1
      N=0
      DO 29 J=26,JMAX
      N=N+1
      R(M,N,1)=P(I,J)
      R(M,N,2)=(P(I,J+1)+P(I,J-1)+P(I+1,J)+P(I-1,J))/4.0
      R(M,N,3)=(P(I+1,J+1)+P(I+1,J-1)+P(I-1,J+1)+P(I-1,J-1))/4.0
      R(M,N,4)=(P(I+2,J+1)+P(I+2,J-1)+P(I-2,J+1)+P(I-2,J-1)
      1+P(I+1,J+1)+P(I+1,J-1)+P(I-1,J+1)+P(I-1,J-1))/8.0
      R(M,N,5)=(P(I+2,J+2)+P(I+2,J-2)+P(I-2,J+2)+P(I-2,J-2))/4.0
      R(M,N,6)=(P(I+2,J+3)+P(I+2,J-3)+P(I-2,J+3)+P(I-2,J-3)
      1+P(I+3,J+2)+P(I+3,J-2)+P(I-3,J+2)+P(I-3,J-2))/8.0
      R(M,N,7)=(P(I+5,J)+P(I-5,J)+P(I,J+5)+P(I,J-5)
      1+P(I+3,J+4)+P(I+3,J-4)+P(I+4,J+3)+P(I+4,J-3)
      2+P(I-3,J+4)+P(I-4,J+3)+P(I-3,J-4)+P(I-4,J-3))/12.0
      R(M,N,8)=(P(I+7,J+1)+P(I+1,J+7)+P(I+7,J-1)+P(I+1,J-7)
      1+P(I-7,J+1)+P(I-1,J+7)+P(I-7,J-1)+P(I-1,J-7)
      2+P(I+5,J+5)+P(I+5,J-5)+P(I-5,J+5)+P(I-5,J-5))/12.0
      R(M,N,9)=(P(I+10,J+6)+P(I+6,J+10)+P(I+10,J-6)+P(I+6,J-10)
      1+P(I-10,J+6)+P(I-6,J+10)+P(I-10,J-6)+P(I-6,J-10))/8.0
      R(M,N,10)=(P(I+7,J+15)+P(I+15,J+7)+P(I-7,J+15)+P(I-15,J+7)
      1+P(I+7,J-15)+P(I+15,J-7)+P(I-7,J-15)+P(I-15,J-7))/8.0
      R(M,N,11)=(P(I,J+25)+P(I,J-25)+P(I-20,J+15)+P(I-15,J+20) +
      1P(I-20,J-15)+P(I-15,J-15)+P(I+20,J+15)+P(I+15,J+20)
      2+P(I+20,J-15)+P(I+15,J-20)+P(I+25,J)+P(I-25,J))/12.0
29  CONTINUE
28  CONTINUE

```

GEOPHYSICAL COMPUTER PROGRAM 1

10

C

C

C

C

C

C

C

C

C

C

C

C

C

C

C

C

C

C

C

C

C

C

```
*****
FOR EACH MAP THERE IS A SET OF COEFFICIENTS C(K,L),
WHERE K IS THE RING NOS AND L IS THE CODED INTEGER
FOR THE DESIRED MAP. CODES ARE A 'ONE' IF THE MAP IS
DESIRED, OR A 'ZERO' IF IT IS NOT. CODES ARE ENTERED
ON THE ISELECT CARD FROM COLUMNS 1 TO 19. THE
FOLLOWING LIST GIVES THE CODES. THUS, A 'ONE' IN
COLUMN 1 REQUESTS A MAP CONTINUED UPWARD ONE
GRID UNIT. A 'ZERO' IN COLUMN 2 WILL SUPPRESS THE
MAP THAT IS CONTINUED UPWARD 2 GRID UNITS, ETC.
```

```
*****
```

```
*****
```

```
COEFFICIENTS FOR UPWARD CONTINUATION 1. CODE L=1
```

```
*****
```

```
C(1,1)=.11193
C(2,1)=.32193
C(3,1)=.06062
C(4,1)=.15206
C(5,1)=.05335
C(6,1)=.06586
C(7,1)=.06650
C(8,1)=.05635
C(9,1)=.03855
C(10,1)=.02273
C(11,1)=.03015
```

C

C

C

C

C

```
*****
```

```
COEFFICIENTS FOR UPWARD CONTINUATION 2. CODE L=2
```

```
*****
```

```
C(1,2)=.04034
C(2,2)=.12988
C(3,2)=.07588
C(4,2)=.14559
C(5,2)=.07651
C(6,2)=.09902
C(7,2)=.11100
C(8,2)=.10351
C(9,2)=.07379
C(10,2)=.04464
C(11,2)=.05998
```

APPENDIX 1

```

C
C *****
C      COEFFICIENTS FOR UPWARD CONTINUATION 3. CODE L=3
C *****
C
C(1,3)=.01961
C(2,3)=.06592
C(3,3)=.05260
C(4,3)=.10563
C(5,3)=.07146
C(6,3)=.10226
C(7,3)=.12921
C(8,3)=.13635
C(9,3)=.10322
C(10,3)=.06500
C(11,3)=.08917
C
C *****
C      COEFFICIENTS FOR UPWARD CONTINUATION 4. CODE L=4
C *****
C
C(1,4)=.01141
C(2,4)=.03908
C(3,4)=.03566
C(4,4)=.07450
C(5,4)=.05841
C(6,4)=.09173
C(7,4)=.12915
C(8,4)=.15474
C(9,4)=.12565
C(10,4)=.08323
C(11,4)=.11744
C
C *****
C      COEFFICIENTS FOR UPWARD CONTINUATION 5. CODE L=5
C *****
C
C(1,5)=.00742
C(2,5)=.02566
C(3,5)=.02509
C(4,5)=.05377
C(5,5)=.04611
C(6,5)=.07784
C(7,5)=.11986
C(8,5)=.16159
C(9,5)=.14106
C(10,5)=.09897
C(11,5)=.14458

```

GEOPHYSICAL COMPUTER PROGRAM 1

12

C

C

C

C

C

```
*****
      COEFFICIENTS FOR DOWNWARD CONTINUATION 1. CODE L=6
*****
```

```
C(1,6)= 4.8948
C(2,6)=-3.0113
C(3,6)= 0.0081
C(4,6)=-0.5604
C(5,6)=-0.0376
C(6,6)=-0.0689
C(7,6)=-0.0605
C(8,6)=-0.0534
C(9,6)=-0.0380
C(10,6)=-0.0227
C(11,6)=-0.0302
```

C

C

C

C

C

```
*****
      COEFFICIENTS FOR DOWNWARD CONTINUATION 2. CODE L=7
*****
```

```
C(1,7)= 16.1087
C(2,7)=-13.2209
C(3,7)= 0.4027
C(4,7)=-0.9459
C(5,7)= 00.0644
C(6,7)=-00.0596
C(7,7)=-00.0522
C(8,7)=-00.0828
C(9,7)=-00.0703
C(10,7)=-00.0443
C(11,7)=-00.0600
```

C

C

C

C

C

```
*****
      COEFFICIENTS FOR DOWNWARD CONTINUATION 3. CODE L=8
*****
```

```
C(1,8)= 41.7731
C(2,8)=-38.2716
C(3,8)= 01.7883
C(4,8)=-04.7820
C(5,8)= 00.5367
C(6,8)= 00.1798
C(7,8)= 00.1342
C(8,8)=-00.0560
C(9,8)=-00.0900
C(10,8)=-00.0639
C(11,8)=-00.0891
```

APPENDIX 1

```

C
C *****
C      COEFFICIENTS FOR DOWNWARD CONTINUATION 4. CODE L=9
C *****
C
C(1,9)= 92.5362
C(2,9)=-89.7403
C(3,9)= 05.1388
C(4,9)=-09.9452
C(5,9)= 01.7478
C(6,9)= 00.8908
C(7,9)= 00.6656
C(8,9)= 00.0718
C(9,9)=-00.0890
C(10,9)=-00.0802
C(11,9)=-00.1173
C
C *****
C      COEFFICIENTS FOR DOWNWARD CONTINUATION 5. CODE L=10
C *****
C
C(1,10)= 183.2600
C(2,10)=-183.9380
C(3,10)= 011.8804
C(4,10)=-018.6049
C(5,10)= 004.2324
C(6,10)= 002.4237
C(7,10)= 001.7777
C(8,10)= 000.3606
C(9,10)=-000.0571
C(10,10)=-000.0921
C(11,10)=-000.1444
C
C *****
C      COEFFICIENTS FOR FIRST DERIVATIVE ON SURFACE. CODE L=11
C *****
C
C(1,11)= 1.87282
C(2,11)=-1.13625
C(3,11)=-0.05949
C(4,11)=-0.30210
C(5,11)=-0.05857
C(6,11)=-0.07597
C(7,11)=-0.07072
C(8,11)=-0.05758
C(9,11)=-0.03905
C(10,11)=-0.02286
C(11,11)=-0.05020

```

GEOPHYSICAL COMPUTER PROGRAM 1

14

C

C

C

C

C

```
*****
COEFFICIENTS FOR FIRST DERIVATIVE DOWN 1. CODE L=12
*****
```

```
C(6,12)=-0.04007
C(6,12)=-0.04856
C(5,12)= 0.00361
C(3,12)= 0.12727
C(4,12)=-0.88750
C(1,12)= 6.62394
C(2,12)=-5.62446
C(7,12)=-0.04007
C(8,12)=-0.04575
C(9,12)=-0.03615
C(10,12)=-0.02233
C(11,12)=-0.05000
```

C

C

C

C

C

```
*****
COEFFICIENTS FOR FIRST DERIVATIVE DOWN 2. CODE L=13
*****
```

```
C(1,13)= 16.98074
C(2,13)=-16.05517
C(3,13)= 00.76135
C(4,13)=-01.98701
C(5,13)= 00.23820
C(6,13)= 00.09219
C(7,13)= 00.07475
C(8,13)=-00.00768
C(9,13)=-00.02726
C(10,13)=-00.02077
C(11,13)=-00.04934
```

C

C

C

C

C

```
*****
COEFFICIENTS FOR FIRST DERIVATIVE DOWN 3. CODE L=14
*****
```

```
C(1,14)= 36.11116
C(2,14)=-35.96237
C(3,14)= 02.17080
C(4,14)=-03.83054
C(5,14)= 00.76745
C(6,14)= 00.42646
C(7,14)= 00.32573
C(8,14)= 00.06859
C(9,14)=-00.01084
C(10,14)=-00.01812
C(11,14)=-00.04832
```

APPENDIX 1

C
C
C
C
C

COEFFICIENTS FOR FIRST DERIVATIVE DOWN 4. CODE L=15

C(1,15)= 67.88049
C(2,15)=-69.68033
C(3,15)= 04.76651
C(4,15)=-06.69004
C(5,15)= 01.74330
C(6,15)= 01.05352
C(7,15)= 00.77613
C(8,15)= 00.19699
C(9,15)= 00.01469
C(10,15)=-00.01433
C(11,15)=-00.04693

C
C
C
C
C
C

COEFFICIENTS FOR 2ND DERIVATIVE ON THE SURFACE.
CODE L=16.

C(1,16)= 2.82994
C(2,16)=-2.49489
C(3,16)= 0.05173
C(4,16)=-0.39446
C(5,16)= 0.00932
C(6,16)=-.00732
C(7,16)=.00304
C(8,16)= 0.00219
C(9,16)= 0.00040
C(10,16)= 0.00004
C(11,16)= 0.00000

C
C
C
C
C

COEFFICIENTS FOR 2ND DERIVATIVE DOWN 1. CODE L=17.

C(1,17)= 7.08408
C(2,17)=-6.93715
C(3,17)= 0.36265
C(4,17)=-0.80764
C(5,17)= 0.13050
C(6,17)= 0.07231
C(7,17)= 0.06502
C(8,17)= 0.02312
C(9,17)= 0.00565
C(10,17)= 0.00103
C(11,17)= 0.00043

GEOPHYSICAL COMPUTER PROGRAM 1

16

C
C
C
C
C
C

```
*****
      COEFFICIENTS FOR 2ND DERIVATIVE DOWN 2. CODE L=18
*****
```

```
C(1,18)= 14.15751
C(2,18)=-14.51327
C(3,18)= 00.96018
C(4,18)=-01.42970
C(5,18)= 00.35907
C(6,18)= 00.22256
C(7,18)= 00.17330
C(8,18)= 00.05501
C(9,18)= 00.01239
C(10,18)= 00.00210
C(11,18)= 00.00085
```

C
C
C
C
C
C

```
*****
      COEFFICIENTS FOR 2ND DERIVATIVE DOWN 3. CODE L=19
*****
```

```
C(1,19)= 24.74755
C(2,19)=-26.02351
C(3,19)= 01.92719
C(4,19)=-02.30269
C(5,19)= 00.72474
C(6,19)= 00.46253
C(7,19)= 00.33920
C(8,19)= 00.09985
C(9,19)= 00.02070
C(10,19)= 00.00322
C(11,19)= 00.00122
```

C
C
C
C
C
C
C

```
*****
      THIS SECTION MAKES THE FINAL CALCULATIONS FOR THOSE
      MAPS SELECTED BY USER IN HIS ISELECT CODE.
*****
```

```
DO 30 L=1,19
LEVEL=L
IF (ISELECT(L).LT.1) 30,31
31 WRITE(2,7)
   WRITE(2,101)(HEADING(I),I=1,10)
   IF(L.EQ. 1)71,52
52 IF(L.EQ. 2)72,53
53 IF(L.EQ. 3)73,54
54 IF(L.EQ. 4)74,55
55 IF(L.EQ. 5)75,56
56 IF(L.EQ. 6)76,57
57 IF(L.EQ. 7)77,58
58 IF(L.EQ. 8)78,59
59 IF(L.EQ. 9)79,60
60 IF(L.EQ.10)80,61
61 IF(L.EQ.11)81,62
62 IF(L.EQ.12)82,63
63 IF(L.EQ.13)83,64
64 IF(L.EQ.14)84,65
```

APPENDIX 1

```
65 IF(L.EQ.15)85,66
66 IF(L.EQ.16)86,67
67 IF(L.EQ.17)87,68
68 IF(L.EQ.18)88,69
69 IF(L.EQ.19)89,90
71 WRITE(2,171)
171 FORMAT (20X,*MAP CONTINUED UPWARD 1 GRID UNIT*//)
GO TO 320
72 WRITE(2,172)
172 FORMAT (20X,*MAP CONTINUED UPWARD 2 GRID UNIT*//)
GO TO 320
73 WRITE(2,173)
173 FORMAT (20X,*MAP CONTINUED UPWARD 3 GRID UNIT*//)
GO TO 320
74 WRITE(2,174)
174 FORMAT (20X,*MAP CONTINUED UPWARD 4 GRID UNIT*//)
GO TO 320
75 WRITE(2,175)
175 FORMAT (20X,*MAP CONTINUED UPWARD 5 GRID UNIT*//)
GO TO 320
76 WRITE(2,176)
176 FORMAT (20X,*MAP CONTINUED DOWNWARD 1 GRID UNIT*//)
GO TO 320
77 WRITE(2,177)
177 FORMAT (20X,*MAP CONTINUED DOWNWARD 2 GRID UNIT*//)
GO TO 320
78 WRITE(2,178)
178 FORMAT (20X,*MAP CONTINUED DOWNWARD 3 GRID UNIT*//)
GO TO 320
79 WRITE(2,179)
179 FORMAT (20X,*MAP CONTINUED DOWNWARD 4 GRID UNIT*//)
GO TO 320
80 WRITE(2,180)
180 FORMAT (20X,*MAP CONTINUED DOWNWARD 5 GRID UNIT*//)
GO TO 320
81 WRITE(2,181)
181 FORMAT (20X,*MAP OF FIRST DERIVATIVE ON SURFACE*//)
GO TO 320
82 WRITE(2,182)
182 FORMAT (20X,*MAP OF FIRST DERIVATIVE DOWN 1 GRID UNIT*//)
GO TO 320
83 WRITE(2,183)
183 FORMAT (20X,*MAP OF FIRST DERIVATIVE DOWN 2 GRID UNIT*//)
GO TO 320
84 WRITE(2,184)
184 FORMAT (20X,*MAP OF FIRST DERIVATIVE DOWN 3 GRID UNIT*//)
GO TO 320
85 WRITE(2,185)
185 FORMAT (20X,*MAP OF FIRST DERIVATIVE DOWN 4 GRID UNIT*//)
GO TO 320
86 WRITE(2,186)
186 FORMAT (20X,*MAP OF SECOND DERIVATIVE ON SURFACE*//)
GO TO 320
87 WRITE(2,187)
187 FORMAT (20X,*MAP OF SECOND DERIVATIVE DOWN 1 GRID UNIT*//)
GO TO 320
```

18

GEOPHYSICAL COMPUTER PROGRAM 1

```

      88 WRITE(2,188)
    188 FORMAT (20X,*MAP OF SECOND DERIVATIVE DOWN 2 GRID UNIT*//)
      GO TO 320
    89 WRITE(2,189)
    189 FORMAT (20X,*MAP OF SECOND DERIVATIVE DOWN 3 GRID UNIT*//)
      GO TO 320
    320 DO 33 I=26,IMAX
          DO 34 J=26,JMAX
            P(I,J)=0.0
          DO 35 K=1,11
    35   P(I,J)=C(K,L)*R(I-25,J-25,K)+P(I,J)
    34 CONTINUE
    33 CONTINUE

C
C *****
C       NEXT SECTION PRINTS ALL MAPS IN SAME FORMAT AS
C       INPUT MAP (SEE PREVIOUS COMMENTS).
C *****
C
      DO 36 J=26,JMAX
        WRITE(2,223)
    223 FORMAT (4X,24(1H*,4X)1H* )
        WRITE(2,37)(P(I,J),I=26,IMAX )
    37 FORMAT(2X,25(F4.0,1X)/)
        IF(IMAX.LT.50) 700, 36
    700 WRITE(2,701)
    701 FORMAT(1H )
    36 CONTINUE
        IF(JMAX.LT.50) 702, 705
    702 LMAX=(50-JMAX)
        DO 703 LL=1,LMAX
    703 WRITE(2,704)
    704 FORMAT(4X,24(1H*,4X),1H*//)
    705 CONTINUE
    30 CONTINUE
      CALL EXIT
    90 WRITE(2,91)
    91 FORMAT(1X,*ERROR. TOO LARGE L VALUE*)
      CALL EXIT

C
C *****
C               JULY, 1974
C   ANY QUESTIONS REGARDING THIS PROGRAM SHOULD BE DIRECTED TO
C               GEOPHYSICS SECTION
C               INDIANA GEOLOGICAL SURVEY
C               BLOOMINGTON, INDIANA 47401
C
C   NO RESPONSIBILITY IS ASSUMED BY THE INDIANA GEOLOGICAL SURVEY
C   NOR THE INDIANA UNIVERSITY DEPARTMENT OF GEOLOGY FOR ANY ERRORS,
C   MISTAKES OR MISREPRESENTATIONS THAT MAY OCCUR WHEN USING THIS
C   PROGRAM. NOR IS RESPONSIBILITY ASSUMED BY THE INDIANA UNIVERSITY
C   RESEARCH COMPUTING CENTER FOR ITS CORRECT REPRODUCTION.
C *****
C
      END

```

Appendix 2. Input Cards for Test Case

Card 1. 80-column identification card. Information from this card is printed as a heading for each of the maps.

Card 2. Codes to select certain map data as output. Cols. 1-19 are either punched with 1 or zero (Format 19 I1). Codes are described in the program comment cards; for example, if col. 1 is punched with a 1, a map continued upward one grid unit ($a = .5$ km) is printed. For the test case, cols. 7 and 16 were punched to yield two maps: (1) input map continued down two grid units and (2) second derivative of input map (appendices 4 and 5).

Card 3. Gives coordinates of maximum I and J values (I and J begin at 26). For a maximum x

coordinate of 25 data points, a value of 50 is entered. For a 25×25 map input IMAX and JMAX are read in as 50, 50 (Format 2 I2). A base value (F6.2) is also read in on this card. The base value is subtracted from the original data input.

Card 4. A scale value is read in to multiply the output data. In this test case, the output gravity values are expected to be small and a scale value of 10.0 is used (F10.4).

Card 5. Input data for the maps, one item of data per card with Format (17X, F7.2), are in row and column sequence; for example, for a 25×25 data array, 625 cards are now read in.

Card 1 → 25X25 GRAVITY FIELD OF VERTICAL CYLINDER, 2 KM RADIUS, TOP 2 KM DOWN, BOTTOM 50 KM
 Card 2 → 0000001000000001000
 Card 3 → 5050 0.0
 Card 4 → 10.
 Card 5 →
 Card 6 →

2.14
 2.25
 2.35
 2.46
 2.57
 2.68
 2.79
 2.88
 2.97
 3.04
 3.10
 3.13
 3.14
 3.13
 3.10
 3.04
 2.97
 2.88
 2.79
 2.68
 2.57
 2.46
 2.35
 2.24
 2.14
 2.25
 2.36
 2.49
 2.62
 2.75

First 25 data cards are stored as first row
 in 25×25 map array (Appendix 3)

Beginning of second row

Final data values of last row
 of 25×25 map array

Card 627 →
 Card 628 →
 Card 629 →

2.35
 2.24
 2.14

Appendices 3-5. Selected Output Maps for Test Case

A gravitational field over a vertical prism was digitized at a grid interval of 0.5 km and used as a test case for program HNDRSN2. The input data were generated from a program following an algorithm from Talwani and Ewing (1960) and is displayed in appendix 3 as a 25×25 map. Map values are in milligals multiplied by a scale factor of 10 and then rounded off. For example, the first input value of 2.14 (appendix 2) is printed on the map in the northwest corner as 21. The solid heavy line outlines the prism. Contours show that the input field is a smooth function with a maximum value of 8.8 milligals.

In this test case only two computed maps were specified. The first was a map continued downward two grid units toward the source of the anomaly (appen-

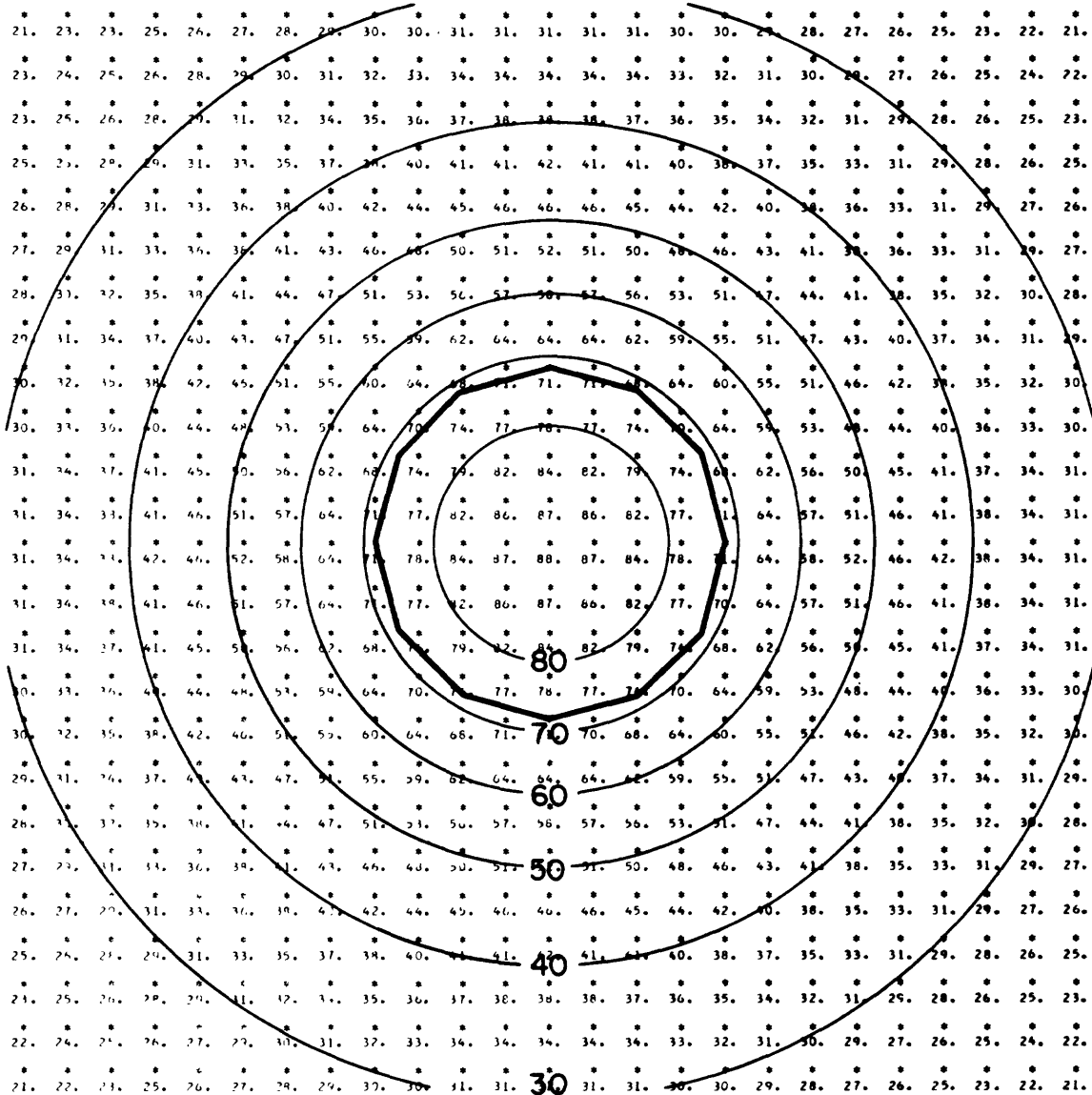
dix 4). The maximum value of the field is greater than the original map data (13.1 milligals), with an overall increase in contour gradient. Contours along the edges of the map are no longer a smooth function, a phenomenon associated with a field as it is continued close to the source and with the inherent limitations imposed on all edge values as discussed previously.

The final map is the second derivative of the input gravity data (appendix 5). Note that the contours display an increased gradient over the center of the anomaly, thus effectively isolating a local source from a regional gradient. In the case of a magnetic field over a vertical prism, the zero contour closely approximates the edges of the source.

Appendix 3. Input Data

[Contours in milligals $\times 10$]

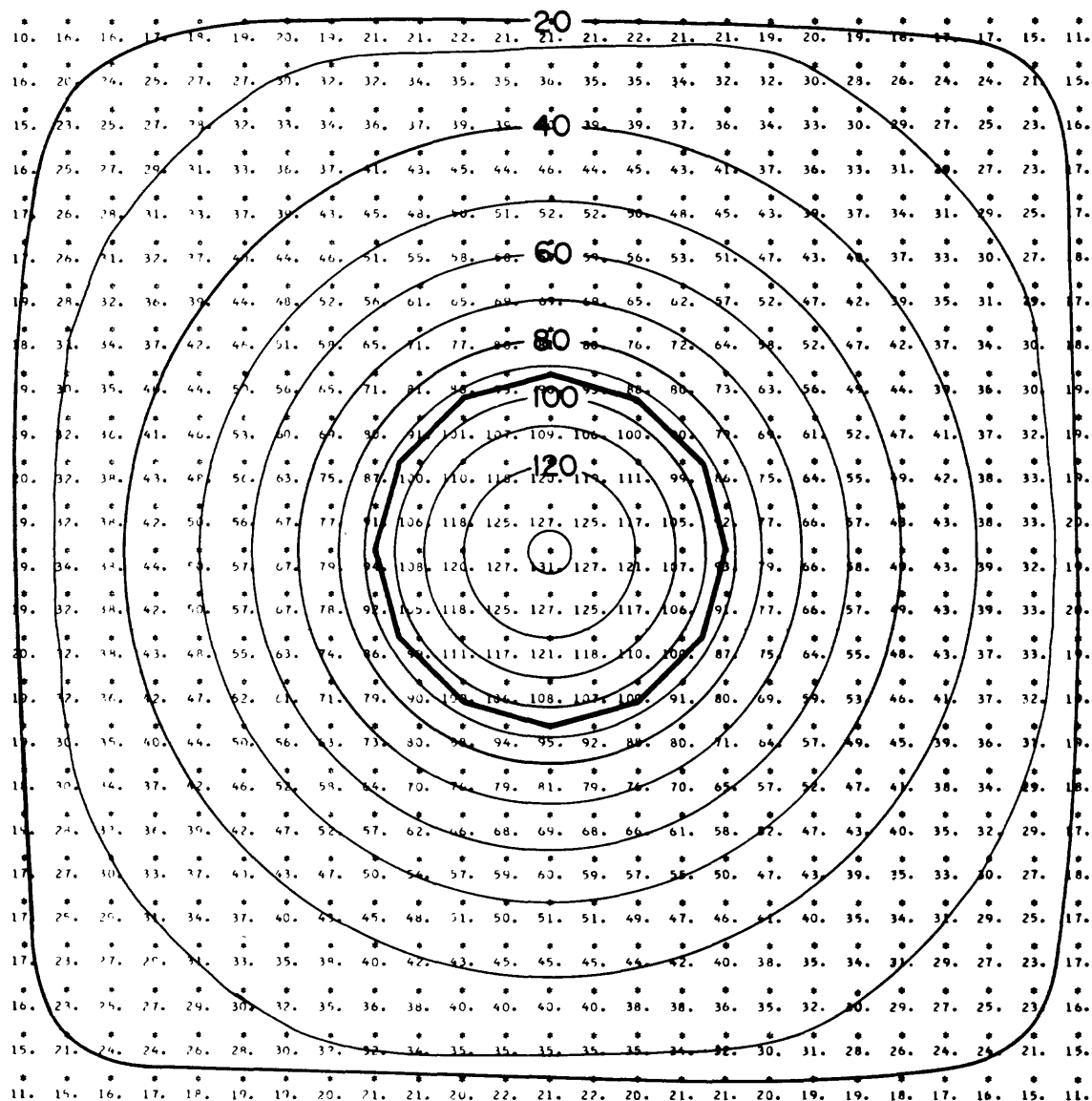
[Gravity field calculated over vertical prism, vertically sided with outline shown by 12-sided figure in center of map]

25 \times 25 GRAVITY FIELD OF VERTICAL CYLINDER, 2 KM RADIUS, TOP 2 KM DOWN, BOTTOM 50 KM
INPUT DATA LESS BASE OF 0.00 MULTIPLIED BY SCALE OF 10.00

Appendix 4. Input Data Continued Down Two Grid Units

[Contours in milligals $\times 10$]

25 X 25 GRAVITY FIELD OF VERTICAL CYLINDER, 2 KM RADIUS, TOP 2 KM DOWN, BOTTOM 50 KM
MAP CONTINUED DOWNWARD 2 GRID UNIT



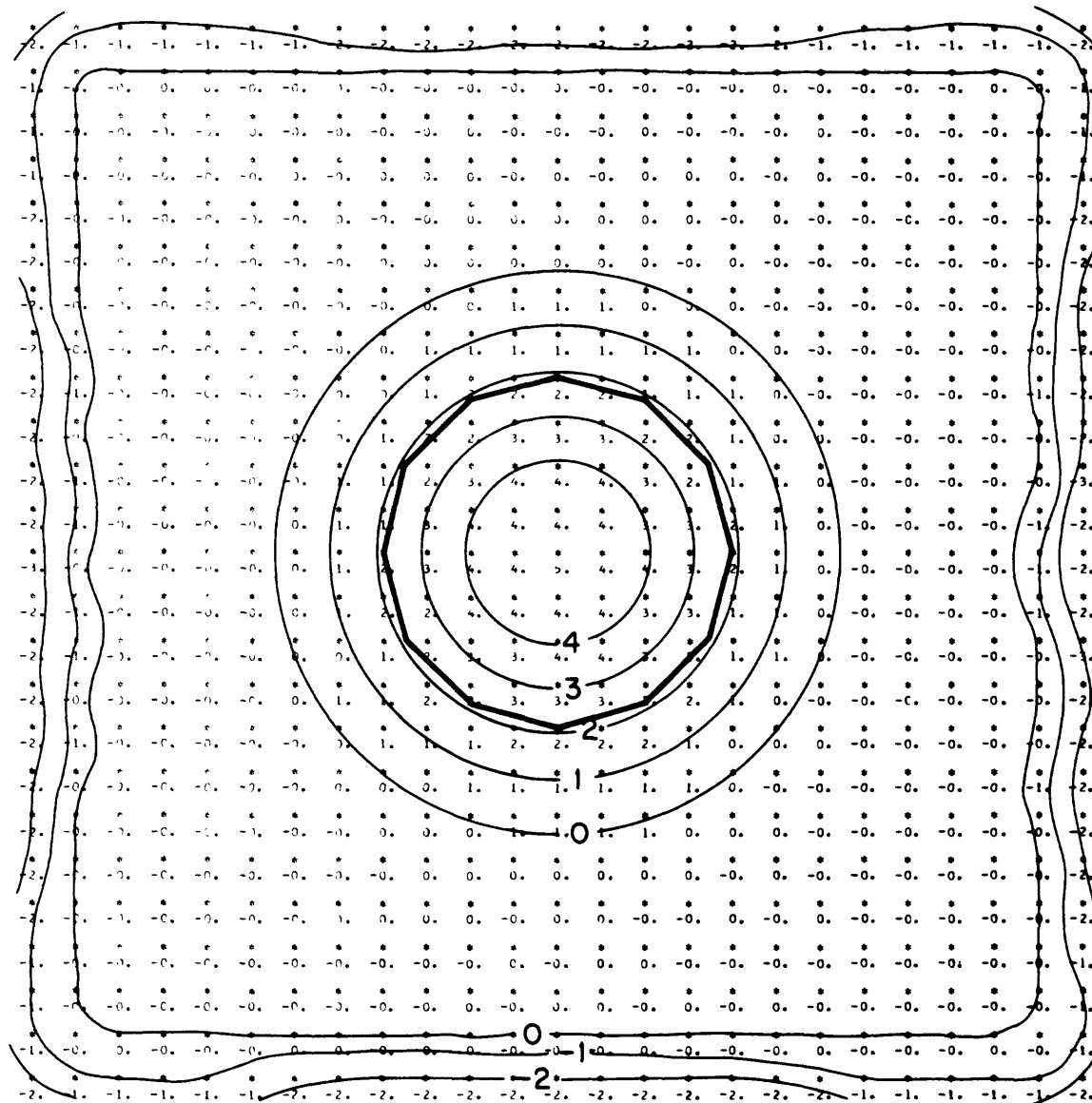
GEOPHYSICAL COMPUTER PROGRAM 1

Appendix 5. Second Derivative of Input Data

[Contours in milligals/.5km/.5km]

[Note additional significant figures can be printed out if the "scale" factor is increased]

25 X 25 GRAVITY FIELD OF VERTICAL CYLINDER, 2 KM RADIUS, TOP 2 KM DOWN, BOTTOM 50 KM
 MAP OF SECOND DERIVATIVE ON SURFACE



Summary

Program HNDRSN2 implements Henderson's (1960) algorithm to calculate derivative and continued fields. The space required to create 19 derivative and continuation maps from an input array of 25 X 25 (625 data

points) was 46,000 octal or 20,000 words. Running time required 26 seconds on a C.D.C. 6600. Single precision arithmetic (14 significant digits) was used in the program.

APPENDIX C

Basic Elements of Fourier Transforms
and ConvolutionLINEAR SYSTEMS

There are two basic types of physical systems - the linear and the non-linear. Linear systems are very useful, for the input-output characteristics of a linear system can be described in a very simple way. Also, linear systems are very common in geophysics (filters, amplifiers, geophones, galvos and even the earth can be considered as linear systems). A simple definition of a system exhibiting linearity is as follows:

- A linear system is one whose action is the same regardless of the amplitude or polarity of the input waveform.

Thus, a telescope may be considered as a linear system - it magnifies a distant object by the same amount regardless of the largeness or smallness of the "input" object. A seismic a.g.c. system, however, is non-linear - it provides an amplification which depends on the magnitude of the input signal.

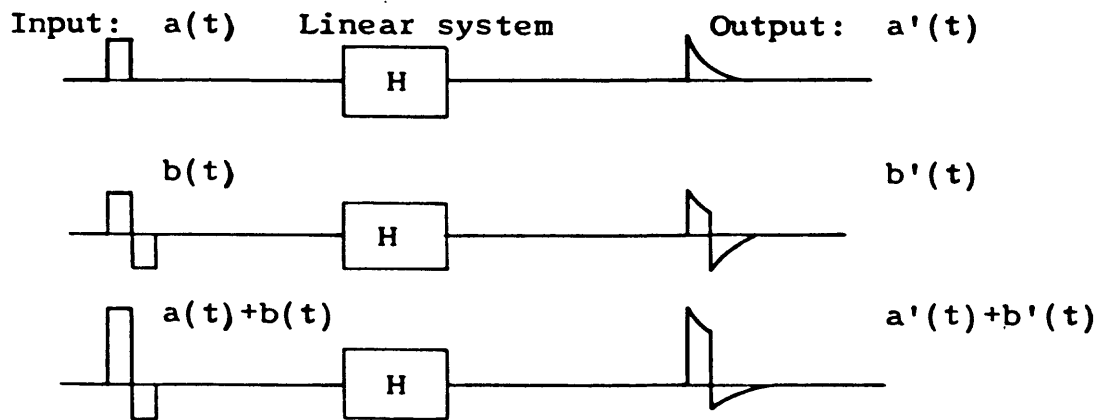
In this chapter, we are concerned with linear operations in the time domain. We shall see that these include such powerful operations as the addition and subtraction of waveforms, normal amplification and attenuation, integration and differentiation, convolution, correlation, harmonic analysis, generation of theoretical seismograms, and others. These powerful processes fail for non-linear systems. We must remember, however, that even a nominally linear device can be linear only up to a certain limit. Hence, the rim of the telescope cuts off images beyond a certain size, an amplifier distorts if it is driven too hard, a magnetic tape saturates if the recording head is over-energized, and a geophone jumps off the ground if the peak acceleration exceeds 1g.

Linear systems are defined by two essential properties:

1. The principle of linear superposition is satisfied.

$$H[a(t) + b(t)] = H(a(t)) + H(b(t))$$

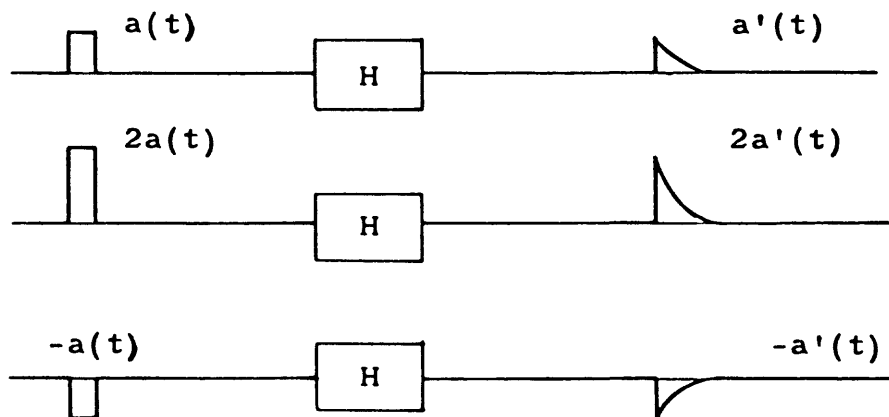
The response to the sum of two inputs is equal to the sum of the two individual responses.



2. The property of homogeneity is satisfied.

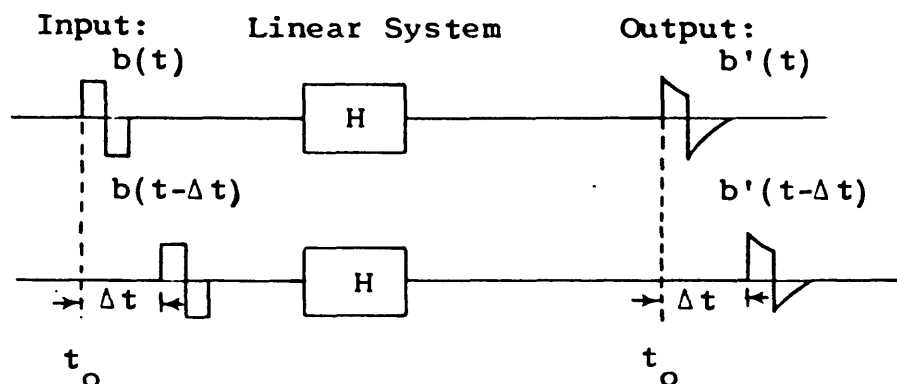
$$H [K a(t)] = K H[a(t)] \quad (K = \text{constant})$$

The response to a constant multiple of any input is equal to the response to the input multiplied by the same constant.



- A system is linear if and only if it is both additive and homogeneous.

A time invariant (stationary) linear system is one in which the input-output relations do not change with time. The shape of the response to an input applied at any instant depends only on the shape of the input and not on the time of application.

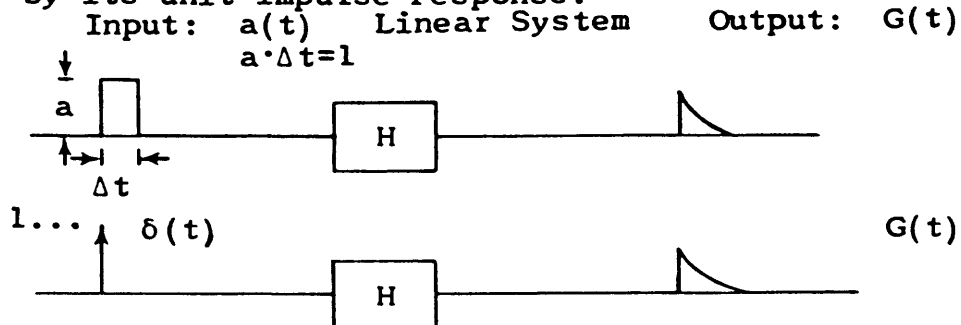


Some of the important characteristics of linear operations are as follows:

- The order in which a sequence of linear operations is performed may be changed without affecting the result.
- A linear system is passive, i.e., no input then no output.
- The output of a linear system contains only those frequencies present in the input; i.e., no new frequencies can appear. A sine wave passes through a linear system and remains a sine wave. It may be changed in amplitude and shifted in phase, but it remains a single frequency sine wave.

UNIT IMPULSE RESPONSE

- A linear system may be completely characterized by its unit impulse response.



$$\text{Unit impulse response} \equiv \lim_{\Delta t \rightarrow 0} G(t)$$

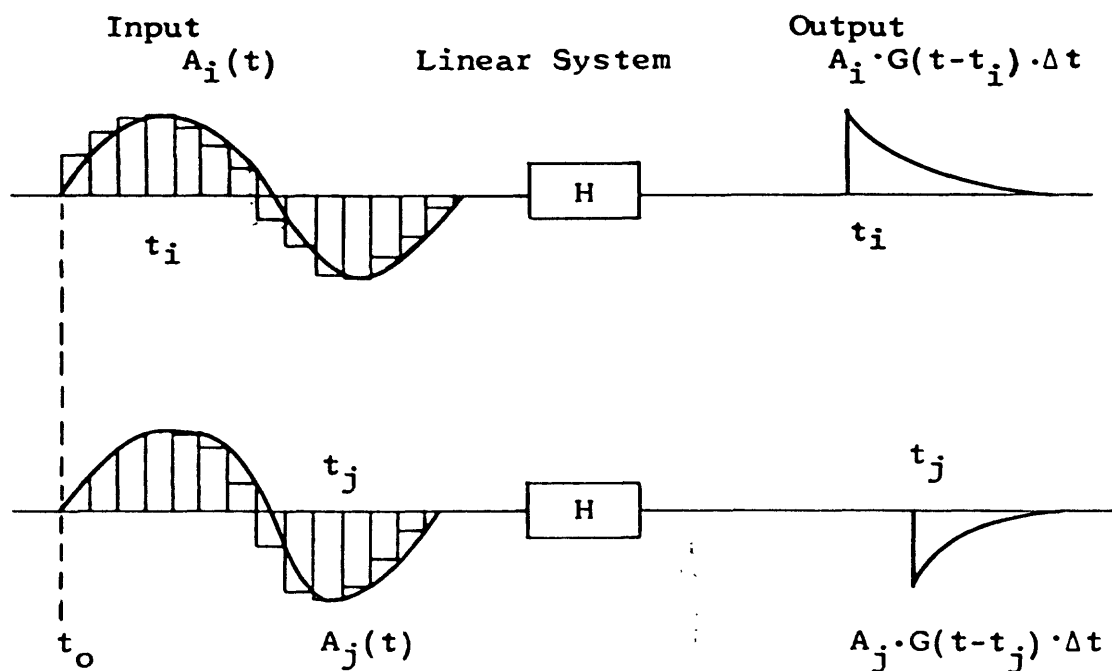
A unit impulse (also called a delta function and a spike) is a pulse which has infinite amplitude and infinitesimal duration. If a unit impulse is the input to a linear system, the response of the system (called the impulse response) specifies the behavior of the linear system uniquely (we will see later that the behavior of a linear system is also specified uniquely by the combination of its amplitude-frequency and phase-frequency responses).

A delta function is a mathematical concept and does not exist in actual practice. However, a very short time interval, Δt , is sufficient for determining the impulse response of most electronic systems. The output changes very little once the duration of the pulse is shorter than the smallest period (highest frequency) passed by the system.

Once the impulse response, $G(t)$, is known, the output of a linear system can be closely determined for any given input. The procedure (illustrated below) can be summarized as follows:

1. The input is approximated as a sum of very narrow pulses, each one approximating a unit impulse delayed in time and multiplied by a constant.

2. The response of the linear system to each individual approximating unit impulse is found using the principles of time-invariance and homogeneity.
3. The response of the linear system to the total input is found by applying the principle of linear superposition.



- For any linear system and for any input waveform, the output waveform is the superposition of all the impulse-responses obtained by regarding the input waveform as a succession of unit impulses.

CONVOLUTION

Convolution is an extremely important and common process in geophysics. Convolution describes the action of a linear system to take a weighted running average of some particular physical quantity over a narrow range. The most common example of convolution in geophysical data acquisition and processing is filtering; filtering by various transmission sub-systems of the earth (Ghosting, water layer reverberation, etc.), filtering of data gathering instrument arrays and systems (geophone arrays, geophone-ground coupling, geophone response, amplifiers, etc.), filtering in the data interpretation phase (downward continuation and 2nd derivative of gravity data, deconvolution, etc.) A good understanding of the physical process of convolution is imperative for understanding many important aspects of the seismic, gravity, magnetics, and electrical geophysical methods and applications in data acquisition and processing.

The Latin roots for convolution have the meaning, "to roll or to twist together". The German word for convolution is "Faltung", which means "to fold". The connotations of the Latin and German meanings, especially folding, help to illustrate the physical concept of convolution. The physical reality behind convolution is exactly the same as that behind the superposition of impulse responses (described earlier) are purely superficial ones.

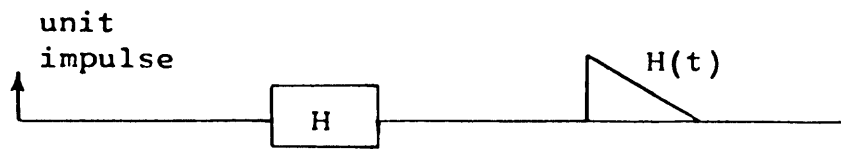
The physical process of convolution may be illustrated in several different ways:

1. Graphically - replacement method
2. Graphically - folding method
3. Moveable strips (serial products)
4. Polynomial multiplication (folding method)
5. Polynomial multiplication - z transforms
6. Matrix multiplication

Each of these methods yields the same answer, but have different applications. Mastery of all the methods will enable you to handle any general convolution problem.

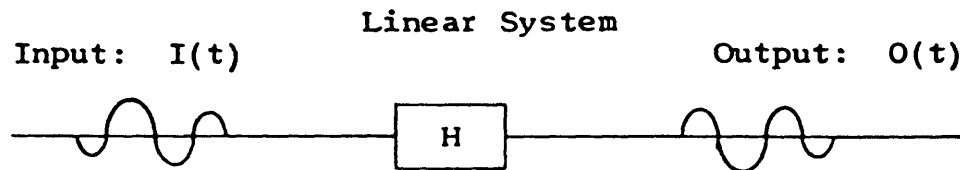
Graphical Representations of Convolution

Suppose we have the linear system, H , which has an impulse response $H(t)$.



We want to find the output, b , at time t_k which results for any general input, $a(t)$, to the linear system H .

- Convolution is the physical process of obtaining an output from some linear system by applying an input.



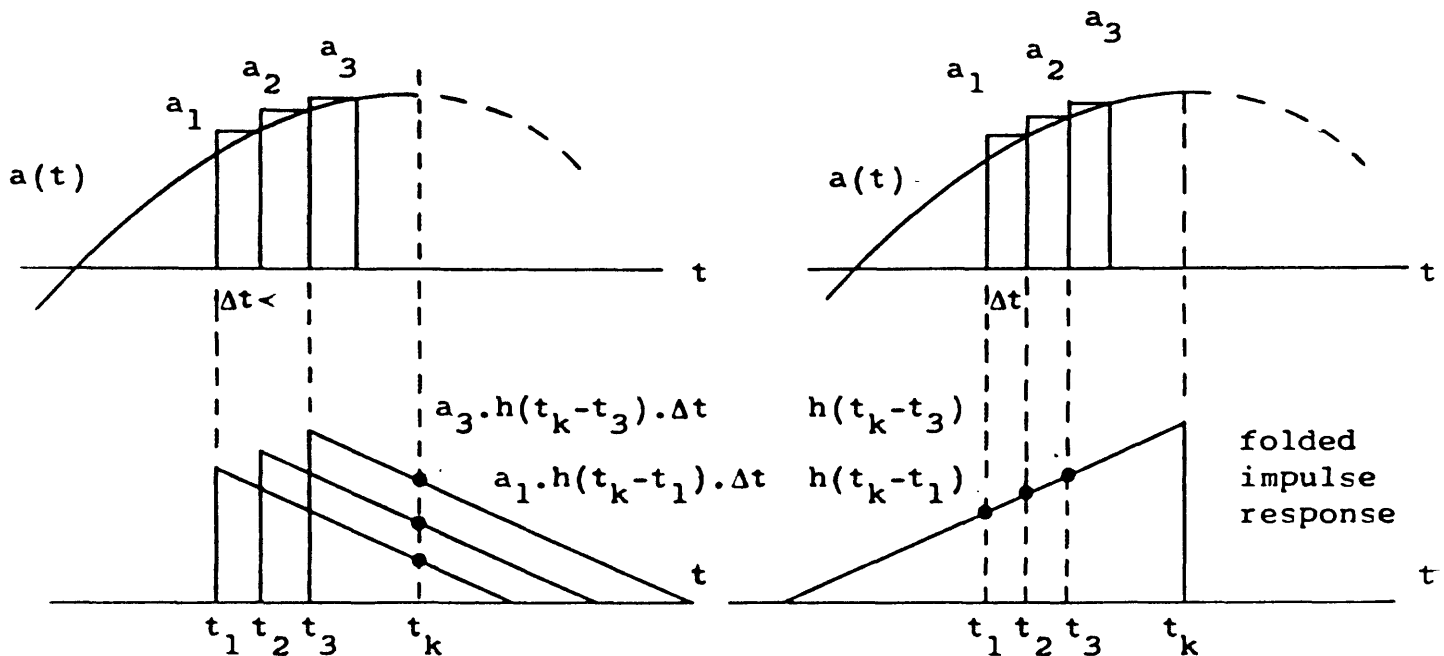
We speak of the above operation as convolving $I(t)$ with the impulse response of the linear system H to obtain the output $O(t)$. In symbols, this operation is written as

$$I(t) * H(t) = O(t)$$

where the symbol $*$ denotes "convolved with".

- Superposition and convolution represent equivalent but procedurally different ways to describe the interaction of an input waveform with an impulse response to produce an output waveform.

The procedure is graphically illustrated below for two equivalent, but different appearing methods, the replacement and the folding methods.



REPLACEMENT METHOD

FOLDING METHOD

Both methods lead to the following result for the output amplitude at time t_k .

$$\begin{aligned}
 b(t_k) &= a_1 \cdot H(t_k - t_1) \cdot \Delta t + a_2 \cdot H(t_k - t_2) \cdot \Delta t \\
 &+ a_3 \cdot H(t_k - t_3) \cdot \Delta t + \dots \\
 &= \sum_i a_i H(t_k - t_i) \Delta t
 \end{aligned}$$

The replacement method can be summarized as follows:

1. Approximate the input as a series of unit impulses of short time duration Δt and amplitude factor a .
2. Replace each impulse used to approximate the input with the impulse response of the linear system multiplied by $a \cdot \Delta t$, the strength of the pulse.
3. Sum at time t_k to obtain the output $b(t_k)$.
The replacement method is clearly an example of the principle of superposition.

The folding method can be summarized as follows:

1. Fold (time reverse) the impulse response, $H(t)$, and shift its time origin to the time t_k .
2. Multiply the area of each impulse used to approximate the input waveform by the value of the folded impulse response for corresponding times.
3. Sum all the product waveforms to obtain the output $b(t_k)$.

The operation is repeated if the output of another time other than $t = t_k$ is desired.

The folding method follows directly from the formula for the convolution integral;

$$b(t_k) = \int_{-\infty}^{\infty} a(\tau) \cdot H(t_k - \tau) d\tau$$

where

$b(t_k)$ = output amplitude at time $t = t_k$,

$a(\tau)$ = input time function (τ is a dummy variable),

$H(t_k - \tau)$ = impulse response of the linear system
folded (reversed) and shifted in time to
 $t = t_k$.

Inspection of the convolution integral reveals that the operations in convolution and their order are as follows:

1. FOLD (reverse in time)
2. SHIFT (shift to time t_k)
3. MULTIPLY (obtain product waveform)
4. SUM (integrate - find the area of all the product waveforms)

Steps 2-4 are repeated if the output at other times is desired.

The replacement and folding methods lead to the following conclusion:

- For any linear system and for any input waveform, the output waveform is the convolution of the impulse response of the system with the input waveform.

The concept of convolution illustrated by the preceding discussion has two merits. First, it makes evident the fact that every physical linear system has a "memory" whose length is the duration of the impulse response, and the output obtained at a particular time is a weighted sum of the input at all past times within this memory. Second, the operation of sliding one waveform past another, while multiplying corresponding ordinates and adding the product waveforms, is basic to other operations on waveforms (such as auto- and cross-correlation which will be discussed (later) and yields insight into the physical processes involved.

Convolution as Moveable Strips (Serial Products)

Consider two polynomials of time;

$$f(t) = a_0 + a_1t + a_2t^2 + a_3t^3 + \dots$$

and

$$g(t) = b_0 + b_1t + b_2t^2 + b_3t^3 + \dots$$

Their product, $h(t)$, is

$$\begin{aligned} a_0b_0 + (a_0b_1 + a_1b_0)t + (a_0b_2 + a_1b_1 + a_2b_0)t^2 \\ + (a_0b_3 + a_1b_2 + a_2b_1 + a_3b_0)t^3 + \dots \end{aligned}$$

This product can be written as

$$h(t) = C_0 + C_1t + C_2t^2 + C_3t^3 + \dots$$

where

$$C_0 = a_0b_0$$

$$C_1 = a_0b_1 + a_1b_0$$

$$C_2 = a_0b_2 + a_1b_1 + a_2b_0$$

$$C_3 = a_0b_3 + a_1b_2 + a_2b_1 + a_3b_0$$

This elementary observation has an important connection with convolution. Suppose two functions $f(t)$ and $g(t)$ are given and it is required to calculate their convolution numerically. We form a sequence of values of $g(t)$ at short regular intervals of width Δt ,

$$\{b_0, b_1, b_2, b_3, \dots b_m\}$$

and a corresponding sequence of values of $f(t)$

$$\{a_0, a_1, a_2, a_3, \dots a_n\}$$

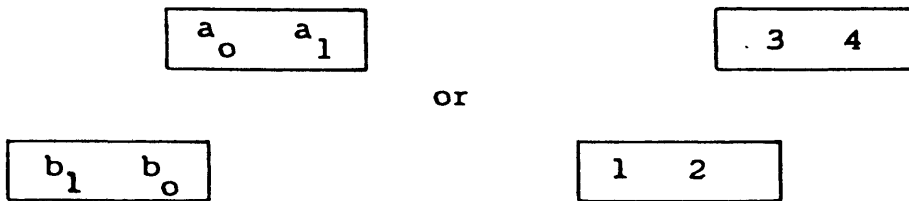
We then approximate the convolution integral by summing products of corresponding values of $f(t)$ and $g(t)$, taking different discrete values of t , one by one. It is convenient to write the values of one sequence, the one to be folded, on a moveable strip of paper which can be slid into successive positions relative to the other sequence.

As a simple example, consider the two sequences

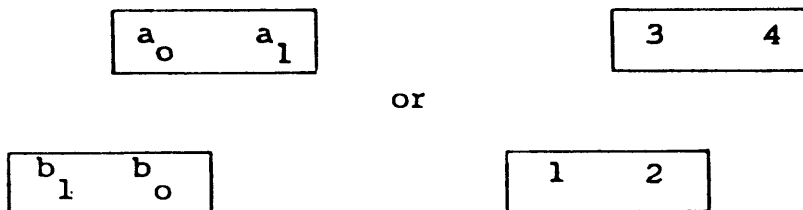
$$f(t) = \{3, 4\}$$

$$g(t) = \{2, 1\} .$$

After folding $g(t)$, the moveable strips can be positioned as follows:



To obtain C_0 , we slide the bottom strip to the position



and multiply adjacent entries;

$$C_0 = a_0 b_0 = 3 \cdot 2 = 6$$

To obtain C_1 , we slide the bottom strip one additional space to the right and repeat the process



$$C_1 = a_0 b_1 + a_1 b_0 = 2.4 + 1.3 = 11.$$

The last coefficient, C_2 , is obtained in an analogous manner;

$$\begin{array}{|c|c|} \hline a_0 & a_1 \\ \hline \end{array}$$

or

$$\begin{array}{|c|c|} \hline 3 & 4 \\ \hline \end{array}$$

$$\begin{array}{|c|c|} \hline b_1 & b_0 \\ \hline \end{array}$$

$$\begin{array}{|c|c|} \hline 1 & 2 \\ \hline \end{array}$$

$$C_2 = a_1 b_1 = 1.4 = 4$$

Therefore,

$$\begin{aligned} f(t) * g(t) &= h(t) \\ &= \{6, 11, 4\} \end{aligned}$$

It can be seen that this procedure generates the same expressions that occur in the multiplication of series; therefore, it is often called a serial product. Also, the serial product is a longer sequence than either of the two individual sequences; the number of terms in the product is one less than the sum of the number of terms in the individual sequences. This relation is important when considering the result of convolving digital operators of different lengths.

One notes that the same result is obtained if $g(t)$ is folded and moved past $f(t)$ in an analagous manner to that described above.

Convolution as Polynomial Multiplication (Folding)

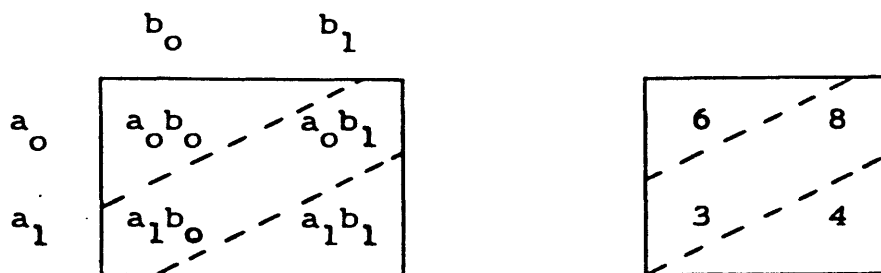
Convolution can be illustrated as polynomial multiplication in another manner. Consider the convolution of the two sequences

$$\{a_0, a_1\} * \{b_0, b_1\}$$

Where $a_0 = 2$, $a_1 = 1$, $b_0 = 3$, $b_1 = 4$. We can write an ordered tabular array as follows;

		b_0	b_1	
a_0	$a_0 b_0$	$a_0 b_1$	or	6 8
a_1	$a_1 b_0$	$a_1 b_1$		3 4

where the entries are the products of corresponding a 's and b 's. If we fold successive diagonals which run from left to right across the tabular array as shown below, we can read the values of the output from the array;



$$C_0 = a_0 b_0 = 6$$

$$C_1 = a_1 b_0 + a_0 b_1 = 11$$

$$C_2 = a_1 b_1 = 4.$$

Therefore,

$$\{2, 1\} * \{3, 4\} = \{6, 11, 4\}.$$

In general, the preceeding discussion leads us to write the following formula for the convolution of sampled (digitized) data;

$$h(t) = f(t) * g(t)$$

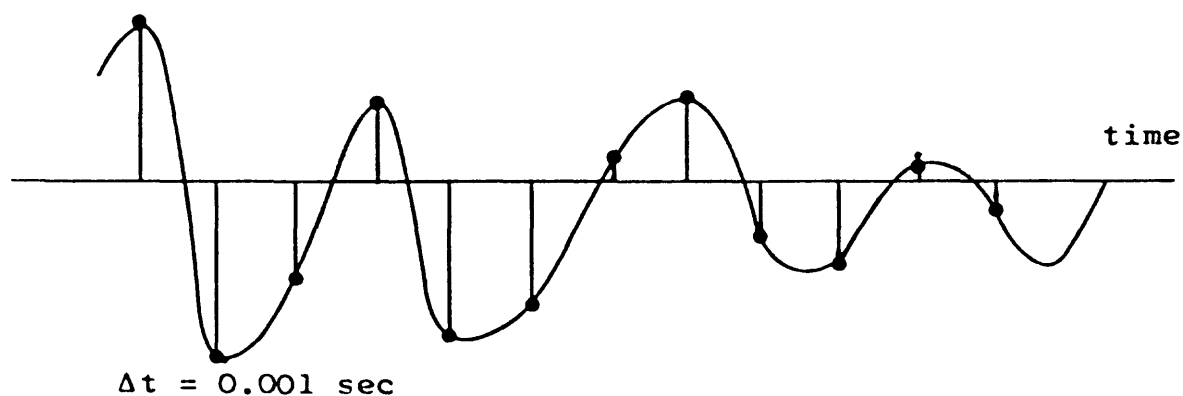
$$C_t = \sum_{s=0}^n a_s \cdot b_{t-s} \quad \text{for } t = 0, 1, 2, \dots$$

Convolution as Polynomial Multiplication (Z Transforms)

In geophysical data processing, it is often convenient to convert a continuous seismic trace or some

other continuous recording of geophysical data as a function of time into discrete numbers which can be processed by a digital computer. The process of converting a continuous seismic trace into a sequence of numbers at equally spaced time points is called digitization.

Consider the following example of digitization:



We can tabulate the results in the following manner:

Time (sec)	1.000	1.001	1.002	1.003	1.004	1.005	etc.
Time Index	t=0	t=1	t=2	t=3	t=4	t=5	etc.
Amplitude	4.0	-5.0	-3.0	2.0	-4.5	-3.5	etc.

If we consider the digitized seismic trace as a sum of unit delta functions having varying time delays and multiplied by a constant, the equation for the digitized trace above can be written as

$$f(t) = 4.0 \delta(t) - 5.0 \delta(t-1) - 3.0 \delta(t-2) + 2.0 \delta(t-3) \\ - 4.5 \delta(t-4) - 3.5 \delta(t-5) + \dots$$

We introduce the mathematical operator

$$z$$

which provides a unit delay. The operator

$$z^n$$

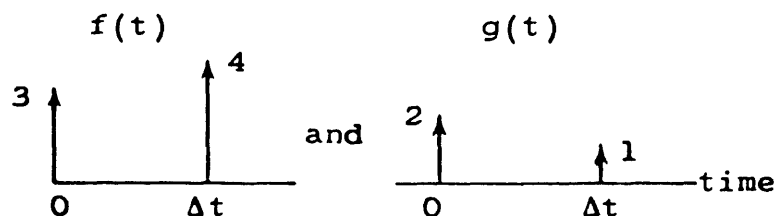
introduces a delay of n time units. Therefore, we can write a polynomial in z for the digitized seismic trace;

$$f(z) = 4z^0 - 5z^1 - 3z^2 + 2z^3 - 4.5z^4 - 3.5z^5 + \dots$$

where $f(z)$ is called the z transform of $f(t)$.

- The z transform of a finite wavelet is the polynomial in z whose coefficients are the coefficients of the wavelet.

As an example, consider the wavelets shown below:



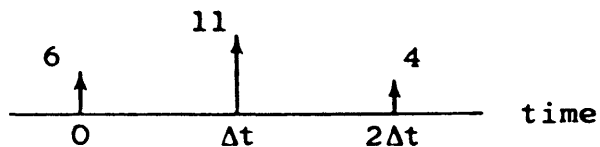
where Δt is the digitization interval. The z transforms for these two wavelets can be written as

$$f(z) = 3 + 4z \quad \text{and} \quad g(z) = 2 + z$$

If we multiply $f(z) \cdot g(z)$, we obtain

$$f(z) \cdot g(z) = 6 + 11z + 4z^2,$$

a function which corresponds to the wavelet



From the preceding section, we realize that the sequence

$$\{6, 11, 4\}$$

is the convolution of $f(t)$ and $g(t)$. Therefore, we can write the important rule;

- Convolution may be performed by multiplication of polynomials; the z transforms of wavelets.

Since polynomial multiplication is a well known operation, we can write the following additional relations:

- Convolution is commutative; i.e.,

$$O(t) = I(t) * H(t)$$

$$= H(t) * I(t)$$

The role of the input, $I(t)$, and impulse response, $H(t)$, may be interchanged in convolution without changing the result.

- Convolution is associative; i.e.,

$$O(t) = I_1(t) * [I_2(t) * H(t)]$$

$$= [I_1(t) * I_2(t)] * H(t)$$

$$= [I_1(t) * H(t)] * I_2(t)$$

These rules illustrate that the order of linear operations does not affect the final output waveform. A typical example is as follows: recording with the playback filter and playing back with the record filter should give the same results as recording with the record filter and playing back with the play back filter (this is the idea behind the dynamic range instrument test). Other familiar examples include preparation of intermediate storage tapes

at various points in a data processing sequence and varying the order of the linear operations in the generation of a synthetic seismogram

Convolution as Matrix Multiplication

Consider the two sequences, $f(t)$ and $g(t)$, defined as

(5 terms) $f(t) = a_0, a_1, a_2, a_3, a_4$ (input)

(3 terms) $g(t) = b_0, b_1, b_2$ (impulse response of filter)

output = 8-1 terms
= 7 terms

The output, $O(t) = f(t) * g(t)$, can be written in matrix notation as follows:

INPUT	FILTER	OUTPUT
$\begin{bmatrix} a_0 & 0 & 0 & 0 & 0 & 0 & 0 \\ a_1 & a_0 & 0 & 0 & 0 & 0 & 0 \\ a_2 & a_1 & a_0 & 0 & 0 & 0 & 0 \\ a_3 & a_2 & a_1 & a_0 & 0 & 0 & 0 \\ a_4 & a_3 & a_2 & a_1 & a_0 & 0 & 0 \\ 0 & a_4 & a_3 & a_2 & a_1 & a_0 & 0 \\ 0 & 0 & a_4 & a_3 & a_2 & a_1 & a_0 \end{bmatrix}$	$\begin{bmatrix} b_0 \\ b_1 \\ b_2 \\ 0 \\ 0 \\ 0 \\ 0 \end{bmatrix}$	$\begin{bmatrix} c_0 \\ c_1 \\ c_2 \\ c_3 \\ c_4 \\ c_5 \\ c_6 \end{bmatrix}$
(7x7)	(7x1)	(7x1)

where

$$\begin{bmatrix} c_0 \\ c_1 \\ c_2 \\ c_3 \\ c_4 \\ c_5 \\ c_6 \end{bmatrix} = \begin{bmatrix} a_0 b_0 \\ a_1 b_0 + a_0 b_1 \\ a_2 b_0 + a_1 b_1 + a_0 b_2 \\ a_3 b_0 + a_2 b_1 + a_1 b_2 \\ a_4 b_0 + a_3 b_1 + a_2 b_2 \\ a_4 b_1 + a_3 b_2 \\ a_4 b_2 \end{bmatrix}$$

The matrix formulation illustrates the basic concepts of convolution:

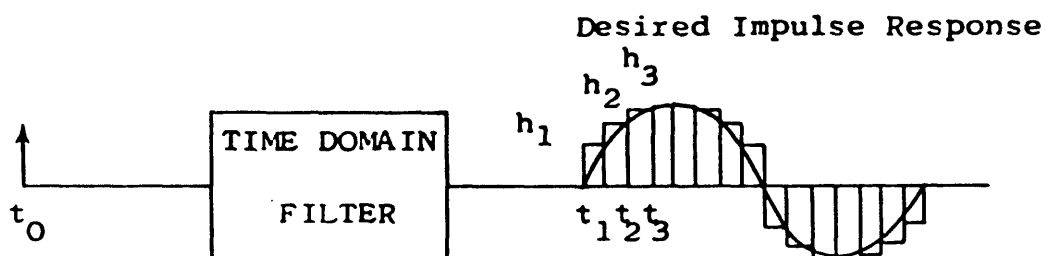
1. FOLD (reverse in time)
2. SHIFT
3. MULTIPLY (obtain product waveform)
4. SUM

Also, the output matrix (the C's) has 7 terms, one less than the sum of the terms in the input and impulse response sequences (the a's and b's).

Design of a Time Domain Filter

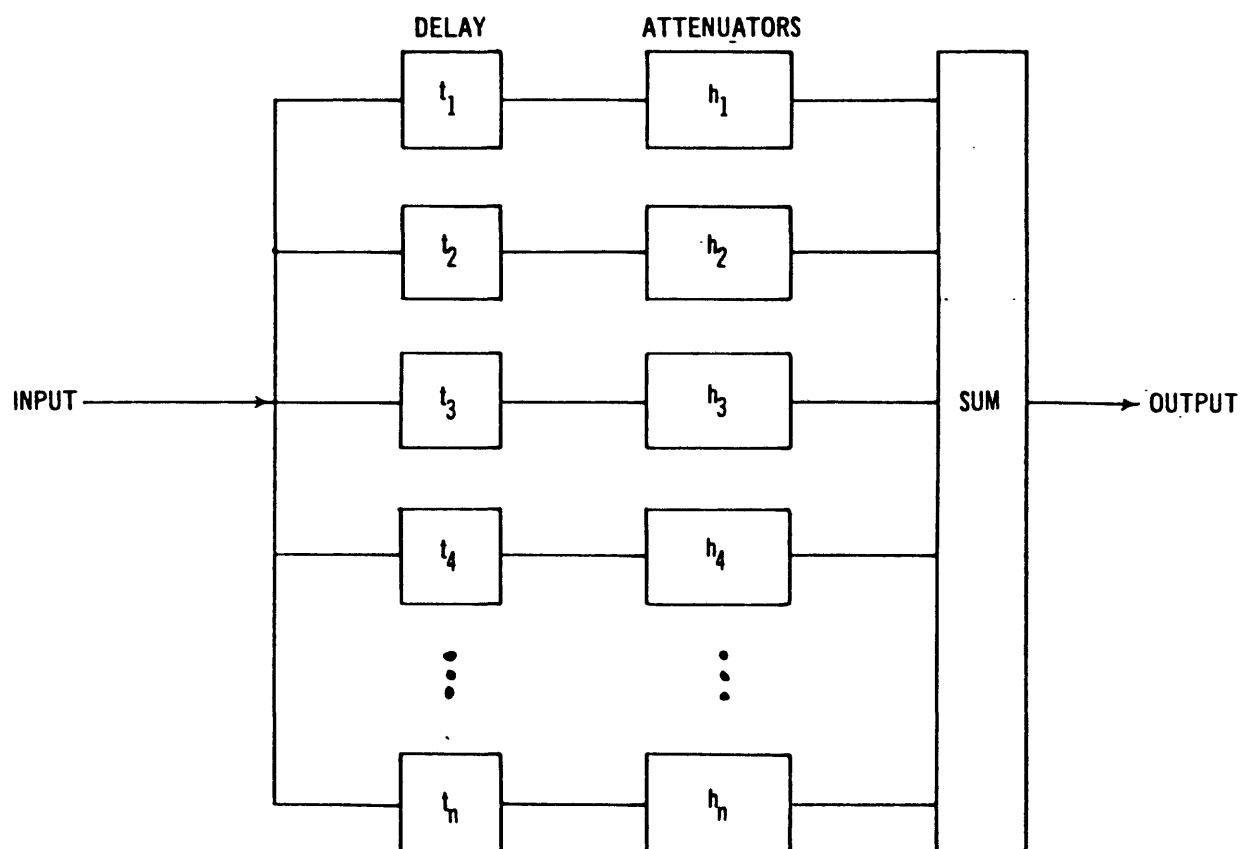
The principle of the time domain filter is based upon the replacement concept of convolution with the role of the input and the impulse response interchanged.

The basic problem is to design a filter which will have a specific impulse response.



The procedure can be described as follows:

1. Divide the waveform representing the desired impulse response into a series of narrow pulses centered at times t_1 , t_2 , t_3 , ... etc., and having heights h_1 , h_2 , h_3 , ... etc., related to the area of the pulse.
2. The filter can be achieved by building a network of time delay devices, attenuators, and a summer.



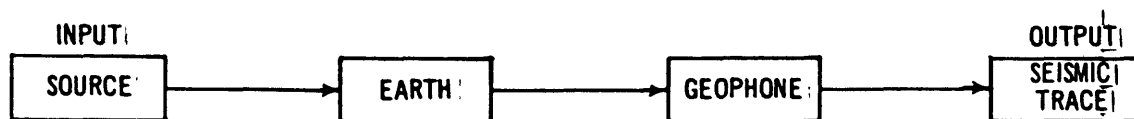
Theoretical (Synthetic) Seismograms

Synthetic seismograms are a powerful tool for estimating the effect which known and postulated changes in the structural attitude and physical properties of the subsurface cause to propagating seismic waves. Significant advances have been made in recent years to develop the capability to duplicate closely in a synthetic seismogram the characteristic features of observed seismic records (see the symposium on Synthetic Seismograms, EAEG, V. 8, p. 231-347, 1966; P.C. Wuenschel, Seismogram Synthesis Including Multiples and Reflection Coefficients, Geophysics, V. 25, p. 106, 1960; S. Treitel and E.A. Robinson, Seismic Wave Propagation in Layered Media in Terms of Communication Theory, Geophysics, V. 31, p. 17, 1966 for details).

A brief review of some of the important aspects of the total seismic process is given below to insure completeness and understanding.

The ground motion recorded by a geophone is the net result of a number of complex physical processes. The physical processes involved, although difficult to generalize, may be classified in terms of communication theory as occurring in three areas: 1) the source, 2) the seismic or elastic wave transmission region of the earth, and 3) the geophone and near surface area. The

total process may be described schematically as a lumped parameter system;



Research and experimental observation through the years has added considerable knowledge of each parameter of the system. Details of each parameter are as follows:

1. The Source - Many seismic energy sources are employed today: dynamite, air gun, aqua pulse, Dinoseis, Vibroseis, GASSP, WASSP, Flexotier, etc. The object of all these different energy sources is to produce an input signal which is either close to or performs the same function as the idealized delta function; a sharp impulsive disturbance with enormous amplitude. (The delta function, as we will see later, has a white amplitude spectrum; i.e., all frequencies are present with the same amplitude.)

If the energy source is dynamite and the detonation medium is rock, the rock behavior is extremely non-linear and complex in the area immediately surrounding the source. Approximately 50% of the available initial energy immediately feeds a shock wave which propagates radially outward from the wall of the shot cavity. The

general characteristics of the intense shock wave are a function of the explosive as well as the shot cavity geometry and the properties of the rock medium in which wave propagation takes place. These characteristics are known to be complex and are the subject of continuing research by many scientists. As the shock wave propagates radially outward, the dissipative characteristics of the rock reduce the loading intensity to the point where the elastic properties of the medium begin to play a significant role.

Water is the closest thing to a perfect source medium. The water layer is essentially homogeneous and isotropic, and consequently, does not exert the extreme dissipative characteristics of rock. It does introduce other problems, however, which offset this advantage.

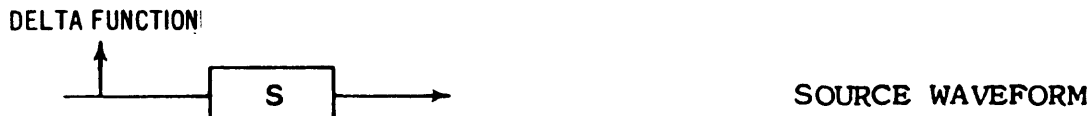
2. The Earth - As the source generated energy propagates into the seismic or elastic region, less than 5% of the original source energy is generally available to propagate as elastic waves. As the elastic wave energy propagates over a distance of a few thousand feet, the pulse changes shape, broadens in time, and decays in amplitude as a consequence of the earth's transmission characteristics. Although the energy source generates a very wide band of frequencies, differential frequency attenuation and absorption by the earth reduces the band.

As a result, the signal is transformed into a spread-out oscillating wavelet. As the disturbance propagates through the earth, it encounters many major and minor geological boundaries. At each boundary, the energy is in part reflected and in part refracted; hence, a great variety of different transmission paths are generated. Other physical phenomena such as ghosting, reverberation within and between layers, scattering, and diffraction occur along each transmission path and compound the complexity of the total process. Processes such as ghosting and reverberation tend to introduce notches and resonant frequencies in the amplitude spectrum, as will be illustrated in later sections. Scattering causes attenuation which increases rapidly with decrease in wave length of the pulse. This action causes the earth to tend to act as a high-cut filter to seismic signals.

3. The Geophone and Near Surface Area - The near surface area, the geophone-ground coupling, and the geophone response are important factors in the total seismic process. The near surface area is often extremely heterogeneous and has a variable thickness and acoustic velocity. These features of the near surface layer introduce an attenuating and broadening effect on the returning reflected pulses in addition to a differential delay (static shift)

from trace to trace. The coupling between the geophone and the ground is a resonant system. The resonant frequency and the sharpness of tuning of this system are controlled by features which may seem insignificant to the seismic emplacement engineer, but which are important. The effect of the resonant system is the same as a filter; each recorded seismic trace is distorted and time shifted as a direct function of the geophone plant as though each trace had a different filter setting. The movement of the earth is measured by a geophone having a restricted bandwidth. This means that the output of a geophone is a distorted version of the actual movement of the free surface of the earth. Also, instrument and system noise tends to complicate the instrument response.

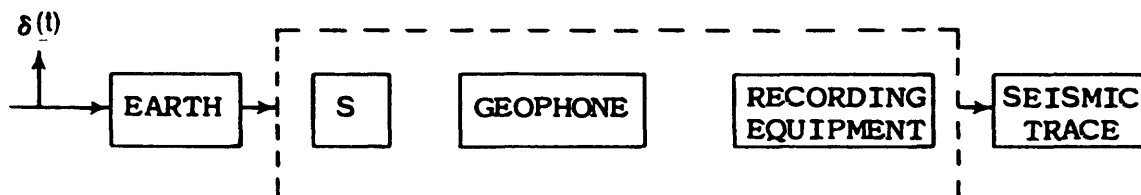
We can describe the process of generating a simple synthetic seismogram in terms of linear systems. First, we consider the source waveform as the impulse response of the source;



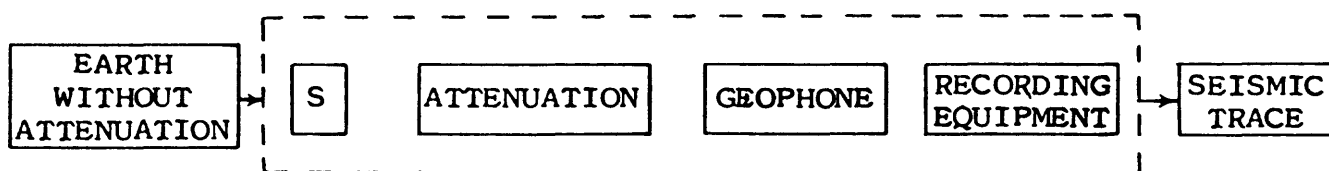
The total seismic process can be shown schematically as



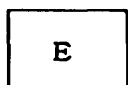
Using the properties of associativity and commutativity of linear systems, we can interchange the order of the linear operations;



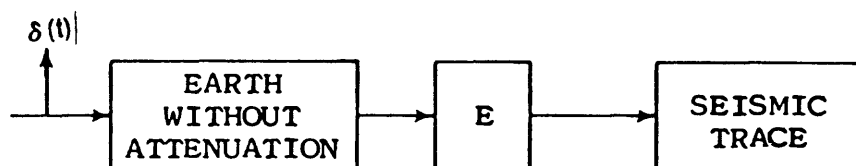
The system designated "Earth" can be subdivided into the Earth Without Attenuation (earth's impulse response) and frequency dependent Attenuation (approximated as a linear system).



The systems contained within the dashed box may be considered as one equivalent linear system



which allows us to approximate the seismic process as a unit impulse interacting with two linear systems;



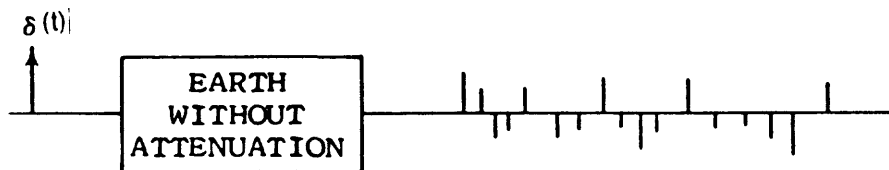
Mathematically, the theoretical seismogram may be considered as

$$\delta(t) * \text{EARTH WITHOUT ATTENUATION} * E = \text{SEISMIC TRACE}$$

or

$$\text{IMPULSE RESPONSE OF THE EARTH} * E = \text{SEISMIC TRACE}$$

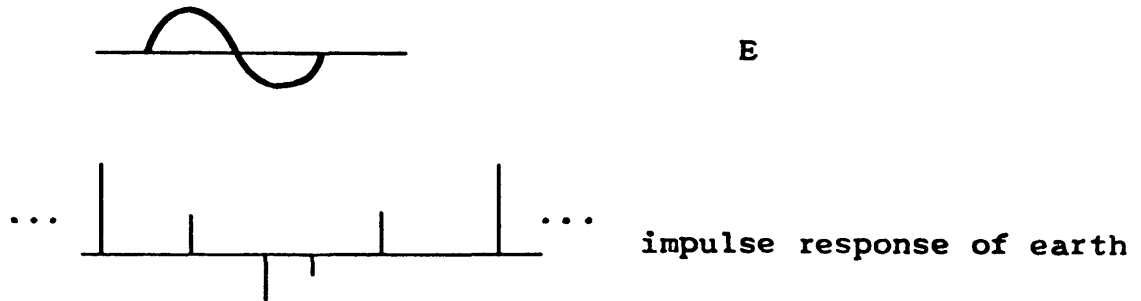
The impulse response of the earth can be considered as a series of impulses, having a spacing related to the occurrence of reflection interfaces within the earth and an amplitude related to the reflection coefficient of each interface. This information can be obtained from continuous velocity and density logs.



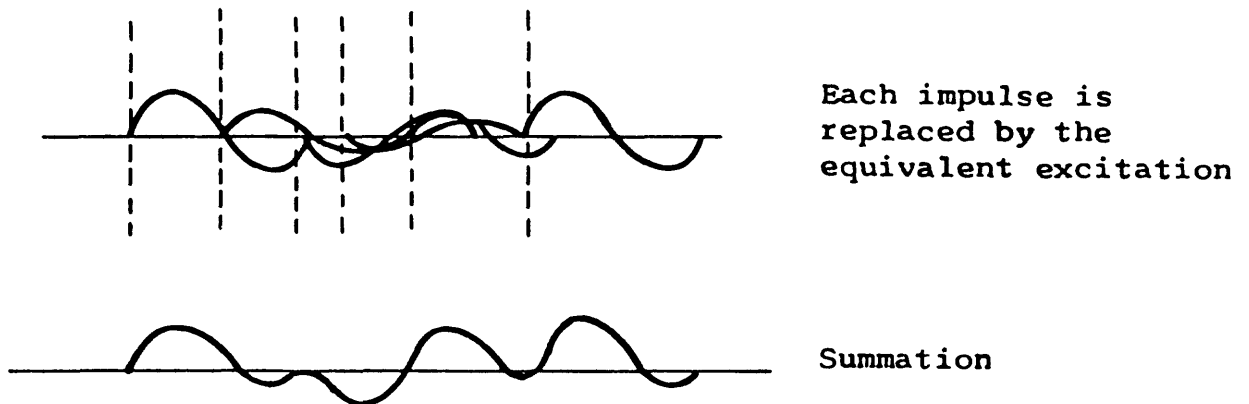
The impulse response of the equivalent system designated E is not as easy to determine, however, and represents the "educated guess" portion of the process.

To illustrate the principles involved in generating a theoretical seismogram, consider the following generalized

example. The impulse response of the equivalent system, E, and the impulse response of the earth are as shown below



The process of convolution can be effected most easily by the replacement method. Each of the reflection impulses are replaced by the waveform for E, appropriately modified in amplitude and polarity. The result of this process and the summation are shown below.

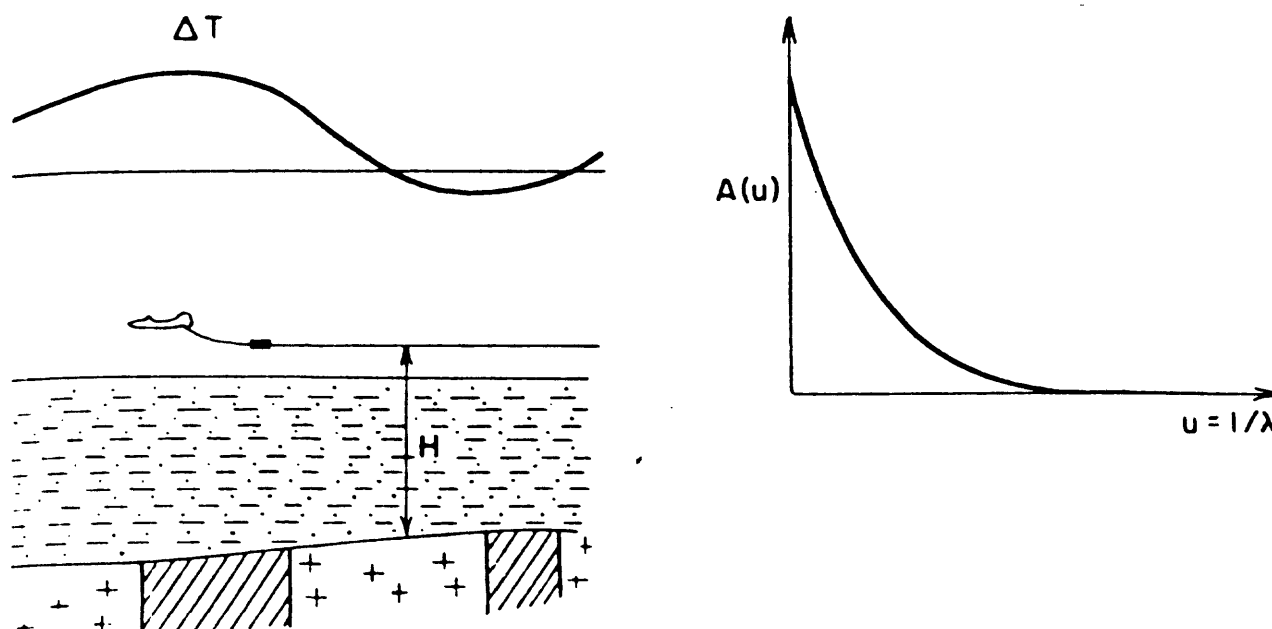


An important result which is apparent from the example above is as follows:

- The waveform for the impulse response of the equivalent system, E, should be short in order to resolve individual reflectors.

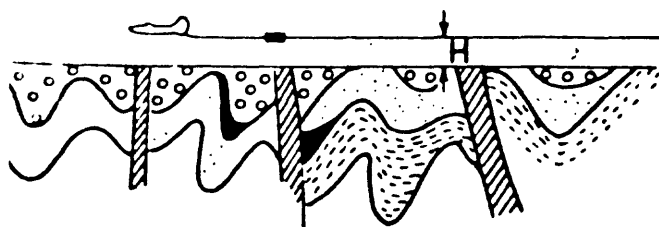
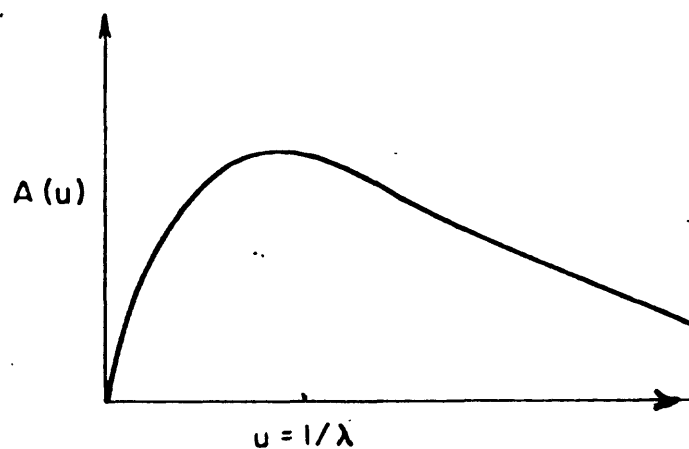
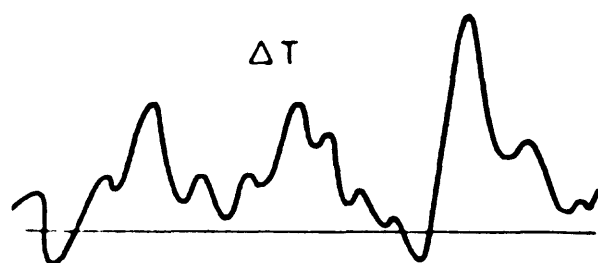
Matched Filtering of Gravity and Magnetic Maps--In this application,* a power spectrum is calculated for the gravity (or magnetic) map and it is divided into: (1) a steeply declining portion at low wave numbers, u , (reflects sources which are very deep and/or broad) and (2) a more gently declining part which is visible at the higher wave numbers (reflects sources which are relatively shallow and localized). The figures which follow illustrate schematically the relative energy spectrum for deep (long wave length-low wave numbers) and shallow (short wave length-large wave number) sources.

DEEP SOURCES



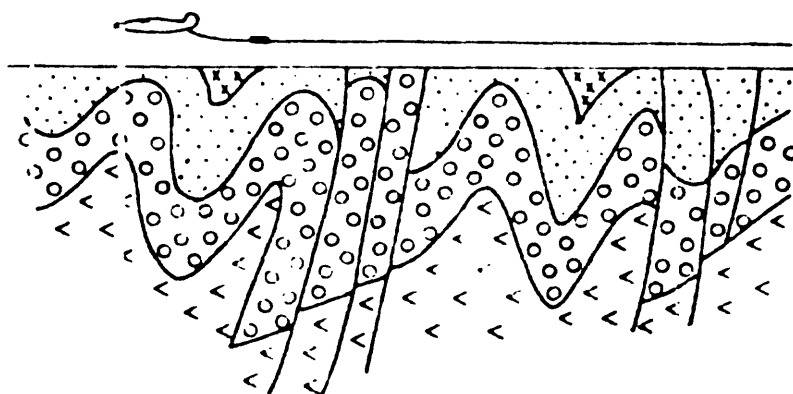
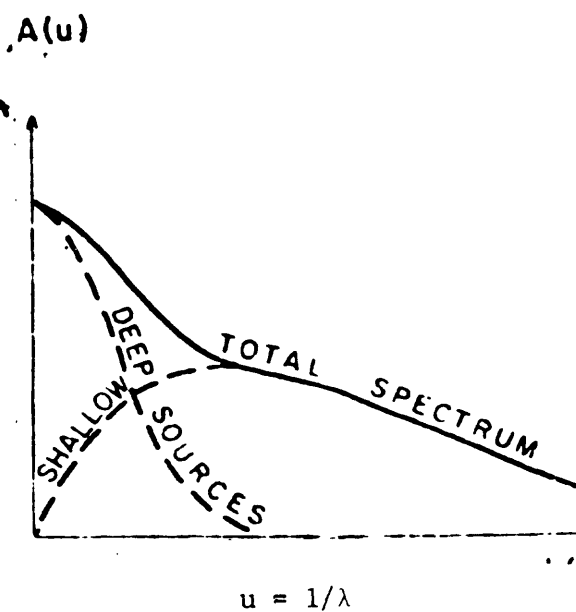
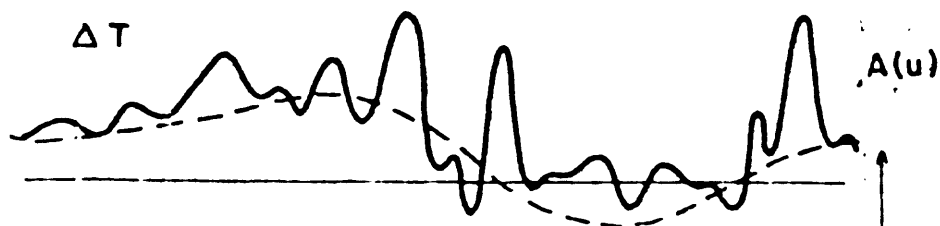
*Spector, A. and Grant, F. S., 1970 Statistical models for interpreting aeromagnetic data, *Geophysics*, v. 35, pp. 293-302.

SHALLOW SOURCES



The composite effect of the shallow and deep sources is shown below.

COMPOSITE EFFECT



A linear filter can be devised which is as close to optimum as one can get for removing one set of sources or the other from the gravity (or magnetic) field. The mathematical concept is as follows. The spectral contribution of the two systems of sources is

$$A(u) = A_R(u) + A_S(u)$$

where $A_R(u)$ is the spectrum of the regional or deeper sources and

$A_S(u)$ is the spectrum of the shallow sources

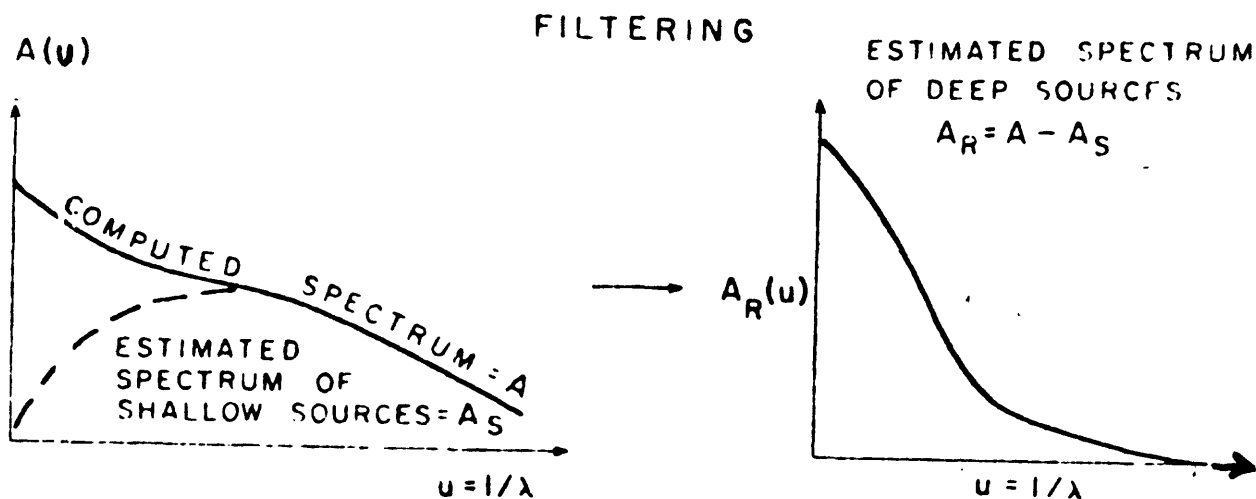
$$A(u) = A_R(u) \cdot \left[1 + \frac{A_S(u)}{A_R(u)} \right]$$

If the spectrum were to be multiplied by the function

$$W(u) = \frac{1}{\left[1 + \frac{A_S(u)}{A_R(u)} \right]}$$

we would in effect filter out the near-surface contribution.

Thus, specifying the mathematical forms of $A_R(u)$ and $A_S(u)$ enables us to design a matched filter. The field data are filtered with the matched filter to achieve the desired data enhancement.



The Fourier Transform--Linear transforms, especially those named for Fourier and Laplace, provide techniques for solving problems in linear systems. Fourier transforms play an important part in the theory of many branches of science. They have both a pure mathematical and a physical basis of meaning. For example, a waveform--optical, electrical or acoustical--and its spectrum are physically picturable and measurable entities and are Fourier transforms of each other.. An oscilloscope enables us to see an electrical waveform; a spectroscope or spectrum analyzer enables us to see optical or electrical spectra. The acoustical appreciation is even more direct, for the ear hears spectra.

The standard formulas for the Fourier transform pair are given by Bracewell.* They are

$$\left. \begin{aligned} F(s) &= \int_{-\infty}^{\infty} f(x) e^{-i2\pi xs} dx \\ f(x) &= \int_{-\infty}^{\infty} F(s) e^{i2\pi xs} ds \end{aligned} \right\}$$

Letting $s=f$ = frequency, $x=t$ =time, $\omega=2\pi f$; or $s=u$ =wave number, and x = distance the transform pair becomes the familiar formulas

Frequency Domain	$S(f) = \int_{-\infty}^{\infty} f(t) e^{-i\omega t} dt$	$\left. \begin{array}{l} \text{Wave number} \\ \text{Domain} \end{array} \right\}$	$S(u) = \int_{-\infty}^{\infty} f(x) e^{-iux} dx$
Time Domain	$G(t) = \int_{-\infty}^{\infty} S(f) e^{i\omega t} df$		$\left. \begin{array}{l} \text{Spatial} \\ \text{Domain} \end{array} \right\}$

*Bracewell, R., 1965, The Fourier Transform and Its Applications, McGraw-Hill, Inc., New York, New York.

Two other formula systems are also commonly used; they give the same result, except for a constant. They are

$$\left. \begin{aligned} F(s) &= \int_{-\infty}^{\infty} f(x) e^{-ixs} dx \\ F(x) &= \frac{1}{2\pi} \int_{-\infty}^{\infty} F(s) e^{ixs} ds \end{aligned} \right\}$$

and

$$\left. \begin{aligned} F(s) &= \frac{1}{2\pi} \int_{-\infty}^{\infty} f(x) e^{-ixs} dx \\ f(x) &= \frac{1}{2\pi} \int_{-\infty}^{\infty} F(s) e^{ixs} ds \end{aligned} \right\}$$

The formula for $S(f)$ can be written in the polar form

$$S(f) = |S(f)| e^{i\phi(f)}$$

where

$|S(f)|$ is the amplitude spectrum and $\phi(f)$ is the phase

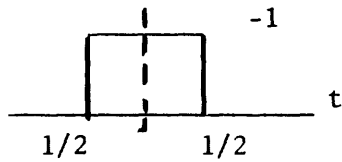
spectrum.

For example, if

$$S(f) = \sin \omega t_0 e^{i \frac{\pi}{2}}$$

$|S(f)|$, the amplitude spectrum, is $|\sin \omega t_0|$ and $\phi(f)$, the phase spectrum,

is $\frac{\pi}{2}$.

Example--Transform of the rectangular pulse

$$G(t) = 1 \quad |t| < 1/2$$

$$= 0 \quad |t| > 1/2$$

$$\begin{aligned} S(f) &= \int_{-\infty}^{\infty} G(t) e^{-i\omega t} dt \\ &= \int_{-1/2}^{1/2} \cos \omega t dt - i \int_{-1/2}^{1/2} \sin \omega t dt \end{aligned}$$

$$= \frac{1}{\omega} \sin \omega t \bigg|_{t=-1/2}^{t=1/2} + \frac{i}{\omega} \cos \omega t \bigg|_{t=-1/2}^{t=1/2}$$

$$= \frac{1}{\omega} \left[2 \sin \frac{\omega}{2} + 0 \right]$$

$$= \frac{\sin \frac{\omega}{2}}{\frac{\omega}{2}} = \frac{\sin \pi f}{\pi f}, \text{ an even function}$$

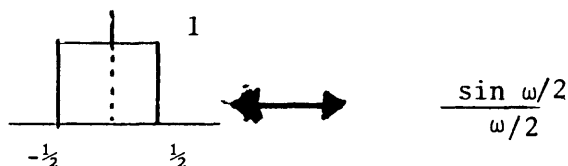
$$\text{The amplitude spectrum} = \left| \frac{\sin \pi f}{\pi f} \right|$$

$$\text{and the phase spectrum} = 0$$

Basic Fourier Transform Pairs--The following transform rules are frequently used in geophysical data analyses.

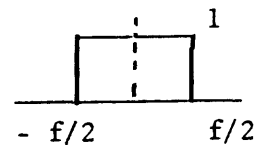
<u>Name</u>	<u>Wave form</u>		<u>Spectrum</u>
1. Basic pair	$G(t)$	\longleftrightarrow	$S(f)$
2. Multiplication by a constant	$KG(t)$	\longleftrightarrow	$KS(f)$
3. Superposition	$G_1(t) + G_2(t)$	\longleftrightarrow	$S_1(f) + S_2(f)$
4. Shift in time	$G(t - t_0)$	\longleftrightarrow	$e^{-i\omega t_0} S(f)$
5. Scaling; reciprocal spreading	$G(Kt)$	\longleftrightarrow	$\frac{1}{K} S(f/K)$
6. Convolution in time domain	$G_1(t) * G_2(t)$	\longleftrightarrow	$S_1(f) \cdot S_2(f)$
7. Truncating in time domain	$G_1(t) \cdot G_2(t)$	\longleftrightarrow	$S_1(f) * S_2(f)$
8. Autocorrelation in time domain	$G_1(t) \otimes G_1(t)$	\longleftrightarrow	$S_1(f) \cdot S_2^*(f)$
9. Cross correlation in time domain	$G_1(t) \otimes G_2(t)$	\longleftrightarrow	$S_1(f) \cdot S_2^*(f)$
10. Differentiation	$G'(t)$	\longleftrightarrow	$2\pi i f S(f)$
11. Higher order differentiation	$G^n(t)$	\longleftrightarrow	$(2\pi i f)^n S(f)$
12. Unit impulse function at $t=0$	$\delta(t)$	\longleftrightarrow	1
13. Unit impulse function at $t=t_0$	$\delta(t - t_0)$	\longleftrightarrow	$e^{-i\omega t_0}$

14. Rectangular pulse



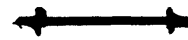
15. Ideal low-pass filtering

$$\frac{\sin \pi t}{\pi t}$$



16. Cosine wave

$$\cos 2\pi f_0 t$$



$$\frac{1}{2} [\delta(f+f_0) + \delta(f-f_0)]$$

17. Gaussian

$$e^{-\pi t^2}$$



$$e^{-\pi f^2}$$

18. Unit step function

$$U(t)$$



$$\frac{1}{i\omega}$$

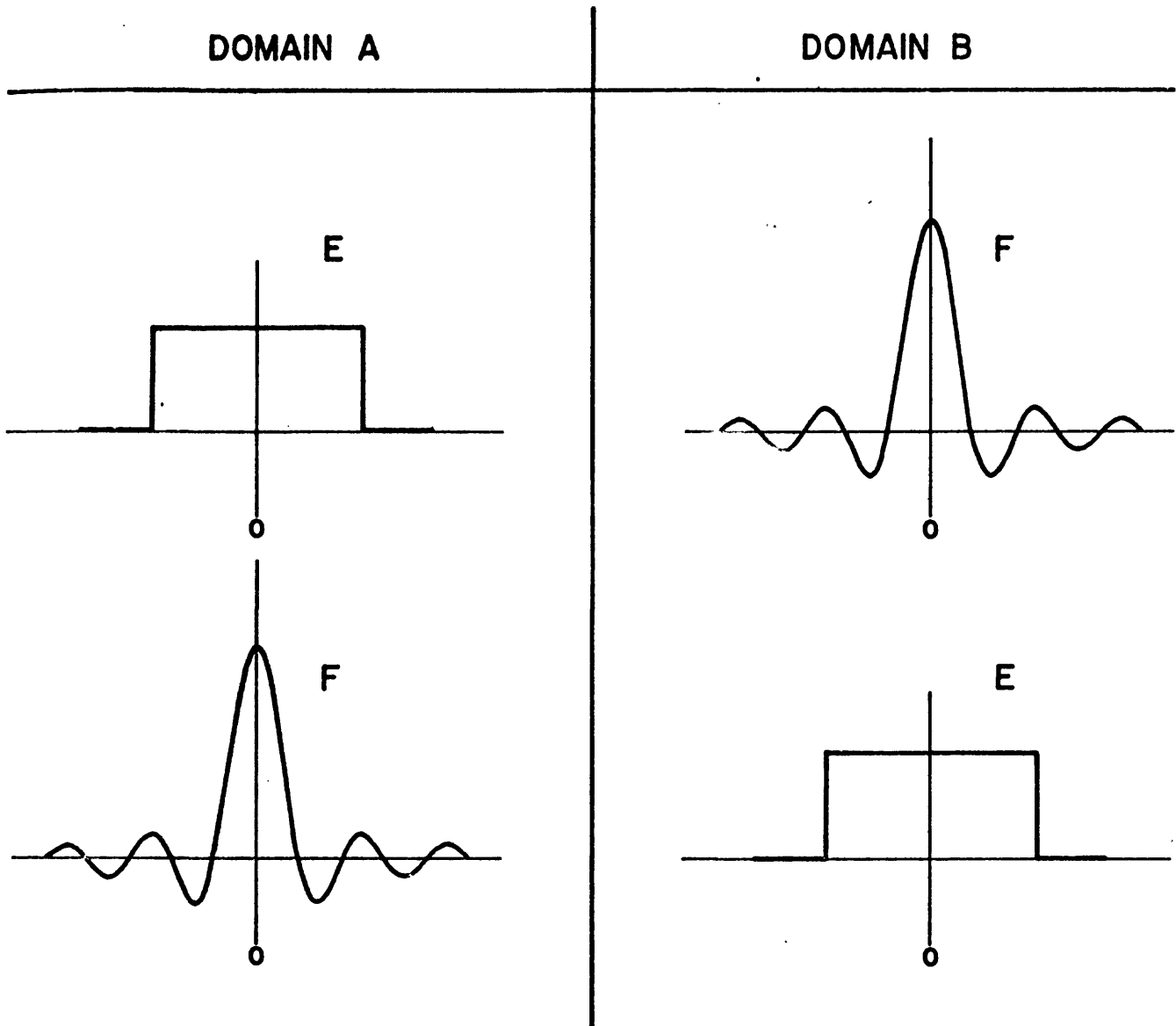
19. Ramp function

$$tU(t)$$



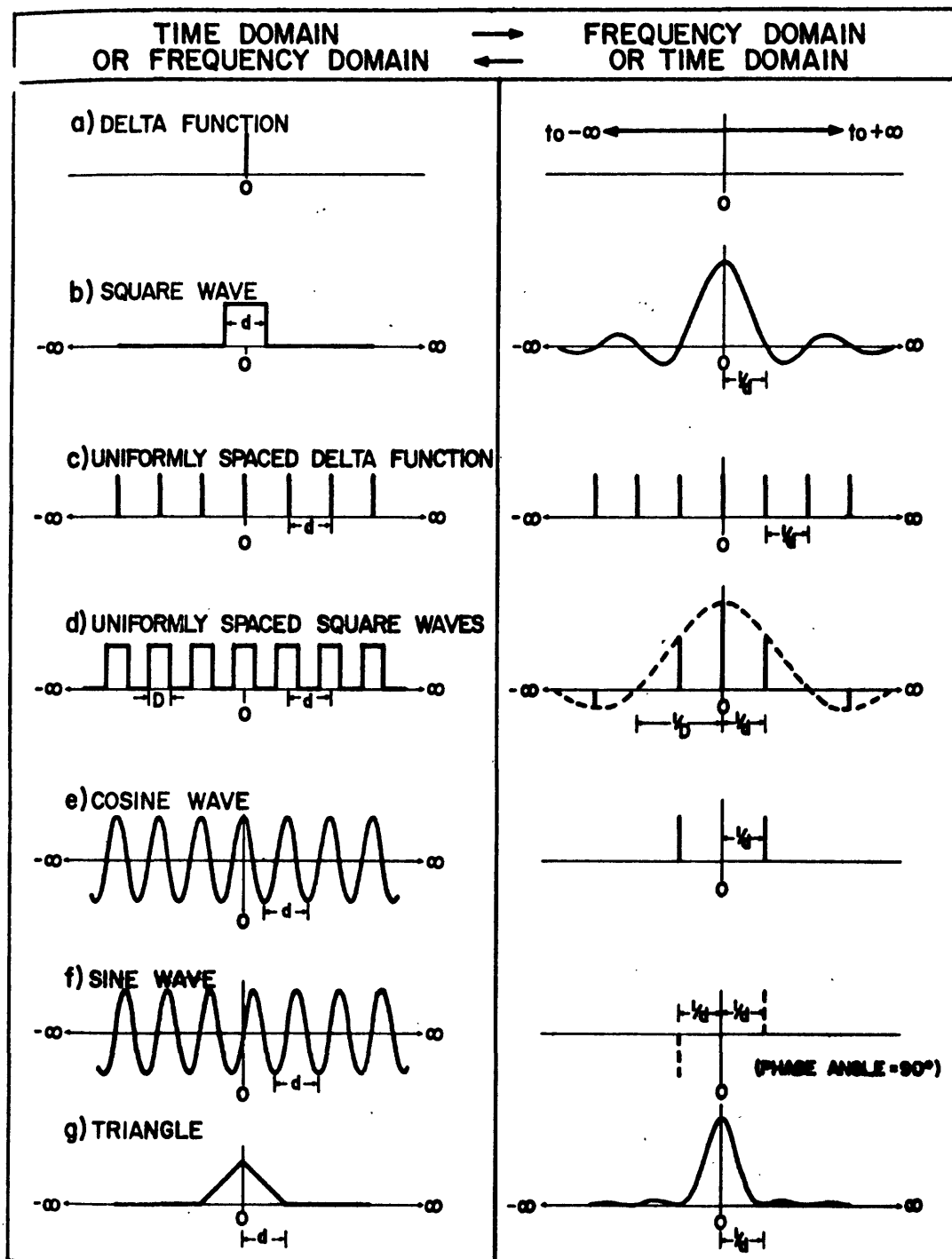
$$-\frac{1}{\omega^2}$$

NOTE: For gravity data, the variables u (wave number) would be substituted for f (frequency) and x (distance) for t (time) in each of the above rules and in the illustrations which follow. The rules are still applicable.

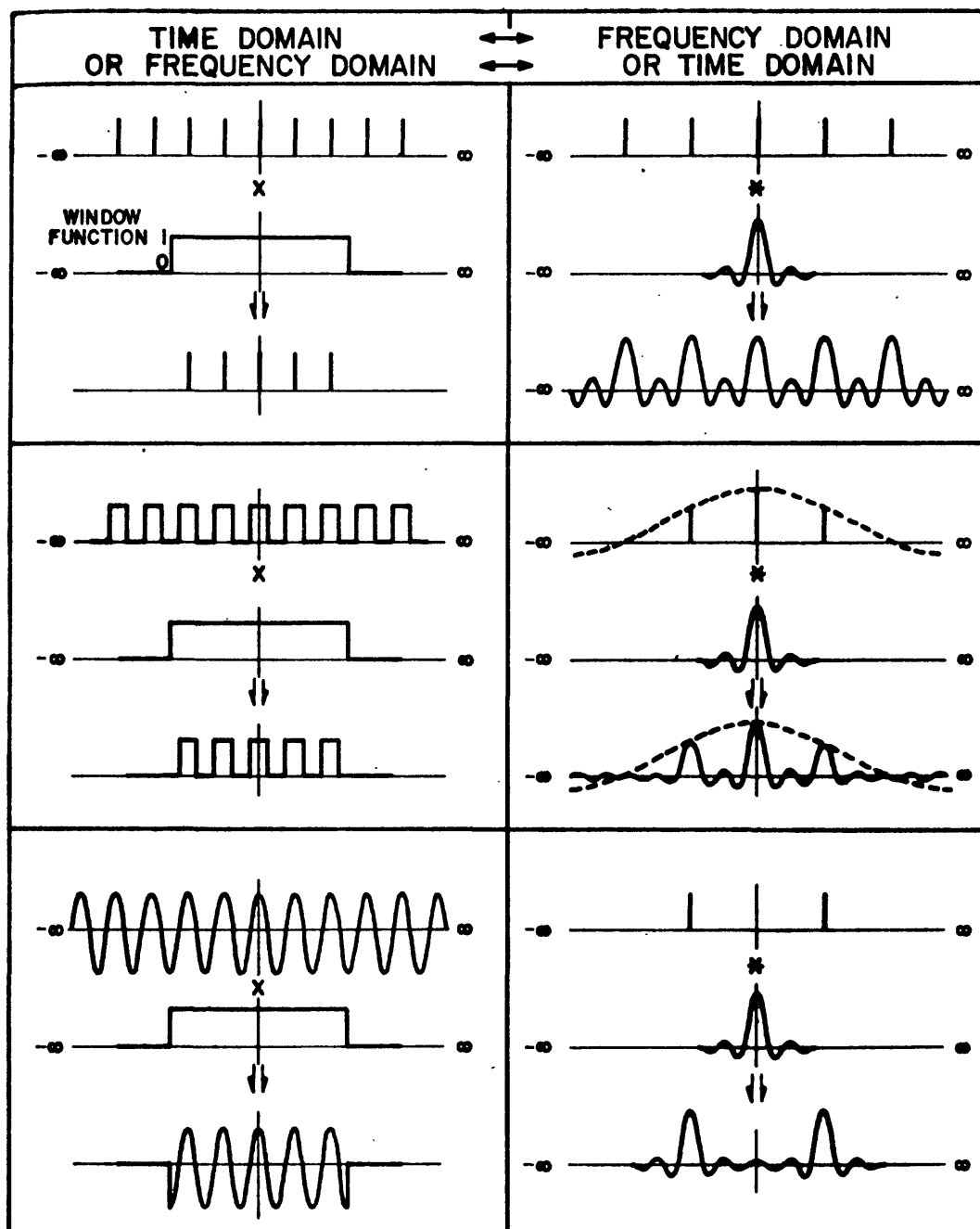


IF DOMAIN A IS TIME, DOMAIN B IS FREQUENCY
IF DOMAIN A IS FREQUENCY, DOMAIN B IS TIME

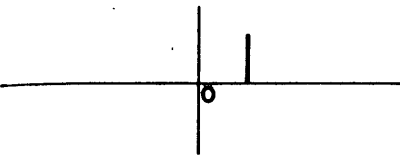
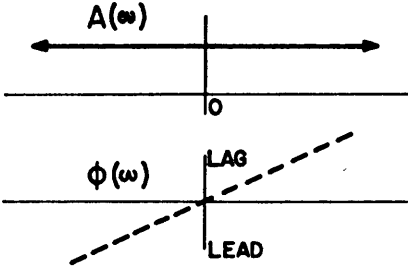
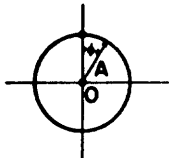
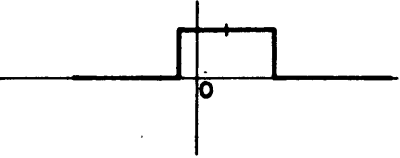
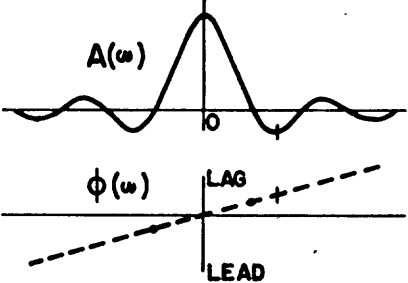
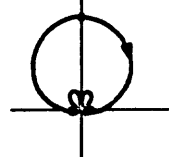
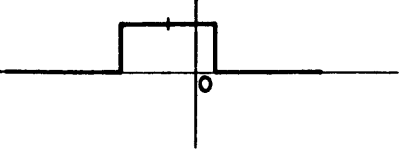
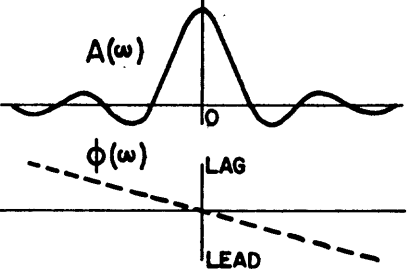
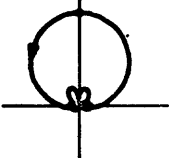
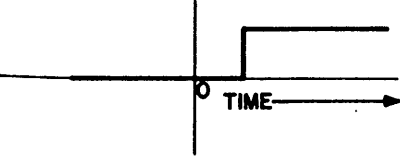
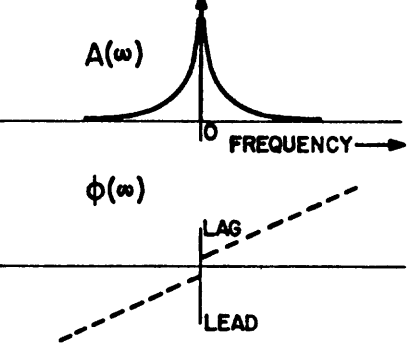
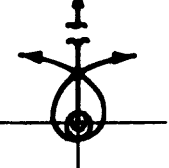
COSINE TRANSFORM PAIRS



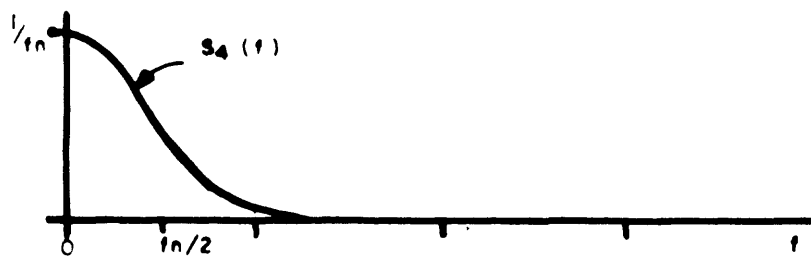
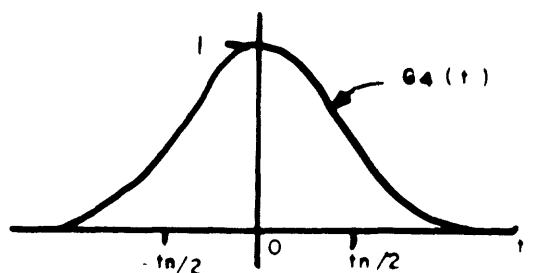
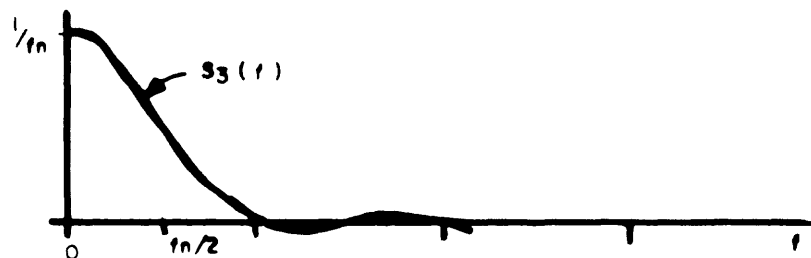
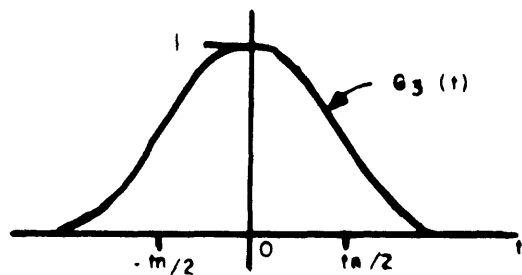
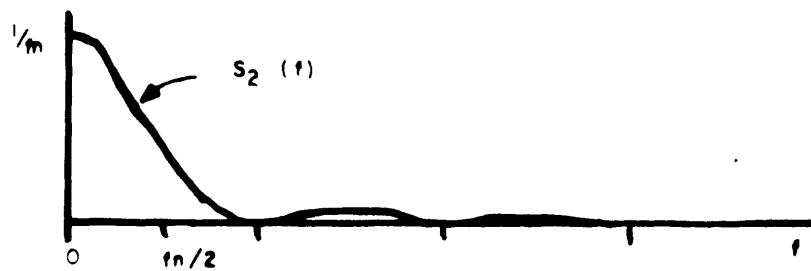
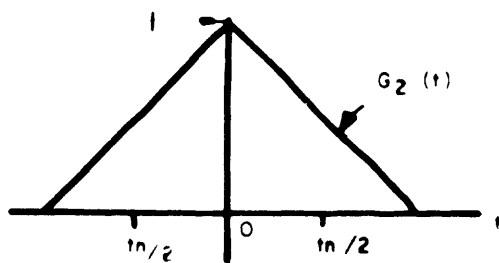
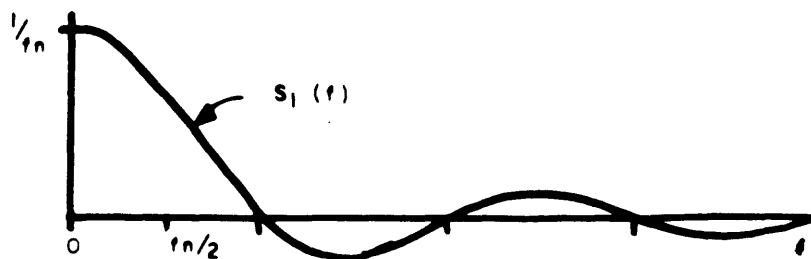
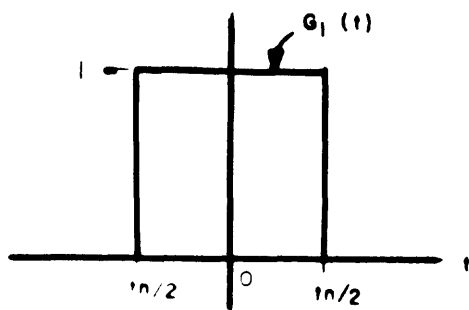
FOURIER TRANSFORM PAIRS
FOR TYPICAL SIGNALS



FOURIER TRANSFORMS OF TRUNCATED FUNCTIONS

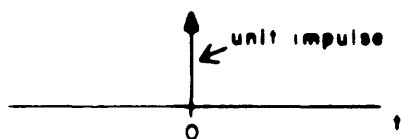
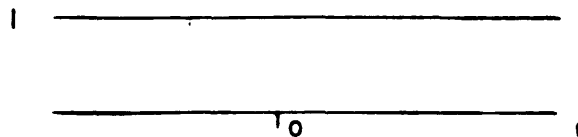
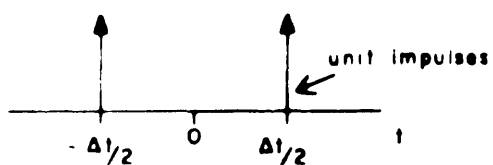
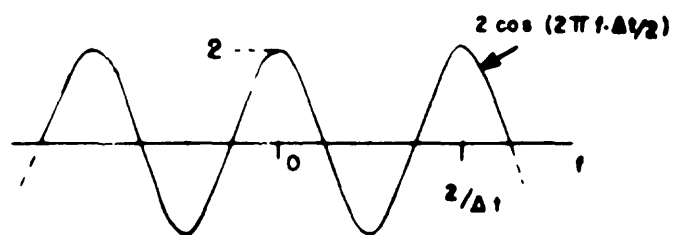
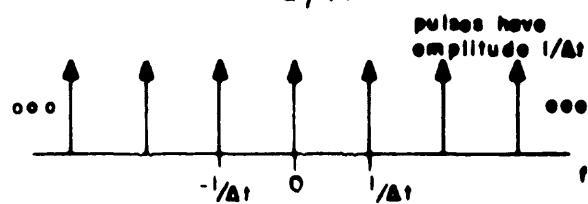
TIME DOMAIN TIME PLOT	FREQUENCY DOMAIN	
	AMPLITUDE AND PHASE SPECTRA	LOCUS PLOT
		
		
		
		

TIME SHIFTED FUNCTIONS



$$t_n = 1/f_n$$

FOURIER TRANSFORMS OF SOME SIMPLE
SYMMETRICAL WAVEFORMS

$G_5(t)$  $S_5(f)$  $G_6(t)$  $S_6(f)$  $G_7(t)$  $S_7(f)$ 

FOURIER TRANSFORMS OF CERTAIN IMPULSIVE WAVEFORMS

Fourier transforms of correlation functions

$$C_{12}(t) = \phi_{12}(\gamma) = \frac{1}{T_2 - T_1} \int_{T_1}^{T_2} G_1(t) * G_2(t+\gamma) dt$$

is the formula for cross correlation.

Alternately, we can write

$$C_{12}(t) = G_1(-t) * G_2(t) ,$$

but the operation of convolution in the time domain is equivalent to multiplication of the individual transforms in the frequency domain.

Thus

$$\begin{aligned} C_{12}(f) &= |S_1(f)| e^{i(-\phi(f))} \cdot |S_2(f)| e^{i\phi(f)} \\ &= A_1(f) \cdot A_2(f) e^{i[\phi_2(f) - \phi_1(f)]} \end{aligned}$$

Thus, the amplitude spectrum of the cross correlation function is the product of the amplitude spectra of each function correlated and the phase spectrum is the difference of the individual phase spectra. Frequencies common to both time functions appear in the amplitude spectrum; whereas, the phase spectrum contains the phase differences.

When we are autocorrelating, $A_1 = A_2$ and $\phi_1 = \phi_2$. So

$$\begin{aligned} C_{11}(f) &= A_1^2(f) e^{i\phi_1(f) - \phi_1(f)} \\ &= A_1^2(f) , \text{ the power spectrum} \end{aligned}$$

Thus, the amplitude spectrum of the autocorrelation function is the power spectrum. The phase spectrum is zero. The autocorrelation function does not contain enough information to reconstitute the original wave form. Two different functions can have the same autocorrelation. The dominant frequency of the autocorrelation is the same as the dominant frequency of the wave form

To determine the power spectrum of a wave form, one can proceed as follows:

1. perform the autocorrelation, $G_1(t) \otimes G_1(t)$
2. take the transform of the autocorrelation function which yields $A^2(f)$.

APPENDIX D

DMAAC Technical Paper No. 73-002

A BOUGUER GRAVITY ANOMALY MAP
OF SOUTH AMERICA

Gerald L. Breville
Charles W. Beierle
Joseph R. Sanders
James T. Voss
Luman E. Wilcox

December 1973

Defense Mapping Agency
Aerospace Center
St. Louis AFS, Missouri 63118

NOTICES

This report is issued to present to organizations and individuals the first mean Bouguer anomaly map of the entire South American continent based wholly upon terrestrial data. It is the paper presented by Mr. Gerald L. Breville of the Gravity Correlation Branch, Research Department, at the 43rd Annual International Meeting of the Society of Exploration Geophysicists held in Mexico City, Mexico on October 25, 1973. Nothing herein is to be construed as Defense Mapping Agency doctrine.

This publication does not contain information or material of a copyrighted nature, nor is a copyright pending on any portion thereof. Reproduction in whole or in part is permitted for any purpose of the United States Government.

ACKNOWLEDGEMENTS

The authors thank Messrs. Gene Woodford, Walter Czarnecki, and Charles Shaw for their valuable assistance in programming techniques and plotter utilization. Thanks also goes to Messrs. Walter Rothermel and Rolf Slettene whose help in the data computations made this map possible.

ABSTRACT

The Bouguer Anomaly Map of South America is a contoured representation of $1^{\circ} \times 1^{\circ}$ mean Bouguer gravity anomaly values. Some of these mean anomaly values are computed directly using observed gravity data held by the DOD Gravity Library. Other means are predicted values involving the application of geophysical-gravity correlation techniques. These geophysical prediction methods are discussed in relation to selected geological and tectonic provinces of South America. The map itself was prepared exclusively by automated map compilation techniques.

CONTENTS

	<u>Page</u>
NOTICES	i
ACKNOWLEDGEMENTS	ii
ABSTRACT	iii
INTRODUCTION	1
DEFINITIONS	1
METHODS USED TO PREDICT $1^{\circ} \times 1^{\circ}$ MEAN BOUGUER ANOMALIES	2
1. NORMAL GRAVITY ANOMALY PREDICTION (NOGAP)	2
2. UNREDUCED GRAVITY ANOMALY PREDICTION METHOD (UNGAP)	6
3. THE EXTENDED GRAVITY ANOMALY PREDICTION METHOD (EXGAP)	8
GEOLOGIC AND TECTONIC CHARACTERISTICS OF SOUTH AMERICA	8
1. THE ANDEAN CORDILLERA COMPLEX	9
2. THE SOUTH AMERICAN PLATFORM	9
3. PLATE TECTONIC INFORMATION	10
DISCUSSION AND CONCLUSIONS	12
APPENDIX A. MAP PARAMETERS, AUTOMATED EQUIPMENT, AND COMPUTER PROGRAMS	14
APPENDIX B. TECTONIC REGIONS AND PARA-PLATFORMS	15
LEGEND	16
APPENDIX C. GRAVITY FORMULA FOR THE 1967 GEODETIC REFERENCE SYSTEM (GFGRS67)	17
APPENDIX D. GFGRS 1967 CORRECTION GRAPH	19
REFERENCES	20
BOUGUER ANOMALY MAP OF SOUTH AMERICA	Inside Back Cover

A BOUGUER GRAVITY ANOMALY MAP OF SOUTH AMERICA

INTRODUCTION

The Bouguer Anomaly Map of South America is a contoured representation of 1° x 1° mean Bouguer gravity anomalies for the South American continent. These Bouguer anomalies were predicted using observed gravity data holdings of the Department of Defense Gravity Library in conjunction with gravity correlation techniques. The entire map - contours, continental outline, geographic graticule, and boundary information - was computer generated and drawn by automatic plotting equipment. A list of the map parameters, equipment and Fortran V programs used for the final map is given in Appendix A.

DEFINITIONS

The general formula to describe the mean Bouguer anomaly as it is used in this paper is as follows:

$$\overline{\Delta g_f} = \overline{g_0} + .3086\overline{h} - \gamma_{1967}$$

$$\overline{\Delta g_B} = \overline{\Delta g_f} - .1119\overline{h}$$

where

$\overline{\Delta g_f}$ = mean free air anomaly

$\overline{g_0}$ = mean observed gravity

$.3086\overline{h}$ = vertical gradient of gravity - reduces observed data to
sea level (geoid)

γ_{1967} = normal gravity at center of $1^\circ \times 1^\circ$

$.1119\bar{h}$ = mass correction = $2\pi K\sigma\bar{h}$, K is the universal gravitational constant, and σ is the density 2.67 gm/cm^3

\bar{h} = mean elevation in meters

$\bar{\Delta g_B}$ = mean Bouguer anomaly

The entire gravity holdings of the DOD Gravity Library have been adjusted to the 1971 International Gravity Standardization Net (IGSN 71). Normal gravity was computed using the gravity formula for the 1967 Geodetic Reference System (GFGRS 67), Appendix C.

METHODS USED TO PREDICT $1^\circ \times 1^\circ$ MEAN BOUGUER ANOMALIES

In general, when observed data is abundant for any given area, statistical prediction and data averaging methods are used to determine mean Bouguer anomalies. These methods are well-known and described elsewhere. When gravity data is lacking or available in smaller quantities, gravity correlation methods are applied. Three gravity correlation methods were used for South America. They are:

- (1) The normal gravity anomaly prediction method (NOGAP)
- (2) The unreduced gravity anomaly prediction method (UNGAP)
- (3) The extended gravity anomaly prediction method (EXGAP)

1. Normal Gravity Anomaly Prediction (NOGAP)

The basic formula of the NOGAP method as used for the South American continent is

$$\bar{\Delta g_B} = BP + TEC + \Delta g_L$$

The Basic Predictor (BP) can be visualized as the equation of the straight line which best fits a plot of mean elevations vs. mean Bouguer anomalies. A single relation of this type is often adequate to describe the regional part of the mean Bouguer anomaly field within a given geologic/tectonic province. The Basic Predictors used for the South America predictions were determined using a least squares solution in the areas of each province where good observed gravity data coverage is available. The Basic Predictors were then applied to predict the regional part of Bouguer gravity within the portions of each province where no observed data exists.

The Basic Predictor is given by the slope-intercept form of the straight line equation

$$\overline{\Delta g_B} = \beta \bar{h} + \alpha$$

Where, by least squares,

$$\beta = \text{SLOPE} = \frac{\sum (gh) - \frac{\sum g \sum h}{n}}{\sum h^2 - \frac{\sum h \sum h}{n}}$$

$$\alpha = \text{INTERCEPT} = \frac{\sum g}{n} - \frac{\sum h}{n} \beta$$

$g = \overline{\Delta g_B}$, from observed data, $h = 1^\circ \times 1^\circ$ mean elevation or $3^\circ \times 3^\circ$

mean elevation, n = number points

The Terrain Effects Correction (TEC) as it was applied in South America is of the form

TEC = -13 (ODM - ME) for elevation under 1500 meters

TEC = -20 (ODM - ME) for elevation over 1500 meters

This TEC is necessary when $3^\circ \times 3^\circ$ mean elevations are used to establish a BP. The TEC adjusts the anomaly to the desired $1^\circ \times 1^\circ$ height. The constants -13 and -20 were arrived at empirically. The ODM is the $1^\circ \times 1^\circ$ mean elevation and the ME is the weighted $3^\circ \times 3^\circ$

In determining the Local Geologic Correction (Δg_L), which expresses local variations in Bouguer gravity due to structural variations within a $1^\circ \times 1^\circ$ area, two methods are available: The Empirical Estimation method and the Analytical method. The Empirical Estimation method uses a table established by Strange and Woollard, 1964, Woollard and Strange, 1966, and Wilcox, 1968, which describes pertinent geological situations and recommends appropriate local geologic correction values. This method gives a first approximation of the Δg_L . The following are examples:

GRANITES, INTRUSIVES, VOLCANISM

Δg_L CORRECTION IN MILLIGALS

Large Granitic Batholith.....	-50
Ultrabasic Intrusives.....	+20
Tertiary Extrusions.....	-10

SEDIMENT FILLED DEPRESSIONS (BASINS)

Most Small to Medium Sized Basins	
Containing 10,000 Feet or More	
of Cenezoic or Cretaceous Sediments.....	-20
Large Geosynclinal Type Basins	
Containing 20,000 Feet or More of	
Cenezoic Clastic Sediments.....	-20
Abnormal Basins Superimposed on	
Shield Areas.....	+25

FAULT BOUNDED DOWNWARPS

Major Graben	
Intermountain.....	-40
Not in Mountains.....	-100
Minor Graben.....	-20

MISCELLANEOUS STRUCTURES Δg_L CORRECTION IN MILLIGALS

Folded Mountain Ranges

Mesozoic or Younger..... -10

These first approximations are adjusted considering such factors as lateral extent and depth of structure in order to obtain a final Δg_L prediction for each $1^\circ \times 1^\circ$ area.

The analytical method in which appropriate attraction formulas are applied to compute the local geologic correction, is used when two conditions are satisfied:

a. The Δg_L is produced primarily by density contrast in the near surface geology and not by local crustal or isostatic conditions.

b. The size, shape, depth, and density contrast of the local geologic structures producing the Δg_L can be determined.

Examples of structures which usually produce a Δg_L by near surface density contrast include (Wilcox, 1968):

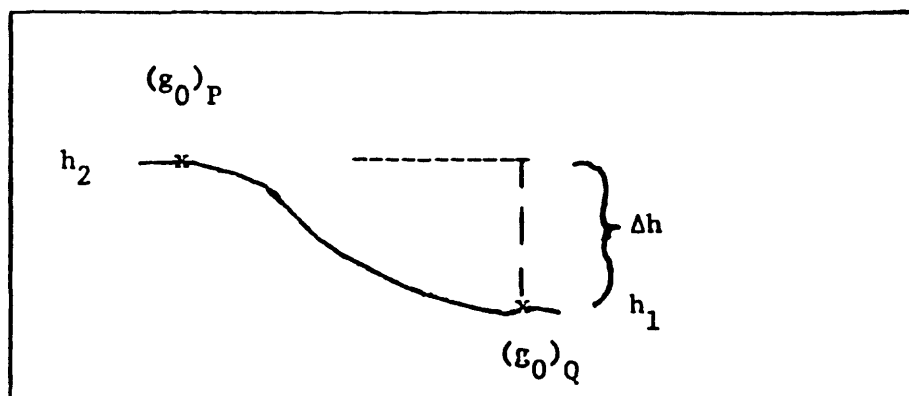
- (1) Most small to medium sediment filled depressions (basins).
- (2) Igneous intrusions.
- (3) Granites.
- (4) Igneous extrusions.

Examples of structures which do not produce a Δg_L by near surface density contrasts include:

- (1) Large geosynclinal type basins.
- (2) Major horst and graben.
- (3) Abnormal basins.
- (4) Folded mountain ranges

2. Unreduced Gravity Anomaly Prediction Method (UNGAP)

In this method, the unreduced vertical gradient of observed gravity data is defined for each geologic/tectonic province. (The accepted theoretical vertical gradient of gravity, $.3086\bar{h}$, is applied in free space above the ground level and should not be confused with the unreduced vertical gradient of gravity.) The procedure is generally described using the following illustration:



PROBLEM: We know the observed gravity, $(g_0)_Q$, and wish to predict the observed gravity, $(g_0)_P$.

The procedure is based upon the following theoretical formulas:

$$(g_0)_P = (g_0)_Q - .3086 \Delta h + .1119 \Delta h - .0316 \Delta h$$

or

$$(g_0)_P = (g_0)_Q - .2283 \Delta h$$

where

$(g_0)_Q$ = known observed gravity

$.3086 \Delta h$ = reduces h_1 to h_2 in free air

.1119 Δh = mass correction for Bouguer plate

.0316 Δh = average terrain correction for points, derived by Voss, 1972.

The empirical testing of 68 individual geologic/tectonic settings in North America and Europe showed that the actual unreduced vertical gradient of observed data with respect to the geoid ranges from approximately .1500 Δh to approximately .4500 Δh , but has an average value close to the theoretical value of 0.2283 Δh . (Voss, 1972)

The empirically derived gradients for South America are as follows:

ANDEAN CORDILLERA COMPLEX

.2960 $\Delta \bar{h}$ for elevations up to 2500 meters

.2433 $\Delta \bar{h}$ for elevations over 2500 meters

SOUTH AMERICAN PLATFORM

Guyana Para-Platform .2100 $\Delta \bar{h}$

Brazilian Para-Platform .2193 $\Delta \bar{h}$

Argentine Para-Platform .2947 $\Delta \bar{h}$

The UNGAP method is applied to obtain $1^\circ \times 1^\circ$ mean values in the following manner: Point observed gravity data is plotted versus point elevation for each latitude band in a geologic/tectonic region. These linear regression lines are then merged to arrive at a mean regression line; the slope of this regression line is the actual mean unreduced vertical gradient of observed data for a geologic/tectonic region.

The mean elevation is then used to determine the predicted mean observed gravity \bar{g}_0 .

The predicted \bar{g}_0 is used in the following equation:

$$\bar{\Delta g}_f = \bar{g}_0 + .3086 \bar{h} - \gamma_{1967}$$

$$\bar{\Delta g}_b = \bar{\Delta g}_f - .1119 \bar{h}$$

3. The Extended Gravity Anomaly Prediction Method (EXGAP)

In general, the method makes effective use of one or two gravity measurements within a $1^\circ \times 1^\circ$ area. The EXGAP predictions take the form:

$$\bar{\Delta g}_B = [\Delta g_B - lgc] - \beta [h - ODM]$$

where

$\bar{\Delta g}_B$ = predicted $1^\circ \times 1^\circ$ mean Bouguer anomaly

Δg_B = observed Bouguer anomaly at any point within the $1^\circ \times 1^\circ$

area

$lgc = \Delta g_L$ at the point where Δg_B is observed

$ODM = 1^\circ \times 1^\circ$ mean elevation

h = elevation at the point where Δg_B is observed

β = slope constant of NOGAP Basic Predictor

The NOGAP and EXGAP methods are explained in detail in, "Summary Of Gravity Correlation Methods For Prediction Of $1^\circ \times 1^\circ$ Mean Free Air Anomalies," by Luman E. Wilcox, January 1968, which is currently under revision and will be available early 1974.

GEOLOGIC AND TECTONIC CHARACTERISTICS OF SOUTH AMERICA

For the purpose of this paper, the South American continent is divided into two general first order provinces -- the Andean Cordillera Complex and the South American Platform.

1. The Andean Cordillera Complex

The delineation of the Andean Cordillera Complex, as shown in Appendix B, is in general agreement with Morrison, 1962. A finer subdivision of this geologic province is given by Childs and Beebe, 1963. This Complex, running the full length of the continent, has undergone extremes of periodic deformation, sedimentation, and volcanism starting in late Cambrian and continuing to the present.

2. The South American Platform

The South American Platform has been defined by many authors as a single enormous cratonic realm undergoing only epeirogenic movements. By analysis of the Bouguer anomaly field, we have further subdivided this vast area into: (1) The Guyana Para-Platform, (2) The Brazilian Para-Platform, and (3) The Argentine Para-Platform. The folded basements of these three Para-Platforms are considered to have been cratonized throughout successive Pre-Phanerozoic cratonization stages (Ferreira, 1972) with ages ranging from 900 - 2,600 million years. These ancient Platforms are partially overlain by extensive sedimentary covers ranging in age from Pre-Cambrian to Cenozoic.

Two of the three Para-Platforms are defined by a unique NOGAP Basic Predictor equation:

- | | |
|----------------------------|-----------------------------|
| a. Guyana Para-Platform | $BP = -.088\bar{h} - 2.513$ |
| b. Brazilian Para-Platform | $BP = -.131\bar{h} - 3.769$ |

where

\bar{h} = slope

\bar{h} = mean elevation

α = intercept

A usable Basic Predictor for the Argentine Para-Platform could not be determined.

In the transition areas between the Para-Platforms, such as the Amazon Trough, the pertinent Basic Predictors were averaged and then applied. In practice, the value falling between the two regression lines was read direct.

Local geologic corrections were determined with reference to the local tectonic regions delineated in Appendix B.

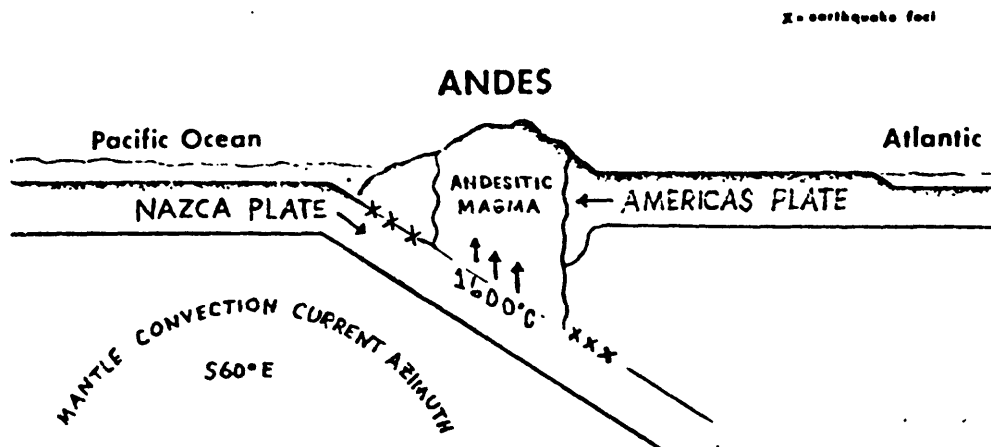
Depth to basement information, such as that shown by Ferreira, 1972, was utilized to establish local corrections for basin structures. Where such information is lacking, an approximation of the depth was made.

Many authors have reported that most of the sedimentary basins of South America are impregnated with massive diabase dikes and sills. Such structures can have a pronounced effect on the local gravity field. The gravitational effects of these structures was considered in determining local corrections for those $1^\circ \times 1^\circ$ areas where these structures are known to exist.

3. Plate-Tectonic Information

Many papers have been written and ideas presented concerning plate tectonics and the various driving forces affecting the plates. For example, an article by D. I. Gough, 1973, presents a very interesting and logical explanation for an uplift mechanism of the Andean Cordillera Complex. The addition of a mantle convection current with an azimuth

of approximately S 60° E as a driving force for the Pacific Ocean Plates further enhances the theory. The general concept is illustrated by the following figure:



An interesting observation is that rising contamination of the vertical column beneath the Andes by the Andesitic Magma from the subducted Lithospheric Plate can account partially for the crustal compensation of the Andes. Also, the contamination of the column cannot be expected to be homogeneous, but occurring in various degrees of contamination, thus causing varying densities within the column. The changes in density should be reflected in the Bouguer anomalies.

Another aspect of these plate movements is that the South American continent, which is riding on the Americas Plate, may be overriding the trench. This aspect lends itself to many diverse opinions of mechanisms that move continents such as: If the Andean uplift is caused by compressional forces exerted against the Pacific Plates, then the continental crust (approximately 32 km. thick) east of the Andes must have rigidity to exert such pressure. If this hypothesis is correct then,

in actuality, the continent may not in the true sense be overriding the existing trench, but constantly creating a new trench as the continent moves along. A combination of all these forces may account for the Andean uplift.

DISCUSSION AND CONCLUSIONS

A pronounced negative zone in the Bouguer anomaly field of South America delineates the Andean Cordillera Complex. This negative area also represents the region where the most apparent present day dynamic tectonics are taking place. The largest Bouguer gravity negative values suggest that the mountain root extends to about 67 kilometers beneath the Andean mountains. If we include the theory of non-homogeneous Andesitic contamination beneath the Andes, the extreme gravity lows may also represent a deep seated change in density contrast due to Andesitic Magma generated at a depth of about 140 kilometers (Gough, 1973).

The South American Platform, as previously stated, has been considered to have been cratonized during the Pre-Cambrian. The regional Bouguer anomaly field appears to be related to this scheme of Pre-Cambrian tectonics. In fact, the regional Bouguer field may represent the roots of ancient mountain ranges that existed in the Pre-Phanerazoic.

When dealing with geophysical prediction techniques, the researcher always starts with some known information, establishes a hypothesis and applies what information is available for a gravity deficient area to arrive at a logical estimation of the gravity field.

The question of accuracy is always raised. Past studies of predicted gravity values evaluated against observed data at a later date has shown that the predicted data agrees to within 9 to 15 milligals (Wilcox, et al, 1972) of the observed data.

Three gravity correlation prediction techniques were used for the continent of South America. A comparison of these methods over the same area revealed that their separately derived values did not differ from each other by more than 5 milligals when a Basic Predictor could be determined for the NOGAP method. This was true for the Guyana Para-Platform and the Brazilian Para-Platform. The Argentine Para-Platform and the Andean Cordillera Complex posed many problems in establishing a solid prediction method. The UNGAP method proved itself to be very dependable in these provinces and the values derived by this method were used exclusively.

The Bouguer Anomaly Map of South America will be continually updated and revised as more data becomes available. Comments and discussions are invited and appreciated.

APPENDIX A'

MAP PARAMETER, AUTOMATED EQUIPMENT, AND COMPUTER PROGRAMS

MAP PARAMETERS

1. Projection: Mercator
2. Graticule: 5° x 5°
3. Scale: 1:20,000,000

AUTOMATED EQUIPMENT

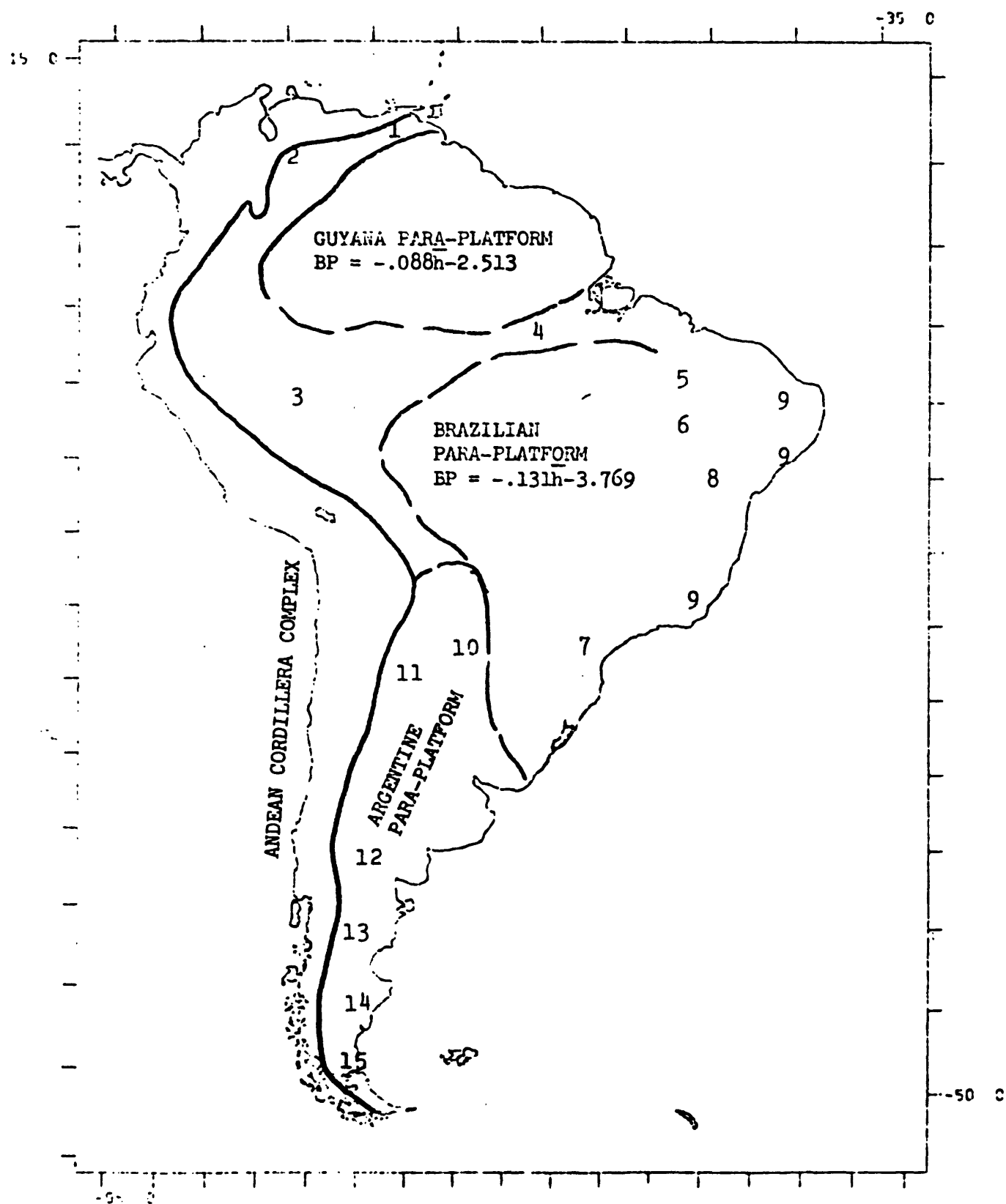
1. NCR 735 Magnetic Tape Encoder
2. IBM 1401 Computer (Converts tape from NCR 735 to tape from UNIVAC 1108)
3. UNIVAC 1108 Computer (Generates plot tape for CALCOMP Plotter)
4. CALCOMP Flatbed Plotter

FORTRAN V COMPUTER PROGRAMS

1. Automated Digitization Program - Uses data output from automated Large Area Record Reader (LARR) for portrayal of continental and political boundaries at various projections and scales.
2. Automated Plot Program - Combines IBM 1401 data, automated digitization, and labeling information into a single run of the CALCOMP Flatbed Plotter for the final map.

TECTONIC REGIONS AND PARA-PLATFORMS

LEGEND (PAGE 16)



LEGEND

1. East Venezuelan Basin
2. Barinas-Apure Basin and Llanos Basin
3. Upper Amazon Basin
4. Amazon Trough
5. Maranhao Basin
6. Sao Francisco Basin
7. Parana Basin
8. Salitre Basin
9. Brazilian Coastal Ranges
10. Pampean Basin
11. Pampean Ranges
12. Rio Colorado and Neuguén Basins
13. Chubut Masiff
14. Deseado Masiff
15. Magellan Basin

APPENDIX C

GRAVITY FORMULA FOR THE
1967 GEODETIC REFERENCE SYSTEM (GFGRS67)

The following data has been extracted from special publication #3
"Geodetic Reference System 1967" published by the Central Bureau of
the International Association of Geodesy 1971.

$$\text{GFGRS67} = \gamma = 978.03185 (1 + 0.005278895 \sin^2 \phi + 0.000023462 \sin^4 \phi) \text{ Gal}$$

GEOMETRIC CONSTANTS

$a = 6\,378\,160\text{m}$ (exact)	Semimajor Axis
$b = 6\,356\,774.5161\text{m}$	Semiminor Axis
$E = 521\,864.6732\text{m}$	Linear Excentricity
$c = 6\,399\,617.4290\text{m}$	Polar Radius of Curvature
$e^2 = 0.006\,694\,605\,328\,56$	e = First Excentricity
$e'^2 = 0.006\,739\,725\,128\,32$	e' = Second Excentricity
$f = 0.003\,352\,923\,712\,99$	Flattening
$f^{-1} = 298.247\,167\,427$	Reciprocal Flattening
$m' = 0.003\,358\,544\,730\,00$	$m' = (a^2 - b^2) / (a^2 + b^2)$
$n' = 0.001\,679\,277\,100\,50$	$n' = (a-b) / (a+b)$
$Q = 10\,002\,001.2313\text{m}$	Meridian Quadrant
$R_1 = 6\,371\,031.5054\text{m}$	Mean Radius $R_1 = (2a+b)/3$
$R_2 = 6\,371\,029.9148\text{m}$	Radius of Sphere of same surface
$R_3 = 6\,371\,023.5234\text{m}$	Radius of sphere of same volume

PHYSICAL CONSTANTS

$$GM = 398\,603 \cdot 10^9 \text{ m}^3 \text{ s}^{-2} \text{ (Exact)}$$

Geocentric Gravitational
Constant

$$\omega = 7.292\,115\,1467 \cdot 10^{-5} \text{ RAD/S}$$

Angular Velocity

$$U_0 = 6\,263\,703.0523 \text{ KGAL} \cdot \text{m}$$

Normal Potential at
Ellipsoid

$$J_2 = 0.001\,082\,7 \text{ (Exact)}$$

$$J_4 = -0.000\,002\,371\,264\,40$$

$$J_6 = 0.000\,000\,006\,085\,16$$

$$J_8 = -0.000\,000\,000\,014\,28$$

Spherical-Harmonic
Coefficients

$$m = 0.003\,449\,801\,434\,30$$

$$m = \omega^2 a^2 b / GM$$

$$\gamma_e = 978\,031\,845\,58 \text{ Gal}$$

Normal Gravity at Equator

$$\gamma_p = 983\,217\,727\,92 \text{ Gal}$$

Normal Gravity at Pole

$$f^* = 0.005\,302\,365\,523\,30$$

$$f^* = (\gamma_p - \gamma_e) / \gamma_e$$

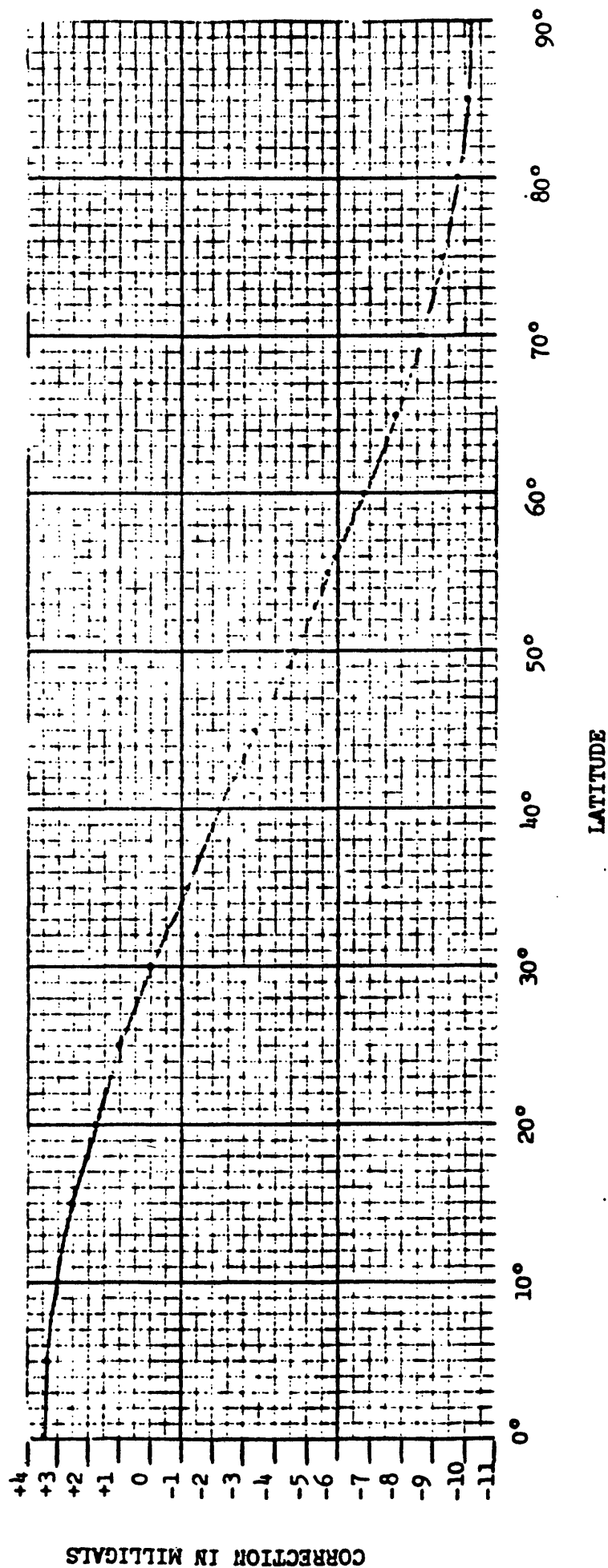
$$k = 0.001\,931\,663\,383\,21$$

$$k = (b\gamma_p - a\gamma_e) / a\gamma_e$$

APPENDIX D'

CORRECTION GRAPH TO CONVERT ANOMALIES COMPUTED FROM THE INTERNATIONAL GRAVITY FORMULA 1930 "POTSDAM SYSTEM"
 $\xi = 981.274$ GAL, TO THE INTERNATIONAL GRAVITY FORMULA 1967.

$$\gamma_{1967} = 978.03185 (1 + 0.005278895 \sin^2 \theta + 0.000023462 \sin^4 \theta) \text{ GAL}$$



REFERENCES

1. Childs, Orlo E., and B. Warren Beebe, Editors, Backbone of the Americas, Tectonic History From Pole to Pole. The American Association of Petroleum Geologists, Memoir 2, 1963.
2. Ferreira, E. O., 1972, Tectonic Map of Brazil, Bulletin No. 1, Ministerio Das Minas E Energia, Departamento Nacional Da Producao Mineral.
3. Gaskell, T. F., Editor, 1967. The Earth's Mantle.
4. Geodetic Reference System, 1967; 1971, Special Publication No. 3, Bureau Central, De L'Association Internationale de Geodesie.
5. Geologic Map of South America, 1:5,000,000, 1964.
6. Gough, D. I., 1973. Dynamic Uplift of Andean Mountains and Island Arcs, Nature Physical Science, Vol. 242, March 19, 1973.
7. Heiskanen, Weikko A., and Helmut Moritz, 1967. Physical Geodesy. W. H. Freeman and Company.
8. International Geological Congress, Twenty-Fourth Session, Montreal, Canada, 1972; Section 3 Tectonics, Section 8, Marine Geology and Geophysics.
9. International Upper Mantle Project
 Volume 1 -- Planning Seminar on the Andean Geophysical Program and Geologic and Geophysics Related Problems; Conference on Solid Earth Problems, Buenos Aires, Argentina, October 1970.
 Volume 2 -- Symposium on the Results of Upper Mantle Investigations with Emphasis on Latin America, Buenos Aires, 1972.
10. Morrison, R. P., 1962. A Resume of the Geology of South America, Scientific Report No. 1, USAF Contract No. AF 19(628)-22.
11. Sletten, R. L., L. E. Wilcox, R. S. Blouse, and J. R. Sanders, 1973. A Bouguer Gravity Anomaly Map of Africa. Defense Mapping Agency Aerospace Center.
12. Strange, W. E., and G. P. Woollard, The Prediction of Gravity in the United States Utilizing Geologic and Geophysical Parameters, Hawaii Institute of Geophysics, Report HIG 64-18, November 1964.

13. Van Broeckel, J., 1968. Gravitational and Geomagnetic Investigations in Surinam and Their Structural Implications.
14. Vening Meinesz, F. A., 1964. The Earth's Crust and Mantle.
15. Voss, James T., 1972. Vertical Gradients of Gravity. Defense Mapping Agency Aerospace Center.
16. Wilcox, Luman E., 1968. Summary of Gravity Correlation Methods for Prediction of 1° x 1° Mean Free Air Anomalies, Defense Mapping Agency Aerospace Center.
17. Wilcox, Luman E., Walter J. Rothermel, and James T. Voss, 1972. The Bouguer Gravity Anomaly Map of Asia. Defense Mapping Agency Aerospace Center.
18. Woollard, G. P., and W. E. Strange, The Prediction of Gravity, in Gravity Anomalies: Unsurveyed areas, AGU Geophysical Monograph Number 9, pp 96-113, 1966.
19. Wuenschel, P. C., and G. R. Hamilton, 1964, Interpretation of Gravity Anomalies on the Westcoast of South America and in the Caribbean. Lamont Geological Observatory.



DEFENSE MAPPING AGENCY AEROSPACE CENTER
SCALE=1/20,000,000 DECEMBER 1973
CONTOUR INTERVAL=20 MGAL.(50 MGAL GREATER THAN +100 AND LESS THAN -100)

APPENDIX E

Table 1. Conversions between English system of units and Syst me International d'Unit s (SI)

Quantity	English Unit	Conversion Factor =	SI Unit	Reciprocal Conversion Factor
Mass	ounce (oz) (avoirdupois)	0.028349527	kilogram (kg)	35.273957 → oz
	pound (mass) (lb) (slug × 32.17)	0.4535924		2.2046223 → lb
	short ton (tn sh)	907.185		1.1023112 × 10 ⁻³ → tn sh
	long ton (tn l)	1016.047		9.842064 × 10 ⁻⁴ → tn l
Length	inch (in.)	0.0254005	meter (m)	39.3700 → in.
	foot (ft)	0.3048006		3.280833 → ft
	yard (yd)	0.9143992		1.093611 → yd
	nautical mile (st ml)	6.2137 × 10 ⁻⁴		1609.35 → st ml
	nautical mile (n ml)*	5.4000 × 10 ⁻⁴		1852.00 → n ml
Time	second (sec)	1.00 ⁺	second (sec) (no other units)	1.00 ⁺ → sec
	minute (min)	60.00 ⁺		0.016667 → min
	hour (hr)	3600.00 ⁺		2.7778 × 10 ⁻⁴ → hr
	day (da)	8.6400 ⁺ × 10 ⁶		1.1574 × 10 ⁻⁵ → da
Frequency	cycles per second (cps)	1.00 ⁺	hertz (Hz)	1.00 ⁺ → cps
Velocity	inch per second (in./sec)	0.0254005	meter per second (m/sec)	39.3700 → in./sec
	foot per second (ft/sec)	0.3048006		3.280833 → ft/sec
	mile per hour (mi/hr) (statute)	0.447041		2.2369 → mi/hr
Acceleration	inch per second squared (in./sec ²)	0.0254005	meter per second squared (m/sec ²)	39.3700 → in./sec ²
	foot per second squared (ft/sec ²)	0.3048006		3.280833 → ft/sec ²
Area	square inch (in. ²)	6.4516238 × 10 ⁻⁴	square meter (m ²)	1550.0 → in. ²
	square foot (ft ²)	0.09290341		10.76387 → ft ²
	square yard (yd ²)	0.83613		1.195985 → yd ²
	square mile (mi ²) (statute)	2.589998 × 10 ⁶		3.8610 × 10 ⁻⁷ → mi ²
Volume	cubic inch (in. ³)	1.6387162 × 10 ⁻⁵	cubic meter (m ³)	6.1023 × 10 ⁻⁵ → in. ³
	cubic foot (ft ³)	0.02831701		35.314645 → ft ³
	cubic yard (yd ³)	0.76455965		1.3079428 → yd ³
	pound ⁺	0.44482		2.2481 → pound
Force	pound ⁺ per square inch (psi or lb/in. ²)	6.8947 × 10 ³	newton per square meter (N/m ²)	1.4504 × 10 ⁻⁴ → psi
Density	pound per cubic inch (lb/in. ³)	2.768 × 10 ⁶	kilogram per cubic meter (kg/m ³)	3.613 × 10 ⁻⁵ → lb/in. ³
	pound per cubic foot (lb/ft ³)	16.018		0.06243 → lb/ft ³
	pound per gallon (lb/gal)	119.826		8.345 × 10 ⁻³ → lb/gal
	foot pound ⁺ (ft-lb)	1.35582		0.73756 → ft-lb
Work or energy	British thermal unit (Btu)	1054.8	joule (J)	9.480 × 10 ⁻⁴ → Btu
Power	horsepower (hp) (U.S. & Br.)	745.70	watt (W)	0.0013410 hp
	electrical horsepower	746.00		0.0013419 hp (elec)
Illumination	foot candle (ft-cd)	10.764	lux = lumen per square meter (lm/m ²)	0.092902

* American units are equivalent to "metric" units. "Foot-pound" or "pound-foot" are "metric" units. The superscript + indicates previous digit (0) repeating ad infinitum.

APPENDIX F

Problems

PROBLEM SET I: Application of Formulas to Typical Geological Problems

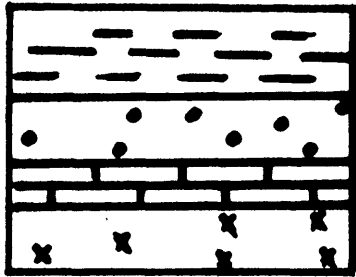
1. Barite occurs in circular disk-like deposits in Washington County, Missouri. The barite is usually found associated with clay material in sink holes of the Potosi dolomite. Usually, the barite constitutes from 12 to 20% of the material. The barite deposits will average about 6 feet in thickness with a radius of 30 feet and be buried about 20 feet beneath the surface. What is the maximum gravity anomaly to be expected when the top of the deposit is 10 feet deep, when 20 feet? Draw a gravity profile that would be expected if measurements were made over such a body buried 10 feet below the surface. (Use solid angle chart in Geophysics V7, L.L. Nettleton)
2. A circular diabase plug with 5 mile radius and infinite depth extent occurs in granite near St. Louis, Missouri. The top of the plug is 300 feet below the surface and is overlain by a series of flat-lying limestones. Construct the gravity profile that would be obtained if a traverse were made across the plug for a distance of 10 miles on either side of the vertical axis.
3. Beach sands containing 50% titaniferous magnetite occur in the form of long horizontal cylinders along the Florida coast. The length of the cylinder usually runs parallel to the coast line and for all practical purposes may be considered to be infinite. These mineralized rolls average 40 feet in diameter and are usually covered concentrically with quartz sands averaging about 10 feet in thickness. Compute and draw a profile at right angles to the axis of the cylinder. Could these deposits be detected using the Worden gravity meter?
4. Two spheres of magnetite occur in limestone. One sphere is 200 feet in radius and buried with its center 250 feet below the surface. The second sphere is 100 feet in radius and buried with its center 650 feet below the surface. The vertical coordinate axis passes through the center of both spheres. Construct profiles for the following cases:
 - A) the upper sphere only assuming a 65% concentration of magnetite
 - B) the lower sphere only assuming a 65% concentration of magnetite
 - C) the gravity profile across both spheres assuming a 65% concentration of magnetite in each
 - D) the gravity profile across both spheres assuming a 65% concentration of magnetite in the upper sphere and a 37 1/2% concentration of magnetite in the lower.
 - E) same as d but with the concentrations reversed

Problem Set I (continued)

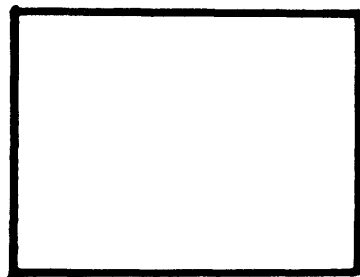
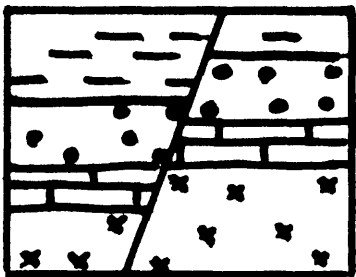
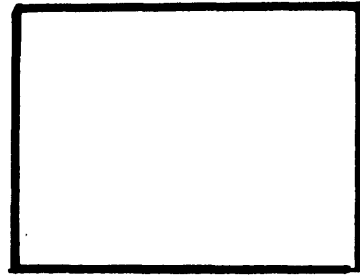
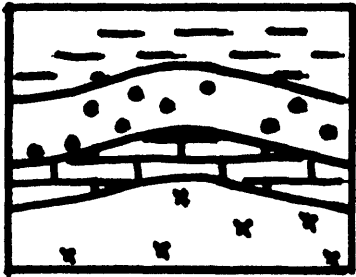
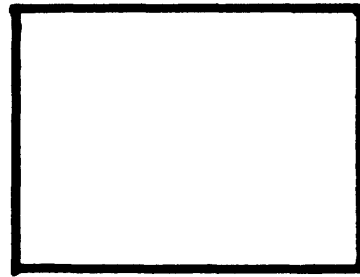
5. One of the largest tunnels in the world was constructed by the Ontario Hydroelectric Power Commission to bring water from above Niagara Falls to the Sir Adam Beck Generating station. The tunnel is a mile long. The diameter is roughly 51 feet and the center of the tunnel is approximately 260 feet below the surface over the length of the tunnel. If the mean specific gravity of the rock removed is 2.7 gm/cm^3 , construct the gravity anomaly profile that would be obtained by measurement at right angles to the axis of the tunnel.
 - A) before the water enters
 - B) if then the water is flowing through the tunnel
6. A vertical vein of pyrrhotite, 20 feet wide and extending to a depth of 1000 feet, occurs in anorthosite. The top of the vein is 100 feet below the surface. Find and construct the gravity profile to be expected if measurements are made across the deposit at right angles to the strike. Consider the vein to be of infinite extent in the strike direction.
7. The Grand Saline salt dome at Grand Saline, Texas has a diameter at its top of 8100 feet. It is covered with a cap rock having a thickness of about 100 feet. The top of the cap rock is 100 feet below the surface. Drilling in the area has revealed the presence of an alternating series of thin-bedded shales and sandstones to a depth of 6800 feet. The drilling also has shown that the dome has flanks which dip at a fairly constant angle of 30° away from the verticle. Construct a gravity profile across the dome for
 - A) the salt dome with vertical sides and no cap rock
 - B) the salt dome with sloping sides and no cap rock
 - C) the salt dome with sloping sides and the cap rock
8. In the western United States, large basin and range areas exist. These are usually north-outh striking grabens formed by granite blocks dropping as much as 1000 feet. The basin originally formed by the graben is now filled with unconsolidated sediments so that there is no noticeable topographic expression of the dropped block. Assume the following:
 - 1) the width of dropped block is 4 miles,
 - 2) the length of the graben is infinite, and
 - 3) the faults are vertical.Construct an east-west profile across the graben area.

PROBLEM SET II--By each block of the 5 diagrams depicting the geologic structure, sketch the effective mass distribution which would give rise to a gravity anomaly.

GEOLOGIC STRUCTURE

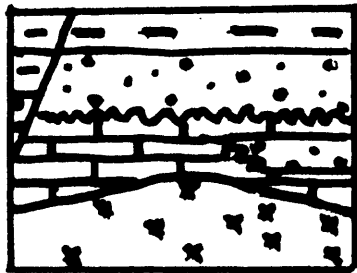


EFFECTIVE MASS DISTRIBUTION

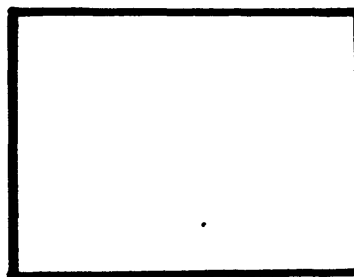
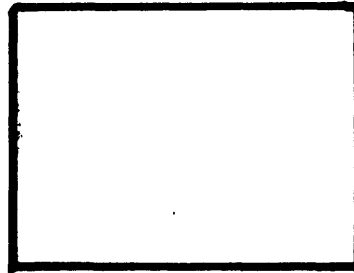


PROBLEM SET II--continued

GEOLOGIC STRUCTURE

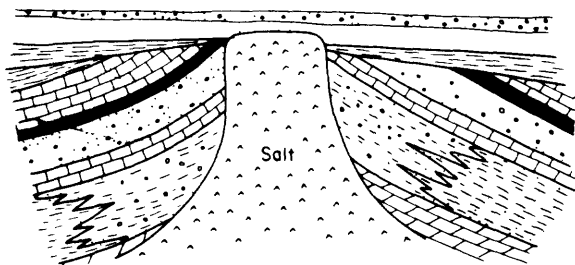


EFFECTIVE MASS DISTRIBUTION

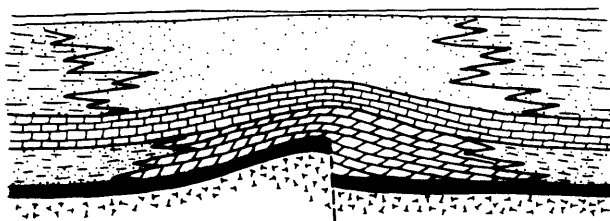


PROBLEM SET III: The four figures below show typical geologic structures: (1) salt dome; (2) structural uplift; (3) normal fault; and (4) a buried valley. For each, draw a sketch of a subsurface geological model using simple geometrical figures which could be used to calculate the gravity effect.

1.

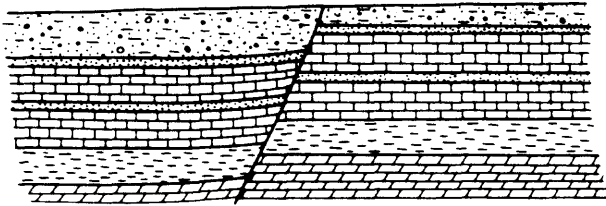


2.

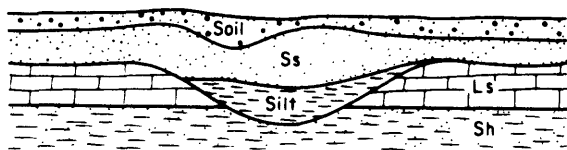


PROBLEM SET III--continued

3.

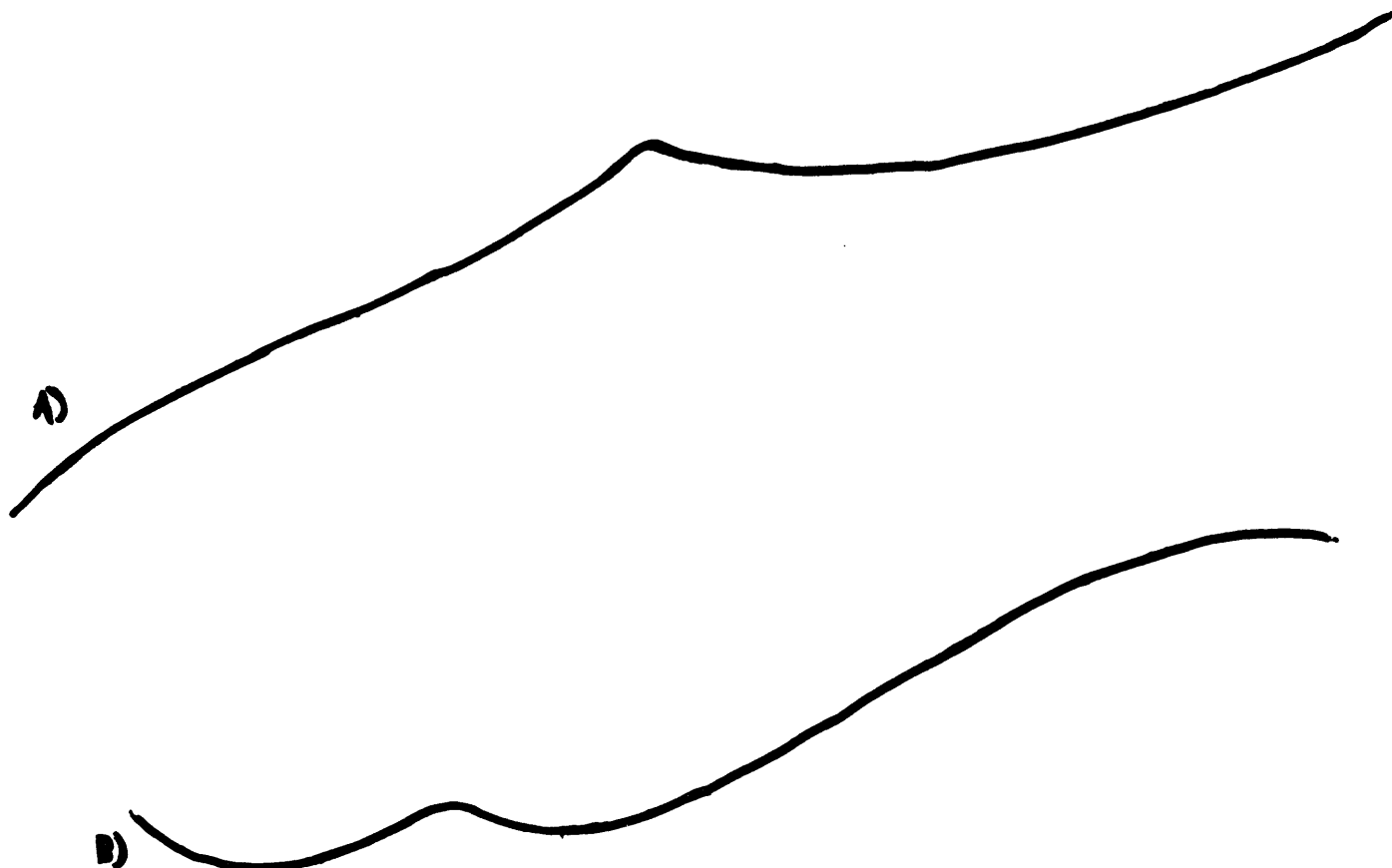


4.



PROBLEM SET IV: Removal of the regional by profile smoothing.

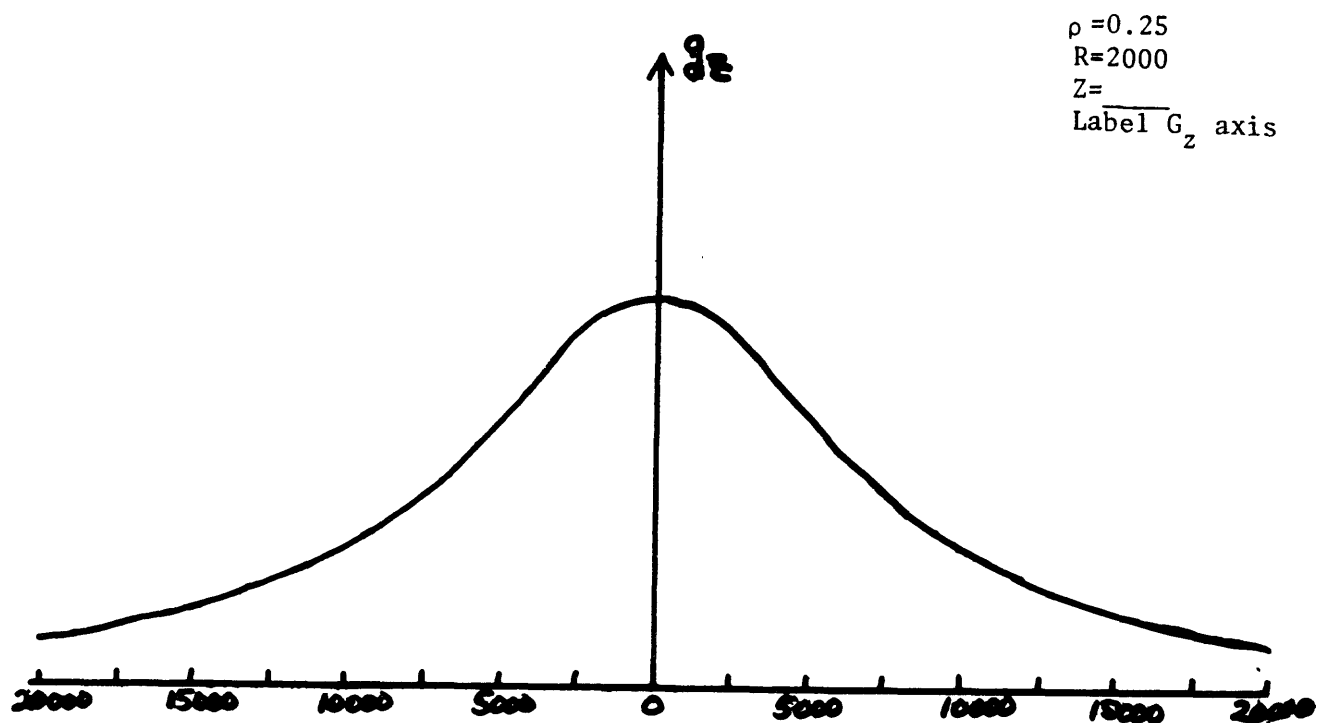
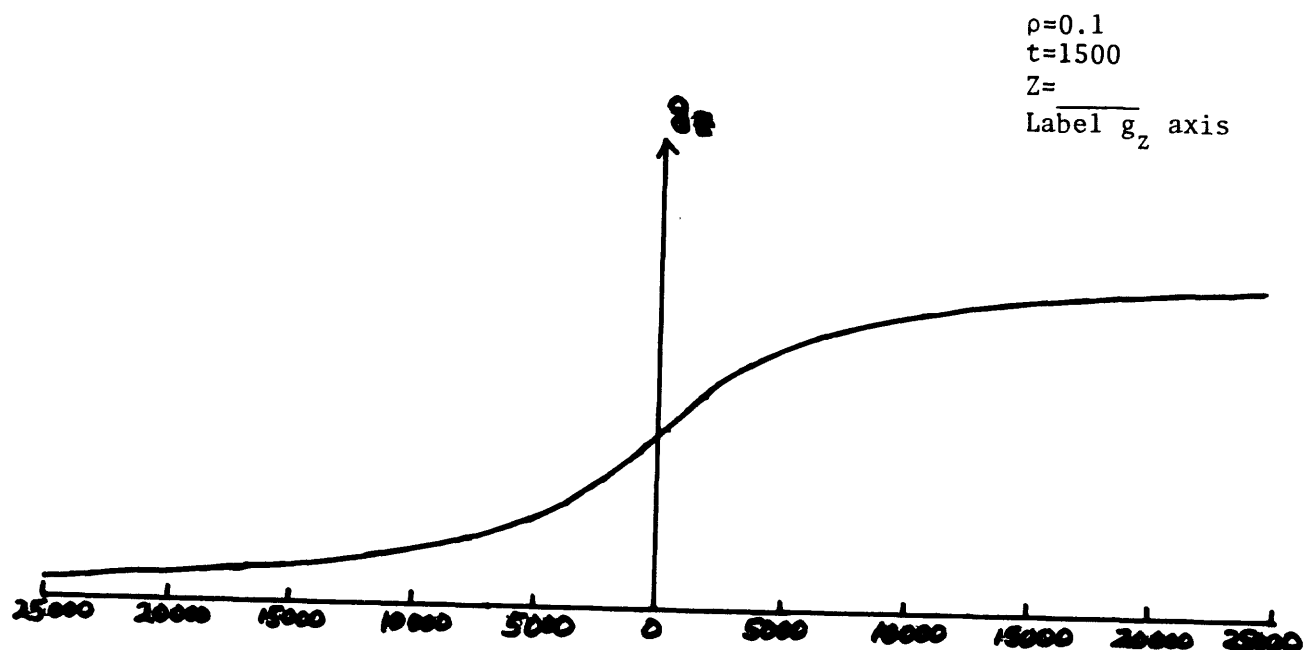
For each of the three Bouguer gravity profiles below, determine the residual gravity anomaly after removal of the regional.



PROBLEM SET IV--continued



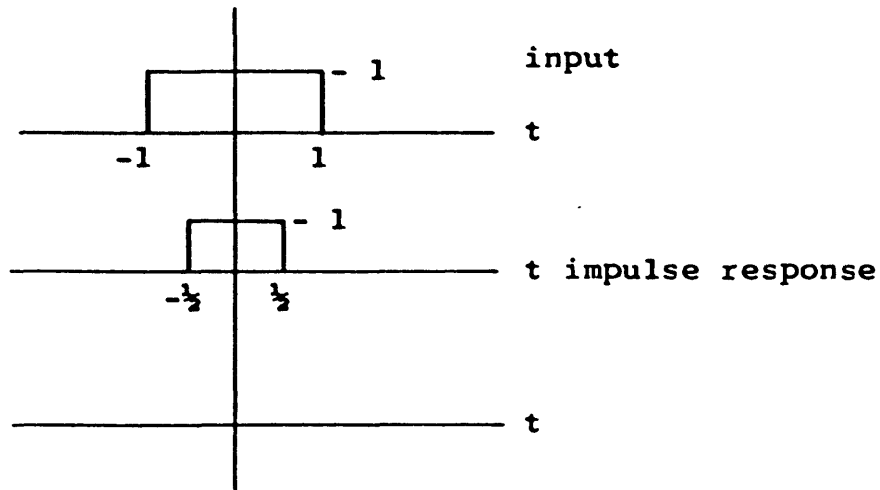
PROBLEM SET V: Given the following two gravity profiles and the indicated information, find the depth to the anomalous mass causing the gravity effect.



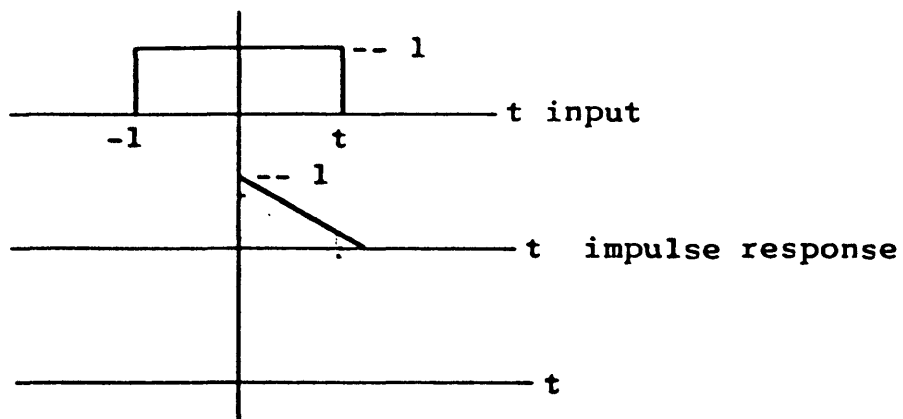
PROBLEM SET VI

CONVOLUTION EXERCISES

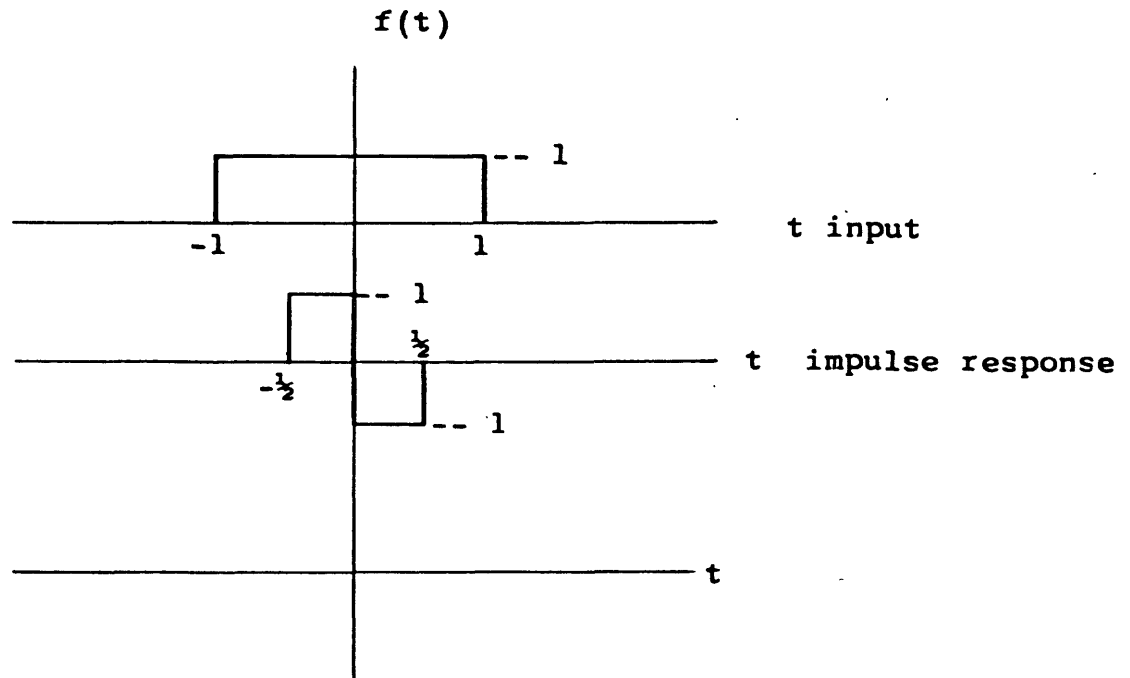
- 1 Use the definition of convolution (FOLD, SHIFT, MULTIPLY, SUM) to find the output when the input and impulse response are as shown below. Sketch the output in the space provided. Reverse the role of the input and impulse response and repeat the problem.



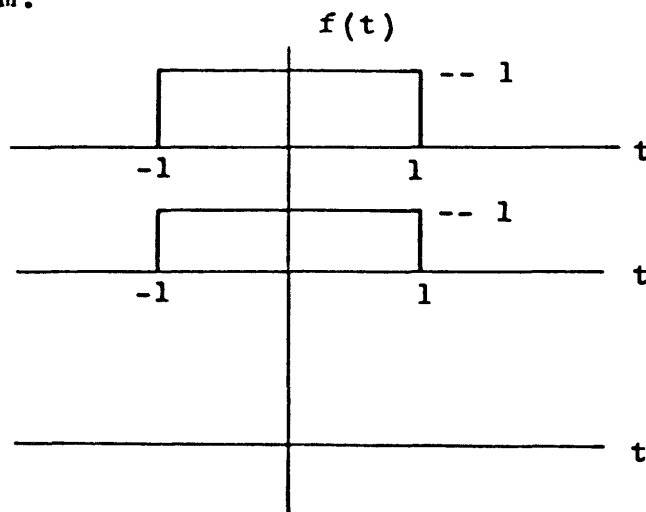
- 2 Find and sketch the output when the input and impulse response are as shown below. Reverse the role of the input and impulse response and repeat the problem.



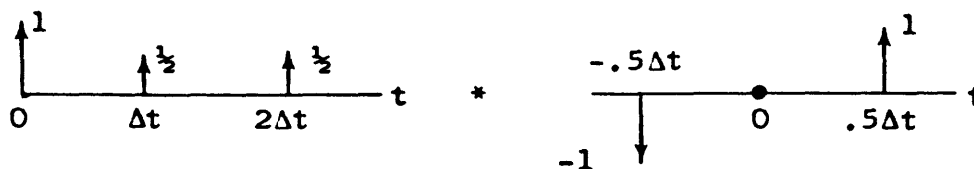
- 3 Find and sketch the output when the input and impulse response are as shown below. Reverse the role of the input and impulse response and repeat the problem.



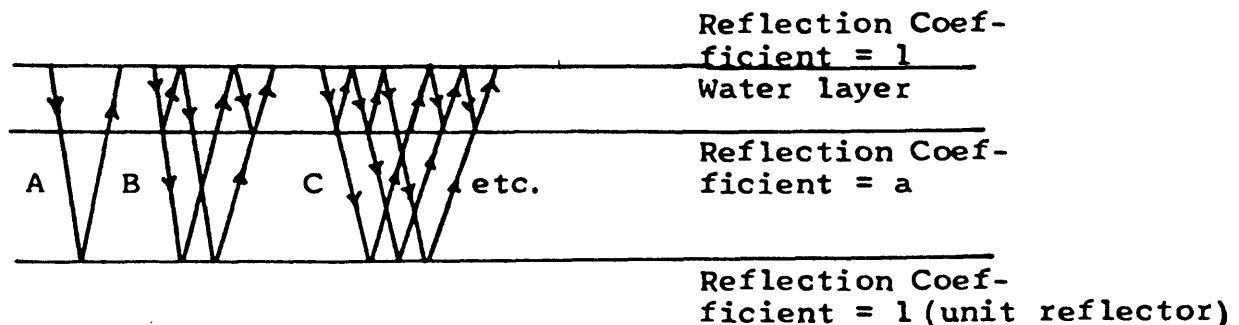
- 4 Find and sketch the output when the input and impulse response are as shown below. Reverse the role of the input and impulse response and repeat the problem.



- 5 Convolve the digitized wavelets shown below. Use the replacement method, the folding method, the moveable strip (serial product) method, polynomial multiplication (folding) method, polynomial multiplication (z transform) method, and the matrix formulation method.



- 6 Write the impulse response of the water layer filter as a time function and as a z transform (i.e., a polynomial in z). Let the 2 way time in the water layer be Δt .



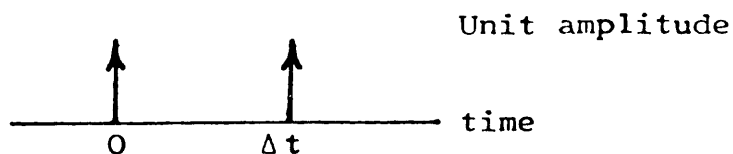
- 7 Write the impulse response of the inverse water layer filter as a time function and as z transform. Sketch the amplitude spectrum of the water layer and the inverse water layer filters.
- 8 Describe the use of auto- and cross-correlation in the vibroseis technique.

- 9 Suppose we have a digitized seismic trace, $G(t)$, sampled at 0.005 sec intervals. What is the highest frequency which can be recovered in an undistorted form? What anti-alias filter should have been used prior to sampling (at $t_s = 0.005$) to assure recovery of the information up to 100 cps? If complete recovery of $G(t)$ is required, what sampling rate should be used?
- 10 Some basic Fourier transform pairs are listed below. Name some common geophysical data processing operations based on each transform pair. $G(t)$ is the time function and $S(f)$ is the frequency function. The arrow means "transforms as" and is a reversible operation.

- a. $K G(t) \longleftrightarrow K S(f)$
- b. $G(Kt) \longleftrightarrow \left| \frac{1}{K} \right| S\left(\frac{f}{K}\right)$
- c. $G_1(t) + G_2(t) \longleftrightarrow S_1(f) + S_2(f)$
- d. $G_1(t) * G_2(t) \longleftrightarrow S_1(f) \cdot S_2(f)$
- e. $G_1(t) \cdot G_2(t) \longleftrightarrow S_1(f) * S_2(f)$
- f. $G(t-t_0) \longleftrightarrow e^{i(-\omega t_0)} \cdot S(f)$

Note: K = constant, $*$ = convolution

- 11 Find the Fourier transform of the time function consisting of the two delta functions below. Sketch the amplitude and phase spectrum. Describe a common operation on geophysical data which this time function represents.



- 12 Design a linear array of geophones which will reject noise wavelengths shorter than 20 ft and longer than 140 ft.
- 13 Draw a block diagram to illustrate the individual parameters of the total marine seismic system. Which elements of the total system can be deconvolved?

In the space on the right, sketch in the amplitude and phase spectrum of the wave form shown on the left.

